Great Lakes Offshore Wind Project: Utility and Regional Integration Study

by

Amirhossein Sajadi, Kenneth A. Loparo
Case Western Reserve University (CWRU)

Rob D'Aquila
General Electric (GE)

Kara Clark
National Renewable Energy Laboratory (NREL)

Joseph G. Waligorski
FirstEnergy (FE)

Scott Baker
PJM Interconnection (PJM)

Final Report Prepared for
U.S. Department of Energy
under the Contract DE-EE0005367

Cleveland, Ohio, 44106

June, 2016

Notice

Acknowledgments

The authors of this report greatly appreciate the continuous engagement and support of the involved organizations throughout this study. In particular, the team would like to acknowledge Richard Kolacinski and Steve Barnes for their assistance.

Executive Summary

Offshore Wind Energy

Wind energy has been known for a very long time. The historians believe that the first windmills were built over 3000 years ago. The first written evidence indicates that the windmill began in Persia, now called Iran [1]. The applications of windmills were to grind or mill grain and to pump water. Although the modern wind turbines look absolutely different than the first windmills, the basic idea behind them is the same; convert the power of the air flow into some other form of desirable energy [1].

This source of electrical energy is relatively new in comparison to other sources such as fossil fuel and hydro power plants which have been around more than a century [2]. In addition, wind power, by its nature is more complex to use in electrical power system due to two key factors: (1) variability and (2) uncertainty [3]. The variability of the wind power means that its available amount is not always at a fixed level and its variability depends on the geographical location and meteorological conditions. Uncertainty of the wind power represents the probability of having the forecasted amount of wind blowing at any given time and depends on the probabilistic method used to forecast as well as aerologic and atmospheric physics and chemistry accuracy. Therefore, the wind power is more sophisticated to dispatch in contrast to the conventional generation units.

Over the last decade, the installed capacity of wind energy conversion systems has grown significantly all across the globe. The American Wind Energy Association reports that the US installed more wind generation capacity in 2015 than other generation sources in 2015, equivalent of 8.6 GW of new wind energy capacity [4]. The US DOE reports that more than 13GW new wind energy generation capacity was installed in the US during 2012 which helped to surpass 60GW of total installed wind capacity at the end of 2012 [5]. Obviously, the share of wind generation has significantly increased and will go on. The most recently released wind vision report by DOE gives a roadmap to 35% wind energy by 2050 for the U.S [6]. In Germany, electricity generation from the wind power increased by around 50 percent in 2015 [7]. In September 2013, Germany reached the record of 1.14GW of new wind capacity installation in the first six months of 2013. This was a 14% expansion in the German wind market by reaching 32.421GW installed capacity of wind turbine in Germany by June 30 2013 [8] and [9]. Contrarily, Spain, Europe's second largest wind market, did not add any new wind power capacity in 2015 [10] while in 2012, it added 950MW new capacity to hit 22.8GW capacity [11]. According to the Ministry of New and Renewable Energy, India has installed 19.662GW of wind power and forecasted to add 2.050GW to this capacity by the end of 2013 [12].

Currently, over 7.7 GW of offshore wind farm are operating all over the world. More than 96% of offshore wind farms are constructed and operating in Europe. England with 3711 MW of operating wind farms is the leader in the world. Denmark with 1272 MW is the second leading country and then Germany with 521 MW is the third.

Non-European countries such as China, Japan, South Korea, and Taiwan have set their road map towards achieving a greater contribution in power generation by offshore wind market by constructing new offshore wind farms or expanding their current capacity. The South Korean government has approved construction of the largest offshore wind farm in the world by 2019. This project is planned to be built in three phases with a total capacity of 2500MW on their southwest coast [13]. The U.S.' first offshore wind farm project is Cape Wind, which is projected to generate 454MW of electrical power [14]. This project is currently ongoing in Nantucket Sound off Cape Cod, Massachusetts, United States. The Indian Government also has approved the construction of the nation's first offshore wind power project [15]. This project with a capacity of 100MW is projected for the coast of Gujarat as a demonstration project and is expected to finish by 2019 [16]. The Taiwanese government aims to install 600 offshore wind turbines with total capacity of 3000MW by 2030 [17]. At this point their success depends upon their available resources and dedication to use the experience of the European countries.

Offshore wind farms are not regarded as a form of distributed generation and typically are installed in scales of 100s of MW. They are located in a distance from the shores and, therefore, high or medium voltage submarine cables have to be used to transmit the generated power to the onshore grid and inject it through the transmission system. Injecting a significant amount of power into an existing power system has a huge impact on its control, stability, and resiliency [18]. In addition, uncertain and variable nature of wind power introduces more complexity in system's control, unit commitment and market operation [19]. Thus, in offshore wind integration studies, the generation and transmission systems planning are the major concerns.

Power System Planning

The power system planning is the process of designing or expanding the system to meet the demand through a secure power delivery, from power generation units to consumptions [20]. The planning process requires a tremendous amount of computer simulation to forecast load growth and evaluate operation and dynamic behaviors of the undertaken power system.

The generation system planning aims to foresee load demand within the period of 2-10 upcoming years or even longer by using historic data to ensure sufficient generation capacity and adequate available reserve will be available. This part of the planning studies determines the fuel mix and the cost of electricity [20]. The ultimate goal of the transmission planning studies is to identify the upgrades required to adopt the new capacity by keeping the existing power systems secure and stable following installation of new generation units.

Planning and operation of generation and transmission systems, however, are highly correlated; bulk generated power is transmitted to the locations where consumers are located through the transmission system. Therefore, they are interrelated and share common operational stability and control issues.

Study Overview

The US DOE initiated the Great Lakes Offshore Wind Project: Utility and Regional Integration Study (DE-FOA-0000414) to address technical challenges and planning requirements concerning integration of large-scale offshore wind power into utility service areas.

This project aims to identify transmission system upgrades needed to facilitate offshore wind projects as well as operational impacts of offshore generation on operation of the regional transmission system in the Great Lakes region including:

Steady State Stability related issues in the system including voltage regulation and reactive power availability in the area as well as power transfer capability of the transmission system.

Small Signal Stability related issues in the system as a result of variability of the offshore wind power including frequency stability and voltage stability.

Large Signal Stability related issues in the system as a result of operation of variable offshore wind power including rotor angle stability, frequency stability, voltage stability.

Accordingly, this study used a simulation model of the US Eastern Interconnection as the test system and focused on the integration of a 1000MW offshore wind farm operating in Lake Erie into FirstEnergy/PJM service territory as a case study.

The project team includes Case Western Reserve University (CWRU), General Electric (GE), FirstEnergy (FE), National Renewable Energy Lab (NREL), and PJM Interconnection (PJM).

The findings of this research provide recommendations on offshore wind integration scenarios, the locations of points of interconnection, wind profile modeling and simulation, and computational methods to quantify performance, along with operating changes and equipment upgrades needed to mitigate system performance issues introduced by an offshore wind project.

Development of Integration Scenarios

Wind power estimation and the geographical locations of wind availability in Lake Erie were provided by the NREL. Accordingly, five possible points of interconnection (POI) in the FirstEnergy transmission grid were identified by GE. The POIs were substations near the shoreline.

Initially, there were seven feasible possible interconnection scenarios proposed that would fit the current grid infrastructure. After team discussions, it was agreed to consider the following scenarios for offshore wind power integration into the FirstEnergy/PJM system for further analysis and investigations:

1. Interconnecting a 1000 MW of offshore wind generation at the Perry 345 kV Substation

2. Interconnecting five cables 200 MW each of offshore wind generation, at the Avon 345 kV Substation, at the Lakeshore 138 kV Substation, at the Eastlake 345 kV Substation, at the Perry 345 kV Substation and at the Ashtabula 138 kV Substation

3. Interconnecting two cables of 500 MW each of offshore wind generation, at the Avon 345 kV Substation and the Lake Shore 138 kV Substation

Computer Simulation Modeling and Implementation

Electrical Generators Wind farms consist of a large number of individual wind turbine generators. The wind farm model may consist of a detailed representation of each wind turbine generator and collector system. However, a single machine model to represent all of the wind farm machines is appropriate for most bulk system studies. Thus, an aggregated model that includes a conventional generator connected to a PV bus for the offshore system was used for the steady state study. The parameters of the machine were calculated based on GE 3.6MW Wind Machine's specifications [21].

Dynamic analysis models to represent the wind turbine generators were developed only for Doubly-Fed Induction Generator (DFIG), also known as Type 3. This decision was based on the North American Electric Reliability Corporation (NERC) and generally accepted practices by North American utilities that recommend new wind interconnections have reactive capability provided by the machines themselves [22].

The original power flow model was modified to represent 2x500 MW paths for the dynamic simulations studies. The equivalent wind farm and collector system could then be partitioned to simulate different offshore wind variability scenarios.

The dynamic scenarios aimed to investigate the impact of variability of the wind generation on stability of the system. The dynamic wind turbine models used in this analysis are not able to provide step changes in generation output during the simulations. Thus, load models were added to the terminals of the wind machines. The loads can then be turned on/off and sizes of the loads are matched to the magnitudes of the step changes that are to be introduced at the terminals of the machine. The loads simulate the variability of the wind farm.

The dynamic models of the offshore wind generation system were represented as defined in the GE PSLF model library [23]:

- *wndtge:* The wind turbine and turbine control model for GE DFIG wind turbines

- *gewtg:* The generator/converter model for GE DFIG wind turbines

- *exwtge:* The excitation (converter) control model for GE DFIG wind turbine generators

Step-Up Transformer In the models, the equivalent wind turbine generator is connected to the collector system via a step-up transformer with specifications equivalent to a typical unit pad-mounted transformer ratings and impedances for standard industry equipment.

Electrical Collector System A typical collector system voltage of 34.5 kV was used in the models. The substation transformer would be suitably rated for the number of wind turbine generators, with impedance of typically around 8%.

Compensation Device In this study, a Static Var Compensator (SVC) with a significant compensation capacity was used and modeled for compensation device at the POIs. This allows assessing the capacity of the compensation device that may be required to provide ancillary service to the grid by looking at the level of reactive power generated/consumed by the SVC.

During steady state analysis, the SVC was modeled as a controllable shunt device. This allowed for automatic voltage control during load flow simulations and the device was modeled to regulate voltage at the POI [22].

In dynamic stability studies, GE PSLF requires that the device be modeled as a voltage independent generator model. Therefore, steady state scenarios with a SVC were modified to include a load flow generator model dispatched with similar reactive capability and no real power output [22].

The dynamic model used to represent these devices was the simple Static VAr device *vwscc* in GE PSLF model library [23]. This analysis looked at a maximum and minimum SVC rating size of ±500 MVAr.

Generation Dispatch Scenarios and Load Assumptions For steady state and dynamic analysis in this investigation, two generation dispatch and load profiles for the Eastern Interconnection were modeled in PSLF:

1. **Summer peak load for steady state analysis:**: contains 68859 system buses, 9091 generators with a total of 936,266 MW and 444,200 MVAr of installed generation capacity to serve the load of 685,469 MW and 201,005 MVar.

2. **Winter light load for dynamic stability analysis:** contains 63608 system buses, 8356 generators with a total of 894,772 MW and 411,288 MVAr of installed generation capacity to serve load of 302,086 MW and 75,596 MVar.

The main objective of this case study was integration of 1000MW offshore wind power generation into the FirstEnergy/PJM system. The second objective was to consider impacts of lack of operation of Perry Power Plant, a major conventional power plant with capacity of 1200MW and 625MVAr. Thus, the generation units in the area were relatively redispatched to maintain the balance between generation and consumption in the area for each of the developed interconnection scenarios.

Contingency List FirstEnergy provided a condensed contingency list that included generation units, transformers, line segments, complete lines, and synchronous condenser outages. This list was used to perform the contingency analysis.

Steady State Stability Analysis

Steady state stability of electrical power systems refers to the behavior of system while operating at any given equilibrium operating point [24]. This section discusses steady state stability analysis in planning studies for offshore wind farm integration.

The steady state stability analysis in power system is practical in generation and transmission planning to ensure that throughout every 24 hours of the day of the year, the system's constraints are not violated at any given operational point. This constitutes that enough generation units are capable and dispatchable with an adequate reserve level and enough line capacity is available to serve the demand load. The outcome of this study determines the required expansion and upgrades to maintain the reliability of the power system.

The steady state analysis in the transmission system is associated with the following criteria: (1) Thermal rating of the lines and (2) Voltage regulation across the system [25]. Typically, the voltage stability margin is much smaller than the thermal stability margin and, therefore, the voltage stability margin determines the overall stability margin for the system [25], in the majority of the cases.

Steady State Contingency Analysis

Power system security is directly related to the ability of the system to maintain normal operation following disturbances so-called contingencies. A contingency represents a credible event that can occur in the system such as an outage of a main component or multiple components. Thus, power system security is then defined as the ability of the power system to survive from and withstand the contingencies and deliver the power to consumers without interruption [24]. It should be noted that power system security is broader concept than stability and integrates reliability and stability, and involves robust and resilient the system [26].

Contingency analysis involves applying a sequence of contingency events to the system. These events could be the outage of a transmission line, a generator or multiple components at the same time. The results represent the response of the system to those contingencies. Then, the events are ranked based on their severity to identify the worst case scenarios and determine how resilient and secure the system will be during long terms [27]. The severity index evaluates how distant the operation points are from the bifurcation point in which voltage collapse occurs. This process is also called contingency ranking and monitoring. Thus, the accuracy of the contingency analysis highly relies on the accuracy of the severity index used by the planner.

Small Signal Stability Analysis

Small signal stability analysis addresses the dynamical behavior of the system following a small disturbance and assesses capability of the system to damp out the oscillations which are excited by the disturbance. In the small signal stability analysis, no contingency occurs and all of the grid components are in operation.

The oscillations in power system contain several frequencies, known as modes. They are the results of interaction of one component, including generators, relative to another. It is highly important to identify these modes and understand their sources in order to develop and design proper controllers to damp them out.

The electromechanical oscillations that involve generator rotating masses occur within range of 0.1 Hz to 3.0 Hz. These modes include Inter-area modes, Interplant modes and Local plant modes and their natural frequency range are 0.1-1.0 Hz, 1.0-2.0 Hz and 2.0-3.0 Hz, respectively.

The sources of the electromechanical oscillations usually are shipping bulk power over long distances as well as high gain automatic voltage regulators (AVRs) [28]. These are critical modes of the system because they can affect tie-line power flows and operational balance in the interconnected power systems. Therefore, system planning studies focus on these types of modes.

The results from the voltage response in time domain do not provide sufficient information for the nature of the oscillation [29]. Therefore, a frequency domain analysis is required to be carried out to identify full list of critical modes of the system.

Frequency stability in a power system is defined as the ability of the system to adequately manage frequency regulation when disturbances occur. Following a disturbance, when frequency decline occurs, it should be adequately arrested so the under-frequency load shedding relays do not operate. The inability of the system to meet such a requirement is an indication of a significant difference between generation and consumption and can lead to the system instability.

Primary frequency control, known as inertial response, refers to the response of the system to frequency changes without changing the governor's reference values. In this stage of control only partially loaded generators participate. The time frame of this stage of frequency control is within in first tens of seconds following a disturbance [24].

It is important to note that it takes a few seconds until governor of generators sense the frequency drop and react and attempt to mitigate frequency deviation by curtailing power generation. Therefore, frequency response of a power system relies on inertial control to prevent an immediate collapse of the system. The inertial response of a power system is generated by rotational mass of its generators and is an index of rotational kinetic energy that they can release [30].

In recent years, higher penetration of renewable energy units such as solar panels and wind turbines has raised the concern for dynamic stability of the power grids. This is because generation units such as solar panels and Type 4 wind turbines are connected to the grid through a power electronic interface which makes them fully isolated from the grid and Type 3 wind turbine are partially isolated from the grid. However, their power electronics interface by using advanced control functions may provide a similar frequency response to the grid as a conventional generator [31].

Large Signal Stability Analysis

Large signal stability analysis addresses the dynamical behavior of the system following a large disturbance to assess whether or not it reaches a new equilibrium operational point [24]. The new equilibrium point attained following a fault may be same the pre-fault equilibrium point or a different equilibrium point. Large signal stability studies include rotor angle, voltage and frequency stability analysis. The voltage stability and frequency response were discussed in detail in the previous section, Small Signal Stability Analysis.

A fault can be short term, such as short circuit faults on transmission lines or generators with a successful clearance, or long term, such as an outage of generation unit(s) or a disconnection of lines by protective relays after a failure in clearing the fault. In the case of short term faults, the systems post-fault topology remains unchanged (assuming that the fault is cleared within the critical clearing time), whereas, in the case of long term faults, the topology is changed.

The oscillations that are excited by the fault should be damped such that ringing decays within the first few cycles to few seconds following the fault. Otherwise, the transient behavior of the system may dominate the system response for sufficiently long that the system trajectory diverges from the stability region associated with the current equilibrium point and potentially lead to system-wide failures.

Rotor angle in a synchronous machine is an electrical angle that is defined by relative angle between rotor and stator magnetic fields. In an interconnected power system, power transfers across the transmission lines happen as a result of the angle difference at ends of the lines. Therefore, the synchronous generators should operate at a mechanical rotational speed so that produce the same electrical speed. This maintains the power flow steady across the system and is so called synchronism in power systems.

Following a severe fault, whether short term or long term, the generators in a power system may reset their operating point to a different operating point than prior to the fault. The change of operating point may result in change in rotor speed and angle. Consequently, change in rotor angle can change the level and direction of power flow among the lines and generators. Rotor angle stability in power systems refers to ability of synchronous machines in the system to maintain their synchronism following a disturbance [24], [32].

A power system is unstable if one or more generators rotor angle starts to deviate from their pre-fault values significantly relative to other angles. This is called loss of synchronism and leads to an unexpected disconnection of a unit(s) or line(s) from the grid which can cause interruption in power delivery and might lead to a blackout if sufficient contingency reserve units are not available in the area.

The longest clearing time that the system remains stable and none of the generators lose the synchronism, is called critical clearing time (CCT) [24]. In multi-machine systems, the CCT is calculated for each of component individually. Calculation of accurate CCT is critically important to set protective equipment appropriate to ensure reliability of power supply.

Recommendations and Findings

Steady State Stability Analysis In steady state stability analysis, operational issues including voltage regulation and power transfer capability of the transmission system were investigated. To accomplish this goal, a novel statistical analytical tool was introduced and used. It was found out that the integration of offshore wind farms could improve the voltage regulation across the system. The results also showed that in lightly loaded power systems, the line congestion is not a concern for adding the wind generation capacity. The introduced tool provided explicit information about the operating conditions of a large scale grid throughout its complete range of operation of the offshore wind farm.

Steady State Contingency Analysis An analytical tool was developed to analyze the contingency operation of large scale power systems for offshore wind farm integration studies. This tool relied on a risk based security index and was used to identify the most severe contingency events by considering variability of the offshore wind farm. Then, feasible offshore wind integration scenarios were examined to identify the most resilient and vulnerable interconnection scenarios and integration topologies within the system. The results proved the effectiveness of the proposed tool. This tool is applicable to integration studies of all types of variable generation units.

Small Signal Stability Analysis In small signal stability analysis, response of the system to variability of the offshore wind power was investigated. This investigation included frequency response and voltage stability analysis. First, it was demonstrated that the voltage oscillatory modes could be captured by applying Prony analysis directly to a time-domain voltage signal. This finding is helpful for large scale interconnected power systems in which applying modal analysis is computationally burdening or impossible. Then, a swing based frequency response metric was introduced to assess the frequency stability where wind power may drop or rise. The results showed the effectiveness of the discussed approaches in assessment of small signal stability of large scale power systems for offshore wind farm integration studies.

Large Signal Stability Analysis In large signal stability analysis, operational issues including rotor angle stability, frequency response, voltage stability as the result of a severe long term and short term faults were examined. This effort was practical to identify worst case scenarios and assess whether or not integration of offshore wind power degrades the stability of the grid.

The results from the short term transient stability showed that upon integration of the offshore wind farm, the CCT was not degraded. Conversely, it was increased significantly in the majority of the cases in a fashion that the system could remain stable after 900 cycles of persisting fault. To be more precise, the CCT for faults on large generators was not improved significantly. The significant improvement of the CCT was for faults on medium capacity generators. The wind farm improved the CCT for the lines depended on their distance from large capacity generators. The

CCT for the fault on the lines close to large generators did not change significantly while for lines close to medium generators, the CCT was significantly improved.

These results also showed that the CCT and dynamics of active power, rotor angle, reactive power and voltage are highly correlated. As the CCT is improved, all other aforementioned variables are improved. Thus, the CCT directly determines short term transient rotor angle and voltage stability margins of system. This study also showed that the additional reactive power support by SVC does not improve the transient stability of the system.

The results from long term transient stability showed that integration of offshore wind farm could improve the transient stability of the system by decreasing the number and amplitude of the oscillatory modes. They also showed that operation of SVC at the POIs does not influence the rotor angle stability of the system following an outage. While the operation of the wind farm at its maximum capacity yielded the worst case scenario in terms of rotor angle oscillations, performance criteria were still met.

The Swing Based Frequency Response (SBFR) metric was introduced and used for all of the studied cases to assess the transient frequency stability. In this study, it was found out that upon integration of the offshore wind farm, the transient frequency stability following a short term fault depends on the size of the faulted component and its inertia contribution. As the larger the capacity of generators are, the more robust and stable they are. This is because of the higher inertia of the larger generators. For faults on medium and small capacity generators and transmission lines, the frequency response relies on the inertial support by the large generators which provide major inertia contribution in the system. The second factor that determines the frequency response is the distance of the faulted component from the large generators. For faults on large capacity generators, frequency response was stronger and independent from the other inertia contributor units. The results from the long term fault outlined that the frequency response of the system was improved upon offshore wind farm integration.

The results from the transient voltage stability showed that the maximum voltage deviation amplitude and oscillations were reduced following a short term fault upon integration of the offshore wind farm. In addition, the transient voltage stability of the system following outage of the grid components was independent from behavior of rotor angle and rotor speeds in the area, for all levels of wind power.

Scope for Future Work

- Development of offshore wind farms in areas where thermal and voltage stability problems already exist may result in some generation not being properly dispatched for some period of time. Because of the fact that the generation dispatch is managed through market processes, it will be necessary to develop and implement methodologies that incorporate stability constraints and market processes. These models will reflect the actual operation of the wind farms that are ultimately deployed in practice. Such studies will give an indication as to whether the offshore wind generation will be economically and technically feasible and viable.

- Additional work is needed to completely understand how operation of neighboring generation units to the POI of the offshore wind farms and their controller systems affect the dynamics and control of both grid and the offshore wind farm.

- Additional work is needed to completely understand how energy storage systems such as battery and ultracapacitor can provide additional support to the power system by preventing or reducing the oscillatory modes in response to the external disturbances. This investigation should be extended to electrochemical effects on those systems including aging effect and ambient conditions such as drastic temperature change. For instance in Cleveland, OH, the summer temperature could reach beyond 100°F whereas the Polar Vortex in the winter could drop the temperature below -30°F. This analysis will allow understanding of their dynamic interaction with the grid and the consequences of these phenomena on the stability and operation of the grid in the presence of large scale offshore wind farms.

Contents

List of Figures

List of Tables

Chapter 1

Introduction

1.1 Power System Operation

Operation of the power systems is a continuous process of maintaining balance between generation of power and its consumption. In large interconnected power systems, the load consumption is constantly changing. This is because of the behavior of consumers. Therefore, the generators should follow the load's fluctuation.

Stability of an electrical power system refers to the ability of the system to reset its operating point to a suitable equilibrium point after a physical disturbance event [24]. In other words, the stability of the power system could be defined as ability of the system to maintain its balance between generation and consumption.

Accordingly, power system studies consist of three major areas:

1. **Steady State Stability**: The behavior of system while operating at any given equilibrium operating point.

2. **Small Signal Stability**: The ability of the system to withstand small signal disturbances including load or generation set point changes. It focuses on the trajectory that it takes from pre-disturbance operating point to post-disturbance operating point.

3. **Large Signal Stability**: The ability of the system during large signal disturbances to maintain its synchronism and regain a new equilibrium operating point following the contingency events, including short circuit faults and outage of electrical circuit elements.

1.2 Power System Planning

The power system planning is the process of designing or expanding the system to meet the demand through a secure power delivery, from power generation units to consumptions [20]. The planning process requires a tremendous amount of computer simulation to forecast load growth and evaluate operation and dynamic behaviors of the undertaken power system. This should be conducted in all levels of generation, transmission and distribution. The generation units transform other forms of energy than electricity into the electrical energy. The transmission system delivers the generated power from generation units to the distribution system. The distribution system is meant to deliver the power to buildings. The roles of buildings are to deliver the power from the distribution level to the end user consumer and provide ancillary services to the grid such as demand response and load management.

The generation system planning aims to foresee load demand within the period of 2-10 upcoming years or even longer by using historic data to ensure sufficient generation capacity and adequate available reserve will be available. This part of the planning studies determines the fuel mix and the cost of electricity [20]. In conventional generation planning studies for power systems, the planners had a vast range of selections from which to choose including hydroelectric, nuclear, coal, gas turbine, etc.

The ultimate goal of the transmission planning studies is to identify the upgrades required to adopt the new capacity by keeping the existing power systems secure and stable following installation of new generation units at minimum cost while the benefits to the system, in particular to the utility companies, are maximized.

Planning and operation of generation and transmission systems, however, are highly correlated; bulk generated power is transmitted to the locations where consumers are located through the transmission system. Therefore, they are interrelated and share common operational stability and control issues.

Operation and planning of traditional power systems with bulk conventional generation units as well as stability related issues have been extensively studied and discussed in papers and textbooks including Machowski [24] and [26], Anderson [33], Kundur [34], Sauer [32] and Gutman [25].

Figure 1.1 shows the flowchart of the studies that are required to be conducted as part of the transmission system planning studies.

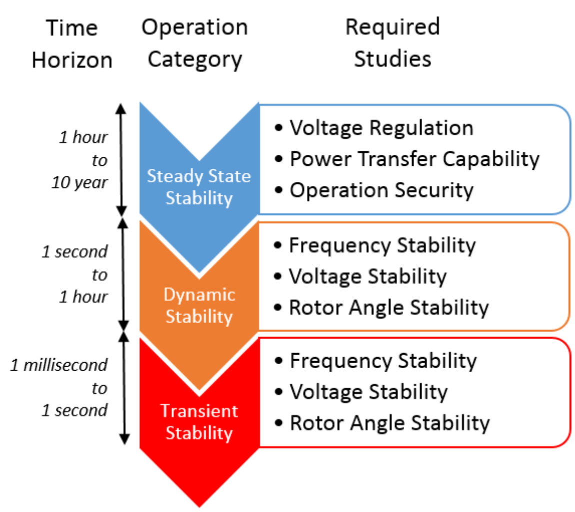

Figure 1.1: Flow chart of studies for power system planning

1.3 Offshore Great Lakes Offshore Wind Project Overview

US Department of Energy (DOE) initiated the Great Lakes Offshore Wind Project: Utility and Regional Integration Study (DE-FOA-0000414) to address technical challenges and planning requirements concerning integration of large-scale offshore wind power into utility service areas.

Offshore wind farms are integrated into an interconnected power system through transmission lines so that system constraints can cause stability, resiliency and reliability issues.

This project aims to identify transmission system upgrades needed to facilitate offshore wind projects as well as operational impacts of offshore generation on steady state operations and dynamic stability of the regional transmission system in the Great Lakes region. The results and recommendation from this work can also be useful in other planned offshore wind developments of the Great Lakes.

The project team includes Case Western Reserve University (CWRU), FirstEnergy (FE), General Electric (GE), National Renewable Energy Laboratory (NREL), and PJM Interconnection (PJM).

1.4 Objectives of This Project

The project has two main objectives:

Objective 1
A Case Study use an appropriate system model, offshore wind profiles, transmission and generation system conditions, and methods for evaluating the wind resource and interconnection of offshore wind to the utility system to identify utility integration needs relative to Lake Erie and recommend appropriate system upgrades including capacity and storage

Objective 2
Development of General Recommendations for Interconnecting Large Great Lakes, and Potentially National, Wind Plants to the Grid including unique requirements on interconnection points, control requirements and the application of system reinforcements for different transmission system characteristics

The overall project scope is decomposed into three main tasks and their associated subtasks:

Task 1 Lake Erie Case Study: Baseline - The objective of this task is to develop the case study scenarios and to obtain the system wind profile data that is necessary to evaluate the impact of offshore wind on utility operations in the proposed service area.

1. Develop Case Study Scenarios: Provide realistic scenarios based on operating conditions, contingencies, and disturbances that need to be evaluated.

2. Develop Utility System Data: Provide system and operating data for the utility service area of interest.
3. Lake Erie Wind Profile Modeling and Statistical Analysis: Provide wind power profiles from the Eastern Wind Integration and Transmission Study database sufficient to generate temporal patterns of power injections that are realizable from the envisioned Lake Erie 1000 MW capacity.
4. Develop Utility System Model: Develop system performance model that is suitable for investigating the impact of variable power injections from Lake Erie on the systems ability to serve load while meeting system performance requirements.
5. Integrate Wind Profile and Utility System Data into the System Model: Develop an operational simulation model that combines the results and data from subtasks 1.1 through 1.3.

Task 2 Lake Erie Case Study: Impact Analysis and Review - The objective of this task is to analyze the impact of 1000 MW of offshore wind in Lake Erie on the utility service area in terms of steady state voltage regulation and dynamic stability (frequency and voltage response).

1. Generate Operating Scenarios: Provide realistic scenarios based on operating conditions, contingencies, and disturbances for the impact study.
2. Acquire simulation data for the operating scenarios.
3. Dynamic and Voltage Stability Analysis: Use computation tools for power system analysis, including small signal, large signal, and voltage stability for evaluating the impacts of wind energy integration on operation stability and security.
4. Energy Storage Modeling for Integration Studies: Build on existing work to develop functional models of energy storage suitable for wind interconnection studies.
5. Analyze simulation data from the case study operating scenarios.
6. Investigate Transmission Upgrades to Achieve Performance Objectives: Integrate energy storage models with the system model, wind power profiles, and the energy storage models to assess system upgrades and the potential for performance and utilization improvements.
7. Submit Case Study Report to DOE: produce a report that summarizes the efforts to date, and submit to DOE for evaluation.

Task 3 Lake Erie Case Study Extensions - The objective of this task is to investigate how the methods developed in the Lake Erie case study can be used regionally/nationally to identify challenges and recommend options for modifications that developers and utilities can use to consider risk and reward scenarios for the integration of offshore wind into utility service areas.

1. Identify challenges and recommend options for modifications that developers and utilities can use to consider risk and reward scenarios.
2. Provide additional information on the effective management of wind energy assets using existing/new technologies to enable the integration of wind power into existing power systems at optimal levels.
3. Develop General Guidelines for addressing the unique aspects of interconnection of wind plants to the established transmission grid. This will include recommendations on scenarios, wind profile modeling, simulations, and computational methods to quantify performance, along with operating changes and equipment upgrades needed to mitigate system performance issues introduced by an offshore wind project.

1.5 Scopes of This Project

1. The project relies on system models that are used by industry and were provided by FirstEnergy/PJM.

2. The computational tool for this analysis was GE PSLF Concordia, the simulation models were prepared by the GE team.

3. The CWRU team used the dispatch and consumption data provided by FirstEnergy/PJM for expected peak load data for summer 2015 for the steady state analysis and recorded winter 2012 data for dynamic analysis.

4. The dynamic databases were developed based on the previous work performed by the 2013 GE Energy Consulting and NREL Report Eastern Frequency Response Study. The 2012 databases were modified slightly from the Eastern Frequency Response Study models to represent the current online and available generation in the FirstEnergy system taking into account plant retirements in the past few years.

5. Wind availability estimation was carried out by NREL and, subsequently, potential geographical locations of offshore plants were identified by NREL/GE.

6. The wind turbines were modeled based on generic models of GE commercial wind machines with one offshore generator representing the entire offshore wind farm.

7. The export cables that ship offshore power to onshore substations were designed and modeled based on data available on ABB commercial offshore cables.

8. The project team selected three possible interconnection scenarios for analysis.

9. FirstEnergy provided a list of contingencies to be considered for analysis, and the project team reviewed and discussed this list before settling on the final set included in this study.

1.6 Organization of This Report

The rest of this report is organized as follows:

Chapter 2 discusses the wind energy and, in particular, offshore wind energy including their history, development and market. The electrical components and topologies as well as available technologies are explained in this chapter. In the end of this chapter, the global status of operating offshore wind farms as the end of 2015 is listed and a selected number of under construction projects are discussed.

Chapter 3 focuses on power system analysis and provides a comprehensive methodology for planning studies in offshore wind farm integration projects including steady state stability analysis, small signal stability analysis and large signal stability analysis.

Chapter 4 describes the FirstEnergy/PJM power system which was used as a case study, highlights the considerations for developing computer models of power systems and offshore wind farms and outlines an instruction for implementation of the introduced methodology.

Chapter 5 presents the results and discusses the findings of this study.

Chapter 6 concludes the findings of this report and provides a scope for future work.

Chapter 2

Offshore Wind Energy

2.1 Introduction to Wind Energy

Wind energy has been known for a very long time. The historians believe that the first windmills were built over 3000 years ago. The first written evidence indicates that the windmill began in Persia, now called Iran [1]. The applications of windmills were to grind or mill grain and to pump water. Although the modern wind turbines look absolutely different than the first windmills, the basic idea behind them is the same; convert the power of the air flow into some other form of desirable energy [1].

In late 1980s, European and U.S. wind atlases produced by scientists at Risø National Laboratory in Denmark [35] and Pacific National Laboratory (PNL) in the U.S. [36] revealed the total resource was astronomically large, not only in Denmark and the U.S. but also in many other countries around the world. By that time, their estimation was that the available wind resource in U.S is sufficient to solely supply the entire energy consumption of the country in 1989 [1]. Ever since, the research toward improving those atlases has been going on and they have been superseded by much higher resolution maps with higher accuracy [37] and [38]. Figures 2.2 through 2.3 show onshore and offshore wind resource potential maps in the US and Europe.

From a business standpoint, wind energy systems are the most rapidly growing business in the world energy sector. Spiegel in [41] has reported that the recent economic crisis made the authorities change their policy to keep this business still leading in the expansion of the energy sector. In another report [42], the LA Times denotes the U.S. wind energy as the fastest growing energy source in 2012. Broadly speaking, in European markets, due to the progress in deployment of the wind and the solar generation units, the marginal cost has dropped dramatically to zero. Consequently, the wholesale prices have significant decreased in markets in which wind energy has played a significant role to achieve this aim.

Over the last decade, the installed capacity of wind energy conversion systems has grown significantly all across the globe. The American Wind Energy Association reports that the US installed more wind generation capacity in 2015 than other generation sources in 2015, equivalent of 8.6 GW of new wind energy capacity [4]. The US DOE reports that more than 13GW new wind energy generation capacity

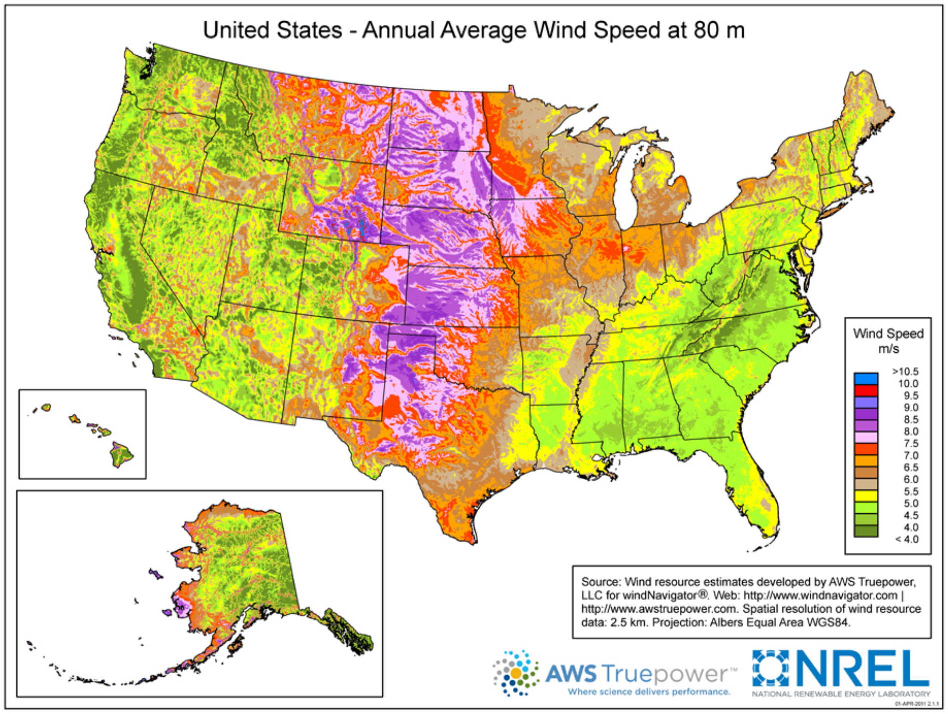

Figure 2.1: Utility-scale land based 80- meter wind resource potential map in the US [37]

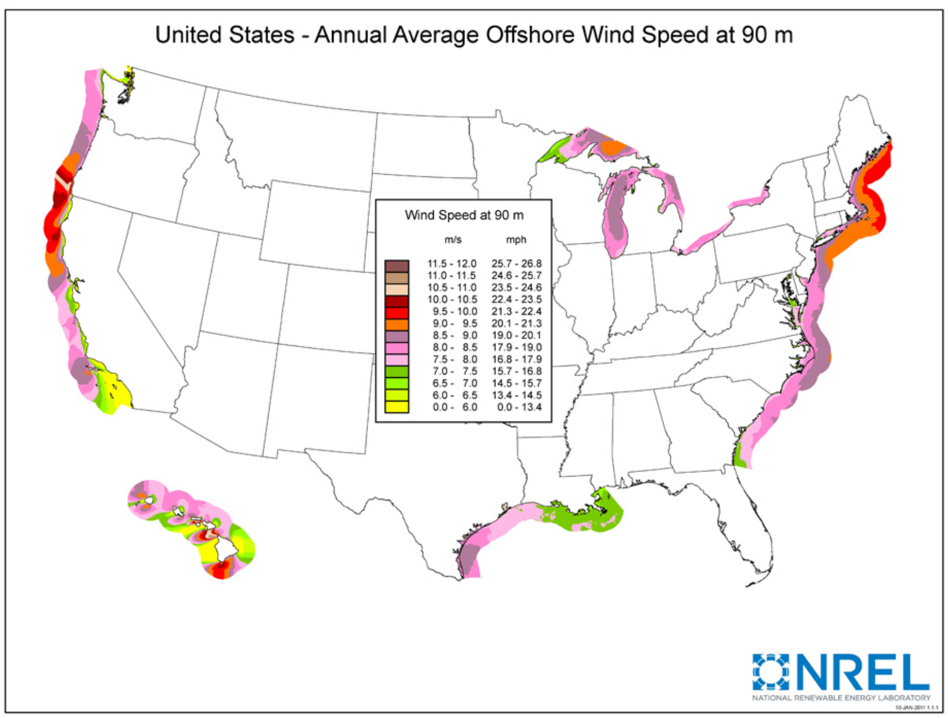

Figure 2.2: Offshore 90-meter wind resource potential map the US [39]

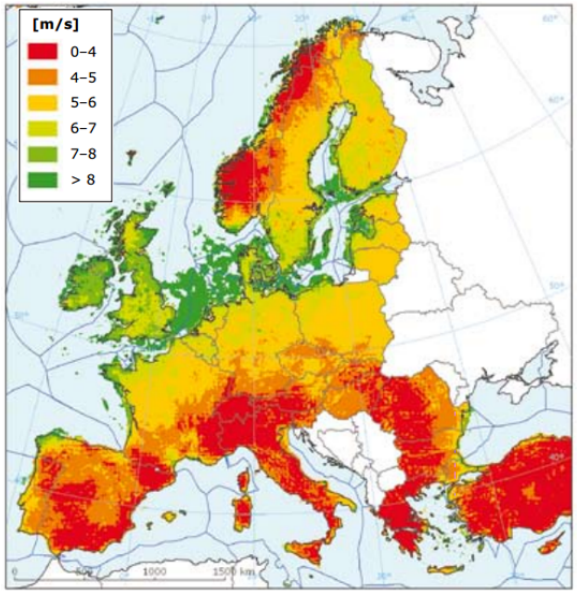

Figure 2.3: Onshore, 80 m onshore, and offshore, 120 m, wind resource potential map Europe [40]

was installed in the US during 2012 which helped to surpass 60GW of total installed wind capacity at the end of 2012 [5]. Obviously, the share of wind generation has significantly increased and will go on. The most recently released wind vision report by DOE gives a roadmap to 35% wind energy by 2050 for the U.S [6]. In Germany, electricity generation from the wind power increased by around 50 percent in 2015 [7]. In September 2013, Germany reached the record of 1.14GW of new wind capacity installation in the first six months of 2013. This was a 14% expansion in the German wind market by reaching 32.421GW installed capacity of wind turbine in Germany by June 30 2013 [8] and [9]. Contrarily, Spain, Europe's second largest wind market, did not add any new wind power capacity in 2015 [10] while in 2012, it added 950MW new capacity to hit 22.8GW capacity [11]. According to the Ministry of New and Renewable Energy, India has installed 19.662GW of wind power and forecasted to add 2.050GW to this capacity by the end of 2013 [12].

This source of electrical energy is relatively new in comparison to other sources such as fossil fuel and hydro power plants which have been around more than a century [2]. In addition, wind power, by its nature is more complex to use in electrical power system due to two key factors: (1) variability and (2) uncertainty [3]. As illustrated by Figure 2.4, the variability of the wind power means that its available amount is not always at a fixed level and its variability depends on the geographical location and meteorological conditions. Uncertainty of the wind power represents the probability of having the forecasted amount of wind blowing at any given time and depends on the probabilistic method used to forecast as well as aerologic and atmospheric physics and chemistry accuracy. Therefore, the wind power is more sophisticated to dispatch in contrast to the conventional generation units.

The wind farms are divided into two categories: (1) onshore wind farms that refer

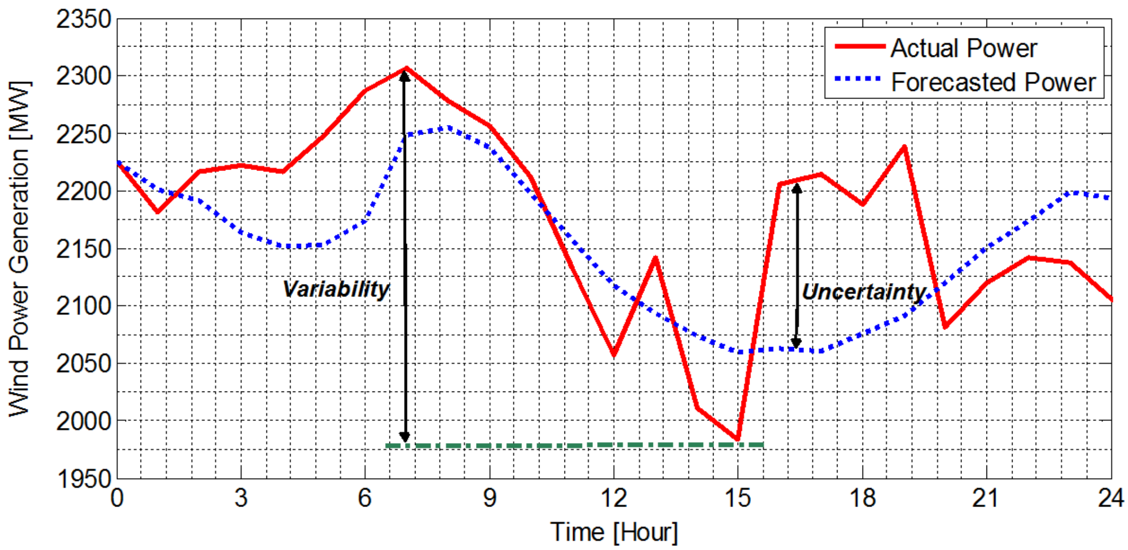

Figure 2.4: Comparative visualization of uncertainty vs. variability [3]

to the wind farms built on land vs. (2) offshore wind farms that are located in the water. Initially, the commercialized wind farms were built and owned onshore. Due to their lower cost to build and operate, onshore wind farm became known as the most affordable renewable energy source [43]. The cost of the generated electricity from an onshore wind farm could plunge to about 7 cent/kwh [44]. Eventually, public concerns for landscape impact, land occupation, noise pollution and risk of lives around the wind towers pushed the affordable onshore wind farms to expensive offshore wind farms. The offshore wind farms are associated with environmental impacts for marine organisms and very costly transport and manufacturing process. On the other hand, offshore wind farms trade off higher efficiency and larger sizes of generators. The estimated cost of the generated electricity by offshore wind farm in the US is 20 cent/kwh and US DOE's objective is to reduce it to 7 to 9 cent/kwh [44].

2.2 What is an Offshore Wind Farm?

An offshore wind farm refers to a wind farm that is constructed and operates in water and away from land. The water could be an ocean, a sea or a lake. The generated power from the offshore wind farm is transmitted to the shore and injected into a power system in form of AC or DC power. Currently, generation capacity of the world's largest operating offshore wind farm is 630MW, London Array wind farm in the UK [45].

An offshore wind farm consists of: (1) wind turbines (2) electrical generators (3) step-up transformers (4) collector systems and (5) a transmission system. In some cases, compensator devices are installed at the POIs to provide additional reactive and voltage support to meet satisfy the required grid codes. Figure 2.5 shows one-line diagram of a typical offshore wind farm.

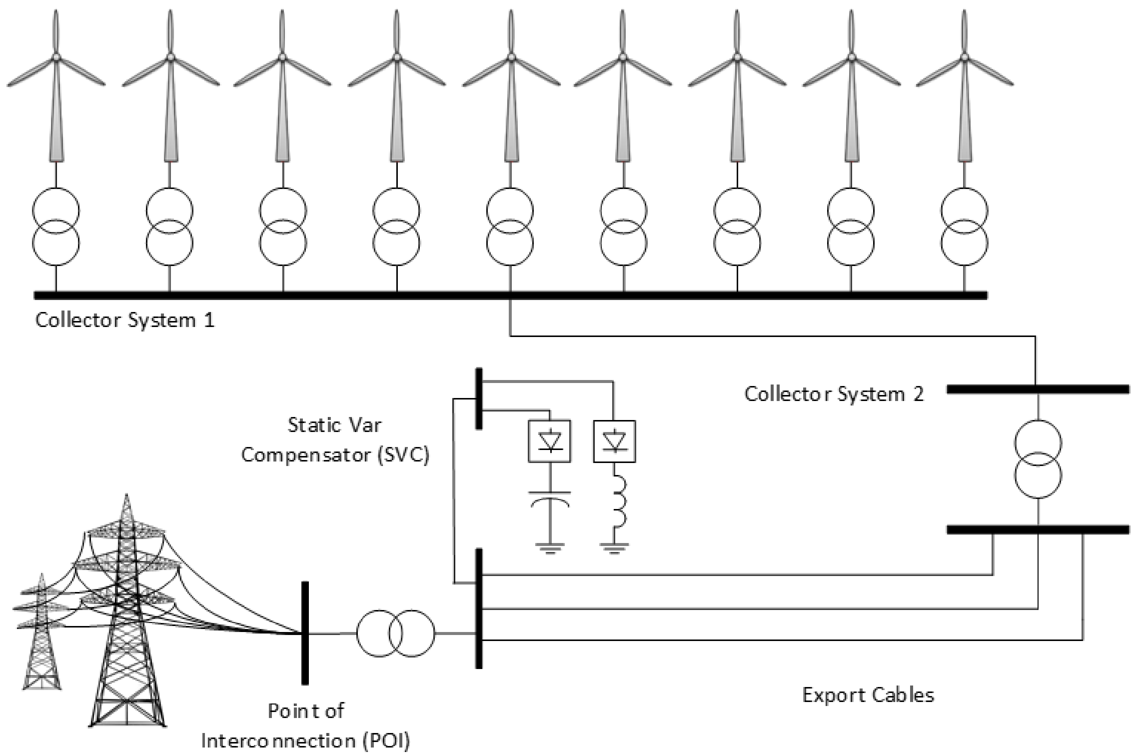

Figure 2.5: One-line diagram of an offshore wind farm [19]

This section briefly discusses these components.

2.2.1 Wind Turbine

A wind turbine is a necessary component to convert wind energy from horizontal direction into rotational trajectory. The wind energy is essentially converted into electrical energy in two major steps, as illustrated by Figure 2.6:

1. From kinetic energy to rotational mechanical energy by the wind turbine

2. From rotational mechanical energy to electrical energy by the electrical generator

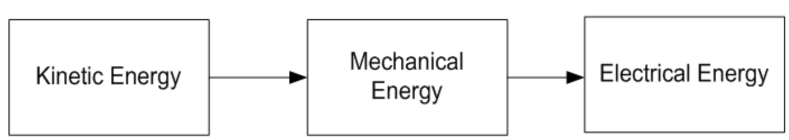

Figure 2.6: Conversion stages of wind energy

Typically, in order to capture the wind energy most efficiently, wind turbines are designed vertically with three blades. The mechanical power derived from the wind according to the aerodynamic characteristics is a function of air density, area swept by a turbine, wind velocity power coefficient of the turbine.

Theoretically, the Betz limit proves that power coefficient of a wind turbine, the ratio of the turbine power over the power of wind stream, is limited to 59% [46]. The power coefficient depends on the aerodynamic design and structure of the turbine. The extracted power from a wind turbine is also highly dependent on tip speed ratio and blade pitch angle, rotor rotational speed and rotor radius.

Practically, during the wind turbine design, the power coefficient curve is a highly important consideration to ensure extracting peak power at any given wind velocity and it is a unique characteristic for any given manufactured turbine. Figure 2.7illustrates an example of wind turbine characteristics for various wind speeds.

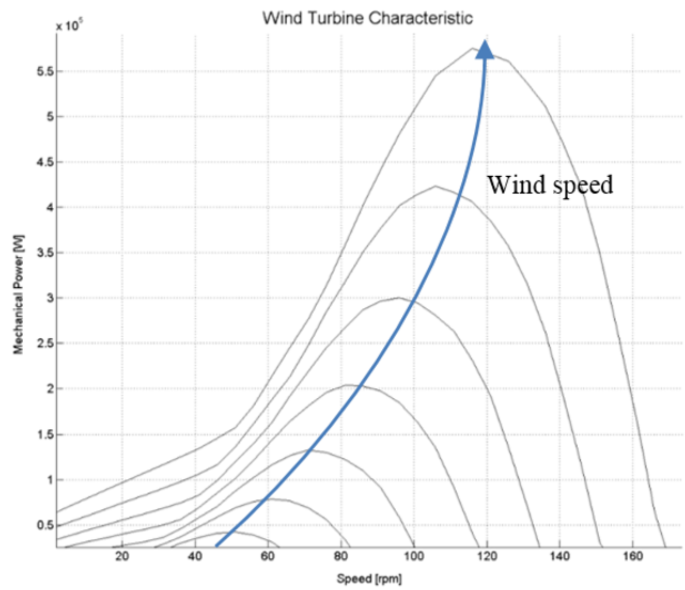

Figure 2.7: Turbine power as a function of shaft speed [52]

Machowski in [24] calculated the relation between diameters and rotational speeds of some wind turbines and showed that for the same wind speed, the bigger wind turbines require the larger blade diameter and slower rotational speed.

Power curve represents the power generated by wind turbine in respect to wind velocity, in the range of cut in and cut off velocities. In fact, wind turbine at the wind velocities lower than cut in velocity and higher than cut off velocity does not operate. The rated wind velocity for small machines is between 16-17 m/s while this value for big machines is between 11-12 m/s [47].

The size of offshore turbines in Europe nowadays has passed the level of 7.5MW as an individual turbine while this number for the turbines in the US is around 3.6MW [48]. The Enercon E126 with power rating of 7.5MW [49] follows the Vestas V164 with power rating of 8MW [50] as two largest offshore wind turbines in the market.

2.2.2 Electrical Generator

Electrical generator is a component that converts rotational mechanical energy into electrical energy. The typical terminal voltage for these machines is less than 690V [51]. In the latest turbines, this has been increased up to 6.9kV [49] and [50]. Therefore, offshore wind turbines are equipped with a step-up transformer in the turbine nacelle to reduce the power losses by increasing the machine terminal voltage level to collector system voltage level, usually between 25-40 kV [52].

The DOE Lawrence Berkeley National Laboratory (LBNL) classifies the type of machine technology being using in offshore wind farms into four major categories [53].

Squirrel Cage Induction Generator (Type 1)

The squirrel cage induction generator, as shown in Figure 2.8, basically operates in fixed speed mode. Therefore, this type of machine does not have the capability to maximize the extraction of energy from wind. Additionally, a capacitor bank is required to produce the magnetizing flux for system start-up. Lack of the capacitor bank would cause voltage dip at the POI [54].

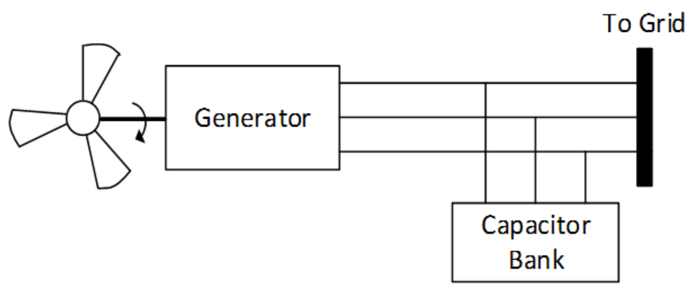

Figure 2.8: Schematic diagram of Type 1

Wound Rotor Induction Generation (Type 2)

Wind energy conversion systems utilizing wound-rotor induction generators, as shown in Figure 2.9, provide more functionality in the system. Placing the rotor in series with variable resistors allows an increase in the operational speed range of the system [54].

Doubly-fed Induction Generator (Type 3)

The predominant technology deployed in the wind industry is the doubly-fed induction generator (DFIG), as shown in Figure 2.10, with about 75% of the market share in the world [46]. Due to its continuing popularity, the major manufacturers of wind turbine generators have focused on developing DFIG systems in the multi-megawatt range. In these systems, the stator of the system operates at the frequency of the power grid and the rotor is supplied by a power electronic converter at the slip frequency [55] and [56].

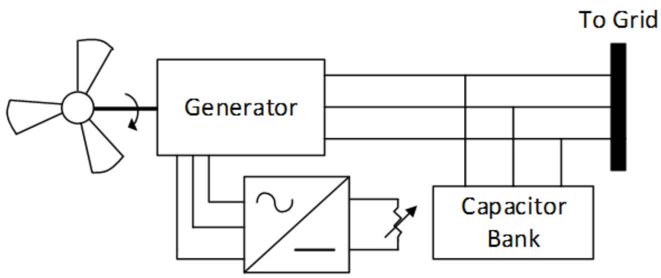

Figure 2.9: Schematic diagram of Type 2

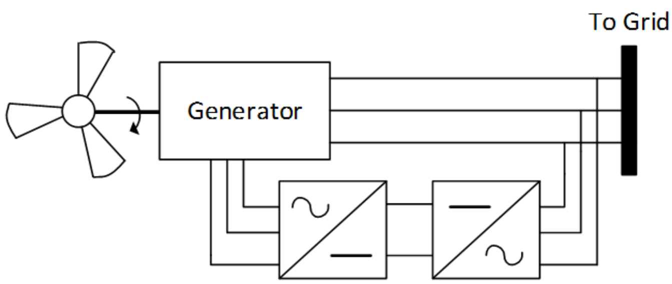

Figure 2.10: Schematic diagram of Type 3

Synchronous Generator with Fully Rated Converter (Type 4)

Synchronous machines are known primarily for their role in traditional bulk generation power stations. This type of generator runs at constant speed and are popular for offshore wind farms.

In this type of wind generators, as shown in Figure 2.11, generated power from the wind machine is transferred through a power converter [57]. This requires the power electronic converter operate at full rating [58] which is a disadvantage of this type. However, using advanced controllers in the converter and turbine permits a great degree of control.

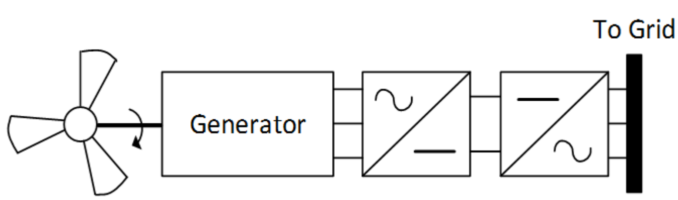

Figure 2.11: Schematic diagram of Type 4

2.2.3 Electrical Transformer

Electrical transformers adjust the level of voltage and current in electrical systems to facilitate the individual equipment interface and interconnect without disruption. In offshore wind farms, electrical transformers are used to raise the level of voltage through multiple steps in the offshore system to reduce power losses during power transfer to the onshore substation. In onshore substations, electrical transformers adjust the voltage level to interconnect offshore export cables to the transmission system in order to inject the power generated by offshore wind farm.

It should be noted that the space available in the offshore system, in the turbine nacelles and on the collector systems, is very limited. In addition to a difficult and costly maintenance situation, the ambient conditions offshore are severely more windy and humid than onshore. Therefore, the electrical transformers for offshore applications must be very compact, durable and reliable [59].

2.2.4 Offshore Collector System

The offshore collector system collects the generated electrical power from individual wind machines and ships it to onshore power systems through export cables. The electrical system of offshore collector systems is equipped with step-up transformers at an offshore substation to increase the level of voltage to the transmission level. The collector feeders could be designed and operating in AC, DC or mixed AC/DC system [60]. In case of the DC feeders, the power electronics inverters or converter, depending on the design, as well as DC switchgears are required that adds additional cost to the design [61]. If the transmission system to shore is DC, the collector system is also equipped with additional power electronic convertors on the high voltage side.

The architecture of the collector system is a function of wind farm size and desired level of reliability. Commonly known topologies for offshore collector system are summarized in this section.

Radial Design

Radial design, as shown in Figure 2.12, is the simplest collector system in which the electrical power generated by a group of wind machines is aggregated through individual feeders. The overall power from all feeders is aggregated through a medium voltage collector hub. This is an inexpensive design [62] because of the simplicity of the design. The rating and the capacity of the cable within each string is determined by number of connected machine to each feeder [61].

Single-Sided Ring Design

This design is similar to the radial design. The difference is the additional cable connected to the last wind machine in the row in the feeder. This allows a redundant pathway for power flow for both intact and contingency conditions that increases the reliability of the system and enhances the energy delivery [61]. In a similar way to the radial design, the overall power from all feeders is aggregated through a medium voltage collector hub. In this design, a greater number of wind machines, in contrast to the radial design, can be connected to each feeder due to the higher cable capacity as result of additional pathway for the energy to flow. This topology is expensive

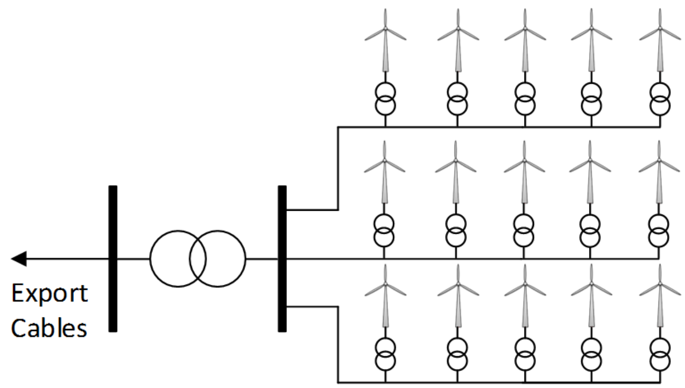

Figure 2.12: One-line diagram of radial design for offshore collector systems

because of additional cabling cost [62]. Figure 2.13 shows a one-line diagram of this design.

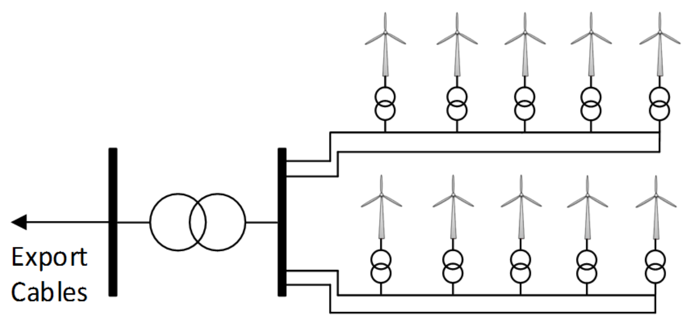

Figure 2.13: One-line diagram of single-sided ring design for offshore collector systems

Double-Sided Ring Design

This design, shown in Figure 2.14, is a mixture of the two previously introduced designs. In this topology, wind machines are connected to the feeders and the feeder within a string, similar to the radial design, and every two neighboring feeders are connected together through the end of the strings. This provides a higher level of reliability and additional pathway for power to flow during the contingency operation, similar to the single sided string design [61].

Star Design

In this design, shown in Figure 2.15, the wind machines are distributed over several feeders. This allows the designer to use the equipment with lower ratings [[62] in some parts of the design and that directly lowers the cost of the system. The downside of this topology is the complexity of the design and switchgear requirement [61].

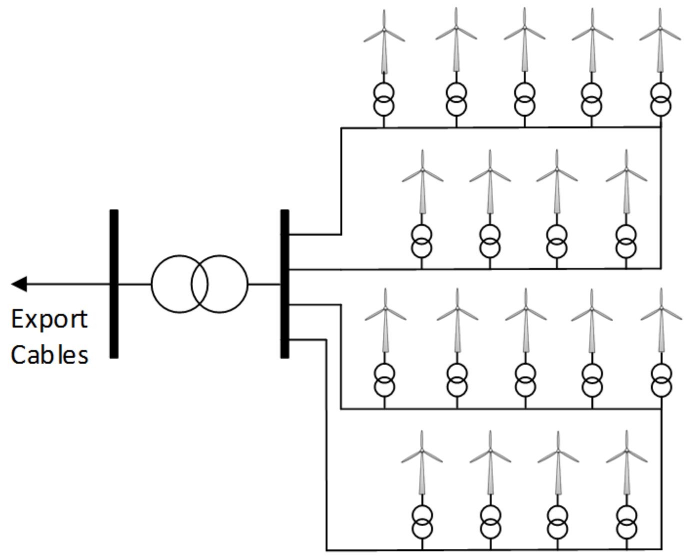

Figure 2.14: One-line diagram of double-sided ring design for offshore collector systems

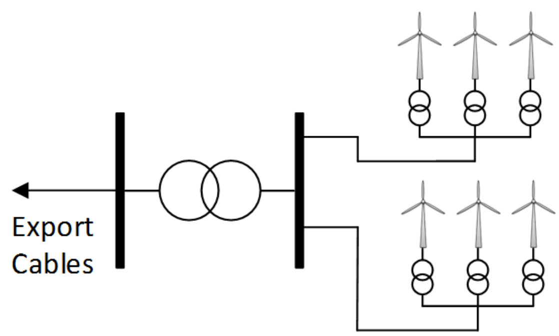

Figure 2.15: One-line diagram of star design for offshore collector systems

Mixed Design

The collector system could be eventually designed using a mixture of the introduced designs. In this case, the system operational reliability and flexibility and cost depend on the quantity of equipment and their rating and no general rules can be stated [62]. An example of the mixed design is shown in Figure 2.16.

Currently, operating offshore wind farms have very little redundancy or none at all [63]. In small scale wind farms (capacity less than 100 MW), the probability of a fault and the associated costs are lower than the costs associated with additional equipment [61]. Therefore, the topologies with redundant paths for power flow and higher levels of reliability are recommended only for large-scale wind farms.

2.2.5 Transmission System

The transmission system or subsea cables to transfer generated power by offshore wind farm to onshore power grid are known in the power industry as export cables.

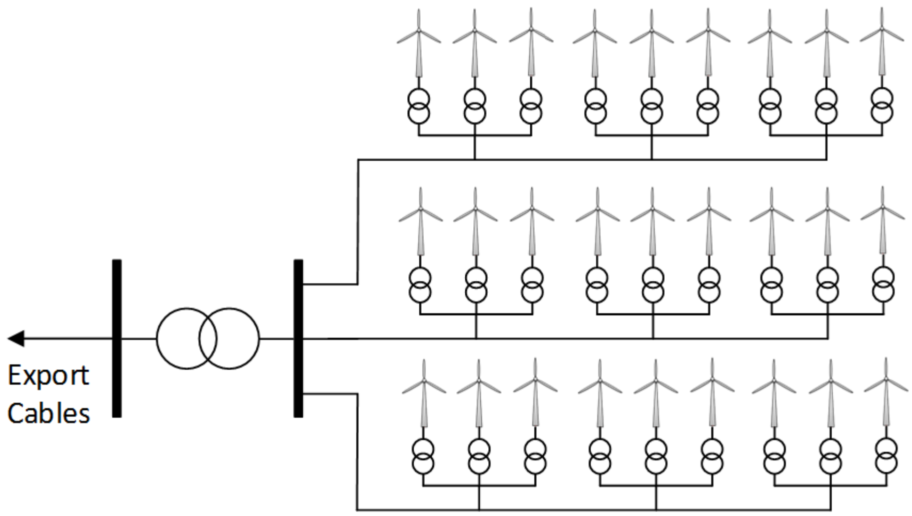

Figure 2.16: One-line diagram of a mixed design for offshore collector systems

In practice, it is being done in two forms - High Voltage AC (HVAC) or High Voltage DC (HVDC).

HVAC

The HVAC systems use AC subsea cables and typically work in the ratings of the transmission system, 138kV or 345kV at 60 Hz (in North America). In this type of export system, shunt reactors are required to compensate the cables' charging currents and avoid voltage fluctuations [64]. Therefore, the cost of the compensation devices is one limitation for the long distance transmissions. The other limitation for long distance transmissions is cable power losses. Figure 2.17 shows a one-line diagram of HVAC export systems.

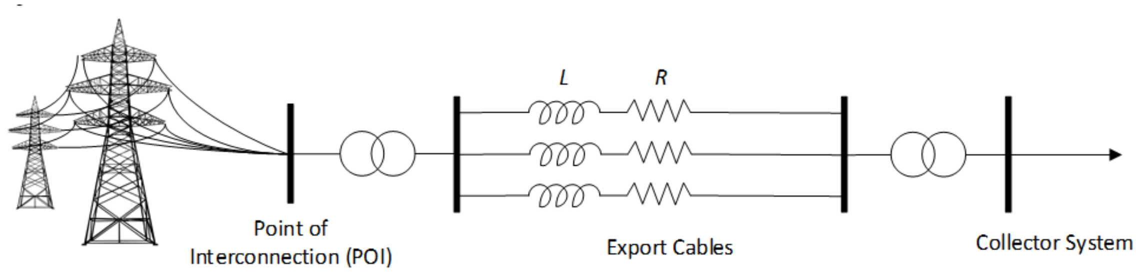

Figure 2.17: One-line diagram of a HVAC export system

In AC connections, choosing the right sea cables is very important. The key issues with the cables are their transmission capability as well as reactive power regulation across them. The reactive power charging current of a sea cable is a function of the cable's rated voltage and capacitance of the cylindrical capacitor of the cable. Their transfer capability is a function of their length and their voltage rating level [65]. XLPE cables are the most common sea cable technology used in industry [66].

HVDC

HVDC system uses DC subsea cables and powerful power electronic convertor and inverters at both ends of the cables. In this type of export, the main limitation is the power electronics components where their cost is very high. The voltage rating of the HVDC is typically greater than 500kV. Figure 2.18 shows a one-line diagram of HVDC export systems.

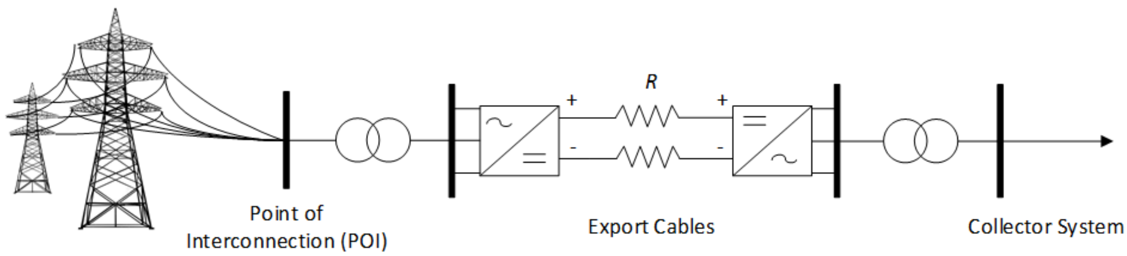

Figure 2.18: One-line diagram of a HVDC export system

Multi-Terminal HVDC

Conventional HVDC connection were meant to be node to node connection and deliver the power from Point A to the Point B. Therefore, it is known as two-terminal HVDC (TTHVDC). There are is a form of HVDC, so called multi-terminal HVDC, that consists of several converters connected to a common HVDC circuit [67]. The MTHVDC connections, in addition to enhance reliability, stability, controllability and flexibility of the power delivery [68], reduce the cost of the system over TTHVDC connection because of reduced number of required converter stations which are very costly [69]. In addition, all technical advantages of TTHVDC connections over HVAC connections are also applied to MTHVDC connections. Figure 2.19 shows one-line diagram of a MTHVDC export system.

As shown in Figure 2.19, instead of using four converter station, three of them were used in this model. A lower number of converter stations means a lower cost. Although the idea of using this type of connection has been discussed since 1960's [67], using them for offshore wind farm is relatively new and there is no operating offshore site that uses this type yet.

The HVAC connections, however, provide higher reliability comparing to the HVDC connections while the HVDC connections provide higher flexibility and 30%-50% less power loss than the HVAC connections [70] as result of higher controllability on the power flow [71]. The cost crossover between HVAC and HVDC systems is a function of distance between the offshore platform and the onshore connection site and depends on the geographical location of the project. In North America, this

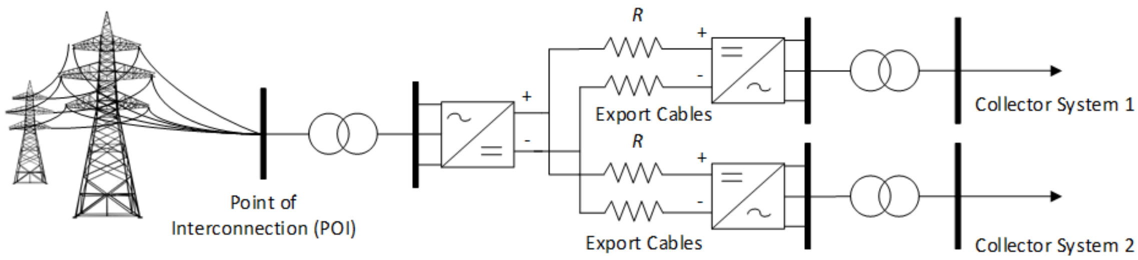

Figure 2.19: One-line diagram of a Multi-Terminal HVDC export system

distance is approximately 50 mi (80 km) [72] while this number in Europe is 20 miles (30 km) and in China and India is greater than 250 miles (400 km) [72]. This cost in different countries is influenced by permitting processes and environmental considerations in design such as deviations from the ideal path and sound protection. In countries such as China and India such barriers are lessened [72].

In some cases in which the offshore wind farm is located close to the shore, medium voltage AC connections are used. This also depends on size of the wind farm because of the cables' power loss. This reduces the cost of the installation by saving an offshore voltage rising platform which is very expensive. The author of [73] recommends medium voltage AC cables for distances within 9 mi (15 km), HVAC for distances within 9 mi (15 km) and 62 mi (100 km) and HVDC for distances greater than 62 mi (100 km) for HVDC for transfer of 100 MW through sea cables.

2.2.6 Compensator Devices

The reactive power compensators are important devices in integration of wind farms to prevent voltage stability issues. The necessity becomes more pronounced in cases in which Type 1 or Type 2 machines are used. In those cases, voltage violations or instability may occur, due to the inability of these types of wind machines to provide reactive power support. Insufficient dynamic performance from the overall wind plant could violate the security of the power system and cause a major blackout if not managed well [64]. In offshore wind farms, the compensation devices are typically installed and operating at the POIs to prevent violation of the grid codes. However, in some cases, these devices might be installed at other points in the grid. Three major solutions for reactive power compensation are available and are explained in the following section.

Mechanical Switched Capacitor (MSC)

This solution is the most economical way to provide reactive power compensation for voltage control [74]. The MSCs are easily operated and require low maintenance. This system could consist of a single switchable capacitor bank or multiple capacitors with back to back switching. In either case, current limiting reactors should be designed and installed to reduce the transient inrush current that is generated due to the inductances on the path from the source to the capacitor during the switching operation [75]. The MSCs, however, could be considered as a fixed capacitor bank if they are switched on or off only a few times during their duty cycle [76]. Figure 2.20 shows one-line diagram of the MSC integration.

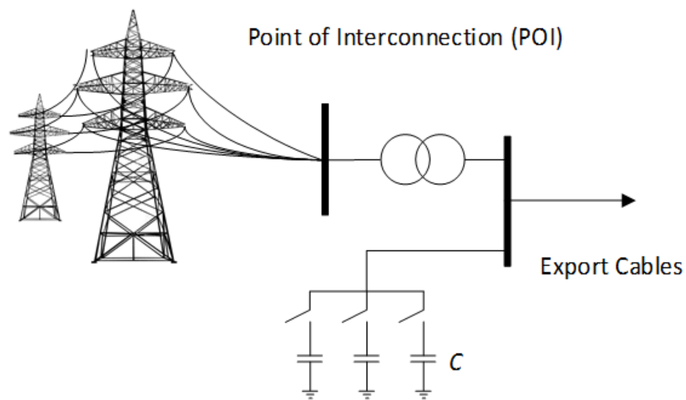

Figure 2.20: One-line diagram of MSC integration

Shunt Reactor

This solution is commonly used in AC transmission systems to regulate the excessive reactive power. Shunt reactors provide a robust performance and are an economical solution. Since they do not require any additional equipment for the interconnection such as transformer, their power loss is low [77]. This type of system usually is installed at the POI to improve voltage regulation and help with complying with grid code. In some cases, an additional shunt reactor is installed on offshore collector system to improve the compensation. Figure 2.21 shows one-line diagram of shunt reactor integration.

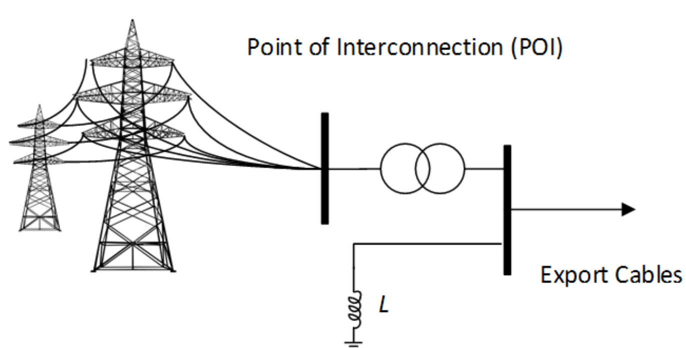

Figure 2.21: One-line diagram of shunt reactors integration

Static Var Compensator (SVC)

This is an effective but costly solution to control power factor or voltage level and to perform as a stabilizer in power systems. The SVC consists of Thyristor Controlled Reactor (TCR) and Thyristor Switched Capacitor (TSC), as shown in Figure 2.22.

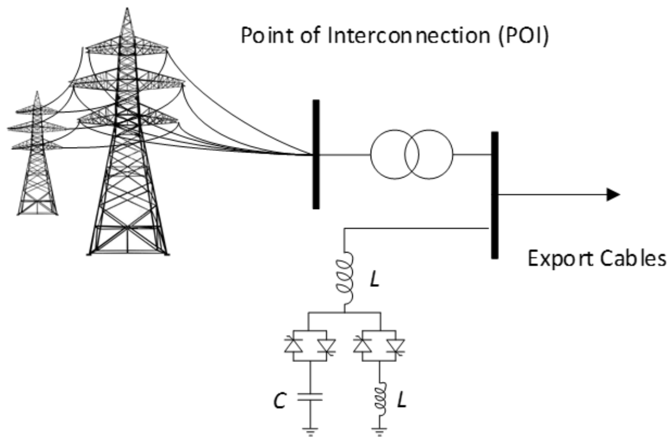

Figure 2.22: One-line diagram of SVC integration

The SVC could provide support for the offshore systems in which the machines do not have sufficient reactive support capability and the export system is HVAC. Because of the fact that the power electronics are used in the SVC, it has a very quick response time and enhances the stability of the voltage under steady state as well as transient conditions. Sometimes, the MSC is added to the SVC to enhance the dynamic control in the system [64] and minimize the cost of the system.

2.3 Operating Offshore Wind Farms around the World

Over 7.7 GW of offshore wind farm are operating all over the world and their list is shown in Table 2.1 and summarized in Figure 2.23.

This list reveals that, currently, more than 96% of offshore wind farms are constructed and operating in Europe. England with 3711 MW of operating wind farms is the leader in the world. Denmark with 1272 MW is the second leading country and then Germany with 521 MW is the third. This shows that in practical terms, the challenges that industry and practitioners are facing is not lack of technology.

Non-European countries such as China, Japan, South Korea, and Taiwan have set their road map towards achieving a greater contribution in power generation by offshore wind market by constructing new offshore wind farms or expanding their current capacity. The South Korean government has approved construction of the largest offshore wind farm in the world by 2019. This project is planned to be built in three phases with a total capacity of 2500MW on their southwest coast [13]. The U.S.' first offshore wind farm project is Cape Wind, which is projected to generate 454MW

Table 2.1: List of Operating Offshore Wind Farms Around the World As End of 2015

Wind Farm	**Capacity (MW)**	**Country**	**Wind Farm**	**Capacity (MW)**	**Country**
Donghai Bridge	131.3	China	Irene Vorrink	17	Netherlands (cnt'd)
Longyuan Rudong Intertidal	102		Lely	2	
Barrow	90	England	Setana Wind Farm	1.2	Japan
Beatrice	10		Sakata Offshore Wind Farm	16	
Blyth Offshore	4		Wind Power Kamisu	14	
Burbo Bank	90		Fukushima Floating Wind Turbine Demonstration Project	2	
Greater Gabbard	504		BARD Offshore 1	400	Germany
Gunfleet Sands 1 & 2	172		Meerwind Sd/Ost	288	
Gunfleet Sands 3 Demonstration Project	12		Borkum Riffgat	113	
Kentish Flats	90		Alpha Ventus	60	
Lincs	270		EnBW Baltic 1	48.3	
London Array	630		Hooksiel	5	
Ormonde	150		Ems Emden	4.5	
Scroby Sands	60		Breitling	2.5	
Sheringham Shoal	317		Kemi	30	Finland
Teesside	62		Thorntonbank Phase 1	30	Belgium
Thanet	300		Belwind Phase 1	165	
Walney	367		Northwind	216	
West of Duddon Sands	389		WindFloat	2	Portugal
Lynn and Inner Dowsing	194		Arinaga	5	Spain
Methil	7	Scotland	Hywind	2.3	Norway
Robin Rigg	180		Anholt	400	Denmark
North Hoyle	60	Wales	Horns Rev II	209	
Rhyl Flats	90		Rdsand II	207	
Arklow Bank	25	Ireland	Nysted (Rdsand I)	166	
Lillgrund	110	Sweden	Horns Rev I	160	
Karehamn	48		Middelgrunden	40	
Vnern	30		Sams	23	
Utgrunden	11		Sprog	21	
Yttre Stengrund	10		Rnland 1	17.2	
Bockstigen	2.75		Avedre Holme	10.8	
Eneco Luchterduinen	129	Netherlands	Frederikshavn	7.6	
Princess Amalia	120		Tun Knob	5	
OWEZ	108		Vindeby	4.95	

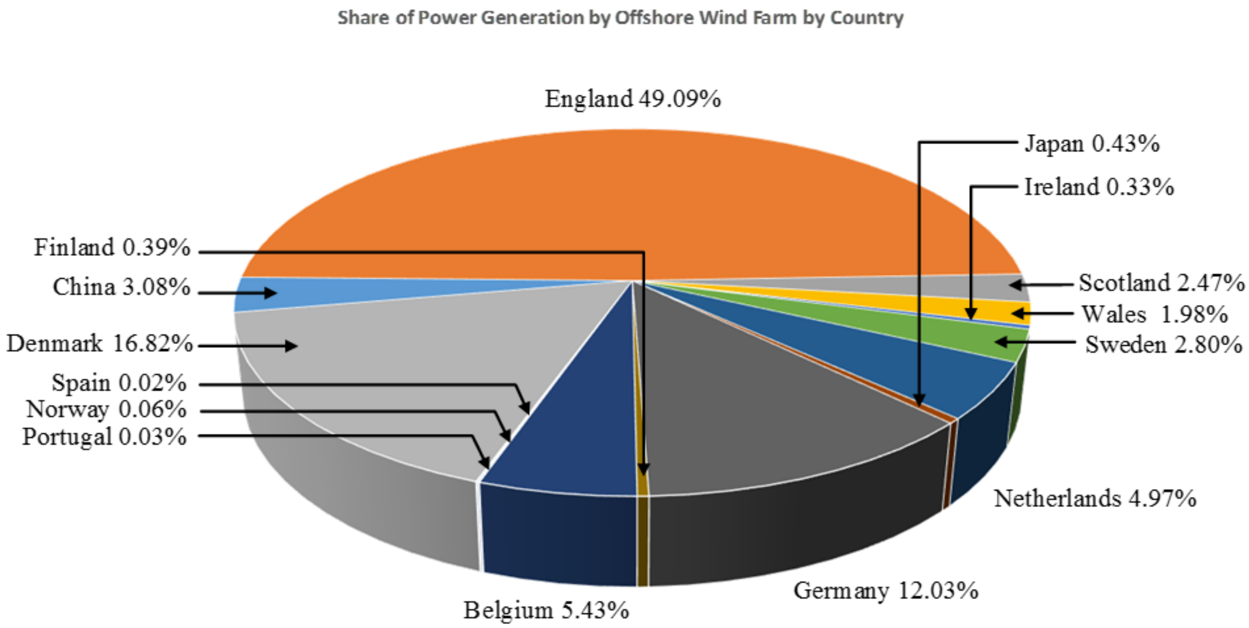

Figure 2.23: Share of countries in global installed offshore wind power capacity as the end of 2015

of electrical power [14]. This project is currently ongoing in Nantucket Sound off Cape Cod, Massachusetts, United States. The Indian Government also has approved the construction of the nation's first offshore wind power project [15]. This project with a capacity of 100MW is projected for the coast of Gujarat as a demonstration project and is expected to finish by 2019 [16]. The Taiwanese government aims to install 600 offshore wind turbines with total capacity of 3000MW by 2030 [17]. At this point their success depends upon their available resources and dedication to use the experience of the European countries.

Chapter 3

Methodology

3.1 Steady State Stability Analysis

Steady state stability of electrical power systems refers to the behavior of system while operating at any given equilibrium operating point [24]. This section discusses steady state stability analysis in planning studies for offshore wind farm integration.

The power systems operate under two constraints [78]:

1. Load

2. Operating variables

The first constraint ensures load demand is being met by system operation, and the second constraint directly addresses the physical limits of the components (e.g. current, voltage, and frequency) [24].

The steady state stability analysis in power system is practical in generation and transmission planning to ensure that throughout every 24 hours of the day of the year, the system's constraints are not violated at any given operational point. This constitutes that enough generation units are capable and dispatchable with an adequate reserve level and enough line capacity is available to serve the demand load. The outcome of this study determines the required expansion and upgrades to maintain the reliability of the power system. However, transmission and generation planning studies are strongly correlated because of the fact that transmission lines have to deliver the generated power by the generators to the consumer.

In planning studies, reliability of the system is a major concern. Three metrics are used to determine level of reliability [79] of power systems:

1. Loss of Load Expectation (LOLE)

2. Loss of Load Probability (LOLP)

3. Effective Load Carry Capacity (ELCC)

These are probabilistic indices and their computation requires applying probabilistic methods to the entire interconnected power system model including the constraints such as generation capacities and transmission limits between areas and involve the load profiles, scheduled outages and probabilistic model of forced outages. The LOLE is expressed in 1 day per 10 years or 0.1 day per year and represents the expected number of the days in a year in which power generation shortage might occur rather than the total outage time. The LOLP represents, solely, the probability of the event in which power generation shortage occurs without any specific information about the time duration of the shortage. The computation procedure of the LOLE uses the entire daily load profiles when the LOLP uses only the peak values of daily load profiles [20]. The ELCC is expressed in percentage and represents the contribution of any given generator in capacity of a power system in serving pick load [80], [81].

The wind integration projects are typically added to an existing power system. Therefore, it is safe to assume them as generation expansion study. However, due to highly variable nature of the wind power, it is required to conduct reliability studies and compute the reliability for all levels of contribution of the wind farm in power generation, from 0% to 100% of its capacity with a credible step size. The step size could be chosen depending on the planner's preference and experience. If the safe reliability level is not reached, additional generation units may improve the reliability. Note that after every modification in the system including change or adjustment in size or status of generation units or load profile, the computations must be repeated until the reliability requirement are met [20].

The impacts of wind power on reliability of the power systems have been addresses in a number of publications. An IEEE Task Force on Wind Capacity Value of the Wind Power Coordination Committee and Power Systems Analysis, Computing and Economics committee of the IEEE Power and Energy Society (PES) [82] describes a number of the common approximate methods for capacity value of wind and summarizes the results from capacity value studies around the world including Great Britain and Ireland systems study [83], New York State Independent System Operator (NYISO) study [84], Minnesota State Study [85] and Irish Wind Study [86]. This summary shows that the wind powers capacity value is a function of mathematical approaches being applied as well as wind and demand profiles characteristics in the region studied. A survey of methods on reliability models for wind generation and their implementation in different regions of the US has been discussed in [87]. This study concluded that the reliability values of wind farms depend upon their rated capacity and the serving load.

The steady state analysis in the transmission system is associated with the following criteria: (1) Thermal rating of the lines and (2) Voltage regulation across the system [25]. Typically, the voltage stability margin is much smaller than the thermal stability margin and, therefore, the voltage stability margin determines the overall stability margin for the system [25], in the majority of the cases.

Previous studies [88], [89], [90], have shown that interconnecting wind farms to the power system may destabilize the grid, depending on technologies and configurations used in the wind farm. In steady state stability analysis, the main concern associated with wind farm integration is the variability of wind power which introduces new challenges to the control of electric power networks [91]. In fact, its stochasticity increases the uncertainty associated with power system states and the attendant complexity of power systems [19]. Therefore, development of stochastic and statistical methods is required to model the wind power.

The current research proposes a statistical approach to determine how integration of offshore wind generation may affect steady state operation of large scale transmission systems. This investigation assumes that the existing system is stable and secure and is practical in offshore wind integration planning studies. This tool provides an understanding of how associated factors with operation wind generation and integration scenarios might affect the system performance that is a key concern in choosing the best wind integration scenario. This research involves solely normal operation of the system and no contingencies occur.

3.1.1 Mathematical Formulation

Power systems consist of non-linear components that could be modeled using a set of nonlinear algebraic equations to describe their dynamics properly. The equations of power flow in power systems can be expressed by:

$$P(V,\delta) = 0 \tag{3.1}$$
$$Q(V,\delta) = 0 \tag{3.2}$$

where V is voltage magnitude and θ is voltage angle. The power flow equations for a n-bus system can be linearized at any operating point as [24]:

$$\begin{bmatrix} \Delta P \\ \Delta Q \end{bmatrix} = \begin{bmatrix} H & M \\ N & K \end{bmatrix} \begin{bmatrix} \Delta\delta \\ \Delta V \end{bmatrix} \tag{3.3}$$

For transmission systems, the M and N matrices can be neglected due to small resistances. Therefore, the Jacobian matrix, J, can be simplified by:

$$J = \begin{bmatrix} H & 0 \\ 0 & K \end{bmatrix} \tag{3.4}$$

From (3.3) and (3.4), the power flow equations for voltage studies can be simplified to:

$$\begin{bmatrix} \Delta Q_1 \\ \Delta Q_2 \\ \vdots \\ \Delta Q_n \end{bmatrix} = \begin{bmatrix} \frac{\partial Q_1}{\partial V_1} & \frac{\partial Q_1}{\partial V_2} & \cdots & \frac{\partial Q_1}{\partial V_n} \\ \frac{\partial Q_2}{\partial V_1} & \frac{\partial Q_2}{\partial V_2} & \cdots & \frac{\partial Q_2}{\partial V_n} \\ \vdots & \vdots & \ddots & \vdots \\ \frac{\partial Q_n}{\partial V_1} & \frac{\partial Q_n}{\partial V_2} & \cdots & \frac{\partial Q_n}{\partial V_n} \end{bmatrix} \begin{bmatrix} \Delta V_1 \\ \Delta V_2 \\ \vdots \\ \Delta V_n \end{bmatrix} \tag{3.5}$$

$$\big[\Delta Q\big] = \big[K\big] \cdot \big[\Delta V\big] \tag{3.6}$$

To determine the voltage sensitivity to changes in power generation and consumption in the system, voltage sensitivity could be computed by:

$$\big[\Delta V\big] = \big[K\big]^{-1} \cdot \big[\Delta Q\big] \tag{3.7}$$

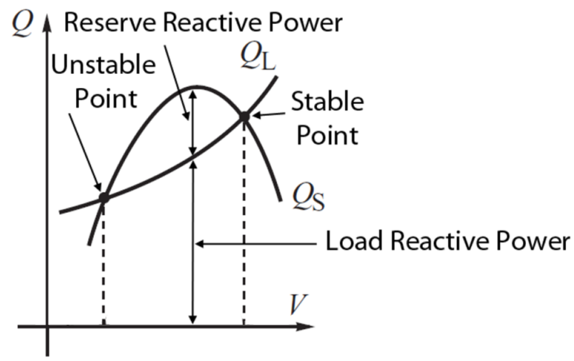

Figure 3.1: Conceptual visualization of the steady state voltage stability assessment

where ΔQ represents the total (generation and consumption) reactive power. This criterion is visualized in Figure 3.1.

As mentioned above, the steady state analysis in the transmission system is associated with two main criteria that ensure the reliability of the system [25]:

1. Emergency thermal rating

2. Voltage regulation

This research uses sensitivity analysis that involves both active and reactive power sensitivity in the transmission system to operation of offshore wind farm. This provides information around all possible operating points to identify high risk scenarios upon injection of wind power.

The dynamic behavior of a power system, using differential-algebraic equations, is given by:

$$\dot{x} = f(x, u) \tag{3.8}$$

where x is a $n \times 1$ state vector and u is a $k \times 1$ representing inputs to the system. For every equilibrium point of x^*, the steady state solution of the system is given by:

$$f(x^*, u) = 0 \tag{3.9}$$

A power system including synchronous generators, wind farms and loads, is shown in Figure 3.2.

To simulate variability of the wind power, a variability component λ, wind variability parameter, in respect to maximum wind generation could be defined such that:

$$0 \leq \lambda \leq \lambda_{max} \tag{3.10}$$

where $\lambda = 0$ represents maximum wind power generation and $\lambda = \lambda_{max}$ represents no wind power generation. This study relies on LOLP reliability metric and uses peak load data. Therefore, the load could be assumed constant.

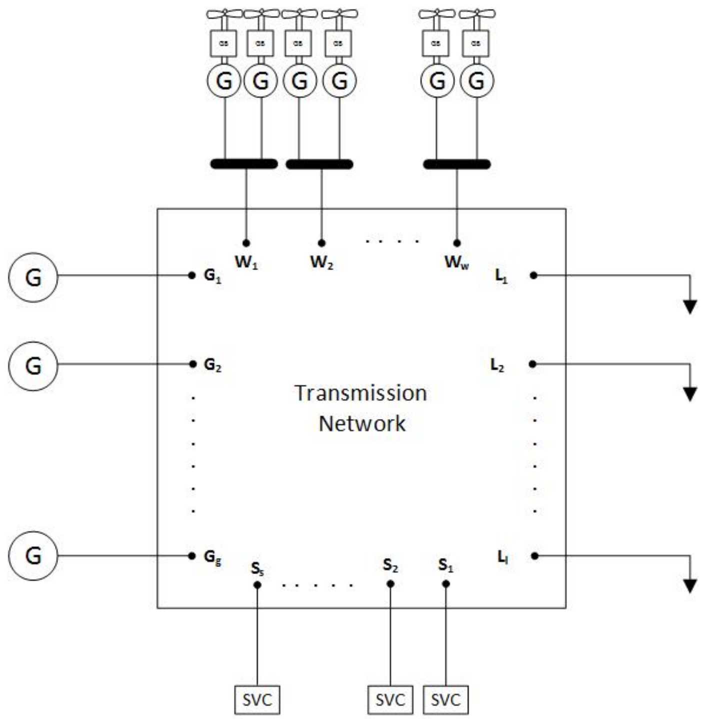

Figure 3.2: One-line diagram of a power system with wind farm

The power equations can be written as:

$$P_{L_i}(\lambda) = P_{L_{i_0}} = const. \tag{3.11}$$

$$P_{G_i}(\lambda) = P_{G_{i_0}}(1 + \lambda K_{P_{G_i}}) \tag{3.12}$$

$$P_{W_i}(\lambda) = P_{W_{i_0}}(1 + \lambda K_{P_{W_i}}) \tag{3.13}$$

where P_{G_i} and P_{W_i} are the active power generation dispatch by conventional power plants while wind power is at its maximum projected capacity and the maximum active power generation by wind farm, respectively, at the i-th bus and $K_{P_{G_i}}$ and $K_{P_{W_i}}$ are their active power participation factors. The participation factor for non-wind generators is positive and for the wind generators is negative. In order to investigate the impact of variability of wind on voltage, the wind real power generation should be shifted in certain steps. Thus, λ is slightly changed in each step. $P_{L_{i_0}}$ is the peak load.

While wind power decreases, the other generators installed at non-wind power plants attempt to compensate the deficit of real power that occurred because of drop of wind power generation. Consequently, according to the reactive capability of the generators, the reactive power at any given P will be determined. Figure 3.3 shows a typical $P - Q$ curve.

Reactive power output of a generator is a function of real power output of the generator which depends on the technology, capability of the machine to provide reactive power support and the machine's controller settings. Therefore, the reactive

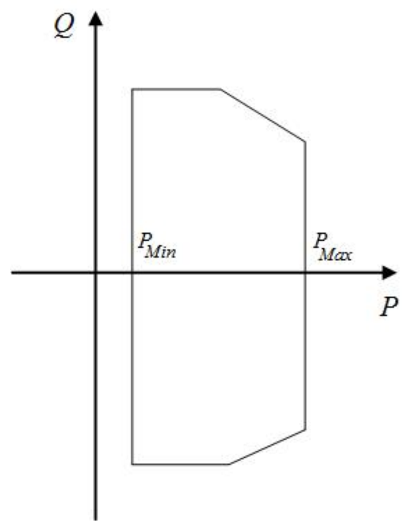

Figure 3.3: A typical reactive capability curve of electrical generators

power equations can be defined by:

$$Q_{G_i}(\lambda) = Q(P_{G_{i_0}}(\lambda)) \cdot (1 + \lambda K_{Q_{G_i}}) \tag{3.14}$$

$$Q_{W_i}(\lambda) = Q(P_{W_{i_0}}(\lambda)) \cdot (1 + \lambda K_{Q_{W_i}}) \tag{3.15}$$

where Q_{G_i} and Q_{W_i} are the reactive power generation by conventional power plants and wind generations, respectively, at the i-th bus. The total reactive generation power is given by:

$$Q_G(\lambda) = \sum_{i=1}^{G} Q_{G_i}(\lambda) + \sum_{i=1}^{W} Q_{W_i}(\lambda) \tag{3.16}$$

The equations that represent the variation of reactive power corresponding to changes in real power can be given by:

$$\frac{\partial Q_{G_i}}{\partial \lambda} = \frac{\partial Q_{G_i}}{\partial P_{G_i}} \cdot \frac{\partial P_{G_i}}{\partial \lambda} \tag{3.17}$$

$$\frac{\partial Q_{W_i}}{\partial \lambda} = \frac{\partial Q_{W_i}}{\partial P_{W_i}} \cdot \frac{\partial P_{W_i}}{\partial \lambda} \tag{3.18}$$

where $\left(\frac{\partial Q_{G_i}}{\partial P_{G_i}}\right)$ and $\left(\frac{\partial Q_{W_i}}{\partial P_{W_i}}\right)$ are determined by the $P - Q$ characteristics of the generators in the area.

Differentiation of (3.12) and (3.13) produces:

$$\frac{\partial P_{G_i}}{\partial \lambda} = P_{G_{i_0}} \cdot K_{P_{G_i}} \tag{3.19}$$

$$\frac{\partial P_{W_i}}{\partial \lambda} = P_{W_{i_0}} \cdot K_{P_{W_i}} \tag{3.20}$$

Substituting (3.19) and (3.20) into (3.17) and (3.18) produces:

$$\frac{\partial Q_{G_i}}{\partial \lambda} = \frac{\partial Q_{G_i}}{\partial P_{G_i}} \cdot P_{G_{i_0}} \cdot K_{P_{G_i}} \tag{3.21}$$

$$\frac{\partial Q_{W_i}}{\partial \lambda} = \frac{\partial Q_{W_i}}{\partial P_{W_i}} \cdot P_{W_{i_0}} \cdot K_{P_{W_i}} \tag{3.22}$$

The reactive power vector could be written by:

$$Q = \begin{bmatrix} Q_{G_i} \\ Q_{W_i} \end{bmatrix} \tag{3.23}$$

By substituting (3.23) into (3.7), the voltage equations for transmission system can be eventually rewritten by:

$$\begin{bmatrix} \Delta V_{G_1} \\ \vdots \\ \Delta V_{G_G} \\ \Delta V_{W_1} \\ \vdots \\ \Delta V_{W_W} \\ \Delta V_{L_1} \\ \vdots \\ \Delta V_{L_n} \end{bmatrix} = \begin{bmatrix} \frac{\partial Q_{G_1}}{\partial V_{G_1}} & \cdots & \frac{\partial Q_{G_1}}{\partial V_{G_G}} & \frac{\partial Q_{G_1}}{\partial V_{W_1}} & \cdots & \frac{\partial Q_{G_1}}{\partial V_{W_W}} \\ \vdots & \ddots & \vdots & \vdots & \ddots & \vdots \\ \frac{\partial Q_{G_G}}{\partial V_{G_1}} & \cdots & \frac{\partial Q_{G_G}}{\partial V_{G_G}} & \frac{\partial Q_{G_G}}{\partial V_{W_1}} & \cdots & \frac{\partial Q_{G_G}}{\partial V_{W_W}} \\ \frac{\partial Q_{W_1}}{\partial V_{G_1}} & \cdots & \frac{\partial Q_{W_1}}{\partial V_{G_G}} & \frac{\partial Q_{W_1}}{\partial V_{W_1}} & \cdots & \frac{\partial Q_{W_1}}{\partial V_{W_W}} \\ \vdots & \ddots & \vdots & \vdots & \ddots & \vdots \\ \frac{\partial Q_{W_W}}{\partial V_{G_1}} & \cdots & \frac{\partial Q_{W_W}}{\partial V_{G_G}} & \frac{\partial Q_{W_W}}{\partial V_{W_1}} & \cdots & \frac{\partial Q_{W_W}}{\partial V_{W_W}} \\ \frac{\partial Q_{L_1}}{\partial V_{G_1}} & \cdots & \frac{\partial Q_{L_1}}{\partial V_{G_G}} & \frac{\partial Q_{L_1}}{\partial V_{W_1}} & \cdots & \frac{\partial Q_{L_1}}{\partial V_{W_W}} \\ \vdots & \ddots & \vdots & \vdots & \ddots & \vdots \\ \frac{\partial Q_{L_n}}{\partial V_{G_1}} & \cdots & \frac{\partial Q_{L_n}}{\partial V_{G_G}} & \frac{\partial Q_{L_n}}{\partial V_{W_1}} & \cdots & \frac{\partial Q_{L_n}}{\partial V_{W_W}} \end{bmatrix}^{-1} \begin{bmatrix} \Delta \frac{\partial Q_{G_1}}{\partial P_{G_1}} \cdot K_{P_{G_1}} \cdot P_{G_{1_0}} \\ \vdots \\ \Delta \frac{\partial Q_{G_G}}{\partial P_{G_G}} \cdot K_{P_{G_G}} \cdot P_{G_{G_0}} \\ \Delta \frac{\partial Q_{W_1}}{\partial P_{W_1}} \cdot K_{P_{W_1}} \cdot P_{W_{1_0}} \\ \vdots \\ \Delta \frac{\partial Q_{W_W}}{\partial P_{W_W}} \cdot K_{P_{W_W}} \cdot P_{W_{W_0}} \end{bmatrix} \tag{3.24}$$

This equation describe voltage behavior of all of the busbars in a transmission system including conventional generation busbars, V_G, wind farm busbars, V_W, and load busbars, V_L, with respect to variability of generated power by wind farms.

Figure 3.4 shows the effects of wind variability on the system's $Q - V$ curve.

As shown in Figure 3.4 and suggested by Machowski [24], operating in the right hand side of the reactive power characteristic curve ensures the voltage steady state stability of the system. Thus, the best indication of steady state voltage instability is voltage drop in transmission system.

The thermal stability in transmission lines is intended to determine power transfer capabilities of the lines by assessing the temperature generated by the energized conductors as result of power transfer. It also assures prevention of line congestion. In this study, the active power loading ratio is used to assess thermal stability in transmission system. In this approach, heavily loaded lines which transfer active power in long distances are an indication of thermal instability.

3.1.2 Approach of This Study

The result of the sensitivity analysis form two data sets for each step that λ shifts. One data set contains information of voltage magnitudes of the busbars. The second

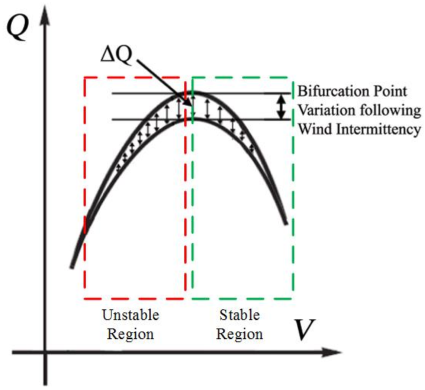

Figure 3.4: Conceptual visualization of the voltage stability assessment in the presence of wind farm

data set contains information of power flow of the transmission lines. To analyze each data set and process them to reveal meaningful information statistical tool was used in this study.

First, kernel density estimation (KDE) was applied to each of the data sets to smooth the data and estimate the density function of each data set with equal weight for all data points. The KDE is a non-parametric method for data smoothing while the degree of smoothing is determined by bandwidth of the kernel function that is used for density estimation. The outcome of the KDE outline the effect of wind power variability on voltage regulation and power flow of the lines.

Then, the data sets of voltage regulation of the lines from all level of wind were merged to form a single set of data sample. Similarly, data sets of power flow of the lines for all level of wind were merged too. The new two sets of data consist of all possible voltage magnitude and power flow data for the system and cover entire operating points of the system.

In an ideally stable power system, voltage magnitudes across the system are regulated at 1.0 p.u. This forms a voltage regulation data for this system with identical measures of mode, maximum, minimum, mean and median of 1 and estimated density function of normal distribution. As the voltage magnitudes across the system begin to deviate from 1.0 p.u. and spread out within a wider range, these measures start to vary. As a result, distribution density function begins to deviate from normal distribution.

Then, maximum, minimum, mode, mean and median of each the merged data sets were calculated. These values provide a sufficient understanding of how the data points are distributed and how close to normal distribution they are distributed. Then maximum and minimum measures indicate whether or not any voltage violation occurs, according to the grid code and its standard range. The mode measure shows what voltage magnitudes have been recorded the most frequently. The closer mode values to 1 is an indication of the greater performance of the system in voltage regulation. The last metric to use was difference between mean and median. The smaller values for this measure indicates that voltage regulation data set tends to form normal distribution density. Positive values for this difference shows likeliness to voltage rise across the system while it negative values indicate likeliness to voltage drop across the system. This measure is similar to Kurtosis and Skewness in which heaviness of tail and shoulders of the distribution is used for interpretation, but easier to compute while in data sets from power systems the tailedness of the probability distribution is not a concern. In fact, this is a technique to measure symmetry of a series of data. The significantly high value of this metric is an indicator of instability of the system. Table 3.1 compares this measure for three data sets within range of 0 and 1 with different distribution density functions.

Table 3.1: Statistical Metrics for Three Distribution Functions

Distribution	Difference between median-mean
Normal	0
Weibull	0.1034
Poisson	0.1568

To derive more information about data sets and measured data points, distribution of data points in relative data sets were compared to the normal distribution to determine whether the data follow a normal distribution. The outcome of this analysis provides information about the probability of any given operating condition, both voltage regulation and line loading level, to occur relative to the wind variability. Figure 3.5 shows a comparative plot for three distributed functions.

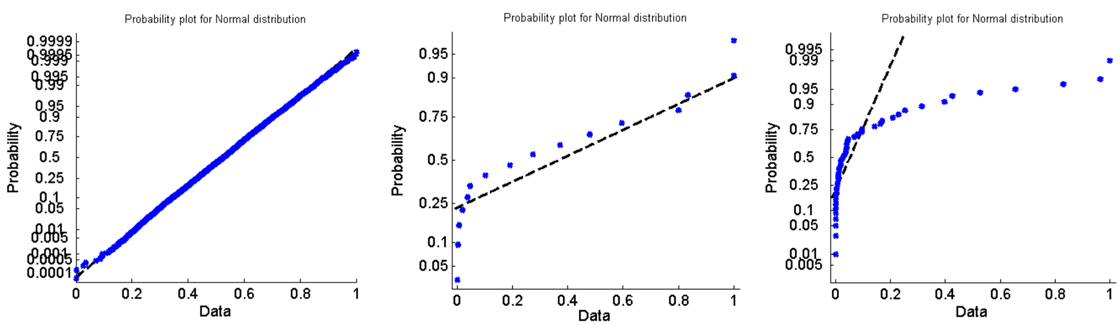

(a) Normal Distribution (b) Poisson Distribution (c) Weibull Distribution

Figure 3.5: Comparative probability plots for three different distribution functions

In this figure, the normal distribution shows the most moderate distribution while 50% of data points are within first 50% of the data set length, and the other 50% of data points are within second 50% of the data set length. The Webibull distribution illustrates the least symmetrical distribution while almost 75% of data points are within first 20% of the data set length and more than 90% of data points are within first 60% of the data set length. The Poisson distribution also indicates an uneven distribution, but closer to a normal distribution than Weibull distribution, while 50% of data points are within first 30% of the data set length and approximately 80% of data points are within first 80% of the data set length.

The last point to note in the Figure 3.5 is that for all of distribution density functions, the probability plots clearly yield the range of data sets. This is tremendously practical in this research to identify whether or not any overvoltage, voltage drop or line overloading occurs in a case studies and with what severity and probability.

3.2 Steady State Contingency Analysis

Power system security is directly related to the ability of the system to maintain normal operation following disturbances so-called contingencies. A contingency represents a credible event that can occur in the system such as an outage of a main component or multiple components. Thus, power system security is then defined as the ability of the power system to survive from and withstand the contingencies and deliver the power to consumers without interruption [24]. It should be noted that power system security is broader concept than stability and integrates reliability and stability, and involves robust and resilient the system [26].

The first step of security assessment is to determine the system operating state. In the power system, presently sensors provide measurements at high rates and resolution. In real-time operation of a power system, measurement devices acquire online data from the grid variables and operating conditions. In current power industry, a centralized supervisory control and data acquisition (SCADA) systems operates a power area. The next step is contingency analysis to perform.

Contingency analysis involves applying a sequence of contingency events to the system. These events could be the outage of a transmission line, a generator or multiple components at the same time. The results represent the response of the system to those contingencies. Then, the events are ranked based on their severity to identify the worst case scenarios and determine how resilient and secure the system will be during long terms [27]. This evaluation is based on how distant the operation points are from the bifurcation point in which voltage collapse occurs. This process is so-called contingency ranking and monitoring.

The most common approach in power system planning studies considers *N-1* security criteria in which a system should curtail outage of any single transmission line or generator to stay in the normal or alert operating state [92].

In practice, one way of computing any possible violation of operating limits during contingency events is to start with a base case and then continue to apply a sequence of events and calculate their severity indices until reaching an unstable case [27]. From that case, the stability margin of the system could be determined. If contingency events do not threaten the security of the system, then the system must be stressed by increasing consumption step by step. Each step requires stability computations until an instability case is found. However, this procedure is computationally complex and may require using multiple processors, parallel computing, and simplified models [27].

The objective of the current section is developing an analytical tool for contingency operation of large scale power systems for offshore wind farm integration studies. The contribution of this section is proposing a risk based approach used to quantify

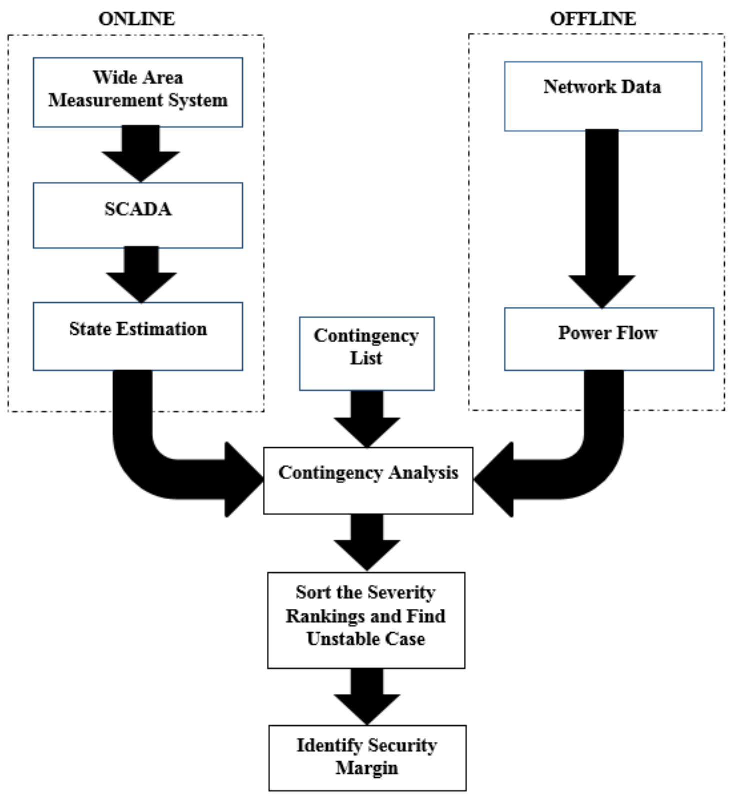

Figure 3.6: Conceptual flow chart of voltage security assessment

variability of the wind power as a single index. This allows in addition to comparing and ranking the severity of events, identifying the most secure integration scenario. This approach is also applicable to all other forms of variable generation units such as onshore wind farms and solar.

3.2.1 Mathematical Formulation

This research introduces a new security index which is capable to identify the most severe contingency events of the system in presence of offshore wind farm and to determine, from a large number of contingencies, those that may lead the system to operational risk. This index also allows to assess operational effects of offshore wind farm on security of the power system and whether or not threats the system to find the best and worst integration scenarios for wind integration projects. This index is a result of combination of multiple severity indices that are address different state variables in the system.

The first step is to initiate the base case with no contingency to ensure it is stable. The next step is to apply contingency events one at a time and conduct sensitivity analysis to acquire voltage magnitude of the busbars, power flow of the lines and active power and reactive power data of generation units. This is to stress the system by varying the wind power. The aforementioned data could be computed using equations described below.

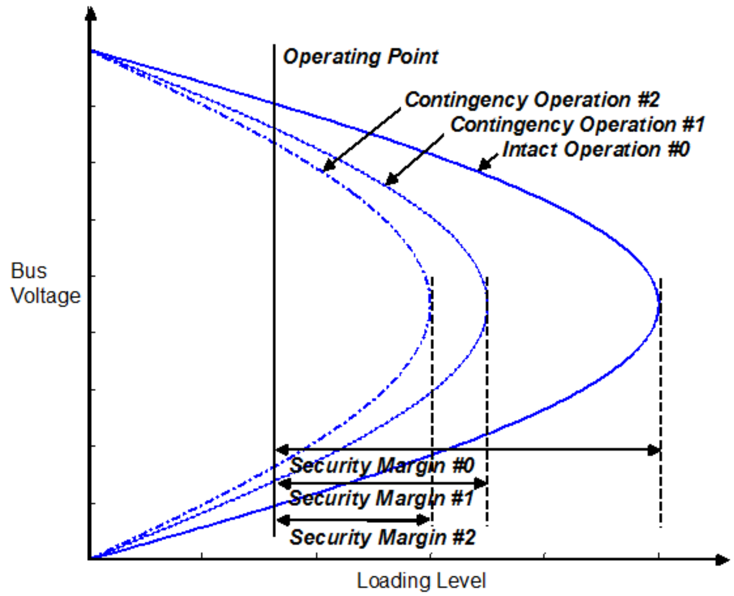

Figure 3.7: Conceptual visualization of voltage security

The dynamic behavior of a power system, using differential-algebraic equations, is given by:

$$\dot{x} = f(x, u) \tag{3.25}$$

where x is a $n\times1$ state vector and u is a $k\times1$ representing inputs to the system. For every equilibrium point of x^*, the steady state solution of the system is given by:

$$f(x^*, u) = 0 \tag{3.26}$$

To simulate variability of the wind power, a variability component λ, wind variability parameter, in respect to maximum wind generation could be defined such that:

$$0 \leq \lambda \leq \lambda_{max} \tag{3.27}$$

where $\lambda = 0$ represents maximum wind power generation and $\lambda = \lambda_{max}$ represents no wind power generation. This study relies on LOLP reliability metric and uses peak load data. Therefore, the load could be assumed constant.

The power equations for a power system including synchronous generators, wind farms and loads could be written as:

$$P_{L_i}(\lambda) = P_{L_{i_0}} = const. \tag{3.28}$$

$$P_{G_i}(\lambda) = P_{G_{i_0}}(1 + \lambda K_{P_{G_i}}) \tag{3.29}$$

$$P_{W_i}(\lambda) = P_{W_{i_0}}(1 + \lambda K_{P_{W_i}}) \tag{3.30}$$

where P_{G_i} and P_{W_i} are the active power generation dispatch by conventional power plants while wind power is at its maximum capacity and the maximum active power generation by wind farm, respectively, at the i-th bus and $K_{P_{G_i}}$ and $K_{P_{W_i}}$ are their active power participation factors. The participation factor for non-wind generators is positive and for the wind generators is negative. In order to investigate the impact of variability of wind on voltage, the wind real power generation should be shifted in certain steps. Thus, λ is slightly changed in each step. $P_{L_{i_0}}$ is the peak load.

While wind power decreases, the other generators installed at non-wind power plants attempt to compensate the deficit of real power that occurred because of wind power generation drop. Consequently, according to the generators' structure and controller, the reactive power generation at any given P will be determined. Reactive power output of a generator is a function of various factors including real power output of the generator, technology used in the generator, capability of the machine to provide reactive power support and the machine's controller settings. Therefore, the reactive power equations can be defined by:

$$Q_{G_i}(\lambda) = Q(P_{G_{i_0}}(\lambda)) \cdot (1 + \lambda K_{Q_{G_i}}) \tag{3.31}$$

$$Q_{W_i}(\lambda) = Q(P_{W_{i_0}}(\lambda)) \cdot (1 + \lambda K_{Q_{W_i}}) \tag{3.32}$$

where Q_{G_i} and Q_{W_i} are the reactive power generation by conventional power plants and wind generations, respectively, at the i-th bus. The total reactive generation power is given by:

$$Q_G(\lambda) = \sum_{i=1}^{G} Q_{G_i}(\lambda) + \sum_{i=1}^{W} Q_{W_i}(\lambda) \tag{3.33}$$

The available reactive power in the area is an accumulation of compensation devices and individual generator's reactive power output in the system including the wind machines.

The equations that represent the variation of reactive power corresponding to changes in real power can be given by:

$$\frac{\partial Q_{G_i}}{\partial \lambda} = \frac{\partial Q_{G_i}}{\partial P_{G_i}} \cdot \frac{\partial P_{G_i}}{\partial \lambda} \tag{3.34}$$

$$\frac{\partial Q_{W_i}}{\partial \lambda} = \frac{\partial Q_{W_i}}{\partial P_{W_i}} \cdot \frac{\partial P_{W_i}}{\partial \lambda} \tag{3.35}$$

where $\left(\frac{\partial Q_{G_i}}{\partial P_{G_i}}\right)$ and $\left(\frac{\partial Q_{W_i}}{\partial P_{W_i}}\right)$ are determined by the $P - Q$ characteristics of the generators in the area.

Rearranging these equations produces:

$$\frac{\partial Q_G(\lambda)}{\partial \lambda} = \sum_{i=1}^{G} \frac{\partial Q_{G_i}}{\partial P_{G_i}} P_{G_{i_0}} K_{P_{G_i}} + \sum_{i=1}^{W} \frac{\partial Q_{W_i}}{\partial P_{W_i}} P_{W_{i_0}} K_{P_{W_i}} \tag{3.36}$$

This equation represents sensitivity of available reactive power in the system to variability of the wind farm.

The acive power and reactive power sensitivity vectors could be given by:

$$\Delta P(\lambda) = \begin{bmatrix}\Delta P_{G_i}(\lambda) & \Delta P_{W_i}(\lambda)\end{bmatrix}^T \tag{3.37}$$

$$\Delta Q(\lambda) = \begin{bmatrix}\Delta Q_{G_i}(\lambda) & \Delta Q_{W_i}(\lambda)\end{bmatrix}^T \tag{3.38}$$

The voltage and rotor angle sensitivities for conventional generation busbars, subscripted by G, wind farm busbars, , subscripted by W, and load busbars, , subscripted by L, following variability of generated power by wind farms could be computed by:

$$\begin{bmatrix}\Delta V_{G_1}\\ \vdots \\ \Delta V_{G_G}\\ \Delta V_{W_1}\\ \vdots\\ \Delta V_{W_W}\\ \Delta V_{L_1}\\ \vdots\\ \Delta V_{L_n}\end{bmatrix} = \begin{bmatrix}\frac{\partial Q_{G_1}}{\partial V_{G_1}} & \cdots & \frac{\partial Q_{G_1}}{\partial V_{G_G}} & \frac{\partial Q_{G_1}}{\partial V_{W_1}} & \cdots & \frac{\partial Q_{G_1}}{\partial V_{W_W}}\\ \vdots & \ddots & \vdots & \vdots & \ddots & \vdots\\ \frac{\partial Q_{G_G}}{\partial V_{G_1}} & \cdots & \frac{\partial Q_{G_G}}{\partial V_{G_G}} & \frac{\partial Q_{G_G}}{\partial V_{W_1}} & \cdots & \frac{\partial Q_{G_G}}{\partial V_{W_W}}\\ \frac{\partial Q_{W_1}}{\partial V_{G_1}} & \cdots & \frac{\partial Q_{W_1}}{\partial V_{G_G}} & \frac{\partial Q_{W_1}}{\partial V_{W_1}} & \cdots & \frac{\partial Q_{W_1}}{\partial V_{W_W}}\\ \vdots & \ddots & \vdots & \vdots & \ddots & \vdots\\ \frac{\partial Q_{W_W}}{\partial V_{G_1}} & \cdots & \frac{\partial Q_{W_W}}{\partial V_{G_G}} & \frac{\partial Q_{W_W}}{\partial V_{W_1}} & \cdots & \frac{\partial Q_{W_W}}{\partial V_{W_W}}\\ \frac{\partial Q_{L_1}}{\partial V_{G_1}} & \cdots & \frac{\partial Q_{L_1}}{\partial V_{G_G}} & \frac{\partial Q_{L_1}}{\partial V_{W_1}} & \cdots & \frac{\partial Q_{L_1}}{\partial V_{W_W}}\\ \vdots & \ddots & \vdots & \vdots & \ddots & \vdots\\ \frac{\partial Q_{L_n}}{\partial V_{G_1}} & \cdots & \frac{\partial Q_{L_n}}{\partial V_{G_G}} & \frac{\partial Q_{L_n}}{\partial V_{W_1}} & \cdots & \frac{\partial Q_{L_n}}{\partial V_{W_W}}\end{bmatrix}^{-1} \begin{bmatrix}\Delta \frac{\partial Q_{G_1}}{\partial P_{G_1}} \cdot K_{P_{G_1}} \cdot P_{G_{1_0}}\\ \vdots\\ \Delta \frac{\partial Q_{G_G}}{\partial P_{G_G}} \cdot K_{P_{G_G}} \cdot P_{G_{G_0}}\\ \Delta \frac{\partial Q_{W_1}}{\partial P_{W_1}} \cdot K_{P_{W_1}} \cdot P_{W_{1_0}}\\ \vdots\\ \Delta \frac{\partial Q_{W_W}}{\partial P_{W_W}} \cdot K_{P_{W_W}} \cdot P_{W_{W_0}}\end{bmatrix} \tag{3.39}$$

$$\begin{bmatrix}\Delta \delta_{G_1}\\ \vdots \\ \Delta \delta_{G_G}\\ \Delta \delta_{W_1}\\ \vdots\\ \Delta \delta_{W_W}\\ \Delta \delta_{L_1}\\ \vdots\\ \Delta \delta_{L_n}\end{bmatrix} = \begin{bmatrix}\frac{\partial P_{G_1}}{\partial \delta_{G_1}} & \cdots & \frac{\partial P_{G_1}}{\partial \delta_{G_G}} & \frac{\partial P_{G_1}}{\partial \delta_{W_1}} & \cdots & \frac{\partial P_{G_1}}{\partial \delta_{W_W}}\\ \vdots & \ddots & \vdots & \vdots & \ddots & \vdots\\ \frac{\partial P_{G_G}}{\partial \delta_{G_1}} & \cdots & \frac{\partial P_{G_G}}{\partial \delta_{G_G}} & \frac{\partial P_{G_G}}{\partial \delta_{W_1}} & \cdots & \frac{\partial P_{G_G}}{\partial \delta_{W_W}}\\ \frac{\partial P_{W_1}}{\partial \delta_{G_1}} & \cdots & \frac{\partial P_{W_1}}{\partial \delta_{G_G}} & \frac{\partial P_{W_1}}{\partial \delta_{W_1}} & \cdots & \frac{\partial P_{W_1}}{\partial \delta_{W_W}}\\ \vdots & \ddots & \vdots & \vdots & \ddots & \vdots\\ \frac{\partial P_{W_W}}{\partial \delta_{G_1}} & \cdots & \frac{\partial P_{W_W}}{\partial \delta_{G_G}} & \frac{\partial P_{W_W}}{\partial \delta_{W_1}} & \cdots & \frac{\partial P_{W_W}}{\partial \delta_{W_W}}\\ \frac{\partial P_{L_1}}{\partial \delta_{G_1}} & \cdots & \frac{\partial P_{L_1}}{\partial \delta_{G_G}} & \frac{\partial P_{L_1}}{\partial \delta_{W_1}} & \cdots & \frac{\partial P_{L_1}}{\partial \delta_{W_W}}\\ \vdots & \ddots & \vdots & \vdots & \ddots & \vdots\\ \frac{\partial P_{L_n}}{\partial \delta_{G_1}} & \cdots & \frac{\partial P_{L_n}}{\partial \delta_{G_G}} & \frac{\partial P_{L_n}}{\partial \delta_{W_1}} & \cdots & \frac{\partial P_{L_n}}{\partial \delta_{W_W}}\end{bmatrix}^{-1} \begin{bmatrix}\Delta K_{P_{G_1}} \cdot P_{G_{1_0}}\\ \vdots\\ \Delta K_{P_{G_G}} \cdot P_{G_{G_0}}\\ \Delta K_{P_{W_1}} \cdot P_{W_{1_0}}\\ \vdots\\ \Delta K_{P_{W_W}} \cdot P_{W_{W_0}}\end{bmatrix} \tag{3.40}$$

$$\begin{bmatrix}\Delta P\end{bmatrix} = \begin{bmatrix}H\end{bmatrix} \cdot \begin{bmatrix}\Delta \delta\end{bmatrix} \tag{3.41}$$

where H is a block of Jacobian matrix which maps relation between busbars angle and power flows in network and shown Equation 3.4.

3.2.2 Approach of This Study

To this end, the network and its components operational data under normal and contingency operations described. The next step is to process the computed data for contingency ranking purposes. The proposed metrics are described below.

Voltage Regulation Index

To assess the effectiveness of voltage regulation across the system for any given level of wind power generation, Voltage Regulation Index (VRI) could be defined by:

$$VRI = \sqrt{\frac{1}{n}\sum_{i=1}^{n}\left(\frac{V_{i_{measured}} - V_{i_{scheduled}}}{V_{i_{scheduled}}}\right)^2} \tag{3.42}$$

where $V_{scheduled}$ and $V_{measured}$ represent the scheduled and computed voltages in the transmission lines and n is the number of transmission lines, respectively. This index measures the error in voltage regulation across the power system. As the voltage regulation performance becomes greater, this index approaches zero. Higher values of this index indicate a considerable error in voltage regulation as a result of poor voltage performance in the system and higher risk of voltage collapse which might require a corrective action in the system.

Power Loss Index

To assess the cumulative power loss in the transmission lines in the system, for any given level of wind power generation, Power Loss Index (PLI) could be defined by:

$$PLI = \frac{1}{n}\sum_{i=1}^{n}\left(\frac{P_{i_{measured}}}{P_{i_{rated}}}\right)^2 \tag{3.43}$$

where $P_{measured}$ and P_{rated} represent the computed active power flow and rated active power transfer capability of the lines and n is the number of lines, respectively. The power loss in the transmission lines and the heating rate are directly correlated. The increase of loading rate in the lines results in higher power loss in the line. Greater values of this index indicate higher rates of line loading.

Transmission Line Loading Index

To quantify loading level of the transmission lines for any given level of wind power generation, Transmission Line Loading Index (TLLI), could be given by:

$$TLLI = \frac{1}{n}\sum_{i=1}^{n}\left(\frac{S_{i_{measured}}}{S_{i_{rated}}}\right) \tag{3.44}$$

where $S_{measured}$ and S_{rated} represent the computed loading level and rated total power transfer capability of lines and n is the number of lines, respectively. This index measures total power that includes active power and reactive power. As loading level in the system increases, this index tends to a greater value which is an indication of a higher likeliness for line congestion to occur. The greater values than 1 for this index are an indication of line overload in the system which might require a corrective action to prevent line congestion and interruption in power delivery.

Reserve Reactive Support Index

Voltage security of the system depends on the availability of reactive support in the system. Therefore, Reactive Capability Index (RCI) could be defined by:

$$RCI = \frac{Q_{reserve_{Area}}}{Q_{load}} \tag{3.45}$$

where $Q_{reserve_{Area}}$ and Q_{load} represent total available reactive power and total reactive power consumption in the power area, respectively. Greater values of RCI is a measure of higher available reactive power for voltage support and is an indicator of higher voltage security since the system's point of operation is more distance from the point of bifurcation in which voltage collapse occurs. Adversely, its smaller values are indicative of the potential for lack of available reactive power in the area that might trigger a voltage collapse in the power area. Figure 3.8 illustrates the relation of available reactive power and voltage security.

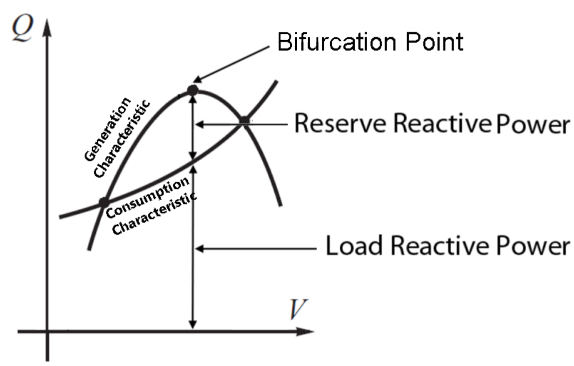

Figure 3.8: Conceptual visualization of relationship between available reactive power and voltage security

The RCI could be also rearranged by:

$$RSSI = \frac{Q_{load}}{Q_{reserve_{Area}}} \tag{3.46}$$

This index is referred to as $RRSI$, the Reserve Reactive Support Index, and the smaller the values of this index indicate higher available reactive power in the area which is an indication of greater voltage security margin. As the state of system begins to move towards bifurcation point, this index tends to greater values and eventually reaches value of infinity when the area runs out of available reactive power and corrective action should be taken.

Security Index

In process of contingency analysis, contingency events must be applied to the system one at a time. For each contingency event, to quantify variability of the wind farm, power system's variables including power flows, voltage magnitudes and generation data should be computed throughout full operational range of offshore wind farm credible steps of power shift, from 0% to 100%. For each step of wind power shift, four introduced indices must be calculated. Then, by incorporation of calculated indices, Security Index (SI) for each level of wind power could be defined by a risk function:

$$SI_i = s_1 VRI_i + s_2 PLI_i + s_3 TLLI_i + s_4 RRSI_i \tag{3.47}$$

where $s_1, \cdots, s_4$ are weighting factors and VRI_i, PLI_i, $TLLI_i$ and $RSSI_i$ are calculated metrics for i-th level of wind power. These weighting factors give importance to each of the indices for calculating the overall SI for each case. The determination the wighting factors depends on the planner's experience and preference as well as condition and topology of the grid. Finally, sum of SIs for all levels of wind power for a particular contingency event forms the SI for that event. This could be formulated by:

$$SI_j = \sum_{i=1}^{m} SI_i \tag{3.48}$$

which security index for the j-th contingency event is by denotes SI_j, security index of i-th level of wind power is shown by SI_i and full span of wind power variability is covered by m steps of power shifts. The greater values of this index represent higher severity of the contingency event.

3.3 Small Signal Stability Analysis

Small signal stability analysis addresses the dynamical behavior of the system following a small disturbance and assesses capability of the system to damp out the oscillations which are excited by the disturbance. In the small signal stability analysis, no contingency occurs and all of the grid components are in operation.

A reliable power system must constantly maintain its operational balance between consumption and generation, and must also ensure that voltage and frequency are within their standard range. It also is important that system operation is secure to withstand disturbances. The disturbances could be, for example, in the form of an expected or unexpected change in the level of generation or consumption.

This section discusses small signal stability analysis in power system planning studies for integration of offshore wind farms.

3.3.1 Small Signal Voltage Stability

Small signal voltage stability analysis addresses the voltage related dynamic behavior of the system following a small disturbance in the system. Figure 3.9 shows dynamics of voltage following a small disturbance.

The oscillations in power system contain several frequencies, known as modes. They are the results of interaction of one component, including generators, relative

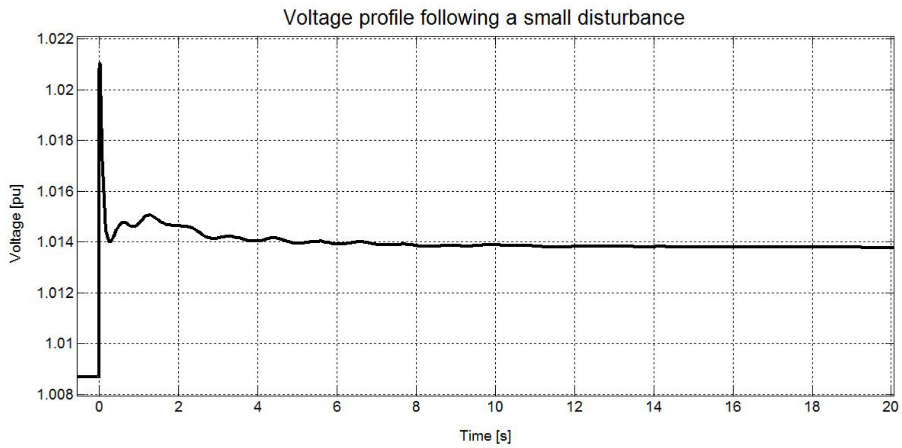

Figure 3.9: Dynamics of voltage following a small disturbance

to another. It is highly important to identify these modes and understand their sources in order to develop and design proper controllers to damp them out. This improves the stability limits of the system from the level of components to the level of the system as whole.

Power system industry classifies the oscillations in the electrical power systems in five major categories [93]:

- **Intraplant mode oscillations:** These modes are the result of a generator rotor swinging against the rest of generator rotors in the same generation site. These modes affect only the machines involved in the oscillation and the rest of the system remains unaffected.

- **Local plant mode oscillations:** These modes are the result of a generator rotor swinging against the rest of generator rotors in the same area. These modes affect only the local machine and grid involved in the oscillation and the rest of the system including the other areas remain unaffected.

- **Inter-area mode oscillations:** These modes are the result of a group of generator rotors in an area swinging against a group of generator rotors in another area. These modes affect a large part of the interconnected power system in more than one area.

- **Control mode oscillations:** These modes are the result of poorly tuned controllers for any given component in the power system such as HVDC, exciter, governor or SVC. These modes affect only the given component and the rest of the system remains unaffected.

- **Torsional mode oscillations:** These modes are the result of turbine-generator mechanical components, typically in multi-stage turbines, with long shafts and low inertias that cause low resonance frequency [94].

The oscillations in power systems always exist and cannot be fully eliminated, because they are a part of the nature of the system [29]. But they can be managed and damped properly to prevent severe instabilities. Power system stabilizers (PSS) have been extensively used in the industry to effectively damp interplant and local plant modes. Supplementary devices such as SVC and HVDC as well as power electronics and their control techniques also impacts on the modes of the system and their damping [29].

The electromechanical oscillations that involve generator rotating masses occur within range of 0.1 Hz to 3.0 Hz. These modes include Inter-area modes, Interplant modes and Local plant modes and their natural frequency range are 0.1-1.0 Hz, 1.0-2.0 Hz and 2.0-3.0 Hz, respectively.

The sources of the electromechanical oscillations usually are shipping bulk power over long distances as well as high gain automatic voltage regulators (AVRs) [28]. These are critical modes of the system because they can affect tie-line power flows and operational balance in the interconnected power systems. Therefore, system planning studies focus on these types of modes. The two other modes, Control modes and Torsional modes, are referred as electrical modes and are the results of mistune of control loops of components and are not in the interest of system planning or expansion studies. These two types of oscillations, their source and suggested solutions are discussed extensively in [95].

For the dynamic stability analysis studies, typically is assumed that the system is steady state stable during the pre-disturbance operating condition. To get a clear and accurate record of oscillation behavior, 20 seconds or longer simulations are required [29]. This time frame is to ensure all dynamics of the systems are captured. In addition, the results from the response in time domain do not provide sufficient information for the nature of the oscillation [29]. Therefore, a frequency domain analysis is required to be carried out to identify full list of critical modes of the system.

The objective of this study is to examine effects of variability of offshore wind farm on small signal voltage stability of a large grid. The contribution of this work is to use Prony analysis to assess large scale power system's voltage response to disturbances introduces by the wind farm, with the main focus on electromechanical oscillation modes and control and torsional modes were not studied. The disturbances applied to the system are modeled as step changes in the level of power generation by the offshore wind farm to model its variability. In practice, the wind power change with a moderate ramp. However, the sudden change was chosen for this study to examine the most severe case such as wind gusts which in many occasions force to a sudden shut down of entire wind farm or a part of it for safety reasons. Recently, it was reported that wind gusts of up to 85mph forced shut down dozens of wind turbines all across the UK [96].

The offshore wind farm was also studied under multiple pre-disturbance operational points. The size of the disturbances was chosen according to the forecasted wind variability for this project which was carried out by NREL [22].

Approach of This Study

To undertake small-signal stability analysis in a multi-machine system using eigenvalue modal analysis, the dynamic models of individual components are needed to be developed first. Then they need to be linearized to form a system's representation using differential algebraic equations. The eigenvalues of system's matrix are the system's modes. The disadvantage of eigenvalue modal analysis is that it is impractical for large interconnected power system. For instance, the Eastern Interconnection model of the US used in this study consists of 63,000 buses. Roughly, more than 20,000 of these buses are equipped with dynamic devices. Depending on the model, every device state variables can range from 2 to 20. In total [28], the state variables range from 40,000 to 400,000. Therefore, the model contains large set of differential nonlinear equations. This is computationally burdening, almost impossible, to calculate using eigenvalue analysis.

In this section, a 3 Machines, 9-Bus Test Case (known as Anderson 9 Bus) [33] were used to examine whether or not Prony analysis could be used to directly identify voltage dominant modes by analyzing voltage signal at any given busbar.

This test model is a benchmark model for the analysis and control of small-signal oscillatory dynamics in power systems and represents an approximation of the Western System Coordinating Council (WSCC) and is composed of 9 buses, 3 synchronous generators, 3 two-winding power transformers, 6 lines and 3 loads. Figure 3.10 shows its one-line diagram. The disturbance examined in this case was the 40% increase of load which is connected to bus 5 at 125 MW. Following this event, the voltage signals from all of the buses were monitored. Figure 3.11 shows these signals.

By comparing the voltage signal, it can be seen that all of them follow a common trajectory with a small variation among their magnitudes. The results from eigenvalue analysis of this system using 6-th order synchronous machine model is shown in Table 3.2. In this table, only oscillation modes are included.

Table 3.2: Eigenvalues of Test System

Eigenvalue	Frequency	Damping Ratio	Machine Number	Variable
-0.8232 $\pm$ j12.593	2.0 Hz	0.06	3	δ, ω
-0.5042 $\pm$ j9.065	1.4 Hz	0.05	2	V_R, E_{f_d}
-5.1660 $\pm$ j7.880	1.2 Hz	0.54	3	V_R, E_{f_d}
-5.1676 $\pm$ j7.816	1.2 Hz	0.55	1	δ, ω
-5.1597 $\pm$ j7.871	1.2 Hz	0.54	2	δ, ω
-0.0988 $\pm$ j4.834	0.7 Hz	0.02	1	V_R, E_{f_d}
-0.4302 $\pm$ j0.899	0.1 Hz	0.43	1	E'_q, R_f
-0.4057 $\pm$ j0.741	0.1 Hz	0.84	2	E'_q, R_f
-0.4161 $\pm$ j0.566	0.0 Hz	0.59	3	E'_q, R_f

In this table, δ, ω, V_R, E_{f_d}, E'_q and R_f correspond to machine's rotor angle, rotor speed, exciter input signal, exciter output signal, voltage behind the transient reactance, and stabilizer feedback variable, respectively.

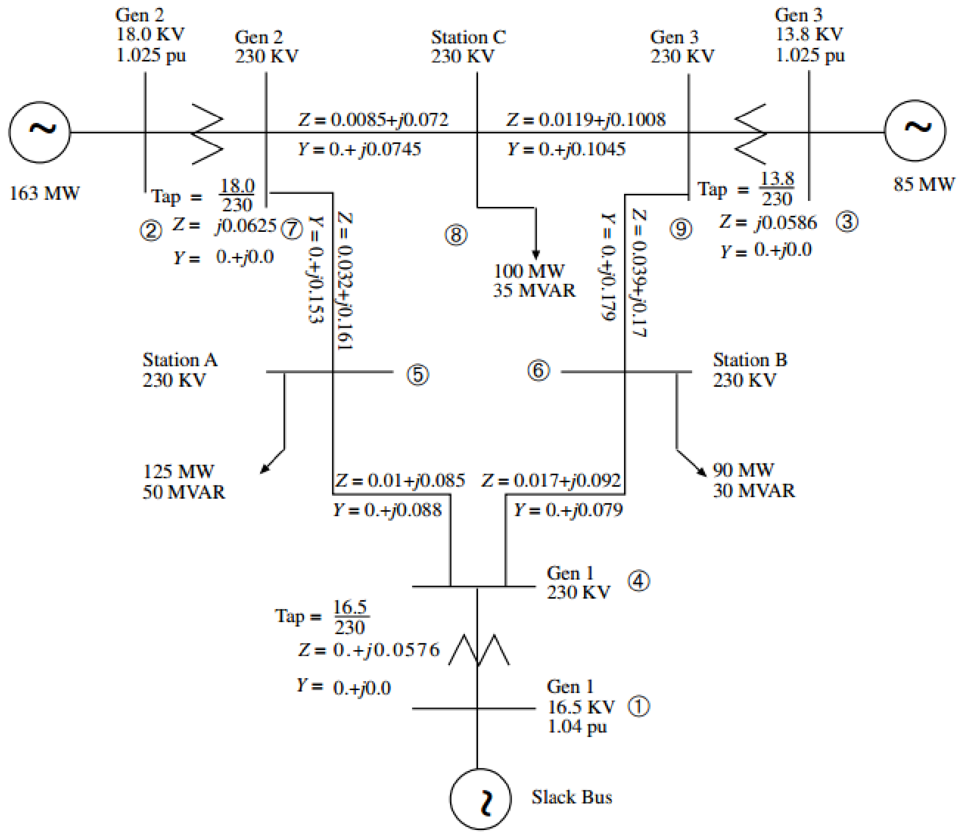

Figure 3.10: One-line diagram of WSCC 9-bus test system [32]

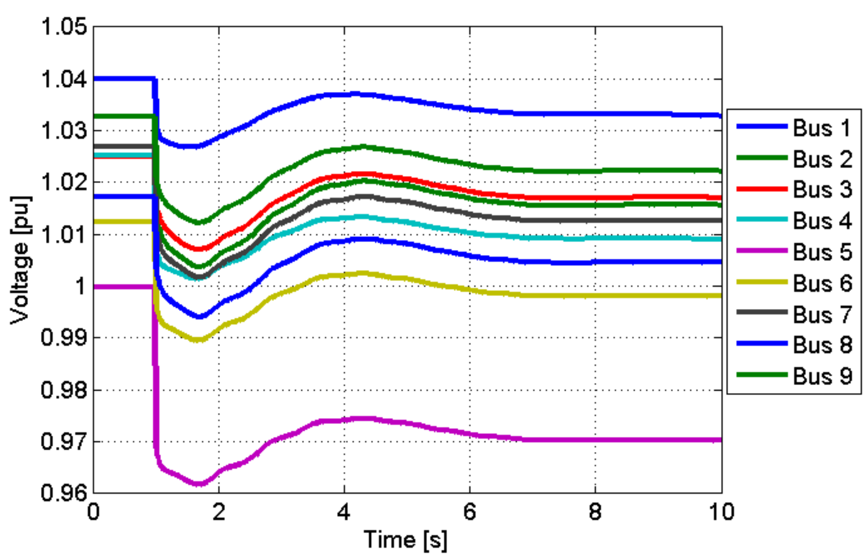

Figure 3.11: Dynamic voltage signals in response to 40% increase of load at bus 5

A Prony analysis was applied to all of the voltage signals to determine the dominant voltage oscillatory modes, magnitude and relative damping ratio. These modes are important of assess magnitude of the initial voltage deviation and time duration needed to damp them out. The results are shown in Table 3.3.

Table 3.3: Results of Prony Analysis on Voltage Signals from the Test System

Bus	Amplitude	Frequency	Damping Ratio
1	1.9×10^{-4}	1.3 Hz	0.05
	1.3×10^{-2}	0.1 Hz	0.43
2	7.6×10^{-4}	1.3 Hz	0.05
	2.2×10^{-2}	0.1 Hz	0.46
3	4.9×10^{-4}	1.3 Hz	0.05
	2.0×10^{-2}	0.1 Hz	0.45
4	6.2×10^{-4}	1.3 Hz	0.05
	1.5×10^{-2}	0.1 Hz	0.44
5	6.6×10^{-4}	1.3 Hz	0.06
	1.7×10^{-2}	0.1 Hz	0.46
6	7.5×10^{-4}	1.3 Hz	0.05
	1.6×10^{-2}	0.1 Hz	0.40
7	8.1×10^{-4}	1.3 Hz	0.05
	1.9×10^{-2}	0.1 Hz	0.44
8	8.0×10^{-4}	1.3 Hz	0.06
	2.1×10^{-2}	0.1 Hz	0.46
9	6.1×10^{-4}	1.3 Hz	0.05
	2.0×10^{-2}	0.1 Hz	0.45

From the prony's analysis results, it can be seen that the dominant frequency of oscillatory modes are 1.3 Hz and 0.1 Hz with damping ratios of approximately 0.05 and 0.43. These modes are consistent for all of the voltage signals. The amplitudes of these modes varied for each signal. The reason for the variation of amplitude is that the network configuration determines the amplitude of oscillations.

From the table 3.2, it can be seen that the modes identified by Prony analysis and the dominant modes identified by eigenvalue analysis are nearly identical. This is not surprising since the change in load at bus 5 triggers a set of changes in the machines' dynamic variables which are connected to both ends of its feeding lines. As a result, dominant modes corresponding to machine 1's E'_q and R_f, machine's voltage behind the transient reactance and stabilizer feedback variable, and machine 2's V_R and E_{f_d}, machine's exciter input signal and exciter output signal are excited. The voltage at any given bus is a function of balance between generation by the generators and consumption by the load in the system. Therefore, voltage oscillatory modes should be consistent with some of the dominant modes of synchronous machines. Those system oscillatory modes that did not appear in voltage modes whether have a very small magnitude that made them impossible to capture or have not been excited.

The analysis completed in this section demonstrates that voltage oscillatory modes for small signal voltage stability analysis could be captured by applying Prony analysis directly to a time-domain voltage signal following a small disturbance. This finding is useful for large scale power system in which applying modal analysis is computationally burdening or impossible.

3.3.2 Small Signal Frequency Response

Frequency stability in a power system is defined as the ability of the system to adequately manage frequency regulation when disturbances occur. Following a disturbance, when frequency decline occurs, it should be adequately arrested so the under-frequency load shedding (UFLS) relays do not operate. The inability of the system to meet such a requirement is an indication of a significant difference between generation and consumption and can lead to the system instability.

UFLS is a system condition addressed by IEEE C37.117 [97] and relies on protective frequency relays for under-frequency shedding of online loads during operating conditions where generation or transmission capacity of the power system is not capable of meeting the demand within prescribed operational limits. UFLS attempts to prevent further loss of generation units. If the mismatch between generation and consumption accommodated by load shedding is sufficient to keep generators online, the system can be restored quickly. Otherwise, a widespread system shutdown will take place [24]. Standard PRC-006-NPCC-1 [98], in coordination with the NERC UFLS reliability standard, has defined the UFLS threshold, as shown in Figure 3.12.

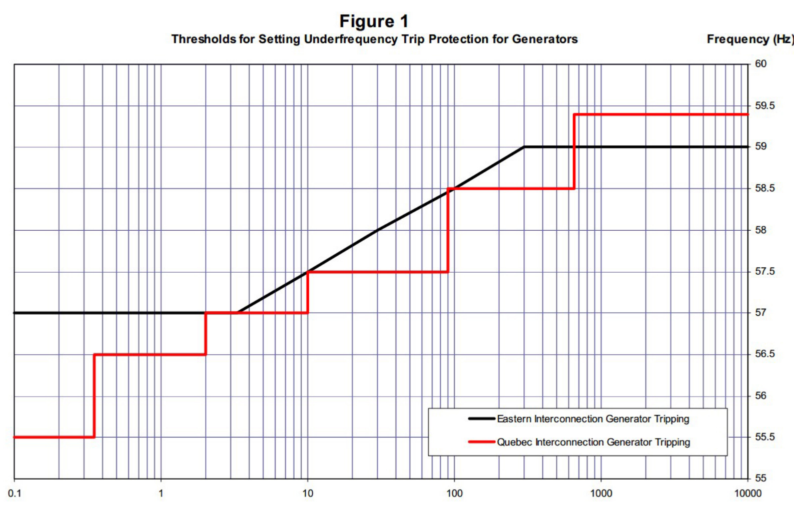

Figure 3.12: Setting under frequency trip protection for generators [98]

Primary frequency control, known as inertial response, refers to the response of the system to frequency changes without changing the governor's reference values. In this stage of control only partially loaded generators participate. The time frame of this stage of frequency control is within in first tens of seconds following a disturbance [24].

Secondary frequency control refers to the action of the balancing reserve units that attempt to mitigate the frequency deviation through Automatic Generation Control (AGC). This control is typically performed by a centralized control system and requires changes in reference values in the governor system of individual turbines. This stage of control can take up to a few minutes to respond following a disturbance [24].

Tertiary control refers to actions that set the reference values for power generation in individual generating units based on the results from optimal dispatch to keep operating conditions normal with adequate spinning reserve available. This stage of control may be performed within 15 minutes following a disturbance [24].

It is important to note that it takes a few seconds until governor of generators sense the frequency drop and react and attempt to mitigate frequency deviation by curtailing power generation. A few seconds after governor response, the frequency deviation becomes ceased and an oscillating transient appears. Eventually, power and frequency are stabilized and reach a new steady state operating point [99], [24]. Figure 3.13 characterizes the frequency control in power systems.

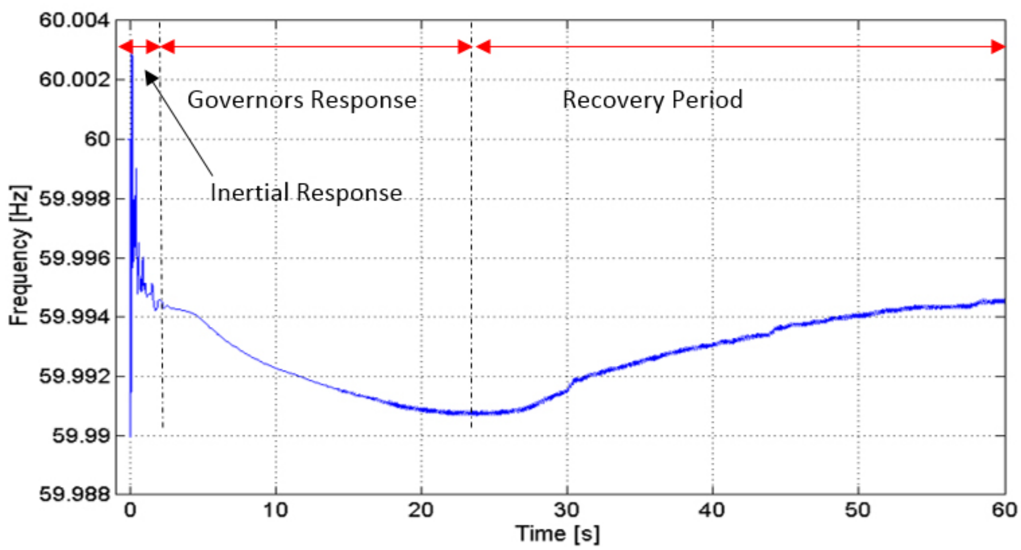

Figure 3.13: Frequency response characteristics

As shown in Figure 3.13, frequency response of a power system relies on inertial control to prevent an immediate collapse of the system and then load damping to keep the system stable and is highly dependent to the inertia of the system. The inertial response of a power system is generated by rotational mass of its generators and is an index of rotational kinetic energy that they can release [30]. In other words, the inertia of a power system is a measure for how the power system resists sudden changes in system frequency, and is highly dependent on the characteristics of the generators in the system.

In recent years, higher penetration of renewable energy units such as solar panels and wind turbines has raised the concern for dynamic stability of the power grids. This is because generation units such as solar panels and Type 4 wind turbines are connected to the grid through a power electronic interface which makes them fully isolated from the grid and Type 3 wind turbine are partially isolated from the grid. However, their power electronics interface by using advanced control functions may provide a similar frequency response to the grid as a conventional generator [31].

This study introduces a new frequency response metric for measuring frequency small signal stability of the power system to variability of the wind farms and intends to assess whether or not the system is capable to arrest initial frequency decline upon the disturbance before the governors sense the frequency deviation and react to it to prevent an unexpected disconnection of line or generator. This metric is useful for both events of increase and decrease in the level of power generation by offshore wind farm. This study is practical in generation and transmission planning and expansion studies.

As was mentioned in previous section, in this study, the changes in level of wind power were simulated by step changes. Normally, pace of change in wind speed is very moderate. However, the reason for choosing step changes to simulate wind variability was that wind gusts are the worst-case scenarios that in many occasions force to a sudden shut down of entire wind farm or a great part of it for safety reasons [96].

Mathematical Formulation

Small signal analysis is the base for small signal frequency response in power systems. Based on fundamental principle of physics, any unbalanced torque acting on the rotor will result in the acceleration or deceleration of the rotor. Therefore, the Newtons equation for rotation of an electrical machine could be written by:

$$J\frac{d\omega_m}{dt} + D_d\omega_m = \tau_m - \tau_e \tag{3.49}$$

where J is the total inertia of the turbine, ω_m the rotor shaft velocity, D_d damping torque coefficient and accounts for the mechanical rotational loss due to winding and friction, τ_m the torque produced by the turbine and τ_e the counter acting electromagnetic torque.

In steady state operation, the rotor shaft velocity remains constant. Therefore, the equation could be rewritten by:

$$\tau_m = D_d\omega_m + \tau_e \tag{3.50}$$

Since the inertial frequency response is interest of this study, it can be assumed that $D_d\omega_m = 0$. Then to describe steady state operation, it could be written:

$$\tau_m = \tau_e \tag{3.51}$$

The consequence of disturbance is determined by:

$$\begin{cases} Rotor\ Decelerates\ , & \text{if } \tau_m < \tau_e \\ Rotor\ Aecelerates\ , & \text{if } \tau_m > \tau_e \end{cases}$$

The disturbance torque, $\Delta\tau_{dst}$ could be defined by:

$$\Delta\tau_{dist} = \tau_m - \tau_e \tag{3.52}$$

Typically, during the small disturbances, the rotation speed remains close to the synchronous speed ω_{sm}. Accordingly, the Newtons equation could be rewritten by:

$$J\frac{d\omega_{sm}}{dt} = \Delta\tau_{dst} \tag{3.53}$$

$$J\omega_{sm}\frac{d\omega_{sm}}{dt} = \Delta P_{dist} \tag{3.54}$$

which ΔP_{dist} is the disturbance power. Replacing $J\omega_{sm} = \frac{2H \cdot S_n}{\omega_{sm}}$ into the previous equation produces:

$$\frac{2H \cdot S_n}{\omega_{sm}}\frac{d\omega_{sm}}{dt} = \Delta P_{dist} \tag{3.55}$$

where H represents the inertia and it quantifies the kinetic energy of the generator's rotor at synchronous speed in terms of the number of seconds it takes the generator to provide an equivalent amount of electrical energy, assuming that generate operates at its rated MVA [24]. Typical values of inertia constant for synchronous machine are in the range of 2 seconds to 10 seconds [100]. S_n is the rated power of the generator.

The electrical speed of the machine is defined by:

$$\omega_s = \frac{\omega_{sm}}{p} \tag{3.56}$$

where p refers to number of poles of the machine.

The Equation 3.55 could be rearranged by:

$$\frac{d\omega_s}{dt} = \frac{\Delta P_{dist}\omega_s}{2H \cdot S_n} \tag{3.57}$$

This equation describes dynamics of electrical rotor speed of the machine following a small disturbance.

The synchronous frequency of the system could be defined:

$$\omega_s = 2\pi f_s \tag{3.58}$$

Replacing Equation 3.58 in Equation 3.57 produces:

$$\frac{df_s}{dt} = \frac{\Delta P_{dst} \cdot f_s}{2H \cdot S_n} \tag{3.59}$$

The Equation 3.59 describes the frequency behavior following a small disturbance for a single machine. This behavior for a multi-machine system with i-generators could be described by:

$$\frac{df_s}{dt} = \frac{\Delta P_{dist} \cdot f_s}{2\sum_{n=1}^{i} H_i \cdot S_{n_i}} \tag{3.60}$$

where H_i and S_{n_i} correspond to inertia constant and nominal rated power of the i-th generator.

Time frame of inertial frequency response is very short so that allows to approximate $\frac{df_s}{dt} \approx \Delta f_s$. Then replacing this into 3.60 and rearranging it produce:

$$\frac{\Delta f_s}{\Delta P_{dist}} = \frac{f_s}{2\sum_{n=1}^{i} H_i \cdot S_{n_i}} \tag{3.61}$$

Equation 3.61 describes the primary frequency response of a multi-machine power system following a small disturbance. Accordingly, the primary frequency response of a system change following a small disturbance is a function of three major factors:

1. Inertia constant of the generators in the area
2. Power rating of the generators in the area
3. Nominal frequency of the system

Frequency Response Metrics

Frequency response metrics in the power industry are used to assess the frequency related performance of an interconnected system is based on the amount of lost generation to the resulting frequency drop in the system.

Frequency response is measured by MW per 0.1 Hz and typically for a loss of a generation unit and must be a negative for an interconnection to be stable. The negative sign is usually neglected and the metric is described as a positive value [99].

Common frequency response metrics in industry are defined by:

- **NERC Primary Frequency Response [101]:** This index is based on the amount of lost generation and the settling frequency and is given by:

$$NERCFR = \frac{Generation\ Loss \quad (MW)}{Frequency\ _{Pre-distrubance} - Frequency\ _{Settled} \quad (0.1Hz)} \tag{3.62}$$

- **LBNL Nadir-Based Frequency Response [53]:** This index is based on the amount of lost generation and the nadir frequency and is calculated by:

$$LBNLFR = \frac{Generation\ Loss \quad (MW)}{Frequency\ _{Pre-distrubance} - Frequency\ _{Nadir} \quad (0.1Hz)} \tag{3.63}$$

- **GE/CAISO Settling-Based Frequency Response [102]:** This index is based on the change in output of all active governors at the time of settling frequency and the settling frequency and is calculated by:

$$GESTLFR = \frac{Change\ in\ Output\ of\ All\ Active\ Governors\ _{Settling} \quad (MW)}{Frequency\ _{Pre-distrubance} - Frequency\ _{Settled} \quad (0.1Hz)} \tag{3.64}$$

- **GE/CAISO Nadir Based Frequency Response [102]:** This index is based on the change in output of all active governors at the time of nadir frequency and the nadir frequency and is calculated by:

$$GENDRFR = \frac{Change\ in\ Output\ of\ All\ Active\ Governors_{\ Nadir} \quad (MW)}{Frequency_{\ Pre-distrubance} - Frequency_{\ Nadir} \quad (0.1Hz)} \tag{3.65}$$

Approach of This Study

This section introduces the proposed frequency response metric for small-signal stability. In this study, the disturbance to the system is introduced to the system in form of a step change (decrease or increase) in level of power generation by the offshore wind farm. This is to examine the impact of wind power variability on frequency stability of the system.

The following measures were used in this study (these points refer to annotations in Figure 3.14 and Figure 3.15):

1. **Setlling Frequency**: Post-disturbance settling frequency (Point B)
2. **Nadir Frequency**: Minimum post-disturbance frequency (Point C)
3. **Frequency Swing Level:** Post-disturbance peak to peak frequency range (Point D to Point C)

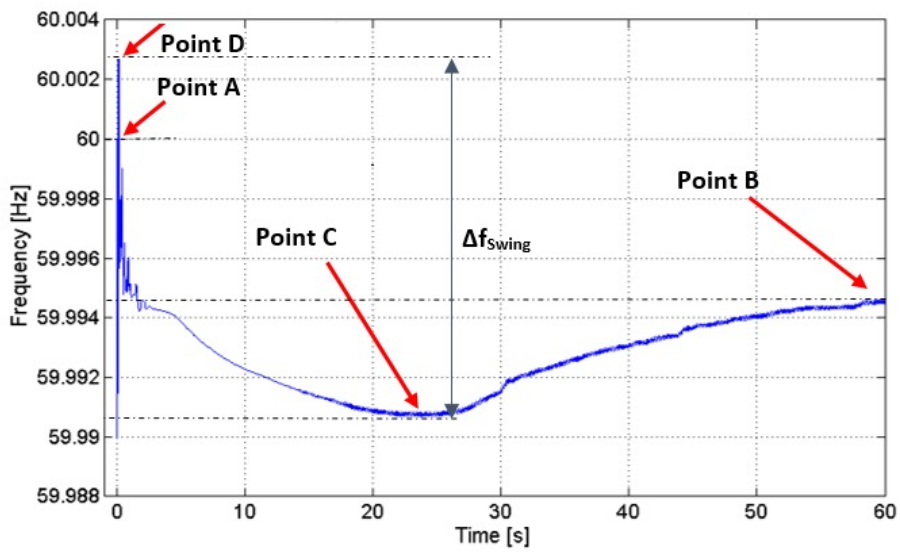

Figure 3.14: Sample frequency response following drop in generation

It is important to note that current studies in the power industry focus on frequency response following a loss of generation while this study focuses on effects of variability of wind power injections into the system. Thus, the industry metrics are not applicable to cases in which wind power increases. The following index was used in this study to assess the frequency response:

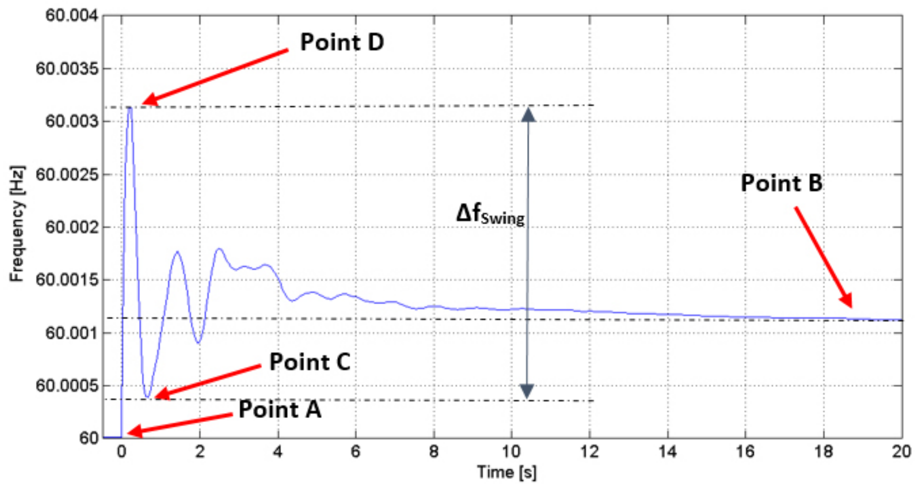

Figure 3.15: Sample frequency response following an increase in generation

- **Primary Frequency Response Index (PFRI)**:

$$PFRI = \frac{Change\ in\ Level\ of\ Wind\ Power\ Generation \quad (MW)}{Frequency\ Swing\ Level \quad (0.1Hz)} \tag{3.66}$$

The value for frequency swing following a decrease in wind power generation event indicates the difference between the nadir frequency and the area nominal frequency while following an increase in wind power generation it indicates the difference between the maximum frequency and the area nominal frequency. Larger absolute values of this index show a greater frequency response of the system.

3.4 Large Signal Stability Analysis

Large signal stability analysis addresses the dynamical behavior of the system following a large disturbance to assess whether or not it reaches a new equilibrium operational point [24]. The new equilibrium point attained following a fault may be same the pre-fault equilibrium point or a different equilibrium point.

A fault can be short term, such as short circuit faults on transmission lines or generators with a successful clearance, or long term, such as an outage of generation unit(s) or a disconnection of lines by protective relays after a failure in clearing the fault. In the case of short term faults, the systems post-fault topology remains unchanged (assuming that the fault is cleared within the critical clearing time), whereas, in the case of long term faults, the topology is changed.

The oscillations that are excited by the fault should be damped such that ringing decays within the first few cycles to few seconds following the fault. Otherwise, the transient behavior of the system may dominate the system response for sufficiently long that the system trajectory diverges from the stability region associated with the current equilibrium point and potentially lead to system-wide failures.

Transient stability is associated with dynamics of three main variables of the system:

- Rotor Angle
- Voltage
- Frequency

Rotor angle in a synchronous machine is an electrical angle that is defined by relative angle between rotor and stator magnetic fields. In an interconnected power system, power transfers across the transmission lines happen as a result of the angle difference at ends of the lines. Therefore, the synchronous generators should operate at a mechanical rotational speed so that produce the same electrical speed. This maintains the power flow steady across the system and is so called synchronism in power systems.

Following a severe fault, whether short term or long term, the generators in a power system may reset their operating point to a different operating point than prior to the fault. The change of operating point may result in change in rotor speed and angle. Consequently, change in rotor angle can change the level and direction of power flow among the lines and generators. Rotor angle stability in power systems refers to ability of synchronous machines in the system to maintain their synchronism following a disturbance [24], [32]. Figure 3.16 illustrates behavior of rotor angles in a stable power system following a fault.

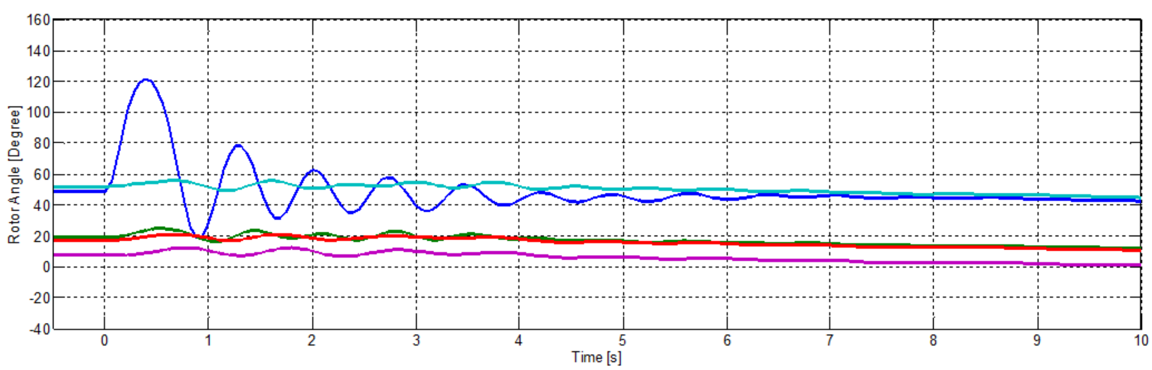

Figure 3.16: Rotor angles maintain their synchronism in a stable system following a severe fault

A power system is unstable if one or more generators rotor angle starts to deviate from their pre-fault values significantly relative to other angles. This is called loss of synchronism and leads to an unexpected disconnection of a unit(s) or line(s) from the grid which can cause interruption in power delivery and might lead to a blackout if sufficient contingency reserve units are not available in the area. Figure 3.17 illustrates behavior of rotor angles in an unstable power system following a fault.

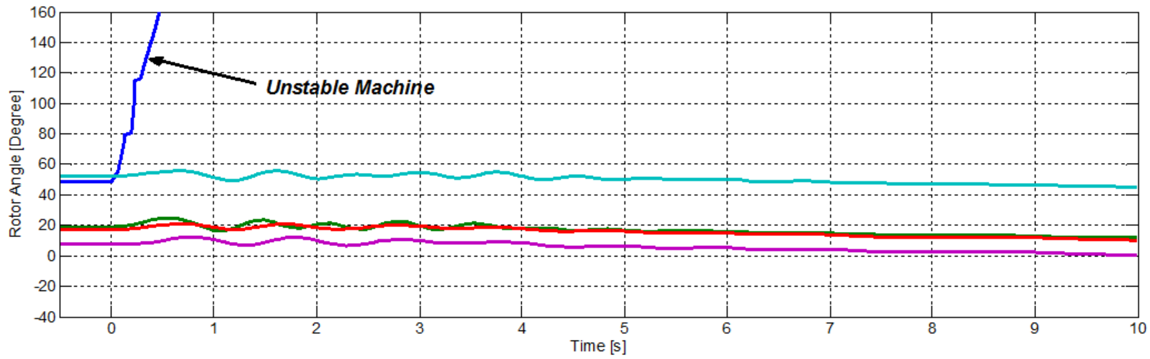

Figure 3.17: Rotor angles lose their synchronism in an unstable system following a severe fault

The longest clearing time that the system remains stable and none of the generators lose the synchronism, is called critical clearing time (CCT) [24]. In multi-machine systems, the CCT is calculated for each of component individually. Calculation of accurate CCT is critically important to set protective equipment appropriate to ensure reliability of power supply.

The objective of this section is to develop a methodology for transient stability analysis of power system for planning studies of offshore wind farm integration projects.

The contribution of this section is to determine relation among transient rotor angle stability, transient voltage stability and transient frequency stability, type and size of the faulted component and operation and variability of the offshore wind farm following all types of faults.

To reach this goal, both types of short term and long term faults were investigated under multiple pre-fault operational level of power generation by the offshore wind farm. The examined components consist of large capacity generator, medium capacity generators, transmission lines and offshore collector system.

3.4.1 Approach of This Study

In stability studies the rotor angle of synchronous machines is the center of the concern. Rotor angle of a machine in power system refers to the relative electrical angle between rotor and stator magnetic fields and in stability studies the electrical angle of synchronous machines is the objective.

The rotor angle and rotor speed are related by:

$$\Delta\omega_m = \frac{d\delta_m}{dt} \tag{3.67}$$

where $\Delta\omega_m$ and δ_m refer to mechanical rotor speed deviation and mechanical rotor anagle of the machine.

The relation between mechanical and electrical angles and speeds are given by:

$$\omega_e = \frac{p}{2}\omega_m \tag{3.68}$$

$$\delta_e = \frac{p}{2}\delta_m \tag{3.69}$$

where ω_e and ω_m refer to electrical rotor speed deviation and electrical rotor anagle of the machine and p represents number of its poles.

Swing equation of power systems is given by:

$$M\frac{d^2\delta_e}{dt^2} + D\frac{d\delta_e}{dt} = P_m - P_e \tag{3.70}$$

where M refers to angular momentum constant, D to damping constant and P_m and P_e to mechanical power on the shaft and electrical power transfer, respectively. Prior to the fault occurance, interconnected generators operate at the synchronous speed, ω_s so that:

$$\omega_e = \omega_s \tag{3.71}$$

$$\frac{d\delta_e}{dt} = 0 \tag{3.72}$$

$$\frac{d^2\delta_e}{dt^2} = 0 \tag{3.73}$$

$$P_m = P_e \tag{3.74}$$

As the fault occurs, electrical power transfer at the faulted machine becomes completely blocked, $P_e = 0$ with short circuit current being flown through the short circuit. Therefore, it becomes zero until fault is cleared. By assuming the damping factor is not a significant value during the severe fault, it could be neglected, $D = 0$. Then, the swing equation for this particular period of operation could be rewritten by:

$$M\frac{d^2\delta_e}{dt^2} = P_m = P_{acc} \tag{3.75}$$

$$\frac{d^2\delta_e}{dt^2} > 0 \tag{3.76}$$

$$\frac{d\delta_e}{dt} \neq 0 \tag{3.77}$$

where P_{acc} is an accelerating mechanical power on the rotor shaft. This shows that during this time, rotor angle begins to deviate from its pre-fault value, $\Delta\delta_e \neq 0$.

The machine rotor speed could be expressed by:

$$\frac{d\delta_e}{dt} = \Delta\omega \tag{3.78}$$

$$\Delta\omega \neq 0 \tag{3.79}$$

Equation 3.78 shows that following a fault, rotor speed begins to deviate from its steady state value. However, the immediate deviation, as the fault occurs, is not significant enough to make turbine governor operate, accelerating mechanical power, P_{acc}, is assumed constant during the fault period.

The angular momentum, M could be expressed by:

$$M = \frac{2HS_n}{\omega_s} \tag{3.80}$$

where H is inertia constant. As was discussed in previous section, (see small signal frequency response), the inertia constant is expressed in seconds and equalizes the kinetic energy of rotating mass of the rotor of synchronous speed at synchronous speed and equivalent amount of electrical energy when operating at the nominal MVA rating of the machine, S_n [24].

Replacing Equation 3.80 into Equation 3.75 produces:

$$\frac{d^2\delta_e}{dt^2} = \frac{\omega_s P_{acc}}{2HS_n} \tag{3.81}$$

In dynamic studies, it is assumed that prior to a disturbance the system operates at synchronous speed. Therefore, Equation 3.81 concludes that transient rotor angle stability is a function of:

1. System's inertia
2. Accelerating power of the fault
3. Capacity rating of the units

During the last decade, higher penetration of renewable energy sources in power systems such as solar panels and wind turbines has raised the concern for stability and dynamics of the power grids. This is because of the fact that renewable energy sources are integrated into the grid through a power electronic interface. This interface decouples them from the grid. Therefore, their contribution to the grid's inertia is not direct and mechanical. Adversely, it is unreliable and complicated and depends on the controller used in their power electronic interface [30]. This could make them unattractive due to the grid stability related concerns.

Following section introduces the methodology of transient stability analysis of power systems for planning studies of offshore wind farm integration projects.

Short Term Fault

1. The first step is to choose right components for undertaking the transient stability analysis. Equation 3.81 revealed that the transient stability of a power system is a function of the accelerating power during the fault. Thus, in planning studies for offshore wind farm integration the main criteria to choose the component for undertaking the stability analysis following short term faults should be based on the level of power that they generate or transmit. This

is to ensure the accelerating power during the fault is significant that makes the fault severe and allows capturing dynamics of the system. Therefore, the components maybe chosen by:

- **Large Capacity Generators**: Generators in the area with largest level of active power generation
- **Medium Capacity Generators**: Generators in the area with level of active power generation equal to approximately half of the area's largest generator
- **Transmission Lines**: Lines in the area with largest level of active power transfer
- **Offshore Collector System**: Half of the offshore collector system

2. The next step is to apply the short term faults were applied as separate events to each of these components (except to offshore collector system) in the system without any wind farm (so-called base case). The CCT is used to assess the rotor angle stability of the system. For each of the studied cases and applied faults, CCT must be computed to assess the transient rotor angle stability performance and identify the stability of margin of the system in each case.

3. The third step is to apply the faults to the components in the system with integrated wind farm. To examine the variability of the wind farm, the level of operation of the wind farm power must be shifted with credible steps throughout its full operational range. The step sizes should be chosen based on the planner's experience and preference. For each of the studied cases, applied faults and level of wind power, CCT must be computed to assess the transient rotor angle stability performance of the system in each case.

4. For assessing the transient voltage stability, following metrics must be computed for each of the studied cases, applied faults and level of wind power, including base case and cases with wind power:

   (a) **Transient Over-voltage (TOV):** Maximum post-disturbance voltage magnitude

   (b) **Transient Low-voltage (TLV):** Minimum post-disturbance voltage magnitude

   (c) **Settling Voltage (SV):** Eventual settling post-disturbance voltage magnitude

5. Frequency response metrics in the power industry are used to assess the performance of an interconnected system upon a contingency event and are based on relating the amount of lost generation to the resulting frequency change in the system. The frequency response of a multi-machine power system following a

disturbance was defined by:

$$\frac{\Delta f_s}{\Delta P_{dist}} = \frac{f_s}{2\sum_{n=1}^{i} H_i \cdot S_{n_i}} \tag{3.82}$$

which ΔP_{dist} is disturbance power, H_i and S_{n_i} correspond to inertia constant and nominal rated power of the i-th generator in the system, and f_s is the synchronous frequency of the system.

Common frequency response metrics in industry [101], [53], [102] are meant to assess capability of the system following an outage and not applicable for short term faults. Thus, in this study, Swing-Based Frequency Response (SBFR) index was defined as follows:

$$SBFR = \frac{Blocked\, Fault\; Power\; (MW)}{Frequency\, Swing\;\; (0.1Hz)} \tag{3.83}$$

This metric was calculated for each of the studied cases, applied faults and level of wind power, including base case and cases with wind power.

6. Finally, by comparing the results from the base case and the cases with different level of wind power, it can be found out how type and size of the faulted components and operation and variability of the wind farm influence on the transient stability of the power system following a short term fault.

Long Term Fault

Following section introduces the methodology of transient stability analysis of power systems for long term faults for planning studies of offshore wind farm integration projects.

1. In planning studies for offshore wind farm integration, the first and important step is to choose right components for undertaking the transient stability. The criteria to choose the components for undertaking the stability analysis following long term faults could rely on the results from analysis of short term fault. The first reason is that in previous section, it was shown that the transient stability of a power system is a function of the accelerating power during the fault. The components for undertaking the stability analysis following short term faults were chosen based on merit of greatest power generation or transmission. This is to ensure the accelerating power during the fault is significant that makes the fault severe and allows capturing dynamics of the system. The other reason is that the CCT was used to identify the rotor angle stability margin of the system. By associating these two reasons, it ensures that relying on the results from short term faults identifies the critical components. Therefore, the components for undertaking rotor angle stability analysis following long term faults were chosen by:

    - **Generators**: The generator with the least CCT

- **Transmission Lines**: The line with the least CCT
- **Offshore Collector System**: Half of the offshore collector system

2. First, an outage of each of these components (except to offshore collector system) should be applied to the system without any wind farm (base case).

3. Next, the faults should be applied to the components in the system with integrated wind farm. To assess influence of variability of the wind farm, the level of power generation by offshore wind farm power should be shifted with credible steps throughout its operational range. The step sizes should be chosen based on the planner's experience and preference.

4. For each of the studied cases and applied faults, the rotor angles, rotor speeds, voltages, active power and reactive power generations of all of the generators as well as the frequency in the area should be recorded.

5. To assess the rotor angle stability of the system, the maximum rotor angle difference deviation in the area should be computed. This shows whether or not the system has been able to maintain its synchronism. In a stable power system, the maximum rotor angle difference deviation should settle approximately at zero within a first few seconds following a fault.

6. For assessing the transient voltage stability, introduced metrics of TOV, TLV and SV (see the previous section) could be computed for each of the studied cases, applied faults and level of wind power, including base case and cases with wind power.

7. In previous section, Swing-Based Frequency Response (SBFR) index was defined. This metric could be used for each fault and level of wind power in the studied cases including base case and cases with wind power.

8. Finally, by comparing the results from each level of wind and base case, the relation between the faulted components and operation and variability of the wind farm and their influence on transient stability of the power system following a long term fault would be observed.

Chapter 4

Case Study: FirstEnergy/PJM Power System

4.1 FirstEnergy/PJM Power System

PJM is a Regional Transmission Organizations (RTO) in the Midwestern United States and is part of the Eastern Interconnection grid operating an electric transmission system that spans 13 states: Delaware, Illinois, Indiana, Kentucky, Maryland, Michigan, New Jersey, North Carolina, Ohio, Pennsylvania, Tennessee, Virginia, West Virginia and the District of Columbia. The PJM service territory is shown in Figure 4.1.

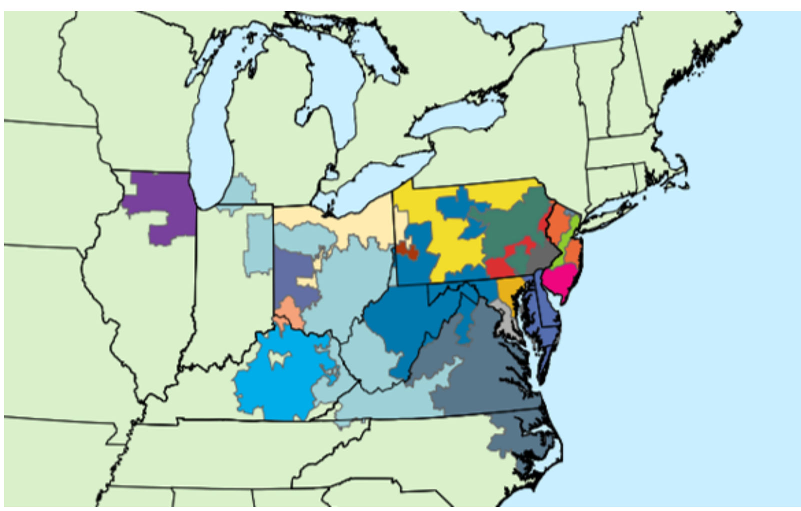

Figure 4.1: Map of PJM service territory [103]

FirstEnergy is the regional utility company, based in Akron, Ohio, within a geographical sub-region of PJM serving 6 million customers within Ohio, Pennsylvania, West Virginia, Virginia, Maryland, New Jersey and New York. Figure 4.2 shows the FirstEnergy service territory.

The power generation dispatch and load consumption in FirstEnergy/PJM area

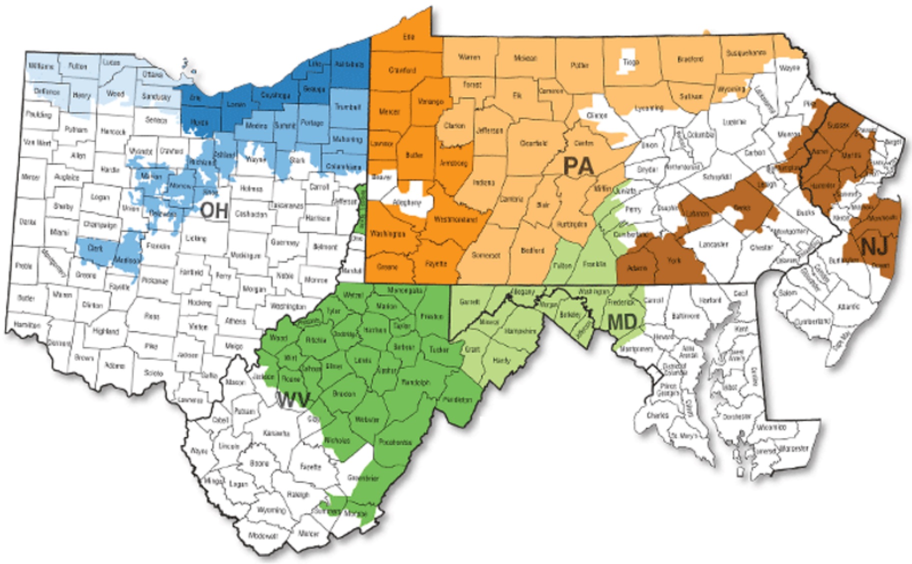

Figure 4.2: Map of FirstEnergy territory [104]

and the operating status of the synchronous condensers and SVC for the base cases are shown in Tables 4.1 and 4.2

Table 4.1: FirstEnergy Area Generation Dispatch (MW) [22]

GENERATION	**Summer Load Data**	**Winter Load Data**
BRUCE MANSFIELD UNITS 1–3	2,375	2,497.8
W.H. SAMMIS UNITS 1–7	2,156	1,483.2
PERRY NUCLEAR	1,202	0
DAVIS BESSE NUCLEAR	855	940
FREMONT COMBINED CYCLE	653	0
AVON LAKE UNIT 7 & UNIT 9	0	758
LEMOYN UNITS 1	572	0
WEST LORAIN GT 2–6	406	0
RICHLAND UNITS 1–6	369	0
BAYSHORE UNIT 1	130	153
CLARK UNITS A & B	48	0
EASTLAKE UNIT 6	23	0
STRYKER CT	16	0

4.2 Estimation of Offshore Wind Energy Generation

Wind power estimation and the geographical locations of wind availability in Lake Erie were provided by NREL, and five possible points of interconnection (substations near the shoreline) in the FirstEnergy transmission grid were identified by GE. Figure

Table 4.2: FirstEnergy Dynamic Reactive Devices (MVAr) [22]

GENERATION	**Summer Load Data**	**Winter Load Data**
EASTLAKE SYNCH COND 1	-7.7	14.1
EASTLAKE SYNCH COND 2	-7.7	14.1
EASTLAKE SYNCH COND 3	-7.7	14.1
EASTLAKE SYNCH COND 4	-18.9	34.5
EASTLAKE SYNCH COND 5	-4.1	26.2
LAKESHORE SYNCH COND 18	-35.9	-14.4
NEWCASTLE SVC	0	0

4.3 shows the selected locations and Table 4.3 illustrates the minimum distances from the nearest possible interconnection point to FirstEnergy substations. These values were determined using Google Earths ruler feature [22].

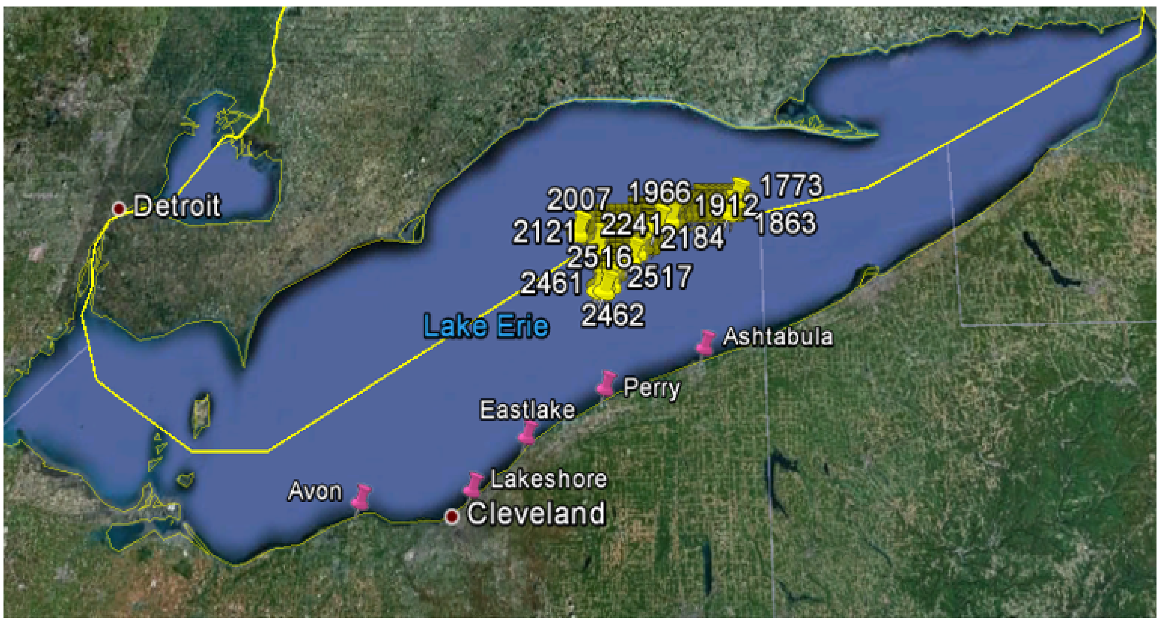

Figure 4.3: Offshore wind farm sites selected for 1000 MW Lake Erie Wind Farm [22]

Table 4.4 illustrates the 10-minute assessment for expected changes in power generation in Lake Erie, provided by NREL.

4.3 Wind Power Integration Scenario Development

Initially, there were seven feasible possible interconnection scenarios proposed that would fit the current grid infrastructure. After team discussions, it was agreed to consider the following scenarios for offshore wind power integration into the FirstEnergy/PJM system for further analysis and investigations:

Table 4.3: Minimum Distance from Offshore Wind Farm to FirstEnergy Substations, provided by GE [22]

FirstEnergy Substation	Miles	Kilometers
ASHTABULA 345 kV SUBSTATION	21.0	33.8
PERRY 345 kV SUBSTATION	17.4	28.0
EASTLAKE 345 kV SUBSTATION	29.6	47.6
LAKESHORE 138 kV SUBSTATION	43.2	69.4
AVON 345 kV / 138 kV SUBSTATIONS	59.2	95.2

Table 4.4: Expected 10-Minute Intermittency for 1000 MW Lake Erie Wind Plant, determined by NREL [22]

Expectation	Frequency	Drop Level	Rise Level
—	Once in 3 Years	360 MW	361MW
99.9%	Once Every 2 Weeks	136	171MW
99.0%	Once Every 1.5 Days	72MW	81MW
95.0%	Four Times Per Day	41MW	44MW
90.0%	Eight Times Per Day	30MW	31MW

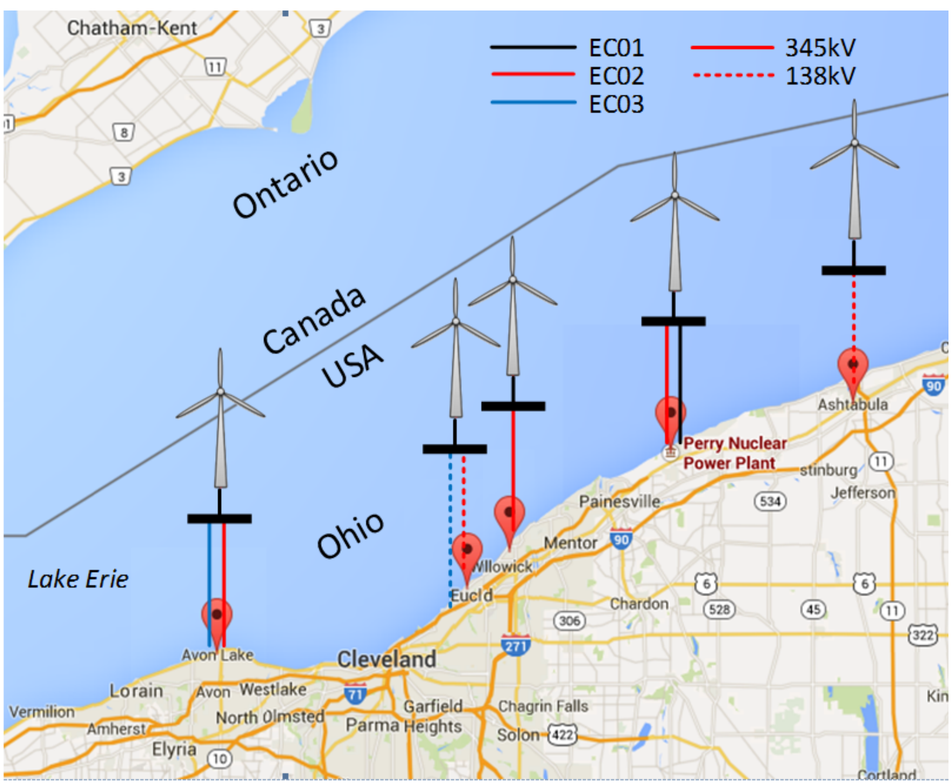

Figure 4.4: Map of Interconnection Scenarios into the FirstEnergy System

1. Interconnecting a 1000 MW of offshore wind generation at the Perry 345 kV Substation, referred to as **EC01**

2. Interconnecting five cables 200 MW each of offshore wind generation, at the Avon 345 kV Substation, at the Lakeshore 138 kV Substation, at the Eastlake 345 kV Substation, at the Perry 345 kV Substation and at the Ashtabula 138 kV Substation, referred to as **EC02**

3. Interconnecting two cables of 500 MW each of offshore wind generation, at the Avon 345 kV Substation and the Lake Shore 138 kV Substation, referred to as **EC03**

The POIs and integration scenarios are illustrated in Figure 4.4.

4.4 Offshore Wind Farm Model Development and Computer Modeling

The offshore wind farm consists of a generator, a step-up transformer, a collector system, export cables and SVCs.

4.4.1 Wind Turbine

Wind farms normally consist of a large number of individual wind turbine generators. The wind farm model may consist of a detailed representation of each wind turbine generator and collector system. However, a single machine model to represent all of the wind farm machines is appropriate for most bulk system studies [22]. Thus, an aggregated model that includes a conventional generator connected to a PV bus for the offshore system was used for the steady state study. Figure 4.5 shows the model in GE PSLF and Table 4.5 describes the models details.

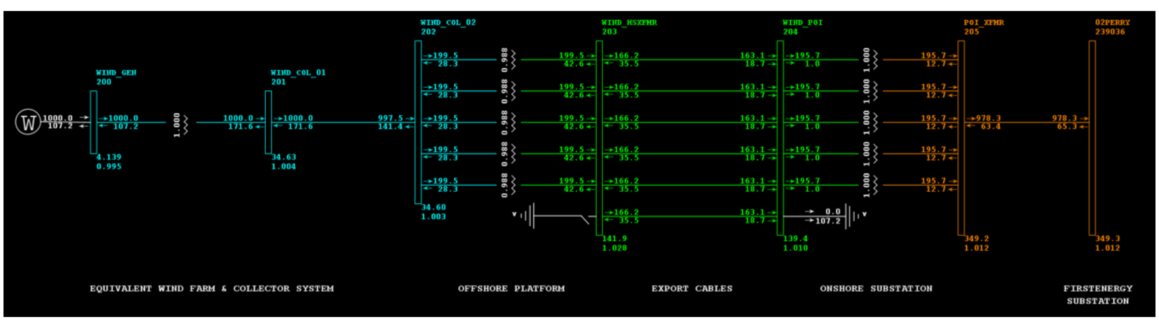

Figure 4.5: Model of 1000 MW wind farm interconnection at Perry 345 kV for steady state analysis in GE PSLF

In Table 4.5, $R00$ corresponds to a machine with no reactive support capability, $R01$ to machine with limited reactive support capability (-7.5% / 7.5%), and $R02$ to machine with full reactive support capability (-43.0% / +57.8%).

Table 4.5: Equivalent Generator Model Data [22]

Scenario		**EC01**	**EC02**	**EC03**
Size of the Wind Turbine in Computer Model		1x1000MW	1x500MW	1x200MW
Total Number of Wind Turbines		278	139	56
Generator Rating (MVA)		1,112	556	224
Maximum Power Capacity (MW)		1000.8	500.4	201.6
Minimum Power Capacity (MW)		44.48	22.24	8.96
R00	Maximum Reactive Power Capacity (MVAr)	0	0	0
	Minimum Reactive Power Capacity (MVAr)	0	0	0
R01	Maximum Reactive Power Capacity (MVAr)	75.06	37.5	15.00
	Minimum Reactive Power Capacity (MVAr)	-75.06	-37.5	-15.00
R02	Maximum Reactive Power Capacity (MVAr)	578.24	289.12	116.48
	Minimum Reactive Power Capacity (MVAr)	-430.9	-215.45	-86.8

In steady state analysis, the minimum power capacity of the turbines in computer models were reset to 0MW. This was to model a complete range of power generation by offshore wind farm from 1000MW to 0MW. However, in dynamic analysis, the minimum power capacity remained as stated in Table 4.5.

The values for wind turbine used in this study rely on a GE 3.6 MW offshore wind turbine, as shown in Table 4.6.

Table 4.6: Specifications of Offshore GE Wind Machine [22]

Parameter	**Value**
Generator Rating	4 MVA
Maximum Real Power Output	3.6 MW
Minimum Real Power Output	0.16 MW
Maximum Reactive Power Capability	2.08 MVAr
Minimum Reactive Power Capability	-1.55 MVAr
Terminal Voltage	4.16 kV
Pad Mounted Transformer Rating	4 MVA
Pad Mounted Transformer Impedance (Z)	7.0%
Typical Collector System Resistance (based on MW rating of wind farm)	0.25%

Dynamic analysis models to represent the wind turbine generators were developed for Type 3 only. This decision was based on NERC and generally accepted practices by North American utilities that recommend new wind interconnections have reactive capability provided by the machines themselves [22].

The original power flow model was modified to represent 2x500 MW paths for the dynamic simulations studies. The equivalent wind farm and collector system could then be partitioned to simulate different offshore wind variability scenarios. Figure 4.6 shows the model with two machines and collector systems in GE PSLF for the dynamic studies [22].

The dynamic scenarios aimed to investigate the impact of variability of the wind generation on stability of the system. The dynamic wind turbine models used in this

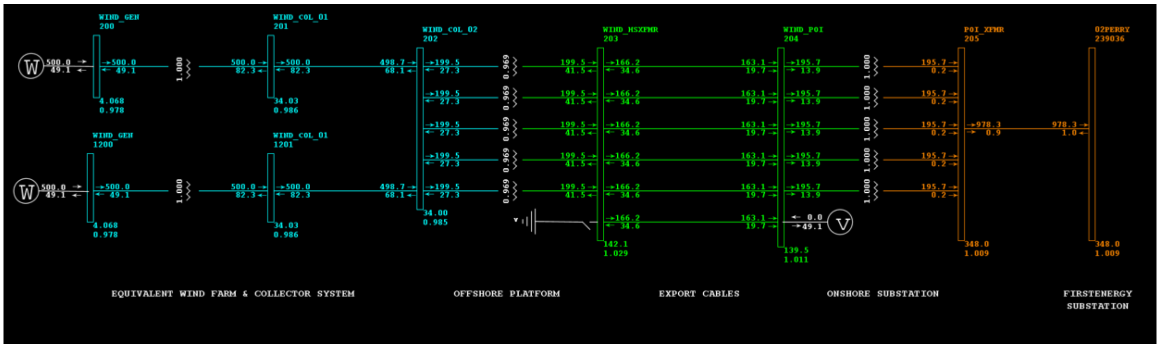

Figure 4.6: Model of 1000 MW wind farm with two separated collector systems - interconnection at Perry 345 kV for dynamic analysis in GE PSLF

analysis are not able to provide step changes in generation output during the simulations. Thus, load models were added to the terminals of the wind machines. The loads can then be turned on/off and sizes of the loads are matched to the magnitudes of the step changes that are to be introduced at the terminals of the machine. The loads simulate the variability of the wind farm. Figure 4.7 shows the model with a machine and a load installed at each platform for two separated collector systems in GE PSLF for the dynamic studies.

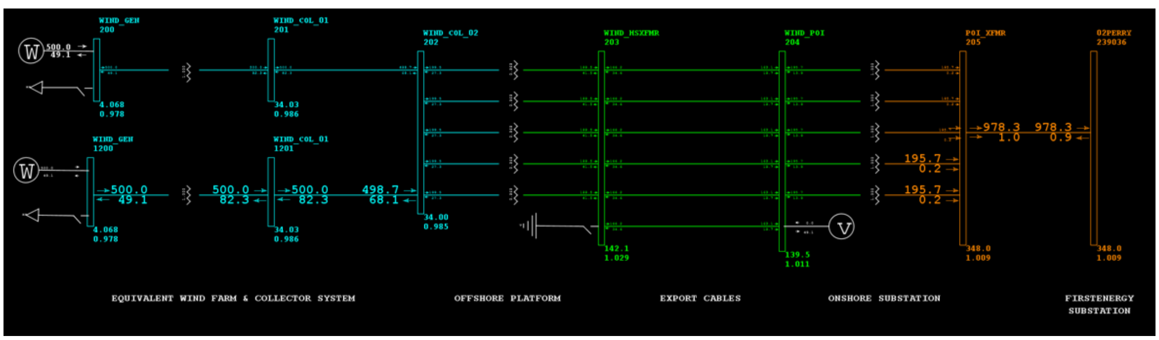

Figure 4.7: Model of 1000 MW Wind farm with two separated collector system and a controllable load in parallel with each wind machine - interconnection at Perry 345 kV for dynamic analysis in GE PSLF

The dynamic models of the offshore wind generation system were represented as defined in the GE PSLF model library [23]:

- *wndtge:* The wind turbine and turbine control model for GE DFIG wind turbines
- *gewtg:* The generator/converter model for GE DFIG wind turbines
- *exwtge:* The excitation (converter) control model for GE DFIG wind turbine generators

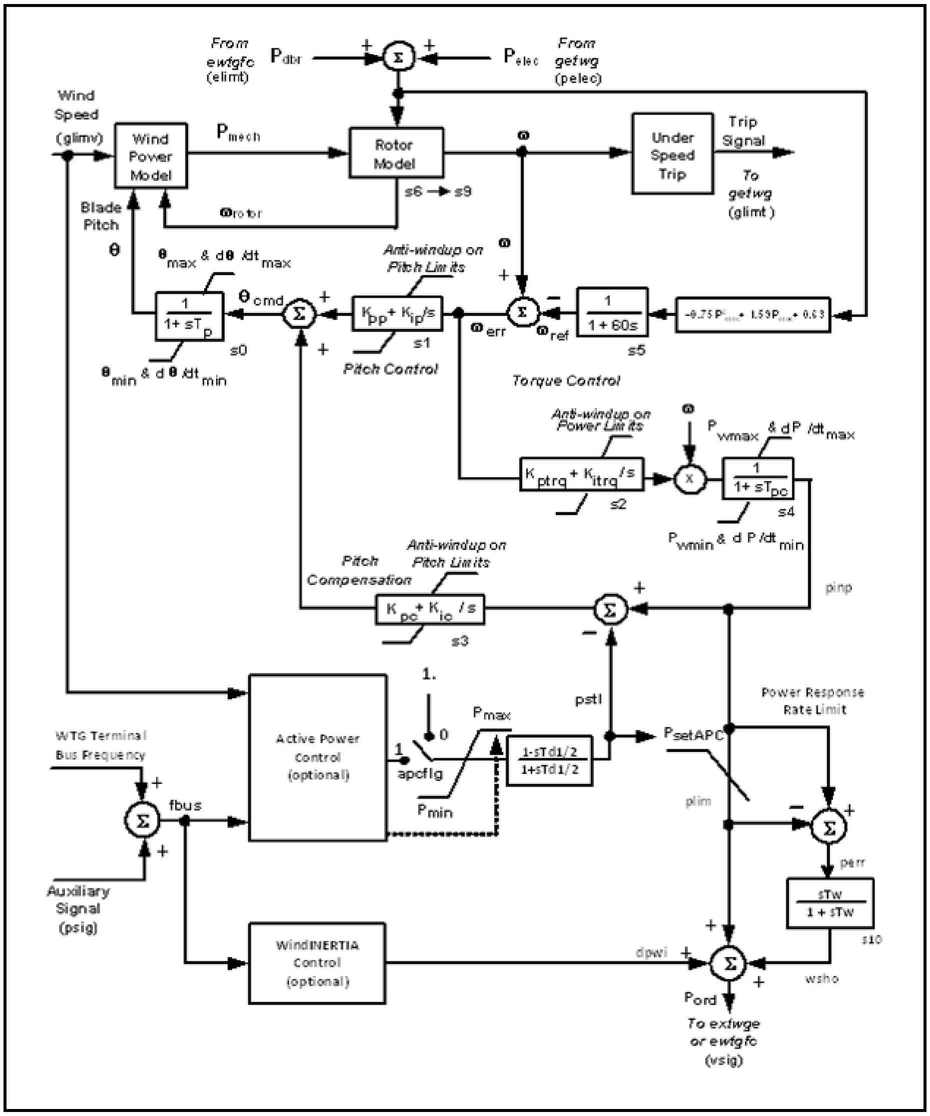

Figure 4.8: Block diagram for PSLF wind turbine and turbine control model *wndtge* [23]

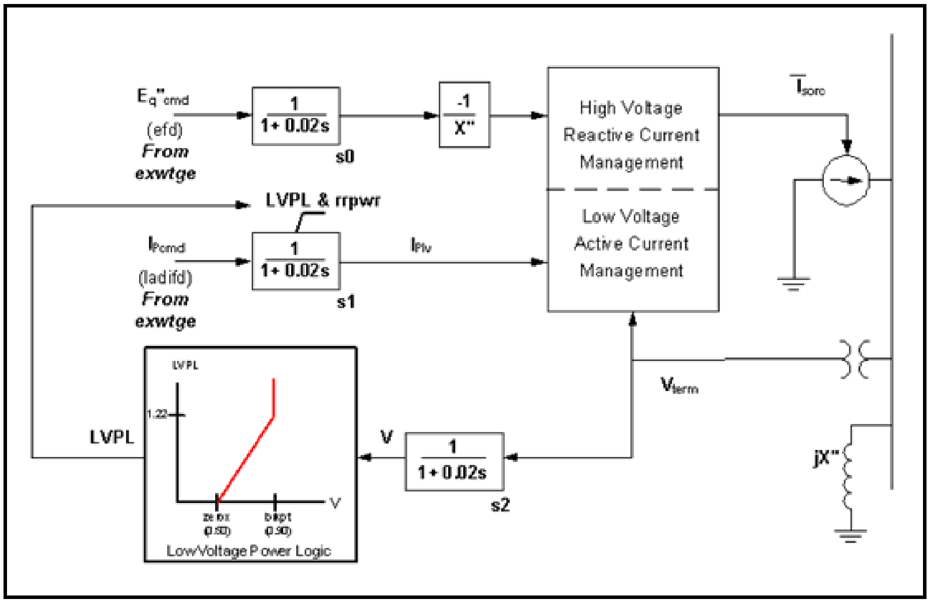

Figure 4.9: Block diagram for PSLF generator/converter model *gewtg* [23]

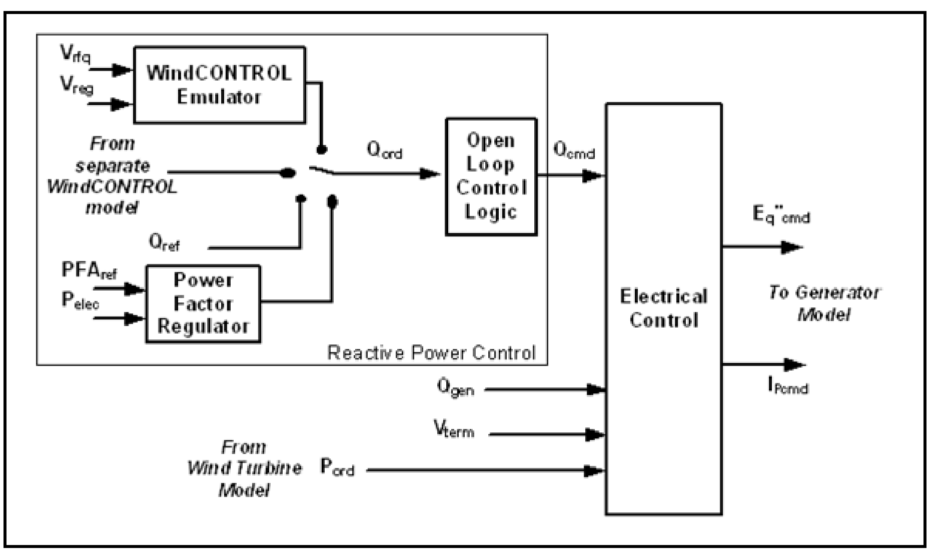

Figure 4.10: Block diagram for PSLF excitation (converter) control model *exwtge* [23]

More information about these models is available in GE PSLF documentation [23].

4.4.2 Equivalent Step-Up Transformer

In the models, the equivalent wind turbine generator is connected to the collector system via a step-up transformer with specifications equivalent to a typical unit pad-mounted transformer ratings and impedances for standard industry equipment, as shown in Table 4.7.

Table 4.7: Equivalent Step-Up Transformer Data [22]

Scenario	**EC01**	**EC02**	**EC03**
Size of Every Machine	1x1000MW	1x500MW	1x200MW
Total Number of Wind Turbines	278	139	56
Transformer Rating (MVA)	1,112	556	224
X (p.u.)	0.07	0.07	0.07
Low Voltage Rating (kV)	4.16	4.16	4.16
High Voltage Rating (kV)	34.5	34.5	34.5
No Load Tap Positions Available	±2.5%	±2.5%	±2.5%
Fixed Tap Position on H.V. Side (p.u.)	1.00	1.00	1.00

In Table 4.7, p.u. units are calculated based on relative transformer MVA base.

4.4.3 Equivalent Collector System

A typical collector system voltage of 34.5 kV was used in the models. The substation transformer would be suitably rated for the number of wind turbine generators, with impedance of typically around 8%. The equivalent offshore wind farm collector system model data is presented in Table 4.8.

Table 4.8: Equivalent Collector System Data [22]

Scenario	**EC01**	**EC02**	**EC03**
Size of Every Machine	1x1000MW	1x500MW	1x200MW
Collector System Voltage Rating (kV)	34.5	34.5	34.5
R (p.u.)	0.00025	0.00050	0.00125
X (p.u.)	0.00100	0.00200	0.00500
B (p.u.)	0.40000	0.20000	0.08000

In Table 4.8, p.u. units are calculated based on 100 MVA base.

4.4.4 Compensation Device

In this study, a SVC with a significant compensation capacity was used and modeled for compensation device at the POIs. This allows assessing the capacity of the compensation device that may be required to provide ancillary service to the grid by looking at the level of reactive power generated/consumed by the SVC.

During steady state analysis, the SVC was modeled as a controllable shunt device. This allowed for automatic voltage control during load flow simulations and the device was modeled to regulate voltage at the POI [22].

In dynamic stability studies, GE PSLF requires that the device be modeled as a voltage independent generator model. Therefore, steady state scenarios with a SVC were modified to include a load flow generator model dispatched with similar reactive capability and no real power output [22].

The dynamic model used to represent these devices was the simple Static VAr device *vwscc* in GE PSLF model library [23]. This analysis looked at a maximum and minimum SVC rating size of ±500 MVAr.

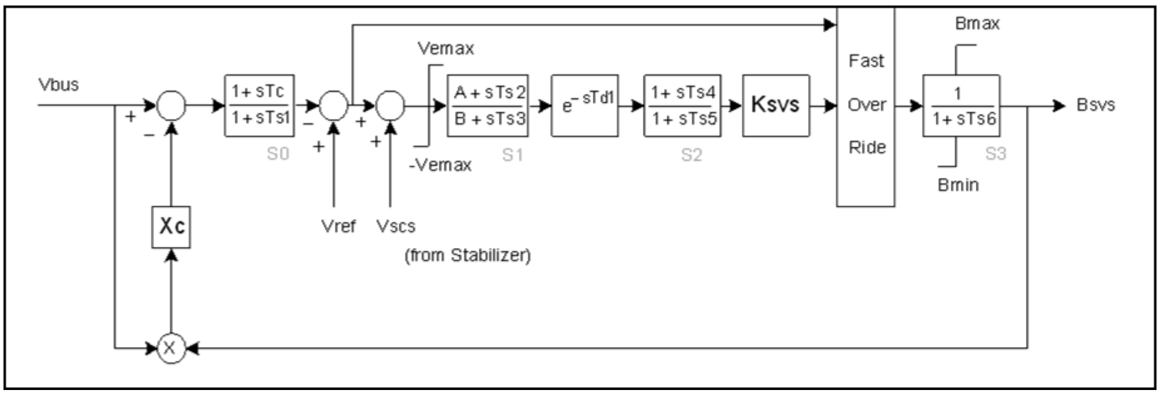

Figure 4.11: Block diagram for PSLF SVC control model *vwscc* [23]

4.5 Generation Dispatch Scenarios and Load Assumptions

For steady state and dynamic analysis in this investigation, two generation dispatch and load profiles for the Eastern Interconnection were modeled in PSLF:

1. **Summer peak load for steady state analysis:**: contains 68859 system buses, 9091 generators with a total of 936,266 MW and 444,200 MVAr of installed generation capacity to serve the load of 685,469 MW and 201,005 MVar.

2. **Winter light load for dynamic stability analysis:** contains 63608 system buses, 8356 generators with a total of 894,772 MW and 411,288 MVAr of installed generation capacity to serve load of 302,086 MW and 75,596 MVar.

System base case models specifications are summarized in Table 4.9.

The main objective of this case study was integration of 1000MW offshore wind power generation into the FirstEnergy/PJM system. The second objective was to

Table 4.9: Specifications of Eastern Interconnection Models Used as Base Case

GENERATION	**Peak Load**	**Light Load**
Number of Buses	68,859	63,608
Number of Generators	9,091	8,356
Installed Generation Capacity (MW)	936,266	894,772
Installed Generation Capacity (MVAr)	444,200	411,288
Load Consumption (MW)	685,469	302,086
Load Consumption (MVAr)	201,005	75,596

consider impacts of lack of operation of Perry Power Plant, a major conventional power plant with capacity of 1200MW and 625MVAr. Thus, the generation units in the area were relatively redispatched to maintain the balance between generation and consumption in the area for each of the developed interconnection scenarios.

4.6 Contingency List

FirstEnergy provided a condensed contingency list that included generation units, transformers, line segments, complete lines, and synchronous condenser outages. This list was used to perform the contingency analysis. The full list of contingencies is shown in Tables 4.10 through 4.15.

Table 4.10: List of 345 kV Transmission Line Outages (Breaker-to-Breaker)

Event ID	Contingency Event Description
1	Loss of Avon to Juniper 345 kV Transmission Line
2	Loss of Avon to Beaver 345 kV Transmission Line Circuit 1
3	Loss of Avon to Beaver 345 kV Transmission Line Circuit 2
4	Loss of Fox to Harding 345 kV Transmission Line Circuit 1
5	Loss of Fox to Harding 345 kV Transmission Line Circuit 2
6	Loss of Harding to Juniper 345 kV Transmission Line
7	Loss of Harding to Inland 345 kV Transmission Line
8	Loss of Harding to Leroy Center 345 kV Transmission Line
9	Loss of Leroy Center to Perry 345 kV Transmission Line
10	Loss of Harding to Chamberlin 345 kV Transmission Line
11	Loss of Juniper to Northfield 345 kV Transmission Line
12	Loss of Northfield to Eastlake 345 kV Transmission Line
13	Loss of Juniper to Star 345 kV Transmission Line
14	Loss of Juniper to Hanna 345 kV Transmission Line
15	Loss of Inland to Northfield 345 kV Transmission Line
16	Loss of Northfield to Perry 345 kV Transmission Line
17	Loss of Eastlake to Perry 345 kV Transmission Line
18	Loss of Bruce Mansfield to Northfield 345 kV Transmission Line
19	Loss of Three-Terminal 345 kV Transmission Line: Perry at Erie West
20	Loss of Davis Besse to Beaver 345 kV Transmission Line
21	Loss of Hayes to Beaver 345 kV Transmission Line
22	Loss of Bruce Mansfield to Hanna 345 kV Transmission Line
23	Loss of Beaver to Carlisle 345 kV Transmission Line
24	Loss of Beaver to West Lorain Plant 345 kV Transmission Line

Table 4.11: List of Planned 345/138 kV Transformer Outages

Event ID	**Contingency Event Description**
25	Loss of Avon 345 / 138 kV Transformer 91
26	Loss of Avon 345 / 138 kV Transformer 92
27	Loss of Fox 345 / 138 kV Transformers 2 & 3
28	Loss of Fox 345 / 138 kV Transformer Q11
29	Loss of Fox 345 / 138 kV Transformer Q12
30	Loss of Fox 345 / 138 kV Transformer Q13
31	Loss of Fox 345 / 138 kV Transformer Q14
32	Loss of Fox 345 / 138 kV Transformers 4 & 5
33	Loss of Harding 345 / 138 kV Transformer Q12
34	Loss of Harding 345 / 138 kV Transformer Q13
35	Loss of Juniper 345 / 138 kV Transformers 4 & 5
36	Loss of Juniper 345 / 138 kV Transformer 4
37	Loss of Juniper 345 / 138 kV Transformer 5
38	Loss of Juniper 345 / 138 kV Transformer 6
39	Loss of Juniper 345 / 138 kV Transformer 3
40	Loss of Inland 345 / 138 kV Transformer 4
41	Loss of Eastlake 345 / 138 kV Transformer 61
42	Loss of Eastlake 345 / 138 kV Transformer 62
43	Loss of Ashtabula 345 / 138 kV Transformer 8
44	Loss of Leroy Center 345 / 138 kV Transformer 1
45	Loss of Leroy Center 345 / 138 kV Transformer 4

Table 4.12: List of Planned 345 kV Transmission Line Segments (Open Breaker)

Event ID	**Contingency Event Description**
46	Loss of Perry to Ashtabula 345 kV Line Segment
47	Loss of Ashtabula to Erie West 345 kV Line Segment

Table 4.13: List of Planned 138 kV Transmission Line Outages (Breaker-to-Breaker)

Event ID	**Contingency Event Description**
48	Loss of Beaver to Black River 138 kV Transmission Line
49	Loss of Beaver to Ford 138 kV Transmission Line
50	Loss of Beaver to Johnson 138 kV Transmission Line
51	Loss of Beaver to Henrietta 138 kV Transmission Line
52	Loss of Beaver to NASA 138 kV Transmission Line
53	Loss of Beaver to West Lorain Plant 138 kV Transmission Line
54	Loss of Carlisle to Lorain Q4 138 kV Transmission Line
55	Loss of Black River to Lorain Q2 138 kV Transmission Line
56	Loss of West Akron to Pleasant Valley Q2 138 kV Transmission Line
57	Loss of West Akron to Hickory Q21 138 kV Transmission Line

Table 4.14: List of Planned Generation Outages

Event ID	**Contingency Event Description**
58	Loss of Avon Unit 9

Table 4.15: List of Planned Synchronous Condenser Outages

Event ID	Contingency Event Description
59	Loss of Eastlake Unit 1
60	Loss of Eastlake Unit 2
61	Loss of Eastlake Unit 3
62	Loss of Eastlake Unit 4
63	Loss of Eastlake Unit 5
64	Loss of Lakeshore Unit 18

Chapter 5

Computational Implementation of Analytical Tools

5.1 Steady State Stability Analysis

Computational implementation of steady state analysis was carried out using sensitivity analysis. Steady state analysis is the first step in power system planning studies. Thus, all of the possible wind integration scenarios should be considered. Accordingly, in this project, 36 case studies were developed for each of interconnection scenarios (EC01, EC02 and EC03). The description of these cases is shown in Table 5.1.

First, accurate models of FirstEnergy/PJM were provided. Then, cases for each of the scenarios were developed and integrated in the base case models. After loading the system, generation dispatch and load data, the wind models were initiated. GE PSLF Version 18.1_01 80K, SSTOOLS simulation tool, was used to carry out this part of this study.

For each studied cases, the wind power generation was shifted from 100% capacity to 0% by steps of 1%. Through every step change in wind power generation, other non-wind generator units in FirstEnergy area were redispatched to pick up missing generation of the wind farm. Then a power flow calculation was computed.

The results of the power flow for each 1% of wind power variability from all transmission lines, generation units and substations in the FirstEnergy operating territory were recorded. These results from two data sets for each step of shift:

- The first data set contains information about voltage magnitudes of the busbars.
- The second data set contains information about power flow of the transmission lines.

In an ideally stable power system, voltage magnitudes across the system are regulated at 1.0 p.u. This forms a voltage regulation data for this system with identical measures of mode, mean and median of 1 and estimated density function of normal distribution. As the voltage magnitudes across the system begin to deviate from 1.0 p.u. and spread out within a wider range, these measures start to vary. As a result, distribution density function begins to deviate from normal distribution. Based on

Table 5.1: List of Studied Cases in Steady State Analysis

Case No.	Voltage Regulation	Reactive Capability	SVC	Perry
1	Terminals of machines	0MVAr	OFF	ON
2	POI			
3	Collector system			
4	Terminals of machines	-7.5%/+7.5%MVAr		
5	POI			
6	Collector system			
7	Terminals of machines	-43.0%/+57.8%MVAr		
8	POI			
9	Collector system			
10	Terminals of machines	0MVAr	ON	
11	POI			
12	Collector system			
13	Terminals of machines	-7.5%/+7.5%MVAr		
14	POI			
15	Collector system			
16	Terminals of machines	-43.0%/+57.8%MVAr		
17	POI			
18	Collector system			
19	Terminals of machines	0MVAr	OFF	OFF
20	POI			
21	Collector system			
22	Terminals of machines	-7.5%/+7.5%MVAr		
23	POI			
24	Collector system			
25	Terminals of machines	-43.0%/+57.8%MVAr		
26	POI			
27	Collector system			
28	Terminals of machines	0MVAr	ON	
29	POI			
30	Collector system			
31	Terminals of machines	-7.5%/+7.5%MVAr		
32	POI			
33	Collector system			
34	Terminals of machines	-43.0%/+57.8%MVAr		
35	POI			
36	Collector system			

this notion, to analyze each data set and process them to reveal meaningful information, following statistical approach were used:

1. First, KDE was applied to each of the data sets to smooth the data and estimate the density function of each data set with an equal weight for all data points. The outcome of this smoothing shows how variability of wind power would effects on voltage regulation and loading levels for each of the studied cases.

2. The next step was to calculate values of maximum, minimum, mode, mean and median of each of the new data sets.

3. The last step was to compare the data sets to the normal distribution to determine whether the data follow a normal distribution. The outcome of this comparison provides information about the probability of any given operating condition, for voltage regulation and line loading level in respect to variability of the wind throughout full operation range of the offshore wind farm.

Then all of the data sets of voltage regulation from all levels of wind power were merged to form a single set of data of lines voltage. Similarly, data sets of power flow from all levels of wind power were merged. The new two sets of data consist of all possible voltage magnitude and power flow data for the system and cover the complete range of operating points for the system. Then, three aforementioned steps were repeated for the new data.

5.2 Steady State Contingency Analysis

Computational implementation of contingency analysis was similar to steady state analysis and was carried out by sensitivity analysis. This analysis is the step after steady state operation analysis in planning studies. Thus, based on the findings from steady state analysis, the integration scenarios in this step may be narrowed down.

In this project, the results from steady state analysis revealed that the point of voltage regulation in the offshore system does not affect the voltage regulation across the transmission system. In addition, FirstEnergy recommended that regulation of voltage for the offshore wind farm should be set at the wind farm POI, onshore, to avoid reactive power injection into the FirstEnergy/PJM grid.

Accordingly, in this project, 12 case studies were chosen for each of interconnection scenarios (EC01, EC02 and EC03) to undertake contingency analysis. The description of these cases is shown in Table 5.2.

First, accurate models of FirstEnergy/PJM were provided. Then, these cases for each of the scenarios were developed and integrated in the FirstEnergy/PJM models. After loading the system, generation dispatch and load data, the wind models were initiated. GE PSLF Version 18.1_01 80K, SSTOOLS simulation tool, was used to carry out this part of this study.

For each of the studied cases, the wind power generation was shifted from 100% capacity to 0% by steps of 10%. Then a power flow calculation was performed. For

Table 5.2: List of Studied in Steady State Contingency Analysis

<table>
<tr><th>Case No.</th><th>Voltage Regulation</th><th>Reactive Capability</th><th>SVC</th><th>Perry</th></tr>
<tr><td>1</td><td rowspan="12">POI</td><td>0MVAr</td><td rowspan="3">OFF</td><td rowspan="6">ON</td></tr>
<tr><td>2</td><td>-7.5%/+7.5%MVAr</td></tr>
<tr><td>3</td><td>-43.0%/+57.8%MVAr</td></tr>
<tr><td>4</td><td>0MVAr</td><td rowspan="3">ON</td></tr>
<tr><td>5</td><td>-7.5%/+7.5%MVAr</td></tr>
<tr><td>6</td><td>-43.0%/+57.8%MVAr</td></tr>
<tr><td>7</td><td>0MVAr</td><td rowspan="3">OFF</td><td rowspan="6">OFF</td></tr>
<tr><td>8</td><td>-7.5%/+7.5%MVAr</td></tr>
<tr><td>9</td><td>-43.0%/+57.8%MVAr</td></tr>
<tr><td>10</td><td>0MVAr</td><td rowspan="3">ON</td></tr>
<tr><td>11</td><td>-7.5%/+7.5%MVAr</td></tr>
<tr><td>12</td><td>-43.0%/+57.8%MVAr</td></tr>
</table>

each step of power shift, the results from all of the 138kV and 345kV transmission lines, generation units and substations in the FirstEnergy operating territory were recorded.

If the power flow calculations converged and intact operation (base case) was stable, then a series of contingency events are applied to the system, one outage event at a time. This list was provided by FirstEnergy consisting of 64 condensed contingency events composed by generation, line segments, entire lines, and synchronous condenser outages. During each outage event, the sensitivity analysis for all levels of wind power was carried out operational variables of the system were recorded.

Then, by using the proposed contingency ranking method, for each level of wind power, four introduced indices of VRI, PLI, $TLLI$ and $RRSI$ were computed. The next step was to compute the overall security index, SI. In this study, weighing factors of $s_1, \cdots, s_4$ were assigned equally. Then, the contingency events were ranked in a descending order by their security index.

To this end, the security index was computed for each step of wind, SI_i for i-th level of wind power. Then for every contingency event, SI_j, the security index for j-th event, was computed by summing up the computed SI_i from all level of wind power, as described in Equation 3.48.

The final results of security index computation were ranked descending to identify the most severe events and the most vulnerable and resilient scenario and interconnection for the offshore wind farm integration.

5.3 Small Signal Stability Analysis

Computational implementation of small signal stability analysis was carried out by a real-time simulation. In dynamic analysis, the reactive capability of the machines were restricted to full capability, R02, and therefore, the integration scenarios were narrowed down to four cases for each of the interconnections (EC01, EC02 and EC03). The studied cases in small signal stability analysis are described in Table 5.3.

Table 5.3: List of Studied in Small Signal Stability Analysis

Case No.	SVC	Perry	Voltage Regulation	Type of Machine
1	OFF	ON	POI	DFIG(-43.0%/+57.8%MVAr
2	ON	ON		
3	OFF	OFF		
4	ON	OFF		

First, accurate models of FirstEnergy/PJM were provided. Then, the aforementioned cases for each of the interconnections were developed and integrated in the FirstEnergy/PJM models. In computer simulation, after loading the system, generation dispatch and load data, the wind models were initiated. Then next step was to load dynamic models of the system including accurate representations of generators and their control systems, stabilizers, governors, dynamic loads and other dynamic components of the grid. GE PSLF Version 18.1_01 80K, DYTOOLS simulation tool, was used to carry out this part of this study.

The main objective of the small signal stability analysis was to investigate impacts of variability of power generation by the wind farm. Therefore, a series of step changes were applied to the offshore wind generators. The sizes of the disturbances were determined consistent with the expected changes in wind power, estimated by NREL. Table 5.4 illustrates the 10-minute assessment for expected changes in power generation in Lake Erie, provided by NREL.

Table 5.4: Expected 10-Minute Intermittency for 1000 MW Lake Erie Wind Plant, determined by NREL [22]

%Expectation	Frequency	Drop Level	Rise Level
—	Once in 3 Years	-360 MW	361 MW
99.9%	Once Every 2 Weeks	-136 MW	171 MW
99.0%	Once Every 1.5 Days	-72 MW	81 MW
95.0%	Four Times Per Day	-41 MW	44 MW
90.0%	Eight Times Per Day	-30 MW	31 MW

Following these disturbances, dynamical parameters of the generation units and transmission lines in the FirstEnergy/PJM area were recorded. The offshore wind farm was studied under multiple pre-disturbance operational points including 1000WM, 800WM, 600MW and 400MW.

The simulations were initiated for the first 5 seconds and then event took place in 5th second. The dynamic simulations covered 20 seconds following the events. This time period was chosen to ensure dynamics of the system in the area is sufficiently captured.

The measurements of voltage and frequency signals were done at POIs with the precision of 1×10^{-7}. It should be noted that the POI was chosen for measurement point since it is the closest onshore location to the source of external disturbance as a result of wind variability. Therefore, the amplitude of the oscillations will be the largest which makes their observation more precise. However, measurement of these signals at any other location on the grid in the area would provide adequate information.

Finally, Prony Analysis was applied to the voltage signals to extract more information from them in frequency domain. Frequency signals were analyzed in time domain and metric of PFRI was calculated for each studied cases.

5.4 Large Signal Stability

Computational implementation of transient dynamic analysis was carried out by a real-time simulation. In transient stability same case as the small-signal stability analysis were used, as described in Table 5.5. However, the results from the small signal stability analysis identified the EC01 as the most sensitive interconnection scenario to external disturbances. Therefore, the interconnection scenarios were narrowed down to only EC01 for transient stability analysis. This interconnection scenario corresponds to interconnecting a 1000 MW of offshore wind generation at the Perry 345 kV Substation.

Table 5.5: List of Studied in Large Signal Stability Analysis

<table>
<tr><th>Case No.</th><th>SVC</th><th>Perry</th><th>Voltage Regulation</th><th>Type of Machine</th></tr>
<tr><td>1</td><td>OFF</td><td>ON</td><td rowspan="4">POI</td><td rowspan="4">DFIG(-43.0%/+57.8%MVAr)</td></tr>
<tr><td>2</td><td>ON</td><td>ON</td></tr>
<tr><td>3</td><td>OFF</td><td>OFF</td></tr>
<tr><td>4</td><td>ON</td><td>OFF</td></tr>
</table>

5.4.1 Short Term Faults

First, accurate models of FirstEnergy/PJM were provided. Then, these cases for each of the scenarios were developed and integrated in the FirstEnergy/PJM models. After loading the system, generation dispatch and load data, the wind models were initiated. Then next step was to load dynamic models of the system including accurate representations of generators and their control systems, stabilizers, governors, dynamic loads and other dynamic components of the grid. GE PSLF Version 18.1_01 80K, DYTOOLS simulation tool, was used to carry out this part of this study.

Following short term faults were investigated in this study:

1. **Short Term:** Three-phase short circuit faults were applied to the following components and successfully cleared after 4.5 cycles:
   (a) Two generators in the area with largest level of power generation (based on the base case)
      i. Perry Generator
      ii. Davis-Besse Generator

(b) Two generators in the area with level of power generation equal to approximately half of the area's largest generator (based on the base case)

   i. Avon Unit 9 Generator

   ii. W.H. Sammis Unit 7 Generator

(c) Three 345kV lines in the area with largest MW level of power transfer (based on the base case)

   i. HYD-MNS: Hoytdl to Bruce Mansfield

   ii. HNN-JNP: Hanna to Juniper

   iii. DVB-LMN: Davis-Besse to Leymon

(d) Half of the offshore collector system, only in the cases with the offshore wind farm

The offshore wind farm was studied under multiple pre-disturbance operational points. The simulations were initiated for the first 5 seconds and the event takes place in 5th second. The transient dynamic simulations covered 10 seconds following the events. This time period was chosen because of the nature of fast transient dynamics of power system and to ensure they are sufficiently monitored and identified. Following these faults, dynamic behavior of the generation units and transmission flows including rotor angles, speeds, power generation and voltage profiles in the FirstEnergy/PJM area were recorded. During a 3-phase to ground short circuit, it is assumed that the system is symmetrical and the short circuit occurs simultaneously and identically on all three phases. The measurements of signals were done with precision of 1×10^{-7}. The measurement of frequency signal was done at wind POI. The voltage and rotor angle and speed signals of generators were measured at the POI of all of the generators in the area.

5.4.2 Long Term Faults

First, accurate models of FirstEnergy/PJM were provided. Then, these cases for each of the scenarios were developed and integrated in the FirstEnergy/PJM models. After loading the system, generation dispatch and load data, the wind models were initiated. Then next step was to load dynamic models of the system including accurate representations of generators and their control systems, stabilizers, governors, dynamic loads and other dynamic components of the grid. GE PSLF Version 18.1_01 80K, DYTOOLS simulation tool, was used to carry out this part of this study.

Following long term faults were investigated in this study:

1. Immediate outage of the generator with the least CCT, Davis-Besse

2. Three-phase short circuit fault applied to the line with the least CCT and after 12.5 cycles of fault, the line was opened, Davis-Besse to Leymon 345kV line

3. Immediate outage of half of the offshore collector system (except in base case)

The offshore wind farm was studied under multiple pre-disturbance operational points. The simulations were initiated for the first 5 seconds and the event takes place in 5th second. The transient dynamic simulations covered 10 seconds following the events. This time period was chosen because of the nature of fast transient dynamics of power system and to ensure they are sufficiently monitored and identified. Following these faults, dynamic behavior of the generation units and transmission flows including rotor angles, speeds, power generation and voltage profiles in the FirstEnergy/PJM area were recorded. During a 3-phase to ground short circuit, it is assumed that the system is symmetrical and the short circuit occurs simultaneously and identically on all three phases. The measurements of signals were done with precision of 1×10^{-7}. The measurement of frequency signal was done at wind POI. The voltage and rotor angle and speed signals of generators were measured at the POI of the generators.

Chapter 6

Results and Discussion

Before discussing the results, following is a brief review of the interconnection scenarios that are undertaken in this study:

- **EC01:** Interconnecting a 1000 MW of offshore wind generation at the Perry 345 kV Substation
- **EC02:** Interconnecting five cables 200 MW each of offshore wind generation, at the Avon 345 kV Substation, at the Lakeshore 138 kV Substation, at the Eastlake 345 kV Substation, at the Perry 345 kV Substation and at the Ashtabula 138 kV Substation
- **EC03:** Interconnecting two cables of 500 MW each of offshore wind generation, at the Avon 345 kV Substation and the Lake Shore 138 kV Substation

6.1 Steady State Stability Analysis

This section shows the results from the steady state stability analysis by using the proposed tool and outlines the findings. The main application of the proposed analytical tool is to assess impacts of offshore wind farms operation on steady state stability of transmission systems by providing an insight into the voltage and thermal stability of the system under normal operation.

During normal operation, no contingency occurred and all of the generation units and load are in operational. The first goal was to investigate how variability of the offshore wind farm impacts on voltage regulation and loading level across transmission system. Whereas the second goal was to understand operational conditions of the transmission system in presence of offshore wind farm. The last goal was to assess whether or not stability of the system was threatened as a result of operation of offshore wind farm within its complete operational span.

6.1.1 Voltage Regulation in Transmission System

The main purpose of this section is to investigate impacts of offshore wind power generation on voltage regulation in transmission lines. FirstEnergy/PJM requires that transmission and subtransmission level apparatus operate within following ranges under normal and single transmission element outage conditions [105]:

- 500kV System: 0.97-1.10 pu
- 345kV and 230kV Systems: 0.92-1.05 pu
- 138kV and 115kV Systems: 0.92-1.05 pu
- 69kV/46kV/34.5 kV Systems: 0.90-1.05 pu
- 25/23kV Systems: 0.90-1.07 pu

Figures 6.1 show the results from voltage regulation across the transmission system, including 500kV, 345kV and 138kV lines (574 lines in total), in the base case. These curves are obtained using probability density estimation of the computed voltage magnitudes data points and comparing their distribution to the normal distribution.

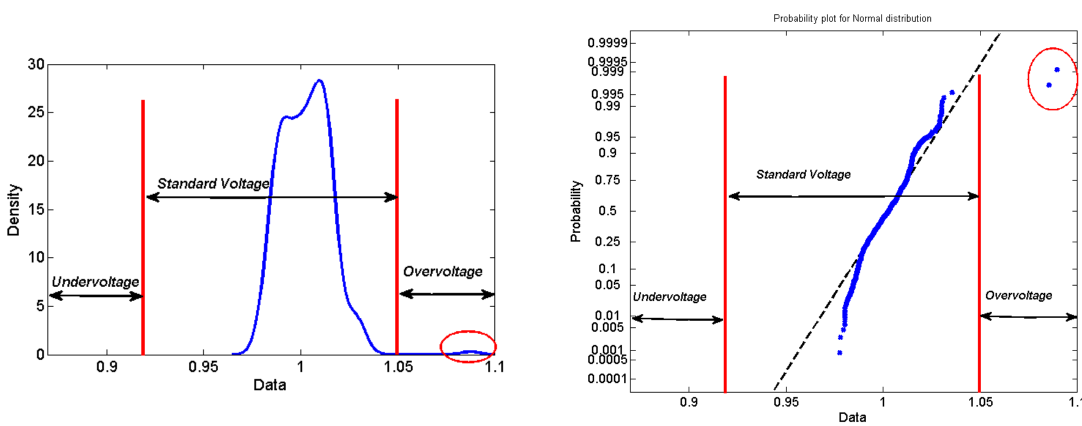

(a) Probability density function

(b) Distribution probability

Figure 6.1: distribution analysis of voltage data in FirstEnergy transmission system-base case

From these two curves, it can be seen that no undervoltage condition has been recorded. However, two 138-kV lines operated in the slightly overvoltage condition. In addition, 99.6% of the lines operate within the range 0.977 pu to 1.035 pu. The mean and mode values of measured voltage magnitudes are 1.002 pu and 1.013 pu, respectively. This is not surprising, knowing the fact that reactive power generation is higher than it demand in this area.

The studied cases in this section are described in Table 5.1.

Figures 6.3 and 6.3 show how density function of voltage magnitudes distribution changes in respect to variability of the wind farm.

As can be seen in these figures, as the level of power generation by the wind farm becomes greater, the distribution of measured voltage magnitudes tends towards a

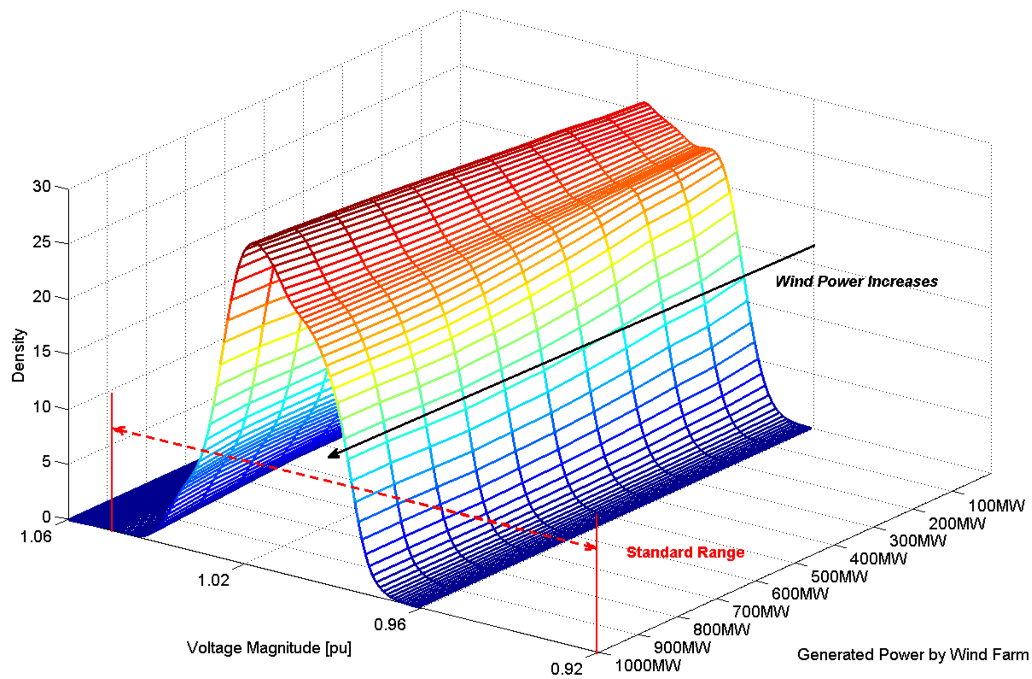

Figure 6.2: Wind power variability vs. probability density function of voltage regulation curve in FirstEnergy/PJM transmission system

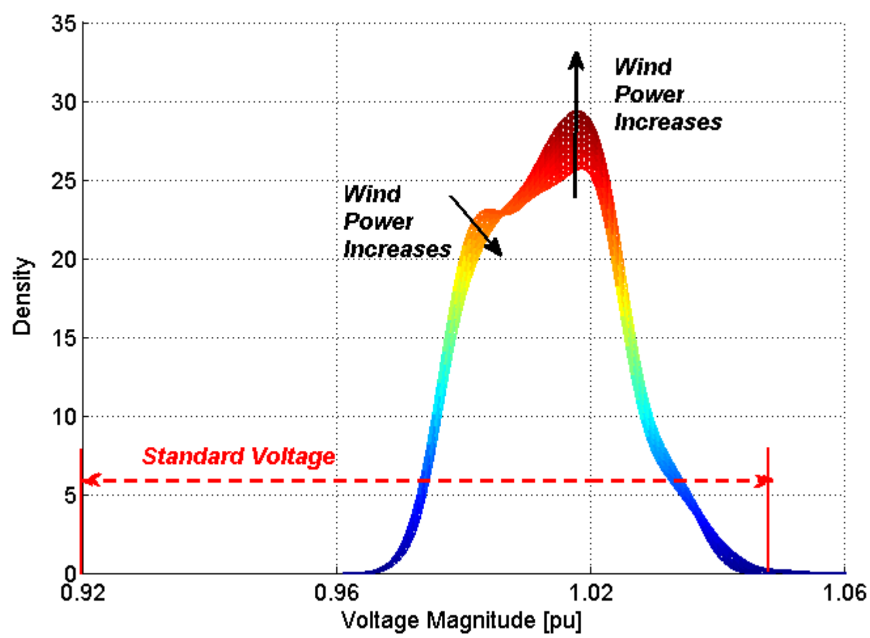

Figure 6.3: Impact of wind power variability on voltage regulation in FirstEnergy/PJM transmission system

normal distribution. It is notable that the higher level of power generation by wind farm becomes, the voltage magnitudes at a greater number of busbars tends towards 1.014 p.u. and the local peak at 0.99 p.u. vanishes. At 1000MW of offshore wind generation, the mode, median and mean values of the data are 1.014 pu, 1.003 pu and 1.004 pu, respectively. This means that as offshore wind farm generates higher power, it improves the voltage regulation across the transmission system and makes the recorded data set more aligned with normal distribution.

The lower the level of offshore wind power generation cause more asymmetry in distribution of the measured voltage data. For instance, at 0MW of offshore wind power generation, the mode value remains at 1.014 pu, while the median and mean values are 1.006 pu and 1.005 pu, respectively. In fact, the level of offshore wind power generation has a direct impact on the median and mode values of the measured voltage magnitudes.

However, it is evident that no voltage violation takes place at all levels of variable wind power. In addition, the bus that experienced overvoltage condition in the base case became properly regulated after adding wind generation.

Figure 6.4 the impacts of variability of the wind farm on distribution probability of voltage magnitudes across the FirstEnergy/PJM transmission system.

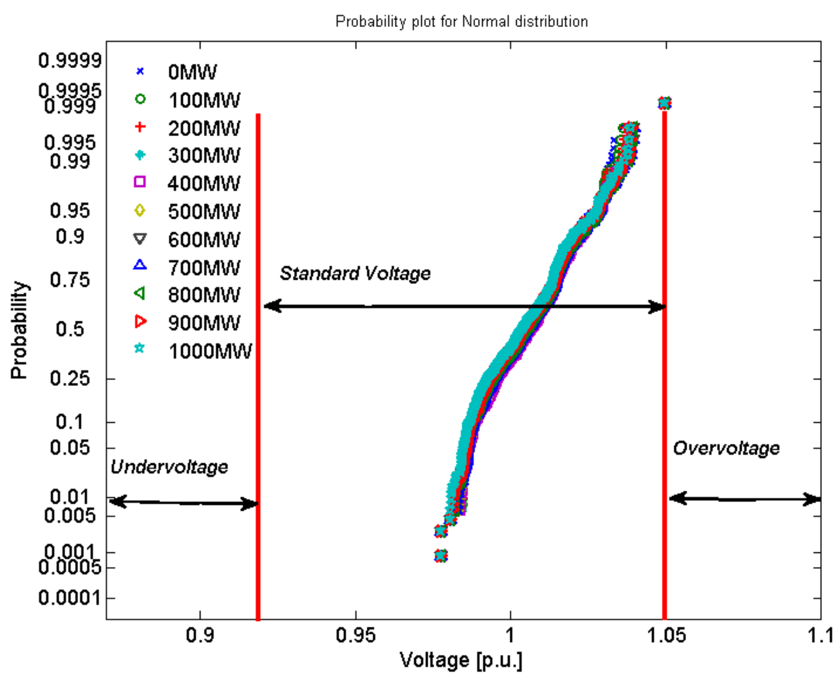

Figure 6.4: Wind power variability vs. distribution probability of voltage regulation curve in FirstEnergy/PJM transmission system

Figure 6.4 consists of a group of curves that each represents the operational performance of voltage regulation in the system for a certain level of offshore wind power generation. Each curve compares the distribution of the voltage data points from a given level of wind power to a normal distribution. These results reveal that after installing the offshore wind farm, for all levels of offshore wind power generation, the FirstEnergy/PJM transmission system were regulated within the standard voltage range. In base case, there was two data point within region of overvoltage which were regulated properly upon operation of the offshore wind farm. This is an indication of voltage stability improvement. In addition, from this figure, it can be seen that the impact of wind power variability on voltage regulation is insignificant as all the data distribution for all levels of the wind power is identical.

Figures 6.2 through 6.4 are illustrate the analysis of the results from EC01 interconnection scenario. The results from EC02 and EC03 are very similar. Thus. they are not shown.

From the last four figures, it can be concluded that integration of the offshore wind farm into FirstEnergy transmission system through EC01 interconnection improves voltage regulation in the FirstEnergy area, regardless of the level of offshore wind power generation. In fact, the buses that experience overvoltage in the base case (FirstEnergy system without wind farm), will be regulated properly. As the level of wind power generation by offshore become greater, the improvement in voltage regulation becomes greater.

In order to take a closer look at voltage regulation in the FirstEnergy/PJM transmission system, simulation results for the distribution of voltage magnitudes for different wind power integration cases and scenarios, corresponding to various levels of wind power generation by offshore wind farm were collected and analyzed. The Figures 6.5 through 6.8 show range, mode, and difference between median and mean of measured voltage for all of the interconnections, EC01, EC02, and EC03.

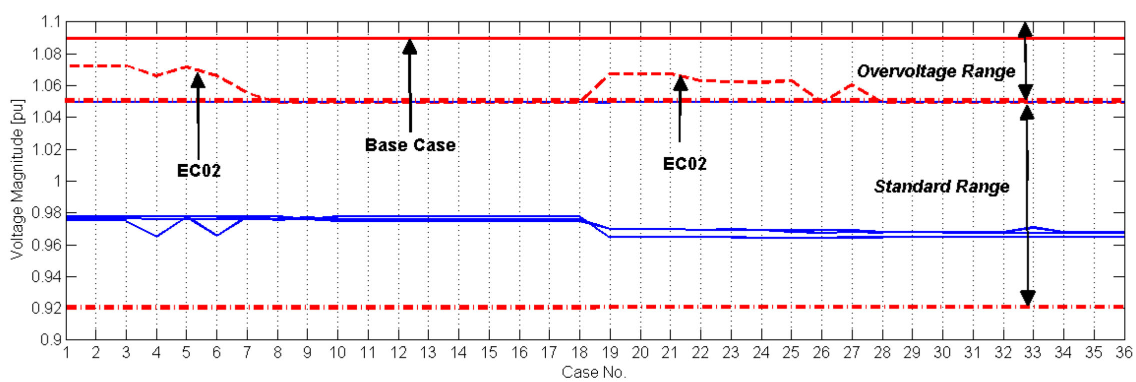

Figure 6.5: Range of voltage magnitudes in FirstEnergy transmission system

Figure 6.5 shows the range of measured voltage magnitudes all across the FirstEnergy/PJM transmission system from all of the studied cases. From 6.5, it can be seen that integration of offshore wind farm into FirstEnergy transmission system improves the voltage regulation in the FirstEnergy area, for all levels of power generation by the wind farm. In fact, the buses that experience overvoltage condition in the base case (system without wind farm), shown in red and dashed line, were regulated properly. This agrees with the findings from Figure 6.2 through 6.4.

The second point to note is that installing a 1000MW offshore wind farm does not violate the voltage regulation in all of the EC01 and EC03 cases and most of the EC02 cases. For EC02, in cases in which machines with no or limited reactive support capability was used, voltage violation occurred, shown in red and dashed line. Figure 6.6 shows the distribution probability of voltage magnitudes for the EC02 cases.

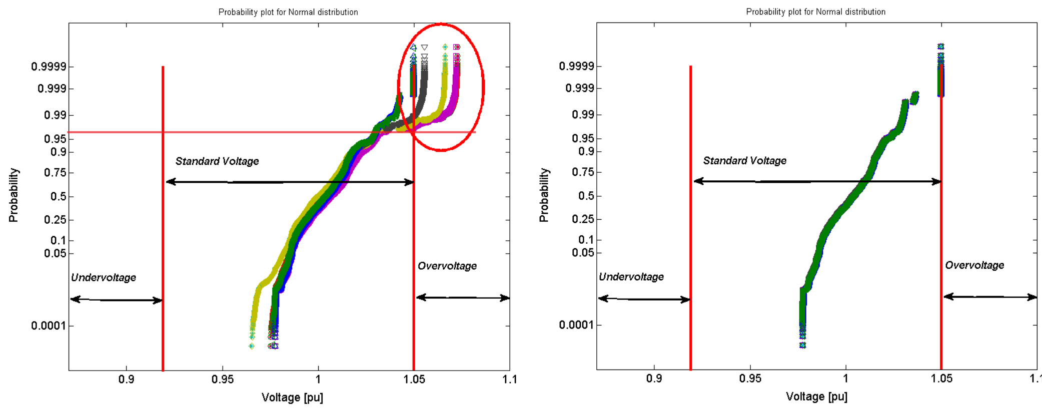

(a) Cases 1-9

(b) Cases 10-18

Figure 6.6: Distribution probability of voltage regulation curves in FirstEnergy/PJM transmission system for selected EC02 cases

In the figure 6.6, it could be seen that in those cases in which voltage violation might occur, the probability of the violation is less than 4% for full operational range of the wind farm. However, operation of SVC at the POI helped with resolving voltage regulation issue superbly.

This indicates that geographical location of the POI according to the topology of the grid and technologies and capability of operating units near the POIs is a factor in determination of effects of integration of the offshore wind farm on the voltage regulation on the grid.

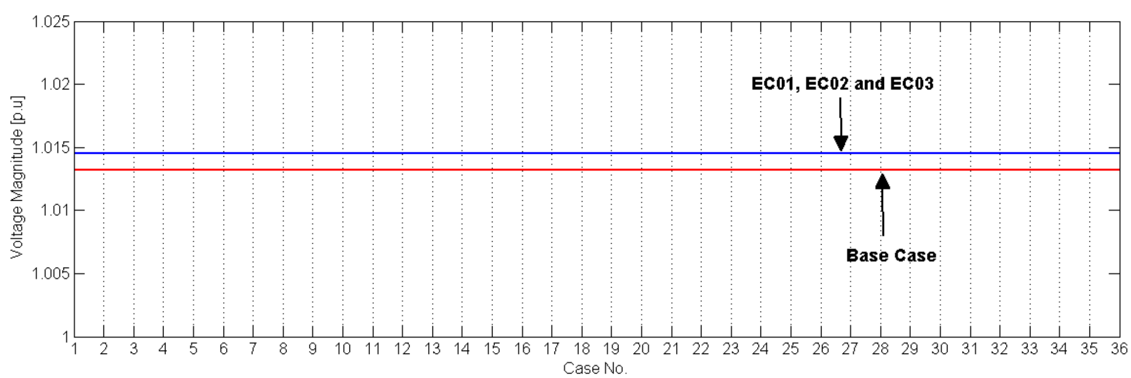

Figure 6.7: Mode of voltage magnitudes in FirstEnergy transmission system

Figure 6.7 shows the voltage mode for all studied cases. The mode value shown in this study is the aggregated mode value for all levels of wind power. As shown, the mode of voltage magnitudes for base case was 1.013 pu. Upon operation of the offshore wind farm, the voltage mode became identically 1.014 pu for all of the studied cases.

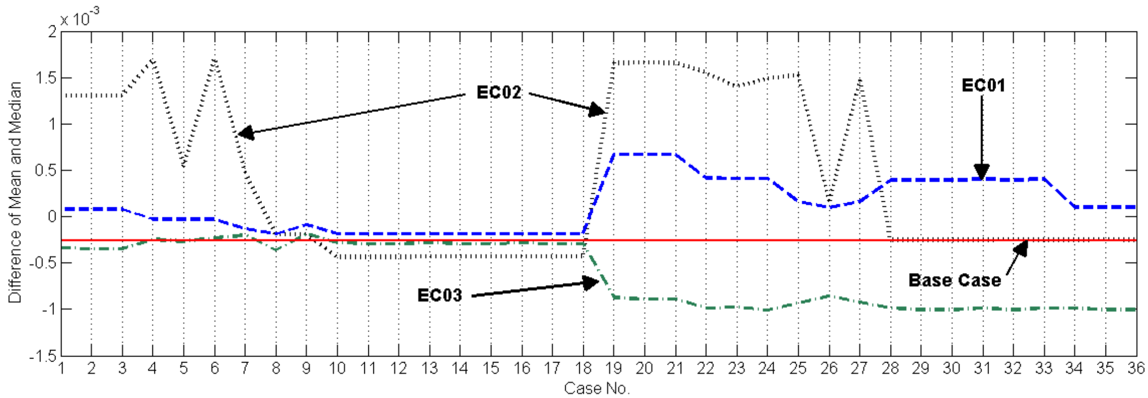

Figure 6.8: Difference between mean and median of voltage magnitudes in FirstEnergy transmission system

Figure 6.8 shows the difference between mean and median of the sets of measured voltage magnitudes for all studies cases. These values were calculated using aggregated voltage data points from all levels of wind power generation. This value for normal distribution is zero. This is a technique to measure symmetry of a series of data.

For a stable operating grid, the expected value for the voltage magnitudes should be nearly zero. Positive values for this index mean likeliness of voltage rise and negative values the likeliness of voltage drop across the power system. The high values of this index are indication of severe threat for voltage security and approaching a significant voltage collapse or violation.

As shown, the symmetry of voltage magnitudes in EC01 and EC03 cases in which Perry was online, remained approximately the same as the base case. The EC01 cases in which Perry was offline showed a tendency towards voltage rise while the EC03 case in which Perry was offline showed tendency towards voltage drop. The EC02 cases in which SVC operated at the POI showed identical distribution as the base case while the EC02 cases in which no SVC operated at the POI showed significant tendency towards voltage rise. The contribution of machine reactive capability and point of voltage regulation are insignificant.

It is noticeable that the EC01 cases deliver the most robust performance in voltage regulation across the FirstEnergy system by maintaining the voltage magnitudes closer to a normal distribution for all level of wind power, with and without Perry.

In all of the studied cases, this metric was very small. Thus, it is safe to that the voltage magnitudes under the steady state operation were symmetrical and formed a normal distribution data set.

6.1.2 Loading level of Transmission System

The aim of this section is to understand how offshore wind power generation will impact loading level of FirstEnergy transmission system.

Figure 6.9 presents the analysis of the transmission system loading result from FirstEnergy system base case in which no wind farm is integrated.

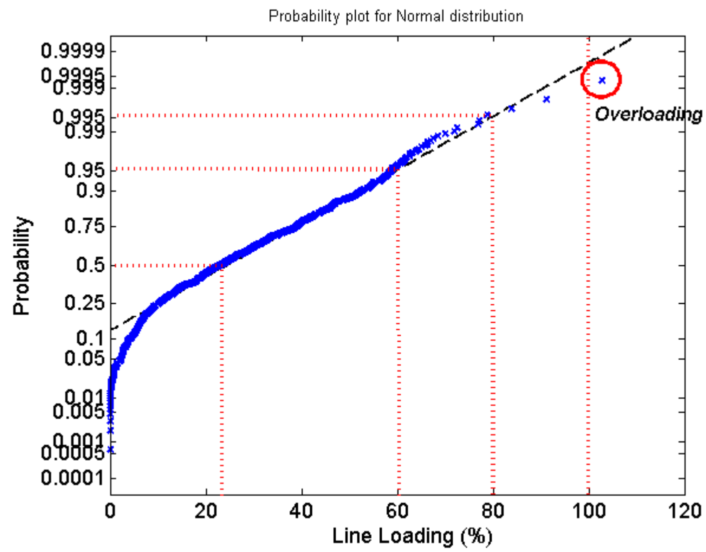

Figure 6.9: Distribution probability of line loading in FirstEnergy transmission system - base case

As shown in this figure, almost 99.5% of FirstEnergy/PJM transmission lines in base case are loaded below 80% of their nominal capacity where the actual loading level for more than 50% of them is below 25%. However, there is a 138-kV line operating in overloaded condition, by exceeding 3.1% of its nominal loading capacity.

Figures 6.10 and 6.11 provide an understating of how wind power variability impacts on loading level of FirstEnergy transmission system.

In these curves, is notable that by higher level of power generation by wind farm, the loading level mode moves to 23% from 21%. In fact, this is because of injecting additional power that is generated by offshore wind farm into the FirstEnergy/PJM system which changes the flow of the power in the system.

As shown in these curves, there is a very small difference in distribution of loading data points of the FirstEnergy transmission system after introduction of the wind farm and for different levels of wind power. This is because more than 95% of the lines in this system are operating below 60% of their nominal capacity in the base case, shown in Figure 6.9.

To investigate how integration scenario of offshore wind farm could impact on lines loading, the results from studied cases are compared in Figure 6.12. This figure illustrates the distribution probability of loading level of the FirstEnergy/PJM transmission system for studied cases.

This figure shows the distribution probability plots for all of the studied cases.

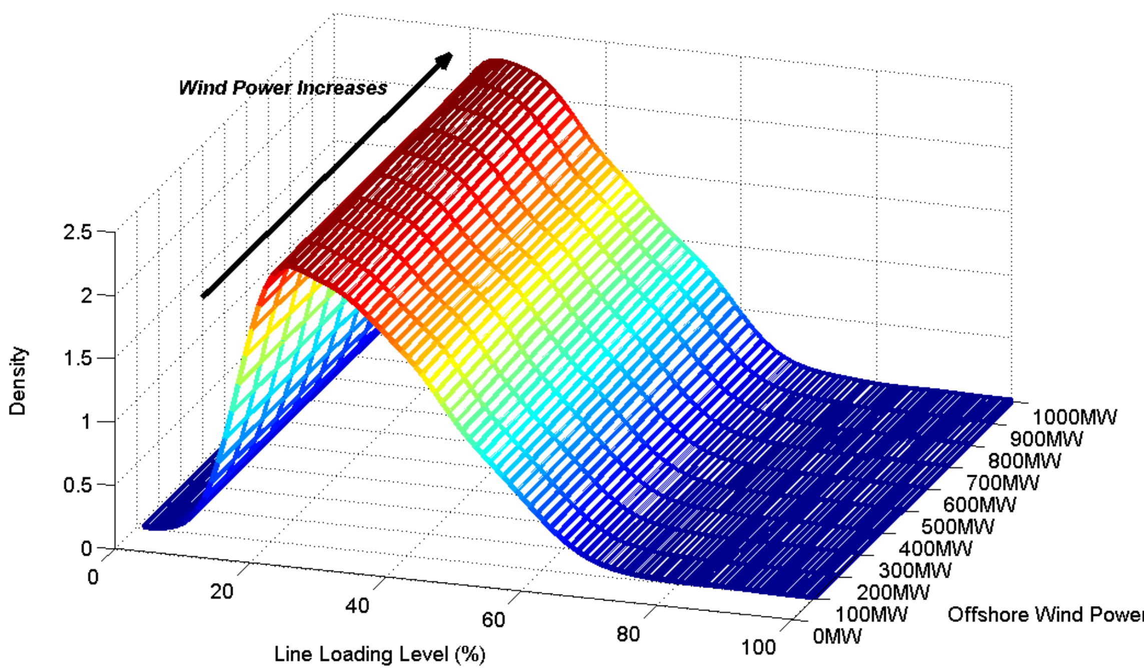

Figure 6.10: Wind power variability vs. probability density function of loading level in FirstEnergy/PJM transmission system

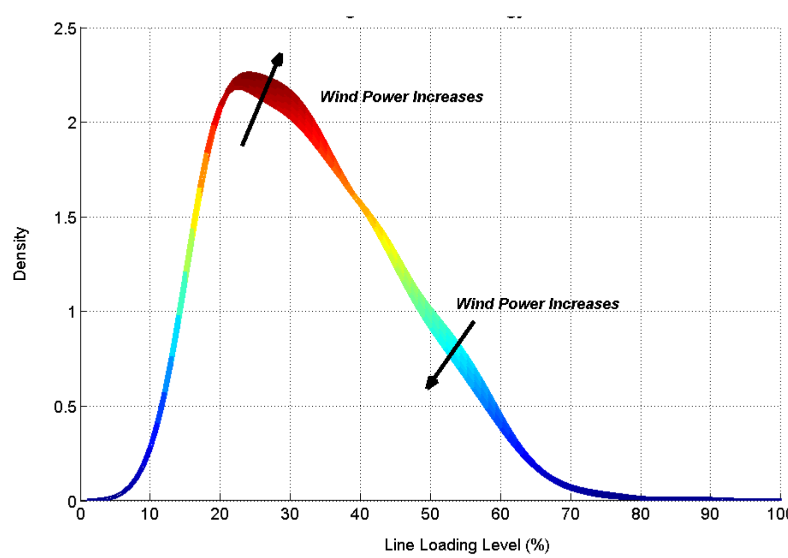

Figure 6.11: Impact of wind power variability on loading level in FirstEnergy/PJM transmission system

However, they follow two main patterns and overlap on each other to form two main plots. The factor that distinguishes the studied cases and their plots is the operational status of Perry. As shown in this figure, in all of the cases, with and without Perry, there is a narrow chance of experiencing overload conditions in a line or multiple lines

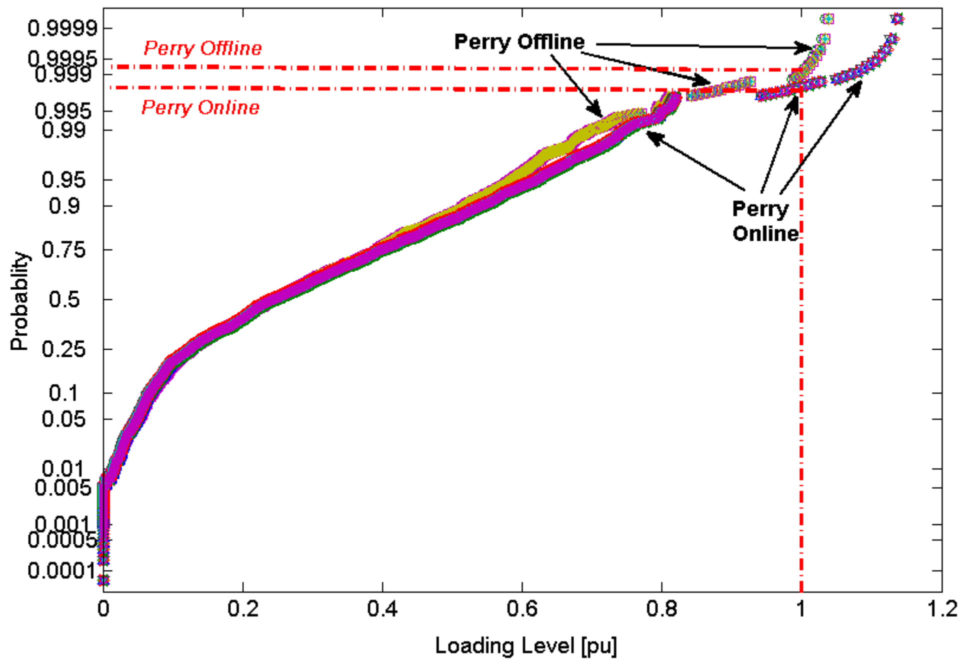

Figure 6.12: Distribution probability of loading level curves in FirstEnergy/PJM transmission system

within the FirstEnergy are. The probability of this condition for lines in cases with online Perry was 0.002% to excess of less than 13% of their nominal rating and in cases without Perry was less than 0.001% to excess of less than 3% of their nominal rating.

The plots shown in Figure 6.12 are from EC01. The results from EC02 and EC03 are identical and, therefore, are not shown.

In sum, the primary factor in loading level of the FirstEnergy transmission system is the operational status of Perry. Lack of operation of this plant, with 1290MW and 625MVAr capacity, causes the loading level to drop slightly. The second factor is the level of power production by the offshore wind farm. The other examined factors have not any notable impact on the loading level of the system.

From the results shown in this section it can be concluded that the FirstEnergy/PJM transmission system is substantially capable to accommodate 1000MW offshore wind power generation introduced in this study, in terms of capacity.

6.1.3 Steady State Voltage Stability

One of the very basic signs for steady state voltage instability is undervoltage violation at any given bus across the system as the operation point begins to approach the voltage collapse point. The results of the voltage range reveal that the FirstEnergy transmission system does not experience this condition. In addition, in all studied cases including the base case, the metric of difference between mean and median was very insignificant. Therefore, for all levels of offshore wind power generation, the system operates in the stable region and it is safe to say that installing an offshore wind farm in Lake Erie will not destabilize the FirstEnergy/PJM transmission system.

6.1.4 Steady State Thermal Stability

Thermal stability is a concern when the transmission lines operate in a heavily overloaded condition. In this study, it was found out that the FirstEnergy transmission system does not experience this condition. In addition, the voltage stability margin is much smaller than the thermal stability margin. Therefore, voltage instability is the dominant factor in determining system stability.

6.2 Steady State Contingency Analysis

This section shows the results from the steady state contingency analysis using the proposed security index and outlines the findings. The main application of the proposed security index is to conduct contingency ranking and monitoring in power systems with variable generation units that provides an assessment of how their variability affects security of the systems.

The first goal was to identify most severe contingency events by considering variability of the offshore wind farm. The second goal was to identify the most resilient and vulnerable integration scenarios for expansion studies.

The studied cases in this section are described in Table 5.1 and the list of contingency events is shown in Tables 4.10 through 4.15.

Figures 6.13 through 6.15 show the security index for studied cases with and without operation of Perry.

The higher values of the proposed security index indicate lower security for the system. In each of the shown figure, the upper plate represents the cases in which Perry was offline while the lower plate represents the cases in which Perry was online. Accordingly, these figures reveal that the loss of Perry adversely impact on security of the system but does not destabilize the system. Total installed generation capacity of the area is 10,344MW which Perry with 1290MW generation capacity contributes by share of 12.47%. This is a significant amount of power generation and, not surprisingly, its loss deteriorate the security of the system but does not threatens it.

6.2.1 Contingency Event Ranking and Monitoring

The *SI* of studied cases holds necessary information to identify the severe events. The greater this index, the more the severe contingency event, for any given case. For comparison purposes, Figure 6.16 shows what contingency events are the most severe for each of the cases. Note that 36 cases presented shown in this figure could be described by:

- **Cases 1-6:** EC01 cases 1-6 with online Perry

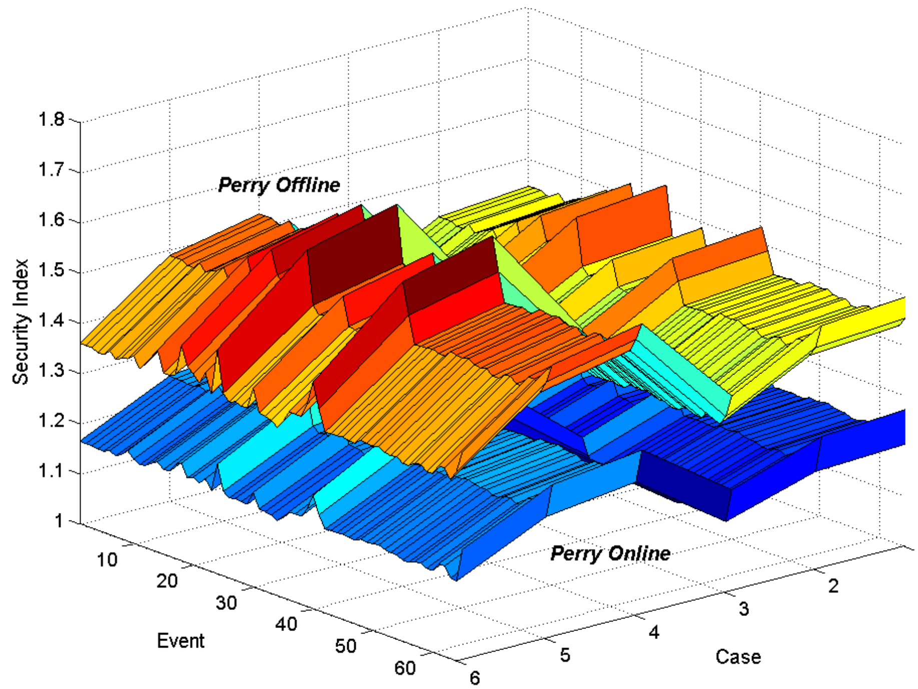

Figure 6.13: Contingency Ranking of EC01 Cases

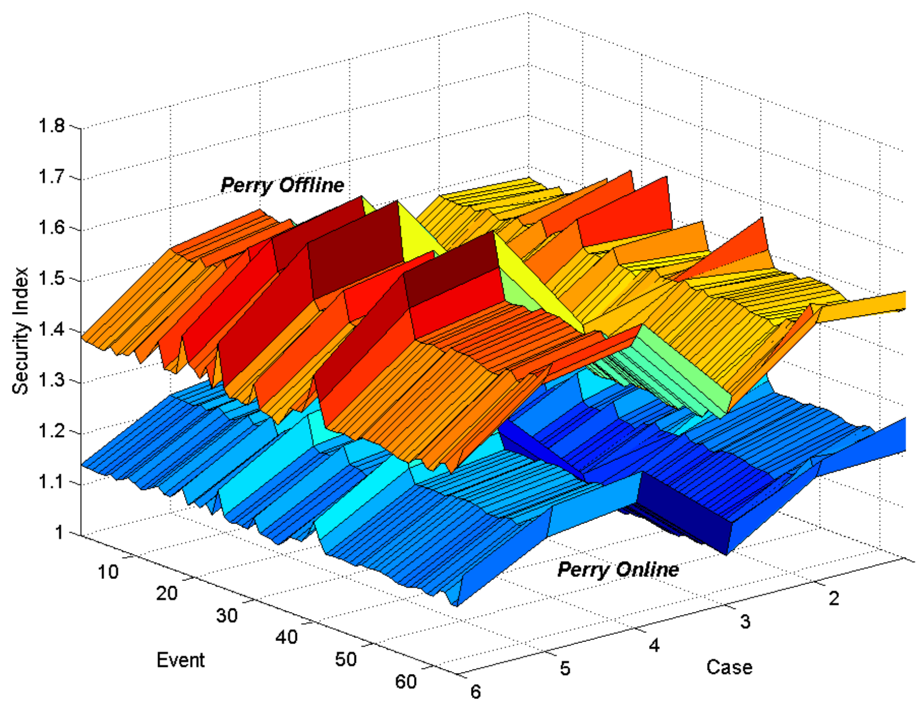

Figure 6.14: Contingency Ranking of EC02 Cases

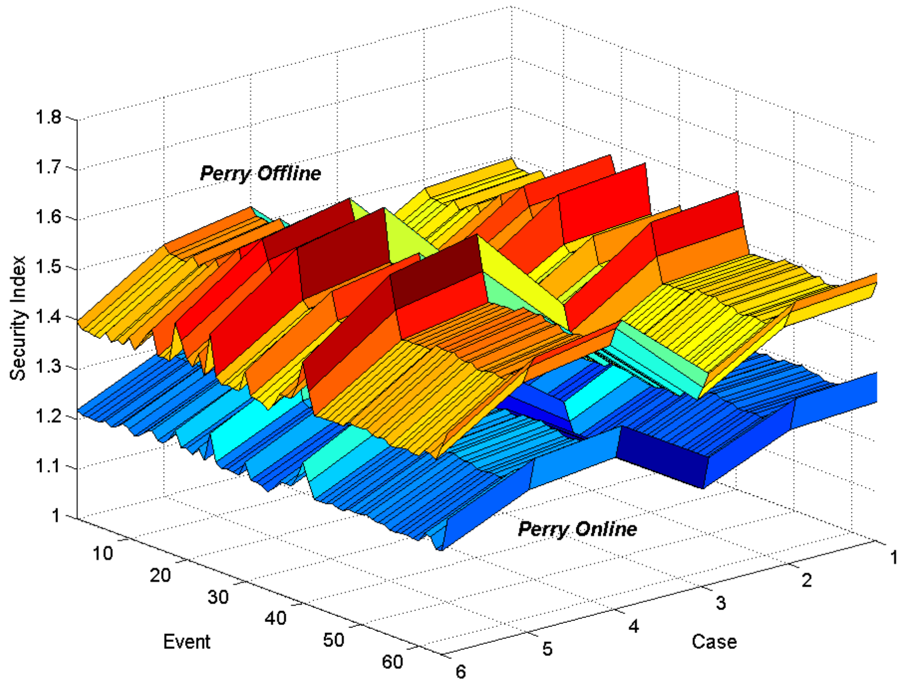

Figure 6.15: Contingency Ranking of EC03 Cases

- **Cases 7-12:** EC01 cases 7-12 with offline Perry
- **Cases 13-18:** EC02 cases 1-6 with online Perry
- **Cases 19-24:** EC02 cases 7-12 with offline Perry
- **Cases 25-30:** EC03 cases 1-6 with online Perry
- **Cases 31-36:** EC03 cases 7-12 with offline Perry

In this figure, it can be seen that severity of events are consistent in all of the studied cases. Tables 6.1 through 6.3 provide a list of top 15 severe contingencies for six selected studied cases. For comparison purposes, the SI for cases with and without Perry is listed.

These results show that the contingency rankings from all interconnection scenarios, EC01, EC02 and EC03 are very similar. For instance, Events 24, Loss of Beaver to West Lorain Plant 345 kV Transmission Line, and 40, Loss of Inland 345 / 138 kV Transformer 4, are consistently ranked 1st or 2nd regardless of interconnection scenario and operational status of Perry. This is because of the fact the operation of Perry and configuration of the offshore wind farm do not influence the power flow of these components.

Note that the ranking of some events in studied cases with and without Perry was noticeably different. As an example, SI value of event 17, Loss of Eastlake to Perry 345 kV Transmission Line, for Case 1, EC01 is 1.240 that makes it stand in 8th in the severity ranking while it value for Case 7, EC01 is 1.446 that ranks this event

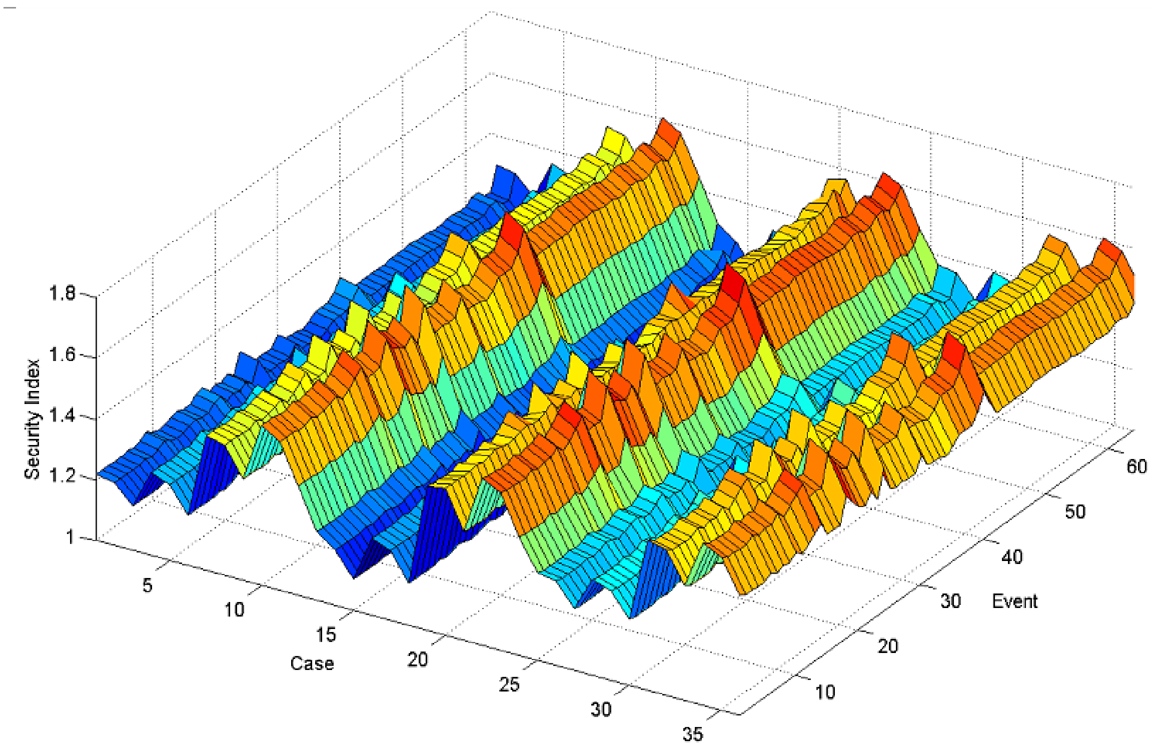

Figure 6.16: Security Indices for studied cases and events

Table 6.1: List of Top 15 Most Severe Contingency Events and Their Ranking for Selected EC01 Cases

	Case 1 - EC01 (Perry Online)		**Case 7 - EC01 (Perry Offline)**	
Event ID.	Ranking	SI	Ranking	SI
40	1	1.280	2	1.530
65	2	1.278	4	1.503
24	3	1.276	1	1.544
39	4	1.247	6	1.488
18	5	1.247	3	1.521
41	6	1.244	7	1.486
30	7	1.243	8	1.484
17	8	1.240	34	1.446
9	9	1.236	25	1.451
22	10	1.234	9	1.479
62	11	1.232	14	1.460
61	12	1.232	13	1.460
14	13	1.231	5	1.490
36	14	1.228	15	1.458
37	15	1.228	16	1.458

Table 6.2: List of Top 15 Most Severe Contingency Events and Their Ranking for Selected EC02 Cases

	Case 1 - EC02 (Perry Online)		**Case 7 - EC02 (Perry Offline)**	
Event ID.	Ranking	*SI*	Ranking	*SI*
40	1	1.287	2	1.564
65	3	1.285	4	1.529
24	2	1.285	1	1.576
39	5	1.255	6	1.521
18	4	1.258	3	1.561
41	7	1.248	9	1.505
30	6	1.251	7	1.516
17	12	1.241	43	1.470
9	13	1.237	42	1.471
22	9	1.237	8	1.512
62	8	1.243	13	1.492
61	11	1.241	14	1.489
14	10	1.242	5	1.527
36	15	1.236	16	1.488
37	16	1.237	17	1.488

Table 6.3: List of Top 15 Most Severe Contingency Events and Their Ranking for Selected EC03 Cases

	Case 1 - EC03 (Perry Online)		**Case 7 - EC03 (Perry Offline)**	
Event ID.	Ranking	*SI*	Ranking	*SI*
40	1	1.362	1	1.593
65	3	1.344	4	1.543
24	2	1.348	2	1.582
39	5	1.322	7	1.534
18	4	1.323	3	1.574
41	6	1.319	8	1.528
30	7	1.311	9	1.522
17	10	1.300	40	1.480
9	17	1.296	44	1.479
22	8	1.304	10	1.522
62	15	1.297	23	1.490
61	11	1.300	22	1.492
14	9	1.303	5	1.537
36	12	1.297	14	1.499
37	13	1.297	15	1.499

34th. This shows that this event becomes less severe as a result of loss of Perry. This is because of the fact following loss of Perry, the flow of power in the system changes.

In addition, the SI values for cases in which Perry was offline, significantly higher than the same cases in which Perry was online. This shows that loss of Perry cause a drop in security of the system which is consistent with the finding evidenced in Figures 6.13 through 6.15.

The proposed approach sought to identify critical credible contingency events for large scale power systems with variable offshore wind farm. The results of this study illustrated that contingency events did not cause voltage collapse or line congestion in the FirstEnergy transmission system. The indication of voltage collapse or line congestion would have been a great value for SI comparing to the found values, greater than 4. Therefore, it is safe to assume that this system is safe. The proposed method was capable to superbly quantify the variability of wind power and perform contingency ranking and monitoring in the power systems with large scale variable generation units.

6.2.2 Resiliency Analysis of Integration Scenarios

In power system planning and expansion studies, the credible and possible integration configurations must be investigated to reach highest resiliency to ensure security of energy delivery. This investigation could be conducted through the same mechanism as contingency ranking and monitoring uses. In fact, the proposed SI of studied cases holds necessary information about resiliency of wind integration scenarios as a particular case in this study. As greater this index is, the more the vulnerable the integration scenario is. Figure 6.17 provides a comparative overview of the resiliency of all 36 studied wind integration cases.

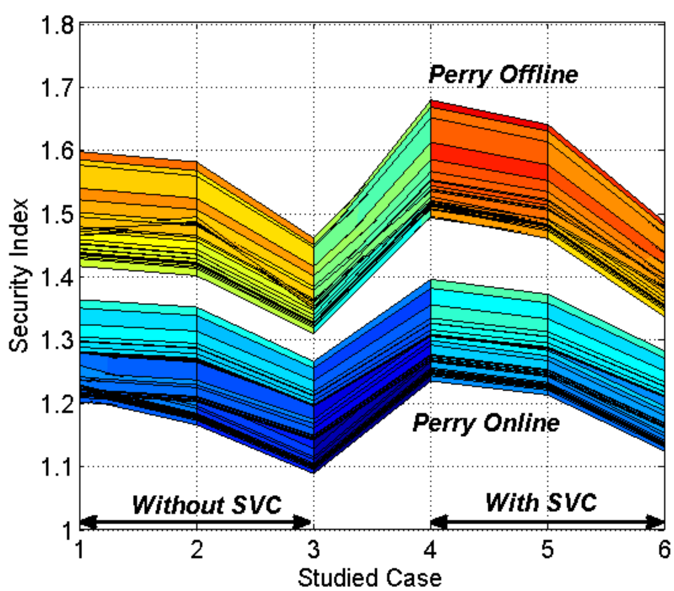

Figure 6.17: Security analysis for studied cases to assess resiliency of the scenarios

This plot consists of series curves that overlap on each other following a similar pattern that create two major groups: (1) top lines that represent cases without Perry and (2) bottom lines that represent cases with operating Perry. The cases 1-3 are not equipped with SVC at the wind POI while cases 4-6 include operation of SVC at the wind POI.

According to this plot, the FirstEnergy system performance was acceptable in this study. The most vulnerable case for all interconnection scenarios, EC01, EC02 and EC03 is Case 4 and the most resilient configuration is Case 3. Case 4 represents integration of offshore wind farm in which machines without any reactive capability were used and operating SVC at the POI. Case 3 represents integration of offshore wind farm case in which machines with full reactive capability were deployed and no operating SVC at the POI.

The first point to note is that the operational status of operation of Perry in the area significantly impacts the resiliency and security of the system. For all three interconnections, there are considerable differences between security indices for the cases with and without the power plant. This agrees with results from previous section.

The second point to note is that the reactive capability of the machines installed in offshore farm is a key factor in the resiliency the system. As shown in Figure 6.17, the greatest resiliency corresponds to the cases with fully capable machines, Case 3 and then Case 6. The cases that used incapable machines in providing reactive power support experienced the greatest vulnerability, weakest resiliency, Case 1 and 4.

The last point to note is that operation of SVC at the POIs has an adverse impact on contingency operation of the system, and this impact was more pronounced in cases in which Perry was offline, Case 4.

6.3 Small Signal Stability Analysis

This section shows the results from the small signal stability analysis and discusses the findings. The studied cases in this section are described in Table 5.3.

6.3.1 Small Signal Voltage Stability

EC01 Interconnection Scenario

Figure 6.18 shows the voltage signals and captured voltage modes at the POI of 205, located at the Perry 345kV substation, following sudden drops and rises in level of power generation by the offshore wind farm in EC01 studied cases.

In this plot, the modes with magnitudes smaller than 1×10^{-3} are neglected due to their insignificance. The first point to note is that variability of the wind did not excite any interplant mode in all of the studied cases. The interplant modes are within range of 2.0 Hz and 3.0 Hz.

The second point to note is that significant amount of modes that appeared in Case 1, 28 modes, and Case 2, 22 modes. These modes are dominantly inter-area modes. The frequency range of inter-area oscillations is between 0.1 Hz and 1.0

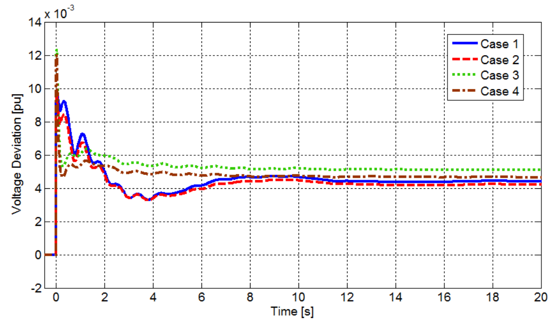

(a) Voltage signals

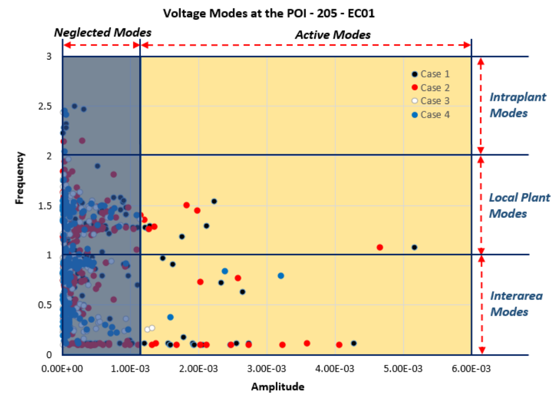

(b) Voltage dominant modes

Figure 6.18: Voltage signals and dominant modes appeared at the POI of 205 following wind power variability - EC01

Hz while the local plant modes are within range of 1.0 Hz and 2.0 Hz. The share of inter-area modes for Case 1 was 75% and for Case 2 was 59%. The inter-area oscillations influence the tie-line power flow and can cause significant stability issues for the system while the local plant oscillations impact local system.

The third point to note is that operational status of Perry was a key influence on voltage modes that appear at the POI. Following loss of Perry, number of oscillating modes dropped drastically from 28 and 22 in cases 1 and 2, to 3 and 4 in cases 3 and 4. Thus, operation of Perry caused a greater number of voltage modes to appear at the POI following variability of the wind. This phenomenon could be caused because of the fact that Perry lacks an active governor and power stabilizer.

The fourth point to note is that the operation of the SVC at the POI did not significantly impact on the voltage oscillation modes and ability of the system to damp them. In fact, the operation of the SVC slightly reduced the amplitude of the inter-area modes. But this effect was inversed for the local plant modes where operation of SVC increased their amplitudes.

It should be noted that the amplitude of captured modes were very small and their damping ratio were fairly high. Thus, it is safe to say that the FirstEnergy/PJM system retained its dynamic voltage stability after integration of the offshore wind farm.

The lists of identified voltage modes including their amplitude and damping ratio are shown for studied cases in Table 6.4 through 6.7.

EC02 Interconnection Scenario

Figures 6.19 thorough 6.23 show the voltage signals and illustrate the voltage modes that were identified at the POIs of 205 located at the Perry 345kV substation, 214 located at the Ashtabula 138kV substation, 225 located at the East Lake 345kV substation, 234located at the Lake shore 138kV substation and 245 located at the

Table 6.4: Voltage modes appeared at the POI following wind farm variability - EC01 - Case 1

Mode No.	Relevant Eigenvalue	Frequency	Amplitude	Damping Ratio
1	-0.004+j0.71	0.1 Hz	0.004	47.34%
2	-0.003+j0.683	0.1 Hz	0.003	53.31%
3	-0.003+j0.697	0.1 Hz	0.003	47.64%
4	-0.002+j0.647	0.1 Hz	0.002	90.91%
5	-0.002+j0.653	0.1 Hz	0.002	54.59%
6	-0.002+j0.652	0.1 Hz	0.002	54.58%
7	-0.002+j0.655	0.1 Hz	0.002	54.78%
8	-0.002+j0.659	0.1 Hz	0.002	53.69%
9	-0.002+j0.651	0.1 Hz	0.002	51.73%
10	-0.002+j0.705	0.1 Hz	0.002	49.19%
11	-0.002+j0.708	0.1 Hz	0.002	48.98%
12	-0.001+j0.67	0.1 Hz	0.001	53.18%
13	-0.001+j0.709	0.1 Hz	0.001	49.05%
14	-0.001+j0.72	0.1 Hz	0.001	48.37%
15	-0.001+j0.668	0.1 Hz	0.001	23.03%
16	-0.002+j1.112	0.2 Hz	0.002	40.93%
17	-0.003+j3.941	0.6 Hz	0.003	81.75%
18	-0.002+j4.559	0.7 Hz	0.002	30.28%
19	-0.001+j4.421	0.7 Hz	0.001	24.37%
20	-0.002+j5.712	0.9 Hz	0.002	12.69%
21	-0.001+j6.115	1.0 Hz	0.001	33.99%
22	-0.005+j6.79	1.1 Hz	0.005	81.64%
23	-0.002+j7.418	1.2 Hz	0.002	22.58%
24	-1.294+j8.133	1.3 Hz	0.002	23.30%
25	-1.294+j8.13	1.3 Hz	0.001	53.61%
26	-1.28+j8.041	1.3 Hz	0.001	17.74%
27	-0.001+j7.979	1.3 Hz	0.001	8.48%
28	-1.543+j9.698	1.5 Hz	0.002	51.17%

Table 6.5: Voltage modes appeared at the POI following wind farm variability - EC01 - Case 2

Mode No.	Relevant Eigenvalue	Frequency	Amplitude	Damping Ratio
1	-0.102+j0.638	0.1 Hz	0.004	57.12%
2	-0.112+j0.701	0.1 Hz	0.004	47.02%
3	-0.107+j0.673	0.1 Hz	0.003	54.31%
4	-0.104+j0.656	0.1 Hz	0.003	51.71%
5	-0.104+j0.651	0.1 Hz	0.002	54.78%
6	-0.105+j0.66	0.1 Hz	0.002	53.74%
7	-0.108+j0.678	0.1 Hz	0.002	50.21%
8	-0.107+j0.674	0.1 Hz	0.002	47.82%
9	-0.102+j0.641	0.1 Hz	0.001	55.97%
10	-0.119+j0.75	0.1 Hz	0.001	49.73%
11	-0.11+j0.689	0.1 Hz	0.001	49.42%
12	-0.735+j4.618	0.7 Hz	0.002	28.16%
13	-0.775+j4.872	0.8 Hz	0.003	37.48%
14	-1.086+j6.822	1.1 Hz	0.005	79.58%
15	-1.059+j6.653	1.1 Hz	0.001	39.75%
16	-1.295+j8.135	1.3 Hz	0.001	26.90%
17	-1.415+j8.888	1.4 Hz	0.001	19.81%
18	-1.271+j7.984	1.3 Hz	0.001	8.49%
19	-1.272+j7.992	1.3 Hz	0.001	8.30%
20	-1.36+j8.545	1.4 Hz	0.001	23.94%
21	-1.455+j9.141	1.5 Hz	0.002	29.46%
22	-1.509+j9.478	1.5 Hz	0.002	24.87%

Table 6.6: Voltage modes appeared at the POI following wind farm variability - EC01 - Case 3

Mode No.	Relevant Eigenvalue	Frequency	Amplitude	Damping Ratio
1	-0.246+j1.544	0.2 Hz	0.001	69.22%
2	-0.269+j1.691	0.3 Hz	0.001	47.25%
3	-1.368+j8.597	1.4 Hz	0.001	28.62%

Table 6.7: Voltage modes appeared at the POI following wind farm variability - EC01 - Case 4

Mode No.	Relevant Eigenvalue	Frequency	Amplitude	Damping Ratio
1	-0.384+j2.412	0.4 Hz	0.002	46.29%
2	-0.798+j5.016	0.8 Hz	0.003	42.96%
3	-0.849+j5.335	0.8 Hz	0.002	31.36%
4	-1.412+j8.874	1.4 Hz	0.001	26.66%

Avon Lake 354kV substation, following sudden drops and rises in level of power generation by the offshore wind farm in EC02 studied cases.

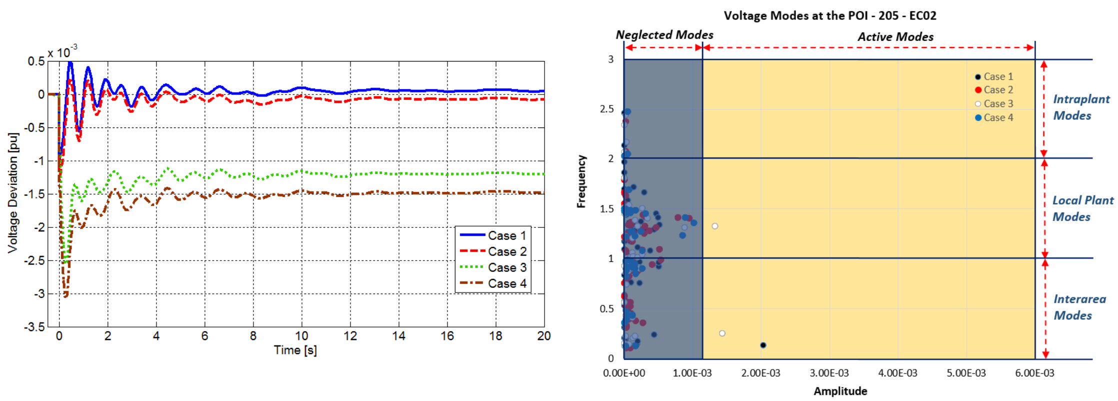

(a) Voltage signals

(b) Voltage dominant modes

Figure 6.19: Voltage signals and dominant modes appeared at the POI of 205 following wind power variability - EC02

From Figure 6.19, it can be seen that there were only three voltage modes captured at the POI of 205. This shows a significantly better performance of the system in respect to voltage dynamics in comparison to the results from the same POI in EC01 interconnection. In addition to lower number of modes, the amplitudes of these modes were also smaller. For Case 1, the only mode was 0.1 Hz which is within inter-area oscillation range. For Case 3, an inter-area mode at 0.260 Hz and a local plant mode at 1.332 Hz appeared. For Case 2 and Case 4 no voltage mode appeared at this POI.

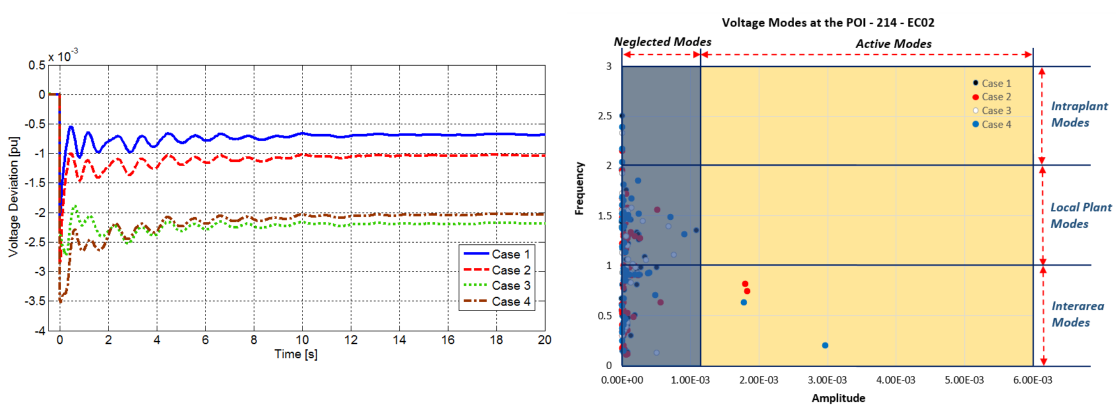

(a) Voltage signals

(b) Voltage dominant modes

Figure 6.20: Voltage singals and dominant modes appeared at the POI of 214 following wind power variability - EC02

The results from the POI of 214, shown in Figure 6.20, show that the voltage modes at this POI appeared only for cases in which SVC operated at the POI. In

Case 2, there were two inter-area modes at 0.1 Hz and 0.6 Hz. For Case 4, two inter-area modes at 0.744 Hz and 0.825 Hz appeared. In Case 1 and Case 3, no voltage mode appeared at this POI.

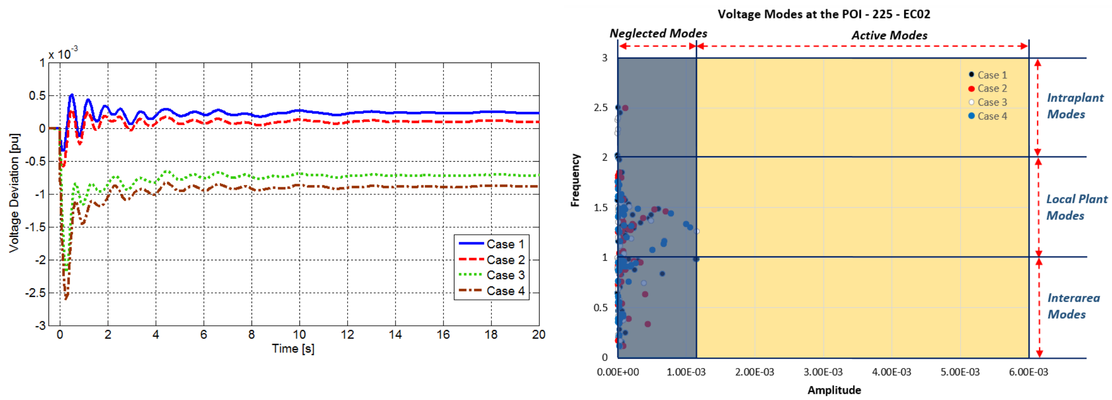

(a) Voltage signals

(b) Voltage dominant modes

Figure 6.21: Voltage signals and dominant modes appeared at the POI of 225 following wind power variability - EC02

The results from the POI of 225, shown in Figure 6.21, remark that the voltage modes at this POI appeared solely in cases without SVC at the POI, similar to the results from the POI of 205. In Case 1, there was only a an inter-area mode at 0.9 Hz. In Case 3, two local plant modes were identified at 1.3 Hz and 1.2 Hz. In Case 2 and Case 4 no voltage mode appeared at this POI.

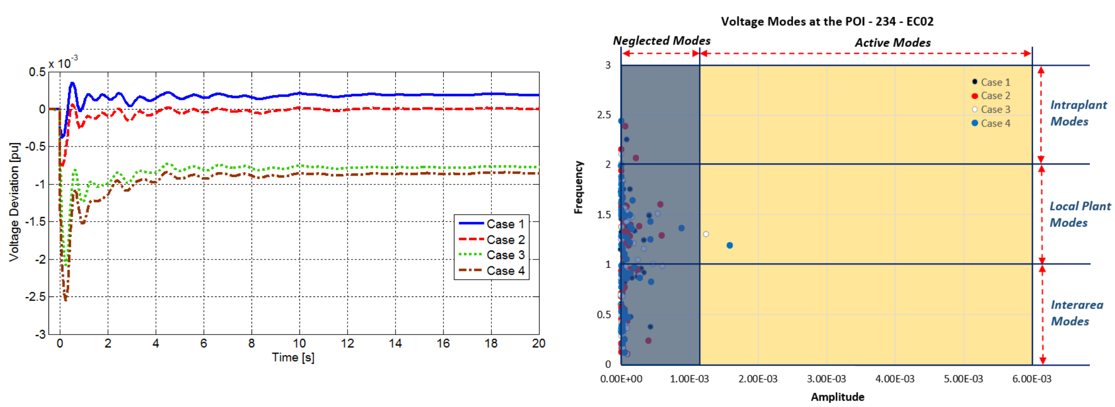

(a) Voltage signals

(b) Voltage dominant modes

Figure 6.22: Voltage signals and dominant modes appeared at the POI of 234 following wind power variability - EC02

The results from the POI of 234, shown in Figure 6.22, show that the voltage modes at this POI appeared only in cases without Perry. In Case 3, there was only a local plant mode identified at 1.2 Hz, Similarly, in Case 4, the identified mode was a local plant mode at 1.1 Hz. In Case 1 and Case 2 no voltage mode appeared at this POI.

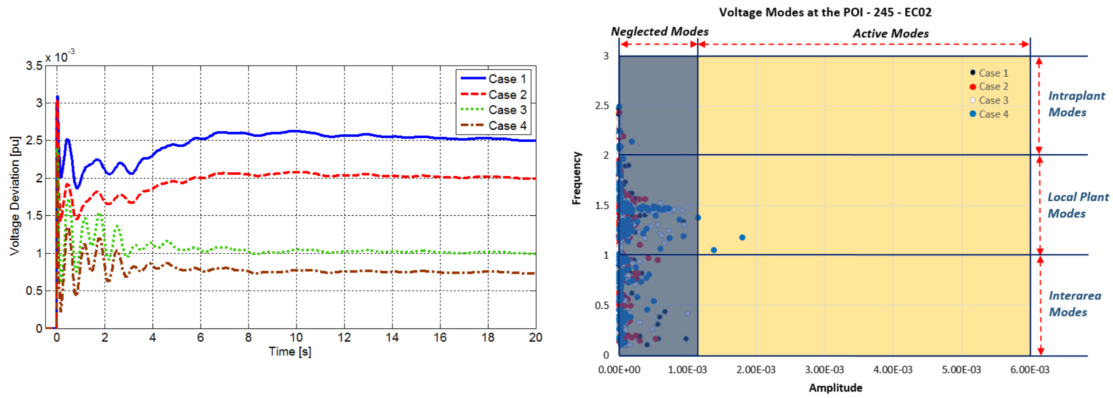

(a) Voltage signals (b) Voltage dominant modes

Figure 6.23: Voltage signals and dominant modes appeared at the POI of 245 following wind power variability - EC02

The results from the POI of 245, shown in Figure 6.23, outline that the voltage modes at this POI appeared solely in Case 4 which represents the loss of Perry and operation of SVC at this POI. The identified modes were local plant oscillation at 1.0 Hz, 1.1 Hz and 1.3 Hz.

The lists of identified voltage modes including their amplitude and damping ratio are shown for studied cases in Table 6.8 through 6.11.

Table 6.8: Voltage modes appeared at the POIs following wind farm variability - EC02 - Case 1

Mode No.	Relevant Eigenvalue	Frequency	Amplitude	Damping Ratio
1	$-0.002+j0.887$	0.1 Hz	0.002	99.55%
2	$-0.001+j6.169$	1.0 Hz	0.001	34.86%
3	$-0.001+j8.484$	1.4 Hz	0.001	24.88%

In all of the studied cases, variability of the wind did not cause any interplant mode in the FirstEnergy/PJM system. It should be noted that the amplitude of identified modes are very small and their damping ratio are fairly high. Thus, it is safe to say that the FirstEnergy/PJM system retains its dynamic voltage stability after integration of the offshore wind farm.

Table 6.9: Voltage modes appeared at the POIs following wind farm variability - EC02 - Case 2

Mode No.	Relevant Eigenvalue	Frequency	Amplitude	Damping Ratio
1	$-0.002+j4.679$	0.7 Hz	0.002	67.10%
2	$-0.002+j5.189$	0.8 Hz	0.002	57.28%

Table 6.10: Voltage modes appeared at the POIs following wind farm variability - EC02 - Case 3

Mode No.	Relevant Eigenvalue	Frequency	Amplitude	Damping Ratio
1	-0.001+j1.64	0.3 Hz	0.001	99.57%
2	-0.001+j2.606	0.4 Hz	0.001	74.88%
3	-0.001+j8.372	1.3 Hz	0.001	32.56%
4	-0.001+j8.154	1.3 Hz	0.001	31.24%
5	-0.001+j7.921	1.3 Hz	0.001	24.84%
6	-0.001+j8.196	1.3 Hz	0.001	24.84%

Table 6.11: Voltage modes appeared at the POIs following wind farm variability - EC02 - Case 4

Mode No.	Relevant Eigenvalue	Frequency	Amplitude	Damping Ratio
1	-0.003+j1.25	0.2 Hz	0.003	97.73%
2	-0.002+j3.998	0.6 Hz	0.002	63.66%
3	-0.001+j6.624	1.1 Hz	0.001	28.80%
4	-0.002+j7.517	1.2 Hz	0.002	43.34%
5	-0.002+j7.41	1.2 Hz	0.002	32.83%
6	-0.001+j8.545	1.4 Hz	0.001	25.88%
7	-0.001+j8.662	1.4 Hz	0.001	19.33%

Operation of SVC at the POIs could improve or degrade the ability of the system to damp out the oscillatory voltage modes. This depended on the geographical location of the POI and type and size of the neighboring generation units and loads.

Operation of Perry did not noticeably impact on inter-area voltage modes from all of the POIs in EC02 studied cases. However, loss of Perry cause local plant voltage modes. This is not surprising since it is the largest generation unit within FirstEnergy/PJM area and its loss influences the dynamic stability of the system.

EC03 Interconnection Scenario

Figures 6.24 and 6.25 show the voltage signals and illustrate the voltage modes that were identified at the POIs of 234 located at the Lake shore 138kV substation and 245 located at the Avon Lake 354kV substation, following sudden drops and rises in level of power generation by the offshore wind farm in EC03 studied cases.

The results from the POI of 234, shown in Figure 6.24, show that no voltage modes, neither interplant, neither local plant nor interplant, at this POI appeared for all of the studied cases. From these results can be concluded that the system is highly capable of preventing any oscillatory voltage mode in the system following variability of the wind farm. The FirstEnergy/PJM system showed a superb dynamic performance for integration of the wind farm through this POI.

The results from the POI of 245, shown in Figure 6.25 reveal that the voltage modes at this POI appeared in all of the studied cases except case 1. In Case 2, an inter-area oscillation appeared at 0.206 Hz. In Case 3, two inter-area and a local plant

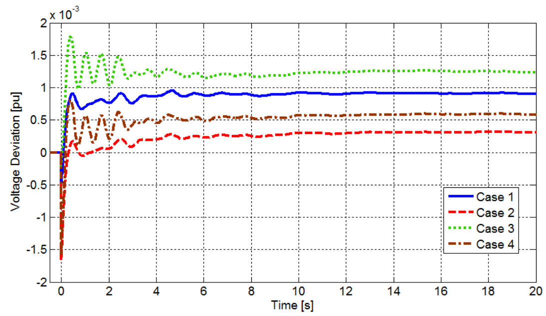

(a) Voltage signals

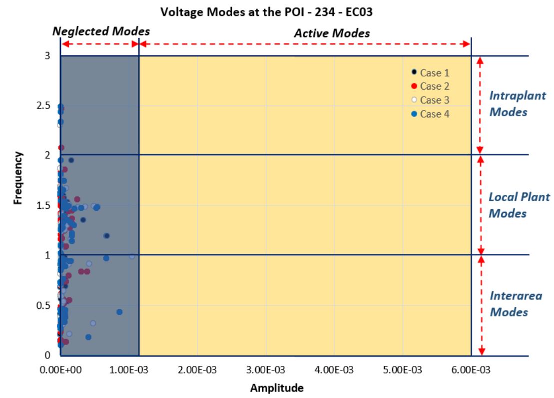

(b) Voltage dominant modes

Figure 6.24: Voltage signals and dominant modes appeared at the POI of 234 following wind power variability - EC03

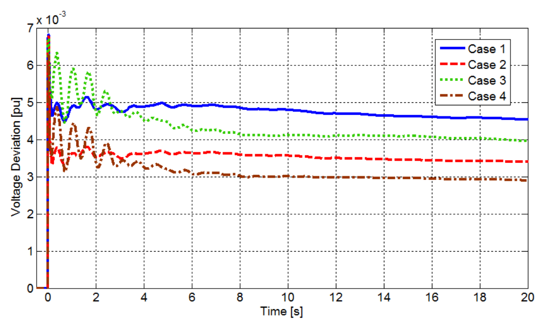

(a) Voltage signals

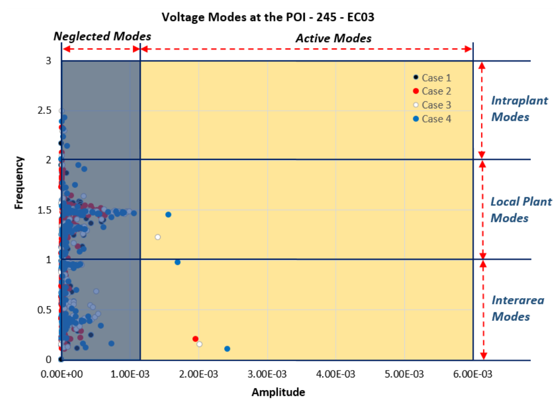

(b) Voltage dominant modes

Figure 6.25: Voltage signals and dominant modes appeared at the POI of 245 following wind power variability - EC03

oscillatory modes were identified at 0.1 Hz, 0.9 Hz and 1.2 Hz. In Case 4, two inter-area modes at 0.1 Hz and 0.9 Hz and two local plant modes at 1.452 Hz and 1.468 Hz appeared. These results show that the operation of Perry could prevent inter-area voltage modes at this POI. In addition, operation of the SVC caused voltage modes, both inter-area and local plant at this POI following variability of the wind power.

The lists of identified voltage modes including their amplitude and damping ratio are shown for studied cases in Table 6.12 through 6.15.

In overall, variability of the offshore wind power in all of the studied cases cause inter-area and local plant voltage oscillation modes at the POI in the FirstEnergy/PJM system. However, their amplitude are very small and their damping ratio are fairly high. Thus, the small signal voltage stability is not a concern in FirstEnergy/PJM system.

Table 6.12: Voltage modes appeared at the POIs following wind farm variability - EC03 - Case 1

Mode No.	Relevant Eigenvalue	Frequency	Amplitude	Damping Ratio
No Voltage Mode				

Table 6.13: Voltage modes appeared at the POIs following wind farm variability - EC03 - Case 2

Mode No.	Relevant Eigenvalue	Frequency	Amplitude	Damping Ratio
1	-0.002+j1.294	0.2 Hz	0.002	97.31%

Table 6.14: Voltage modes appeared at the POIs following wind farm variability - EC03 - Case 3

Mode No.	Relevant Eigenvalue	Frequency	Amplitude	Damping Ratio
1	-0.002+j0.952	0.2 Hz	0.002	96.91%
2	-0.001+j6.178	1.0 Hz	0.001	58.54%
3	-0.001+j7.706	1.2 Hz	0.001	64.94%

Table 6.15: Voltage modes appeared at the POIs following wind farm variability - EC03 - Case 4

Mode No.	Relevant Eigenvalue	Frequency	Amplitude	Damping Ratio
1	-0.002+j0.678	0.1 Hz	0.002	98.82%
2	-0.002+j6.144	1.0 Hz	0.002	61.77%
3	-0.002+j9.125	1.5 Hz	0.002	9.80%
4	-0.001+j9.229	1.5 Hz	0.001	6.46%

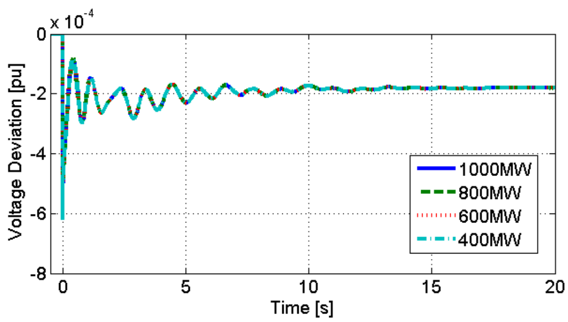

(a) POI 214

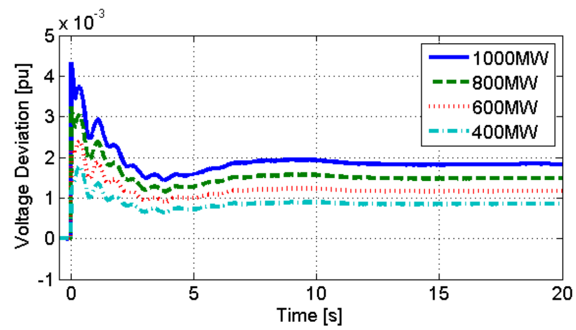

(b) POI 205

Figure 6.26: Voltage signals from the POI 205 and the POI 214 following a given step change in wind power for different pre-disturbance levels of wind power

Figure 6.26 compares the voltage dynamics of the POI 205 and the POI 215. As shown in this figure, the voltage response at POI the 214 for all pre-disturbance levels of wind power is identical while at the 205 is a function of pre-disturbance level of wind power. As the higher the pre-disturbance level of wind power became, the greater the voltage deviation at the POI 205 became. Thus, it could be concluded that the voltage dynamics and level of voltage deviation for different pre-disturbance levels of wind power is a function of the geographical location of the POI and the size and the controller used in the neighboring generation units. Also, it should be noted that in all of the studied cases, the level of voltage deviation was a function of magnitude of change in level of the wind power. Figure 6.27 shows the voltage dynamics for the POI 205 and the POI 245 as two examples.

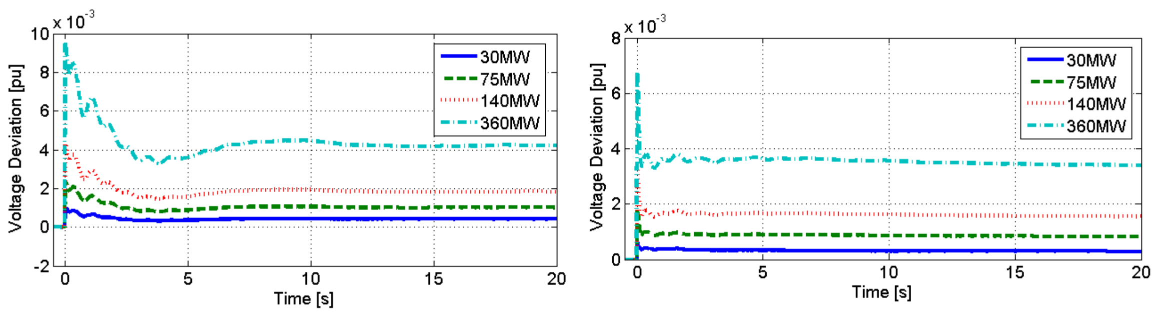

(a) POI 214

(b) POI 205

Figure 6.27: Voltage signals from the POI 205 and the POI 245 following different levels of change in wind power

6.3.2 Small Signal Frequency Response

Wind Power Drop

This section presents the frequency response to a sudden drop in level of power generation by the offshore wind farm. Figures 6.28 and 6.29 present the simulation results for nadir frequency and settling frequency in the FirstEnergy/PJM area for studied cases.

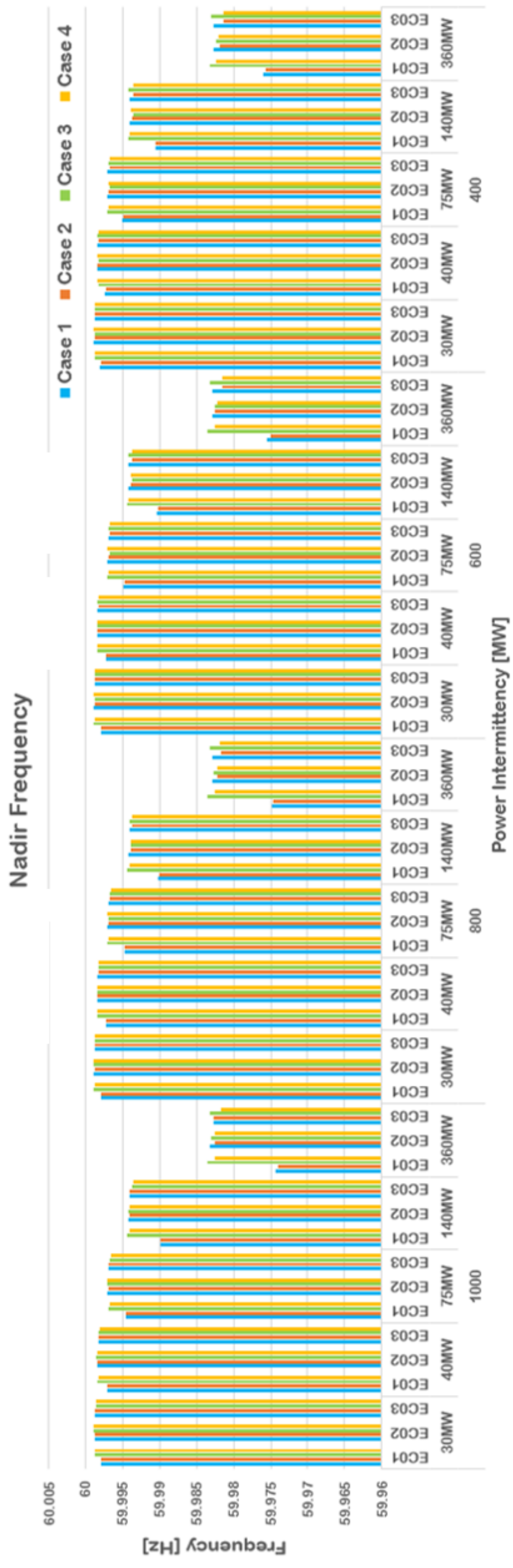

Figure 6.28: Nadir frequency following a drop in the level of power generation by wind farm in the FirstEnergy/PJM area

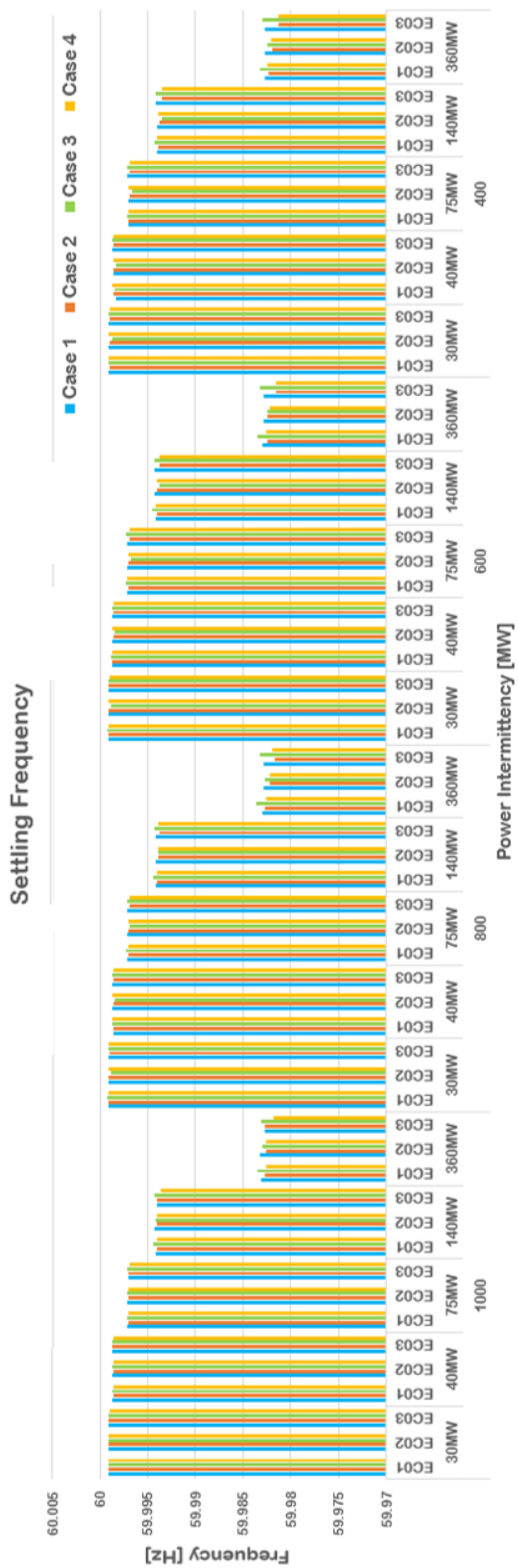

Figure 6.29: Settling frequency following a drop in the level of power generation by wind farm in the FirstEnergy/PJM area

In Figure 6.28, it can be seen that in all of the studied cases, nadir frequency during the inertial frequency response stage remained above the UFLS threshold for all levels of drop and all levels of pre-drop operating point of the offshore wind farm. The lowest nadir frequency was 59.975 Hz in Case 1 and Case 2 of EC01 interconnection, following 360MW wind power drop. According to the NERC UFLS reliability standard in the Eastern Interconnection, the UFLS threshold for generators with 100 MW or more of peak net load must be set at 59.5 Hz [105]. These results also show that the nadir frequency is a function of level of drop in wind power generation. As the greater the level of drop becomes, the lower level of the nadir frequency becomes.

The results from the settling frequency, shown in Figure 6.29, showed that in all of the studied cases, the system regained the area frequency of greater than 59.98 Hz within inertial frequency control stage. These results also show that the settling frequency is a function of level of drop in wind power generation. The greater the level of drop became, the lower the settling frequency became.

For the EC01 interconnection, for all levels of wind power, in Case 1 and Case 2 in which Perry was online, the nadir frequency was lower than in the other cases in which Perry was offline, Case 3 and Case 4. This is an indication of a greater oscillation in Case 1 and Case 2. Figure 6.30 compares the frequency response of these cases with respect to time.

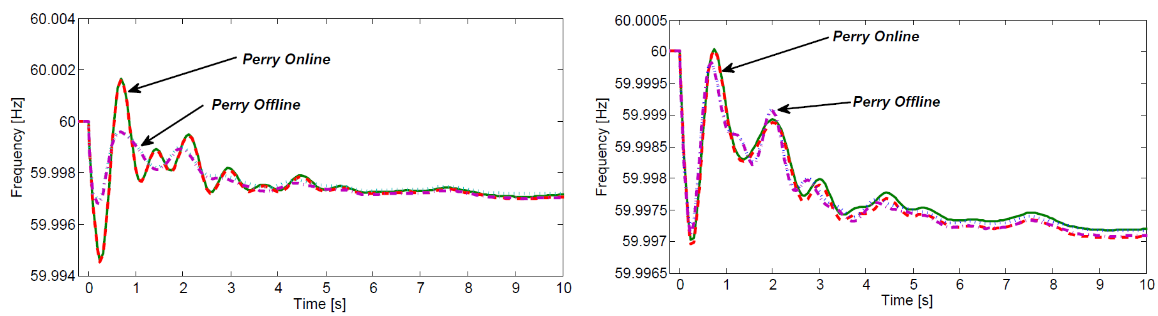

(a) EC01

(b) EC02

Figure 6.30: Primary frequency response in the FirstEnergy area to 140MW drop in level of wind power generation for EC01 and EC02 interconnections

In Figure 6.30, it can be seen that Case 1 and Case 2 for EC01 had significantly higher levels of frequency swing than Case 3 and Case 4, nearly doubled. The main reason for this phenomenon is that for EC01, the POI is situated at the Perry substation. Since Perry was a nuclear power plant with no active governor, it magnifies the disturbances that are caused by wind power intermittency.

Results from the settling frequency, shown in Figure 6.29, also reveal that the pre-disturbance level of offshore wind power generation does not determine the settling frequency. The only factor in determining the primary settling frequency is the level of drop in wind power generation (size of the disturbance). Figure 6.31 and 6.32 illustrate the relationship between the size of wind power drop and the pre-disturbance level of offshore wind power generation and nadir and settling frequencies of the primary frequency response of the system.

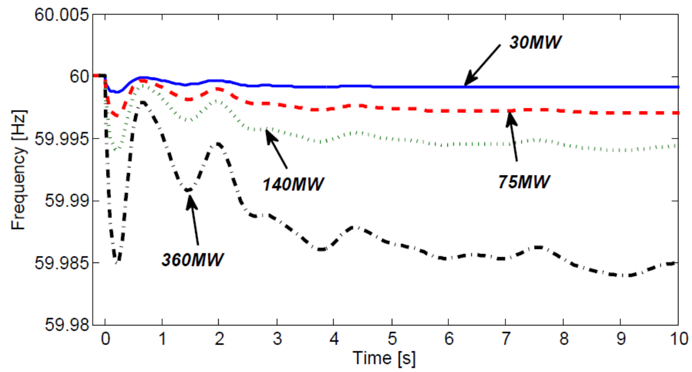

Figure 6.31: Primary frequency response in the FirstEnergy area to different levels of drop in wind power generation level for EC01 interconnection

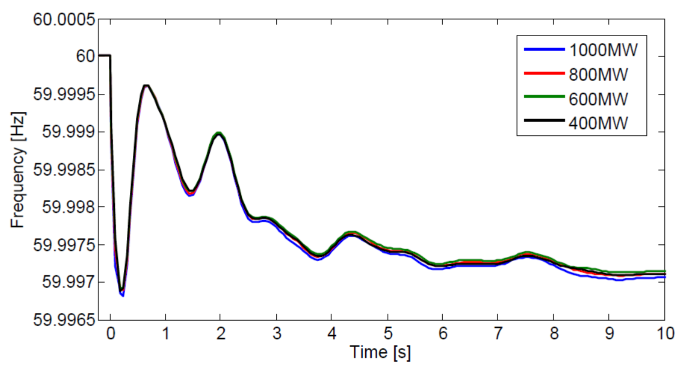

Figure 6.32: Primary frequency response in the FirstEnergy area to 140MW level of drop in wind power generation level at given different pre-drop operating points of the offshore wind farm for EC01 interconnection

Figures 6.33 through 6.36 show computed values of the proposed frequency response metric for the studied cases in this analysis.

The results presented in Figures 6.33 through 6.36 reveal that the system frequency response for EC01 interconnection in cases in which Perry was online (Case 1 and Case 2) was weaker than in cases in which Perry was offline. As mentioned previously, the lack of governor regulation in this generation unit degrades the frequency response of the system while the offshore wind farm is integrated through this POI.

The frequency response metrics were approximately consistent for all pre-drop levels of wind power generation in all studied cases and were a function of the level of drop. The greater the size of the drop was, the weaker frequency response of the system was. Finally, the operation of SVC at the POIs did not have any significant impact on frequency response. The results agree with this notion.

In overall, the primary frequency response metrics by FirstEnergy system showed that it has a great ability to arrest frequency decline within first 20 seconds following

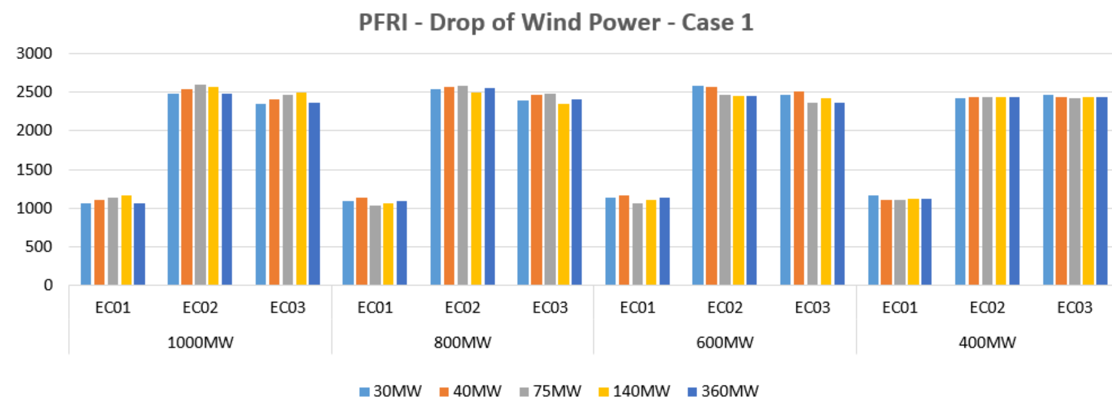

Figure 6.33: Primary Frequency Response Index for wind power generation drop - Case 1

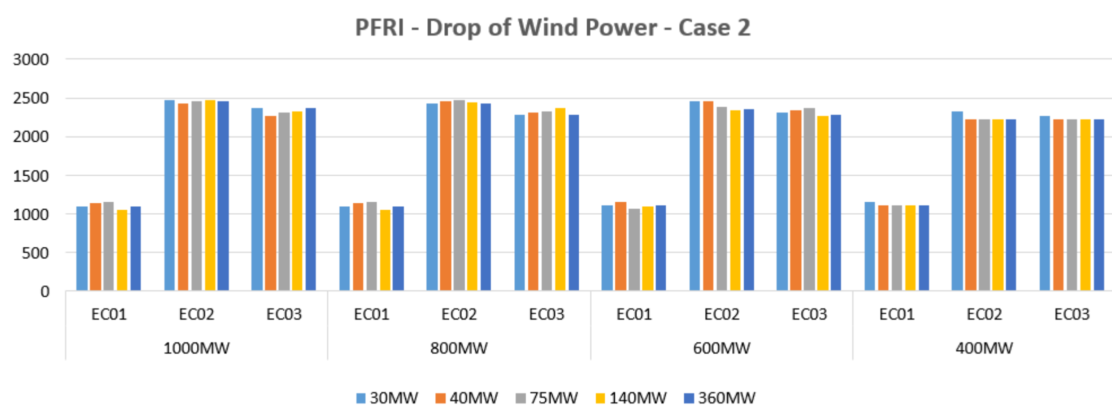

Figure 6.34: Primary Frequency Response Index for wind power generation drop - Case 2

the drop in level of power generation by the offshore wind farm. In all of the studied cases, the nadir frequencies were far distant from threshold of UFLS, 59.5 Hz in Eastern Interconnection [105].

Wind Power Rise

This section presents the frequency response to a sudden rise in level of offshore wind power. Figures 6.37 and 6.38 present the simulation results for nadir frequency and settling frequency in the FirstEnergy/PJM area for studied cases.

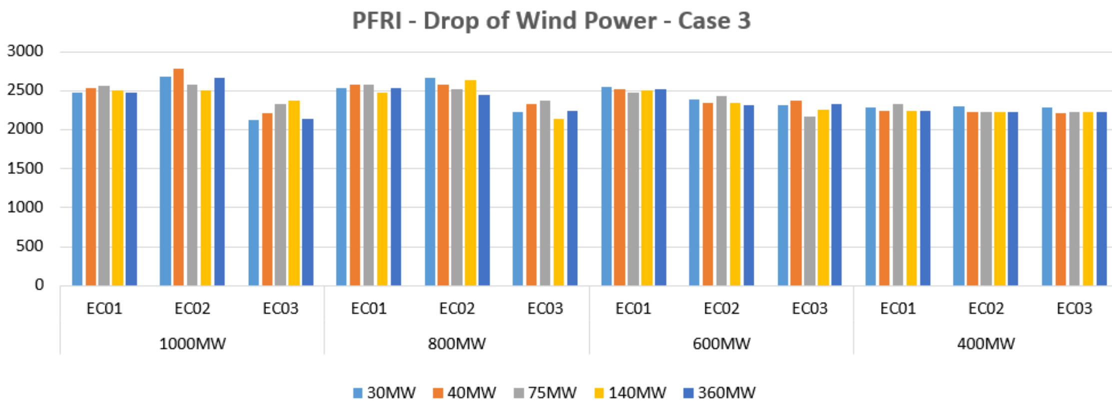

Figure 6.35: Primary Frequency Response Index for wind power generation drop - Case 3

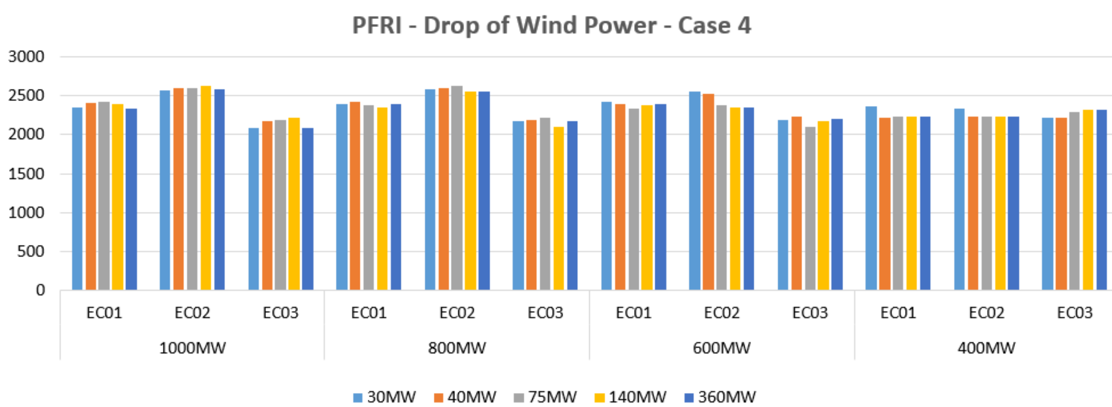

Figure 6.36: Primary Frequency Response Index for wind power generation drop - Case 4

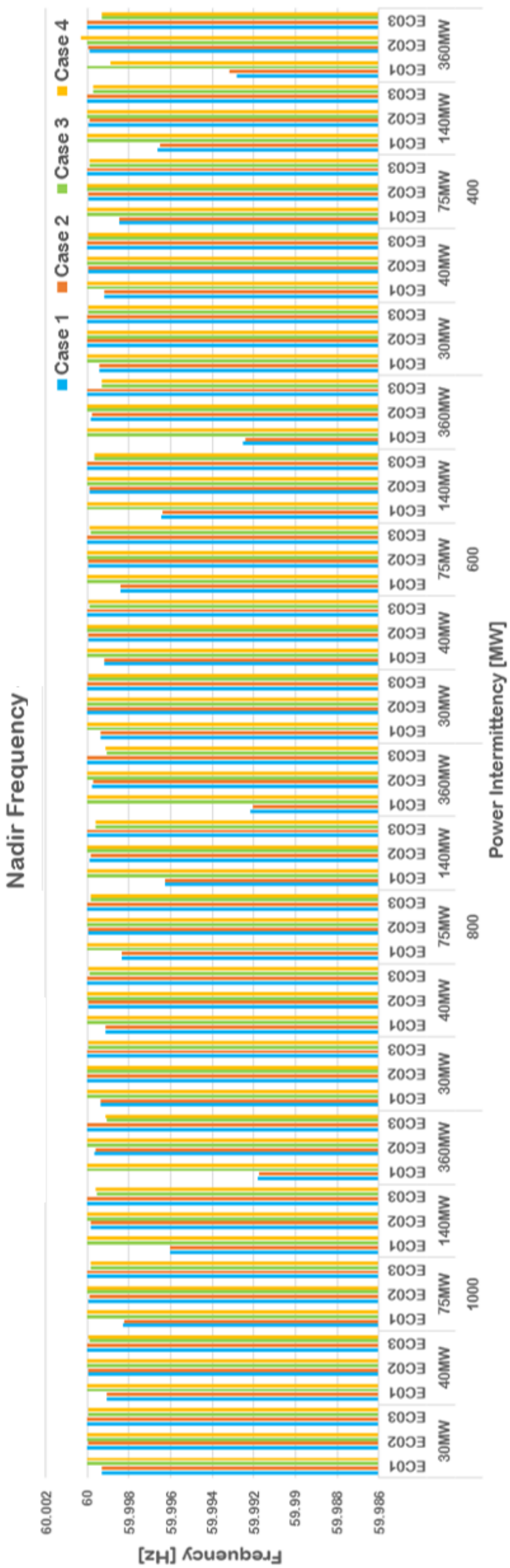

Figure 6.37: Nadir frequency following a rise in the level of power generation by wind farm in the FirstEnergy/PJM area

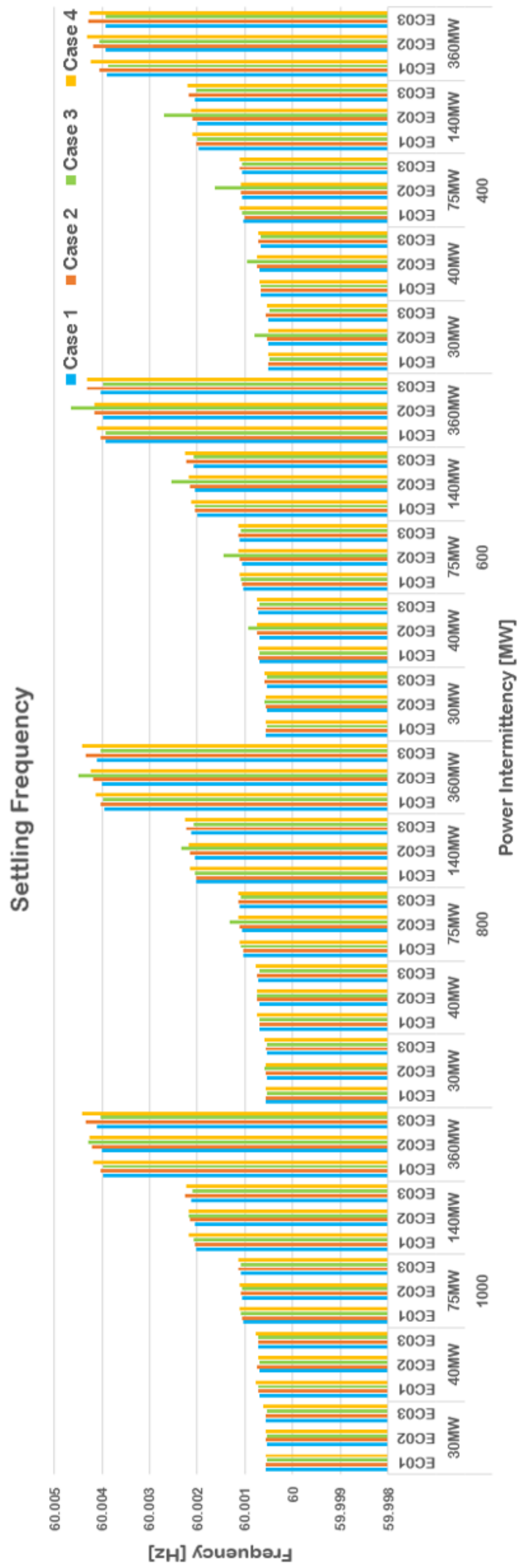

Figure 6.38: Settling frequency following a rise in the level of power generation by wind farm in the FirstEnergy/PJM area

In Figure 6.37, it can be seen that in all of the studied cases, nadir frequency in the inertial frequency response stage remained above the UFLS threshold for all levels of rise and all levels of pre- rise operating point of the offshore wind farm. The lowest nadir frequency was 59.992 Hz in Case 1 and Case 2 of EC01 interconnection, following 360MW wind power rise. These results also show that the nadir frequency is a function of level of rise in wind power generation. As the greater the level of drop becomes, the lower level of the nadir frequency becomes.

The results from the settling frequency, shown in Figure 6.29, showed that in all of the studied cases, within first 10 seconds following the rise, the system regains a new steady state area frequency within range of 60.00 Hz and 60.025 Hz. These results also showed that the settling frequency is a function of level of rise in wind power generation. As the greater the level of rise becomes, the higher the settling frequency becomes.

For the EC01 interconnection, Similar to the results from drop in wind power generation, the Case 1 and Case 2 in which Perry was online, experienced lower levels of nadir frequency and higher maximum frequency which is an indication of a greater oscillation than cases in which Perry was offline, Case 3 and Case 4. Figure 6.39 compares the frequency response of these cases with respect to time.

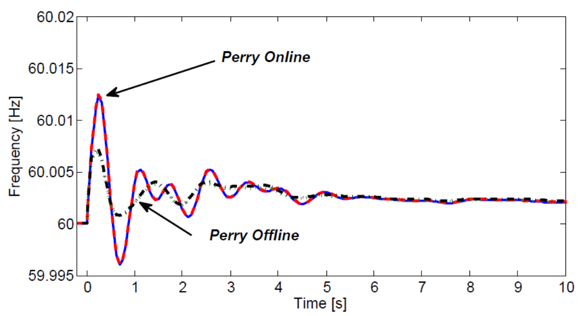

(a) EC01

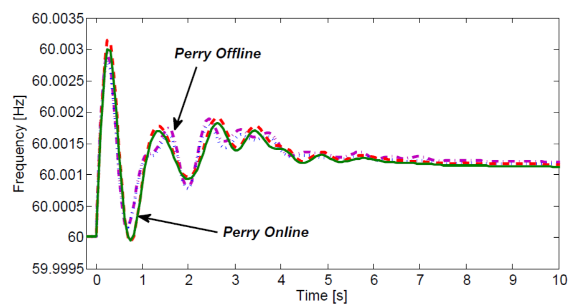

(b) EC02

Figure 6.39: Primary frequency response in the FirstEnergy area to 140MW rise in level of wind power generation for EC01 and EC02 interconnections

In Figure 6.39, it can be seen that, as expected, Case 1 and Case 2 for EC01 had significantly higher levels of frequency swing than Case 3 and Case 4, nearly doubled. As mentioned previously, the EC01 POI is located at the Perry substation. Since Perry is not equipped with an active governor, the capability of the system to damp the frequency oscillations is limited. As a result, greater overshoot (higher maximum frequency) and lower nadir frequency were recorded from the Case 1 and Case 2 of EC01 in contrast with the metrics from the Case 3 and Case 4 of EC01.

Results from the settling frequency, shown in Figure 6.38, revealed that the pre-disturbance level of offshore wind power generation did not determine the settling frequency. The only factor in determining the primary settling frequency was the level of rise in wind power generation (size of the disturbance). Figure 6.40 and 6.41 illustrate the relationship between the size of wind power rise and the pre-disturbance level of offshore wind power generation and nadir and settling frequencies of the primary frequency response of the system.

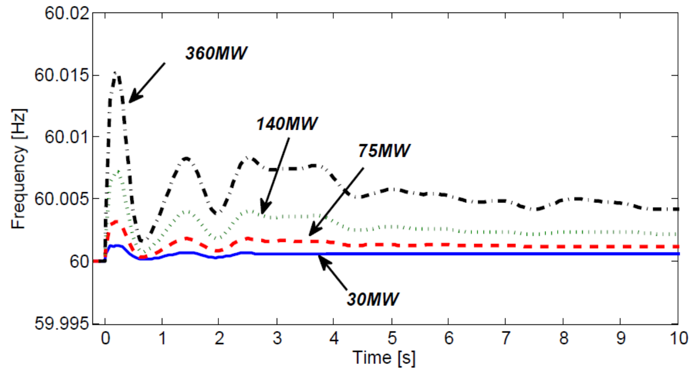

Figure 6.40: Primary frequency response in the FirstEnergy area to different levels of rise in wind power generation level for EC01 interconnection

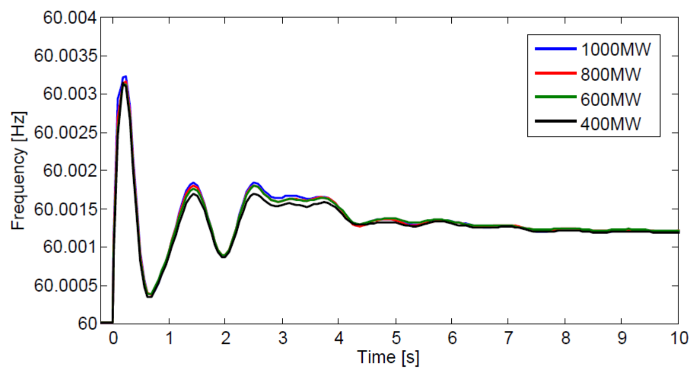

Figure 6.41: Primary frequency response in the FirstEnergy area to 140MW level of rise in wind power generation level at given different pre-drop operating points of the offshore wind farm for EC01 interconnection

Figures 6.42 through 6.45 show computed values of the proposed frequency response metric for the studied cases in this analysis.

The results presented in Figures 6.42 through 6.45 reveal that the system frequency response to rise in level of wind power for EC01 interconnection in cases in which Perry was online (Case 1 and Case 2) was weaker than in cases in which Perry was offline. These results are similar to the results from drop in wind power generation.

The frequency response metrics were approximately consistent for all pre-disturbance levels of wind power generation in all studied cases and is independent from the level of rise.

Finally, the operation of SVC at the POIs did not have any significant influence on the frequency response.

In summary, the FirstEnergy system was able to adequately arrest the frequency decline and oscillations within approximately the first 10 seconds following an rise in the level of offshore wind power generation.

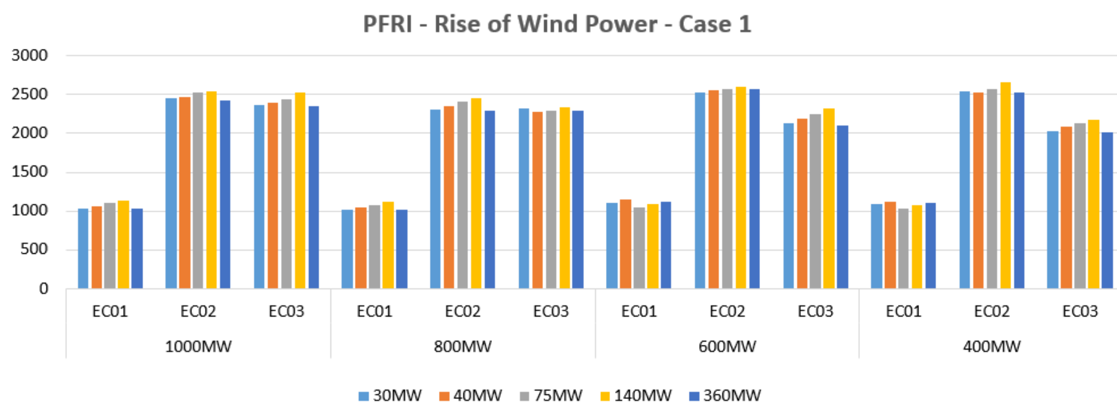

Figure 6.42: Primary Frequency Response Index for wind power generation rise - Case 1

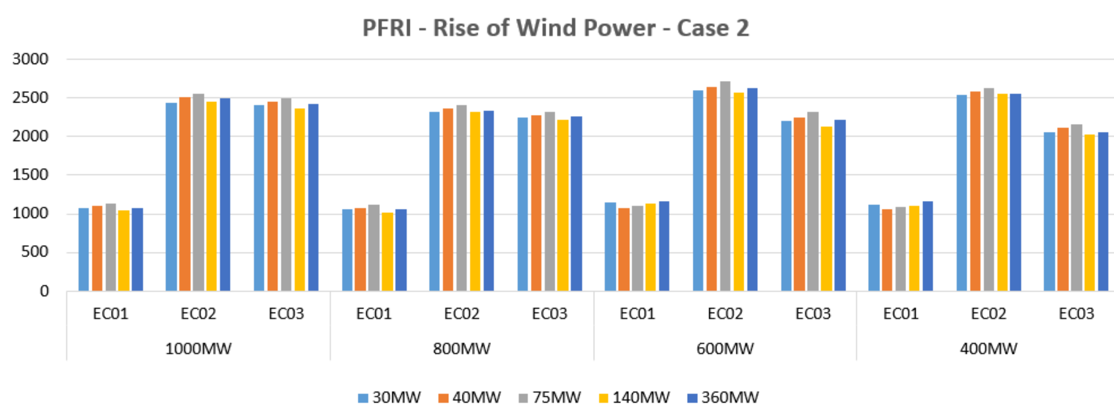

Figure 6.43: Primary Frequency Response Index for wind power generation rise - Case 2

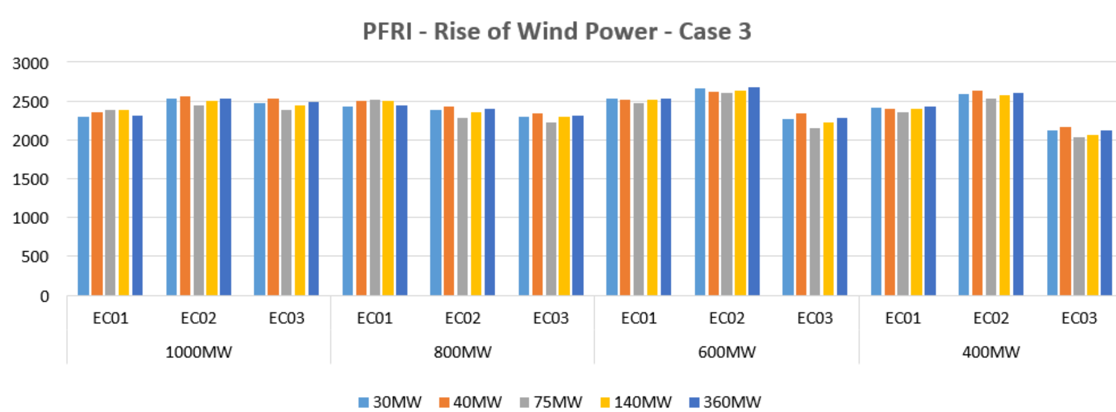

Figure 6.44: Primary Frequency Response Index for wind power generation rise - Case 3

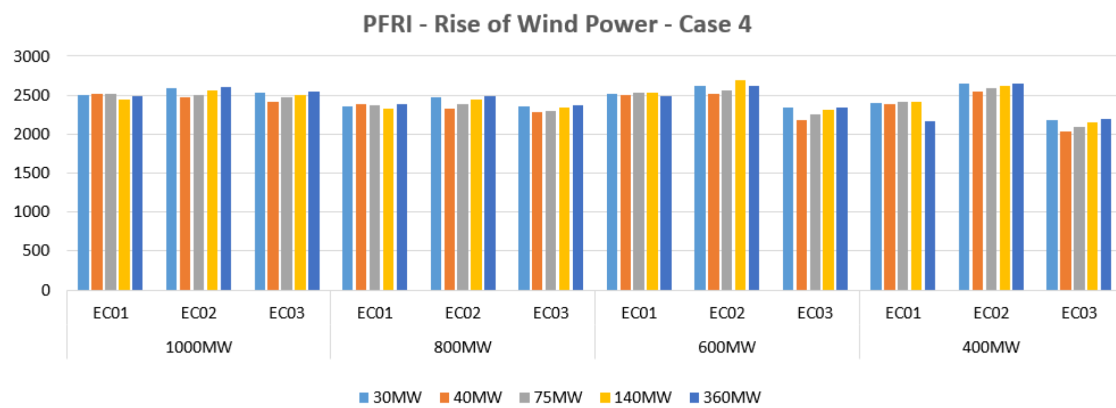

Figure 6.45: Primary Frequency Response Index for wind power generation rise - Case 4

6.4 Large Signal Stability Analysis

This section shows the results from the large signal stability analysis and discusses the findings. The studied cases in this section are described in Table 5.5.

6.4.1 Short Term Fault

Tables 6.16 through 6.19 show the range of CCTs for studied cases and faults in the FirstEnergy/PJM area and the effects of operation of the offshore wind farm on transient stability of the area.

- **Large Capacity Generators**

Table 6.16: CCT for three phase faults on large capacity generators in studied cases

	Base Case	**Case 1**		**Case 2**		**Case 3**		**Case 4**	
Component	CCT	Min	Max	Min	Max	Min	Max	Min	Max
Perry	9.5	9.5	10.5	9.5	10.5	—	—	—	—
Davis-Besse	7.5	7.5	7.5	7.5	7.5	7.5	7.5	7.5	7.5

- **Medium Capacity Generator**

Table 6.17: CCT for three phase faults on medium capacity generators in studied cases

	Base Case	**Case 1**		**Case 2**		**Case 3**		**Case 4**	
Component	CCT	Min	Max	Min	Max	Min	Max	Min	Max
Avon	8.5	21.5	21.5	21.5	21.5	8.5	9.5	8.5	9.5
W.H. Sammis	14.5	23.5	23.5	23.5	23.5	17.5	17.5	17.5	17.5

- **Transmission Lines**

Table 6.18: CCT for three phase faults on transmission lines in studied cases

	Base Case	**Case 1**		**Case 2**		**Case 3**		**Case 4**	
Component	CCT	Min	Max	Min	Max	Min	Max	Min	Max
Hanna to Juniper	15.5	18.5	22.5	17.5	22.5	15.5	15.5	15.5	15.5
Hoytdl to Bruce	31.5	>900	>900	>900	>900	45.5	47.5	45.5	49.5
Davis to Leymon	7.5	7.5	7.5	7.5	7.5	7.5	7.5	7.5	7.5

- **Offshore Collector System:**

Table 6.19: CCT for three phase faults on offshore collector system in studied cases

	Case 1		**Case 2**		**Case 3**		**Case 4**	
Component	Min	Max	Min	Max	Min	Max	Min	Max
Half of the System	>900	>900	>900	>900	>900	>900	>900	>900

The results show that operation of offshore wind farm, for all levels of wind, did improve the CCT for three phase faults in the system. In fact, in all of the studied cases in which Perry was online, the CCT was increased. In the other cases in which Perry was offline, CCT remained the same as was in base case. In two of the cases, fault on collector system and fault on Hoytdl-Bruce Mansfield line, system remained stable after 900 cycles.

These results show that operation of the offshore wind farm did not noticeably improve the CCT for faults on large generators. To compare the CCT in cases with and without offshore wind farm, for fault on Davis-Besse, it remained unchanged and for fault on Perry, it was conditionally improved by only 2 cycles. However, operation of the offshore wind farm significantly improved the CCT for faults on medium capacity generators, as Sammis and Avon experienced higher CCT in cases with the offshore wind farm integrated. In addition, the wind farm improved the CCT for the lines, depending on their distance from large capacity generators. As shown, the CCT for fault on Hoytdl to Bruce Mansfield line was superbly improved from 32 cycles to not losing the synchronism for up to 900 cycles in cases 1 and 2. On the other hand, the CCT for fault on Davis-Besse to Leymon line did not change in cases with operating wind farm.

Integration and operation of the offshore wind farm improved the CCT for fault on Avon generator by 15 cycles, from 8 cycles in base case to 23 cycles while the CCT remained unchanged for fault on the Davis-Besse generator. For comparison purposes, these two faults were chosen to show in this section. The findings of this analysis are applicable to other faults with respect to whether or not their CCT was improved upon integration of the offshore wind farm.

The active power dynamic and relative rotor angle behavior for these two faults are shown in Figures 6.46 and 6.47.

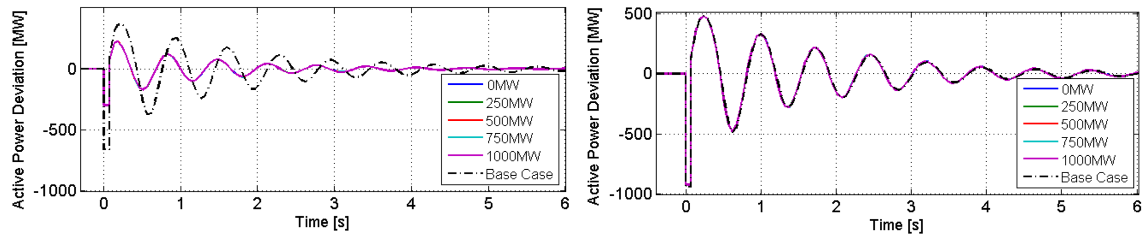

(a) Fault on Avon generator

(b) Fault on Davis Besse generator

Figure 6.46: Active power profiles following a short fault for different levels of wind power

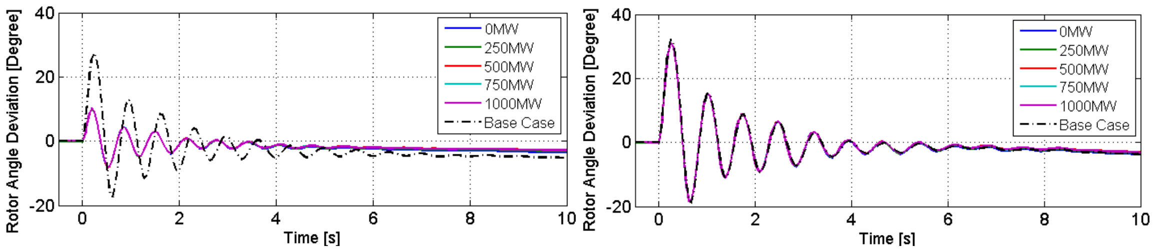

(a) Fault on Avon generator

(b) Fault on Davis Besse generator

Figure 6.47: Rotor angle profiles following a short fault for different levels of wind power

The results from rotor angle behavior show that rotor angle stability was improved in the cases in which CCT was improved by its lowered magnitude and improved damping ratio, for all levels of wind power. In the other cases in which the CCT has not been changed, the rotor angle stability has been degraded. This was an indication that the operation of offshore wind farm improves transient stability of the system.

Figures 6.48 through 6.51 show the transient rotor angle, active power, reactive power, area frequency and voltage dynamics following faults on Davis-Besse and Avon generators for all of the studied cases.

These results show that the dynamics of rotor angle, active power, reactive power and voltage following are related. In case of fault on Avon, as the CCT was improved, the rotor angle stability and active power recovery was improved, and subsequently, reactive power and voltage dynamics are improved. The TOV from 1.020 p.u. in cases 1 and 2 was decreased to 1.003 p.u. in cases 3 and 4. In case of fault on Davis-Besse in which the CCT remained unchanged after wind farm integration, the dynamics of rotor angle and active power remained unchanged. Subsequently, reactive power and voltage dynamics remained unchanged with TOV and TLV at 1.028 p.u. and zero p.u. The settling voltage in all of the studied cases was the pre-fault voltage level (no steady state voltage deviation). Based on presented results, it can be concluded that integration of offshore wind farm into the system, improved the transient voltage stability and transient rotor angle stability of the system following short term faults.

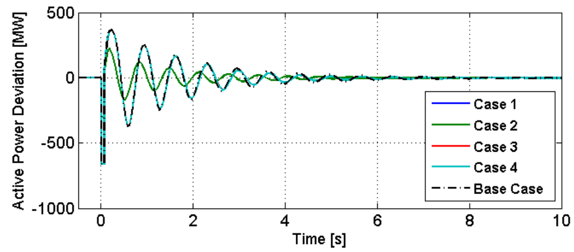

(a) Fault on Avon generator

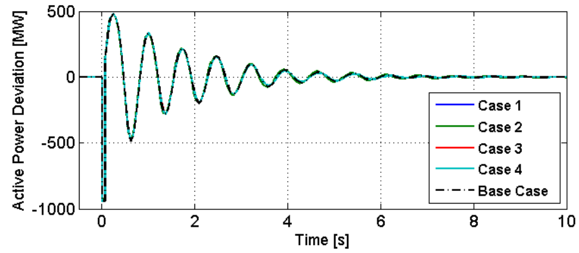

(b) Fault on Davis Besse generator

Figure 6.48: Active power profiles following a short fault in different studied cases

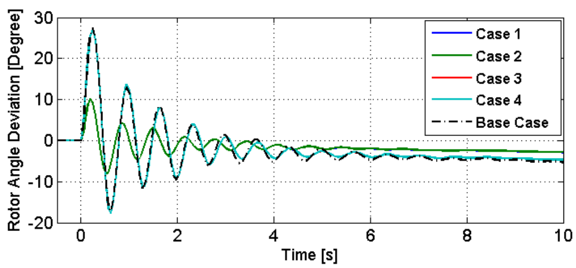

(a) Fault on Avon generator

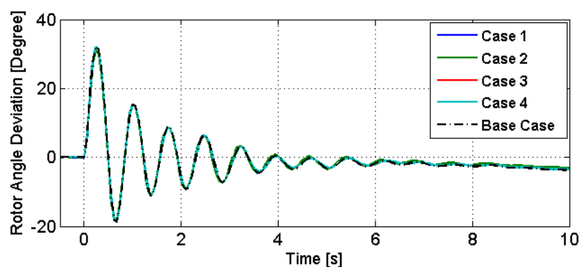

(b) Fault on Davis Besse generator

Figure 6.49: Rotor angle profiles following a short fault in different studied cases

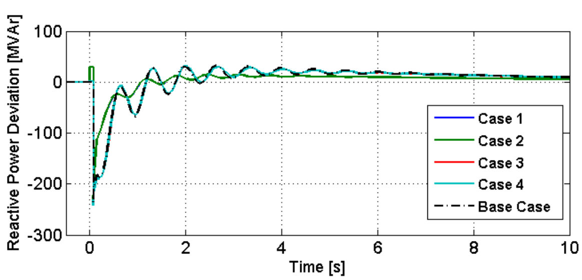

(a) Fault on Avon generator

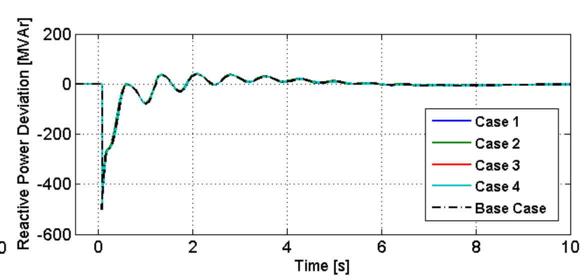

(b) Fault on Davis Besse generator

Figure 6.50: Reactive power profiles following a short fault in different studied cases

From the results, it also can be seen that the CCT directly determines short term transient rotor angle and voltage stability in a power system with a variable offshore wind farm. In the FirstEnergy/PJM power system, the CCT was a function of operation of Perry and independent from operation of SVC at the POI. This was why results from cases 1 and 2 for all studied cases in which CCT was improved are identical as well as the results from cases 3 and 4. This was not surprising since operation of Perry provided additional support and inertia during fault and post fault.

In [106], it was concluded that wind machines with capability of providing reactive support aid the synchronous generators in the area to damp the oscillations since can

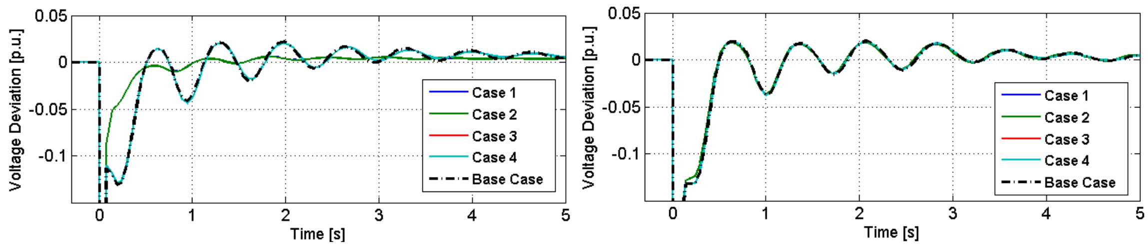

(a) Fault on Avon generator (b) Fault on Davis Besse generator

Figure 6.51: Voltage power profiles following a short fault in different studied cases

provide reactive power support in all range of their operation. Following this notion, operation of SVC at the POI should be able improved the transient stability of the system too. Adversely, in this system, the additional reactive power support did not have any influence on the deviations. In fact, the rotor angle stability improvement was because of higher available synchronous generators reserve in the area following redispatch of the generators in the area to add wind power.

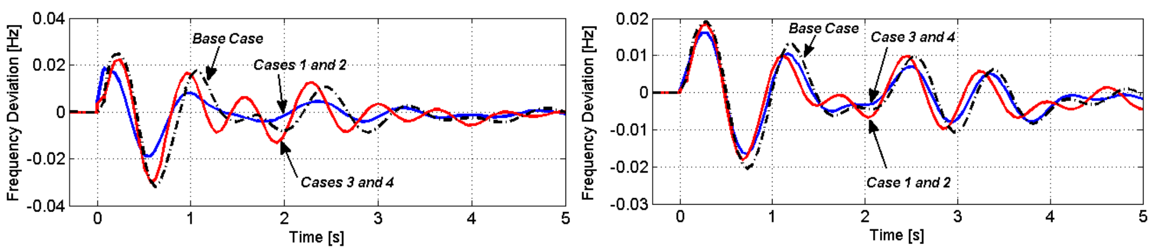

(a) Fault on Avon generator (b) Fault on Davis Besse generator

Figure 6.52: Area frequency profiles following a short fault in different studied cases

The results illustrated in Figure 6.52 show that the area frequency remained within standard range following both faults and the nadir frequency remained above 59.96 Hz. However, the frequency response of a power system is defined by the area frequency behavior in respect to the level of blocked power. Plots shown in Figure 6.53 show the proposed frequency response metric, SBFR, for studied cases for a complete operational range of offshore wind farm. This metric is a function of blocked active electrical power and area frequency swing during a fault.

From Figure 6.53, it can be seen that upon offshore wind farm integration; the frequency response for fault on Davis-Besse was improved in all of the studied cases for all levels of wind power. Cases 1 and 2 in which Perry was online experienced the greater improvement than cases 3 and 4. The level of improvement was approximately consistent following variability of the wind power. By comparing results from case 1 and case 2 as well as case 3 and case 4, it can be seen that the contribution of SVC to frequency response was very insignificant.

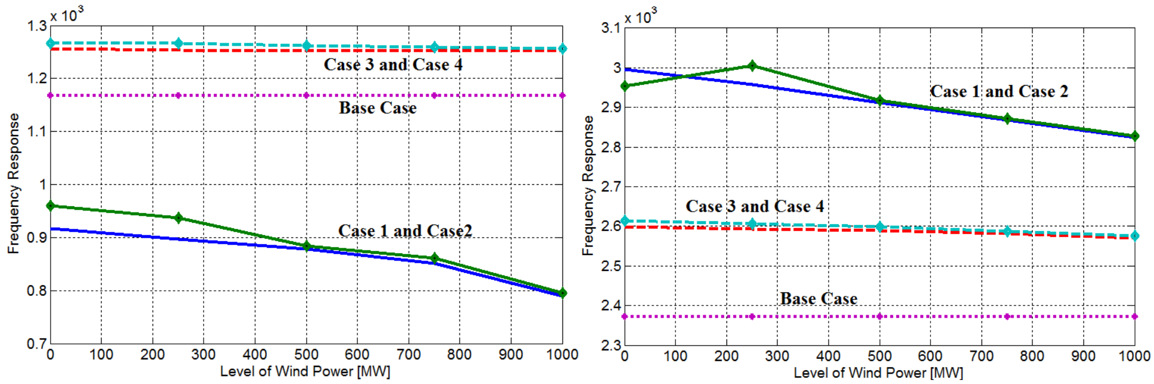

(a) Fault on Avon generator (b) Fault on Davis Besse generator

Figure 6.53: SBFR for short term faults in FirstEnergy/PJM area for different levels of offshore wind power

The frequency response for fault on Avon upon offshore wind farm integration was a function of operation of Perry. In cases 1 and 2 in which Perry was online, upon offshore wind farm integration, the frequency response was weakened whereas in cases 3 and 4 in which Perry was offline, it was improved. The level of improvement was approximately consistent following variability of the wind power. Similar to finding from the previous event, by comparing results from case 1 and case 2 as well as case 3 and case 4, it can be seen that the contribution of SVC to frequency response was very insignificant.

For further investigation, plots shown in Figure 6.54 show the SBFR for faults on Perry generator, large capacity, and Sammis generator, medium capacity.

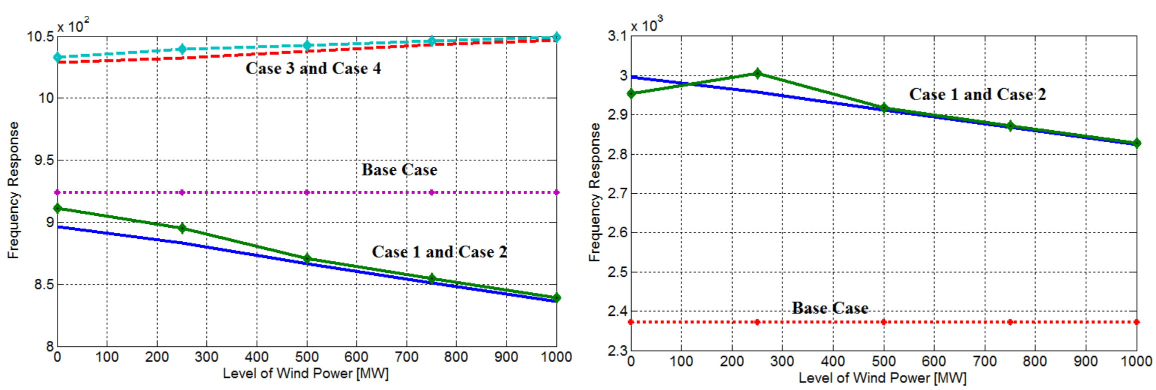

(a) Fault on W.H. Sammis generator (b) Fault on Perry generator

Figure 6.54: SBFR for short term faults in FirstEnergy/PJM area for different levels of offshore wind power

The results shown in 6.54 are consistent with the results from Figure 6.53 and upon offshore wind farm integration, the frequency response for fault on Perry was improved while its improvement for fault on Sammis was a function of operation of Perry. Accordingly, in cases 3 and 4 in which Perry was offline, the frequency response was improved while in cases 1 and 2 in which Perry was online, it was degraded.

In the FirstEnergy/PJM area, as was shown in small signal frequency response section, operation of Perry weakens the frequency response of the system if the wind farm was integrated through the POI at Perry, EC01. Following fault on Avon, since this unit was not able to provide sufficient inertial response, the frequency response depended on the operation and inertial response from the other generators in the area, especially the large capacity generators. Therefore, adverse impact of operation of Perry on frequency response was monitored. On the other hand, following the fault on Davis-Besse, since it was a large unit with capability to provide sufficient inertial response, the operation of Perry did not weaken its frequency response.

plots shown in Figure 6.55 show the SBFR for faults on Hoytdl to Bruce Mansfield and Davis-Besse to Leymon lines.

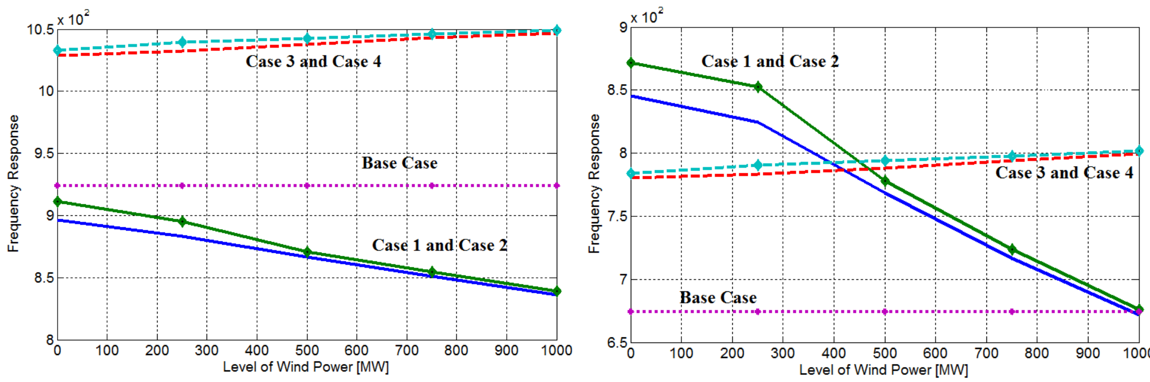

(a) Fault on Hoytdl to Bruce Mansfield line (b) Fault on Davis-Besse to Leymon line

Figure 6.55: SBFR for short term faults in FirstEnergy/PJM area for different levels of offshore wind power

Hoytdl to Bruce Mansfield line transmit the power from Bruce Mansfield power plant which consists of several small units and Davis-Besse to Leymon line transmits the power from Davis-Besse power plant which has a single unit. Thus, these lines are both connected from one end to generation units: (1) Bruce Mansfield, medium capacity and (2) Davis-Besse, large capacity.

The frequency response for fault on Hoytdl to Bruce Mansfield line was similar consistent with the results from faults on medium capacity generators. Thus, in cases 3 and 4 in which Perry was offline, the frequency response was improved while in cases 1 and 2 in which Perry was online, it was degraded. Adversely, the frequency response for fault o Davis-Besse to Leymon line was to consistent with the results from faults on large capacity generators. Therefore, the frequency response was improved in all studied cases and for all level of wind power. Since the transmission lines do contribute to the inertia of the system, the frequency response for fault on them depends on their distance from major contributor units in inertia. Thus, upon offshore wind integration, the closer the lines are to the large capacity generators, to a greater extend the frequency response becomes improved. Additionally, the more distant they are from the large capacity generators, the more their frequency response becomes weaker.

In comparison, the values of SBFR for faults on the medium capacity generators and lines were significantly lower than the fault on large scale generators. For instance, the SBFR while Perry online for Davis-Besse was within range 2,800 to 3,000 while for Avon and Sammis, it was within range of 800 to 1,000 and 850 to 900, respectively. Thus, it could be concluded that relying on the least CCT does not necessary identify the weakest frequency response. In fact, there was an inverse relationship between the CCT and frequency response in which the greater the CCT was, the weaker the frequency response becomes for short term faults.

The results showed that, upon offshore wind farm integration, the transient frequency stability depends on the size of the faulted component and its inertia. As the larger the capacity of generators are, the more robust and stable they are following a short term fault. This was because of the higher inertia of the larger generators. For faults on medium and small capacity generators as well as lines, the frequency response relies on the inertial support by large generators which provide major contribution in inertia of the system and the distance of the faulted component from them. For faults on large capacity generators, frequency response was stronger and less dependent on the other inertia contributor units.

6.4.2 Long Term Fault

Following loss of a major generation unit or transmission line, rotors of generators in the area decelerate due to a deficit of active power. Subsequently, rotor angles begin to deviate. Figure 6.56 showed rotor speed of the synchronous generators in the area following loss of Davis-Besse.

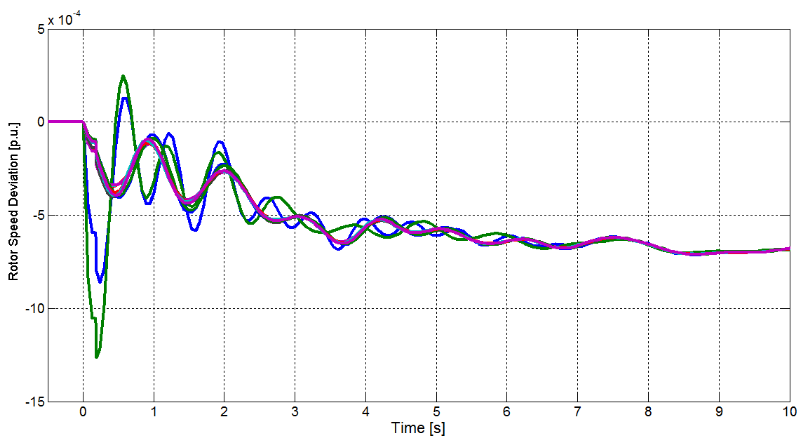

Figure 6.56: Rotor speeds in the FirstEnergy/PJM area following loss of Davis-Besse

As shown in this figure, the rotor speeds reach a steady state point within first 10 seconds. In a stable power system, the rotor speeds should regain their new operating point within few first seconds following an outage. It is normal that the maximum rotor angle difference in the area changes by a few degrees. Otherwise, system loses the synchronism that might lead to a major blackout.

Figures 6.57 through 6.59 show the maximum rotor speed and rotor angle deviations in the area for different levels of wind power following investigated components.

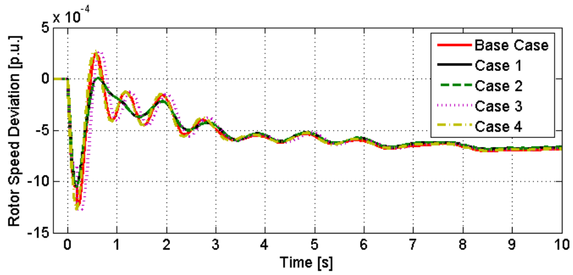

(a) Maximum Rotor Speed Deviation

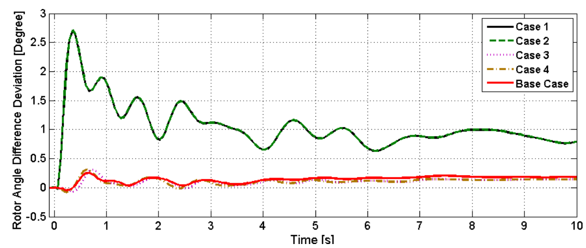

(b) Rotor Angle Difference Deviation

Figure 6.57: Rotor angle and speed deviation in the area following loss of Davis-Besse generator

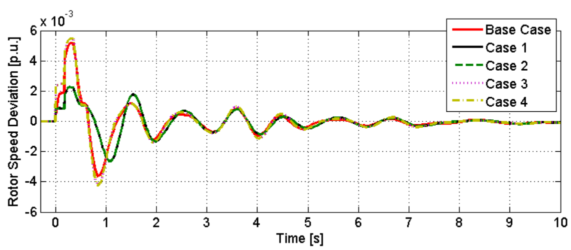

(a) Maximum Rotor Speed Deviation

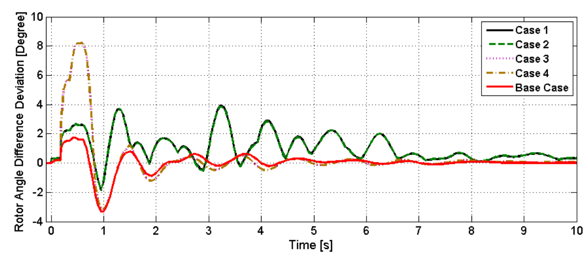

(b) Rotor Angle Difference Deviation

Figure 6.58: Rotor angle and speed deviation in the area following loss of Davis-Besse-Leymon line

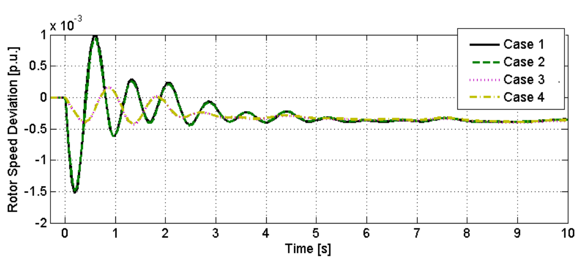

(a) Maximum Rotor Speed Deviation

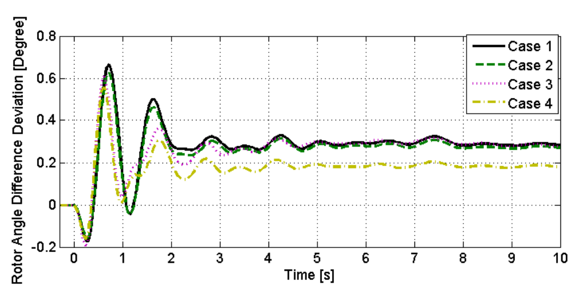

(b) Rotor Angle Difference Deviation

Figure 6.59: Rotor angle and speed deviation in the area following loss of half of offshore collector system

Figure 6.57 showed that in the base case, following loss of Davis-Besse generator, rotor angle difference in the area changes within 0.3 degrees and maximum rotor speed deviation in the area reaches zero within first 7 seconds. Upon integration of the offshore wind farm, in all of the studied cases, the maximum rotor speed deviation settles at 0.0007 p.u, identical as was in the base case. The rotor angle difference in cases 1 and 2 in which Perry was online, after a peak at 2.6 degrees, settles at 0.7 degrees deviation within first 10 seconds. The rotor angle difference in cases 3 and 4 in which Perry was offline, followed the similar trajectory as in the base case and settled within 0.3 degrees deviation.

Figure 6.58 showed that in the base case, following loss of Davis-Besse-Leymon line, rotor angle difference in the area initially deviates to approximately 3 degrees and then after damping out the oscillations, settles at zero within first 8 seconds. The maximum rotor speed deviation in the area also after oscillations amplitudes as high as 0.005 p.u., reaches zero within first 8 seconds. Upon integration of the offshore wind farm, in all of the studied cases, the maximum rotor speed deviation settles at zero within first 10 seconds. In cases 1 and 2 in which Perry was online, the amplitude of maximum rotor speed deviation as high as 0.002 p.u., less than the half of the greatest amplitude in the base case, and in cases 3 and 4 in which Perry was offline, is 0.005 p.u, same as in the base case. The rotor angle difference deviation in cases 1 and 2 after a few oscillations with a greater damping ratio than in the base case, settles at zero within first 10 seconds. The rotor angle difference deviation in cases 3 and 4 after oscillations with greater amplitude but higher similar trajectory and damping ratio as in the base case and settled at zero within first 10 seconds.

Figure 6.59 showed that following loss of half of the offshore collector system, maximum rotor speed deviation settled at 0.0003 p,.u. within first 10 seconds with an amplitude as high as 0.0015 p.u. in cases 1 and 2 in which Perry was online and as high as is 0.0004 p.u. in cases 3 and 4 in which Perry was offline. In cases 1, 2 and 3, the rotor angle difference after a few oscillations with an amplitude as high as 0.7 degree, settled at 0.3 degree deviation within first 2 seconds. In case 4, it settled at 0.2 degree deviation within first 4 seconds with similar oscillations.

By comparing the results from case 1 and 2 and case 3 and case 4 in all of the studied cases, it can be concluded that operation of SVC at the POI does not significantly influence the rotor angle stability of the system including rotor speed and rotor angle difference following an outage.

These results are inconclusive regarding the relation of the rotor angle difference deviation and rotor speeds deviation in the area. Thus, cases 1 and 3 were selected to perform Prony analysis to identify the dominant oscillatory modes of the system. These two cases were selected since the contribution of operation of SVC to the transient stability following a long term fault was insignificant. This provide a better understanding of dynamic performance of the system for each event. The Prony analysis was performed on the entire active power generation profiles in the area in each studied cases.

The results of the Prony analysis are shown in Table 6.20 through 6.22. It should be noted that the only dominant generators modes for each case are shown.

The results presented in Table 6.20 show that following outage of Davis-Besse

Table 6.20: Oscillatory modes appeared in the system following loss of Davis-Besse generator

	Base Case		**Case 1**		**Case 3**	
Mode No.	Frequency	Amplitude	Frequency	Amplitude	Frequency	Amplitude
1	0.9 Hz	16.37	0.9 Hz	20.09	—	—
2	1.0 Hz	28.12	—	—	—	—
3	1.3 Hz	24.75	1.3 Hz	19.02	—	—
4	1.5 Hz	20.35	1.5 Hz	25.40	1.4 Hz	36.99

Table 6.21: Oscillatory modes appeared in the system following loss of Davis-Besse to Leymon line

	Base Case		**Case 1**		**Case 3**	
Mode No.	Frequency	Amplitude	Frequency	Amplitude	Frequency	Amplitude
1	0.9 Hz	116.66	0.8 Hz	18.12	—	—
2	1.0 Hz	179.76	1.0 Hz	123.62	1.0 Hz	129.82
3	1.3 Hz	405.45	1.3 Hz	377.13	1.3 Hz	292.72
4	1.4 Hz	110.37	1.4 Hz	298.61	1.4 Hz	102.92
5	1.5 Hz	121.27	1.9 Hz	170.23	1.5 Hz	119.36

Table 6.22: Oscillatory modes appeared in the system following loss of half of the offshore collector system

	Case 1		**Case 3**	
Mode No.	Frequency	Amplitude	Frequency	Amplitude
1	0.2 Hz	10.33	—	—
2	0.5 Hz	27.93	0.7 Hz	17.48
3	0.9 Hz	31.94	0.9 Hz	20.62
4	1.0 Hz	17.42	1.0 Hz	14.87
5	1.3 Hz	59.22	1.2 Hz	27.57
6	1.4 Hz	85.52	1.5 Hz	19.89

generator, in case 3, three of the dominant modes which also appeared in the base case including an inter-area mode and two local plant modes, were eliminated whereas in case 1, only one of the local plant modes was eliminated. The amplitude of the remaining modes did not change significantly.

The results shown in Table 6.21 reveal that following fault and loss of Davis-Besse to Leymon line in case 3 in comparison with the base case, amplitude of all of the modes were reduced and the inter-area mode at 0.9 Hz was eliminated. In case 1, amplitude of the inter-area mode at 0.9 Hz, was reduced by 90% from 116.66 to 18.12. The amplitude of the low frequency local plant modes at 1.0 Hz and 1.3 Hz were also reduced while the amplitude of higher frequency local plant modes, at 1.4 Hz and 1.5 Hz were boosted.

The results shown in Table 6.22 yields that following loss of the collector system in case 3, amplitude of all of the modes which also appeared in case 1 were reduced and a low frequency inter-area mode at 0.2 Hz was eliminated.

From the presented results, it can be seen that the overall influence of offshore wind farm integration on dynamics of the system is mostly positive by reducing or eliminating the oscillatory modes.

Figures 6.60 through 6.62 shows impacts of variability of the offshore wind farm on transient rotor stability of the system for studied cases.

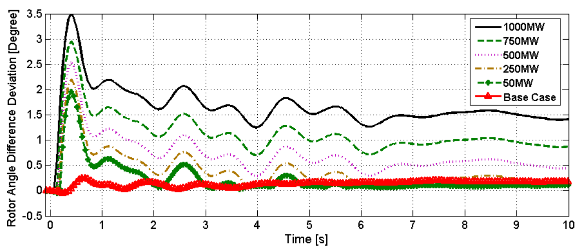

(a) Case 1

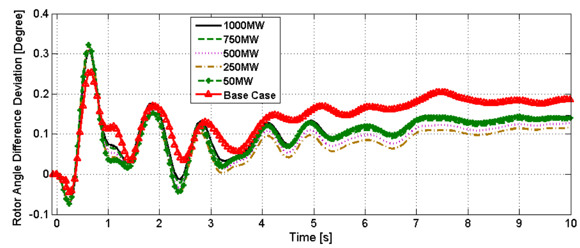

(b) Case 3

Figure 6.60: Maximum rotor angle difference for different levels of wind power following loss of Davis-Besse generator in studied cases

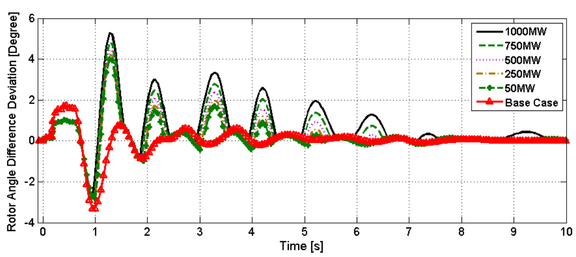

(a) Case 1

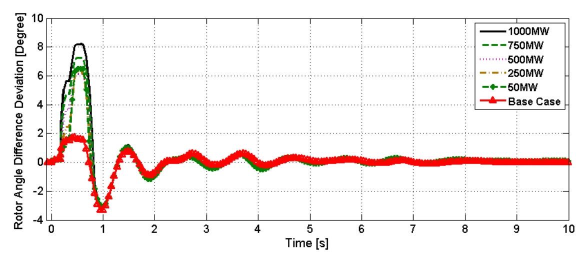

(b) Case 3

Figure 6.61: Maximum rotor angle difference for different levels of wind power following loss of Davis-Besse to Leymon line in studied cases

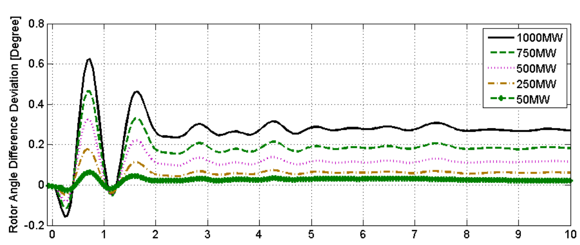

(a) Case 1

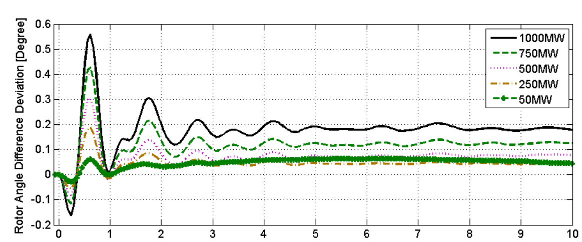

(b) Case 3

Figure 6.62: Maximum rotor angle difference for different levels of wind power following loss of half of the offshore collector system in studied cases

The results shown in Figures 6.60 through 6.62 reveal that the higher levels of offshore wind power amplifies the amplitude of rotor angle oscillations and cause a higher settling rotor angle difference in area. In Figure 6.60, it was shown that the maximum rotor angle difference deviation in base case was less than 0.3 degree whereas in Case 1 for maximum wind power, it was approximately 3.5 degrees. The maximum rotor angle difference deviation in Case 3 is very close to its value in the base case, 0.3 degree.

Figure 6.61 reveals that following a fault on the Davis-Besse to Leymon line, in both cases of 1 and 3, the greatest rotor angle difference deviation was for the maximum level of wind power.

Similarly, in Figure 6.62, it could be seen that the maximum wind power caused the maximum level of rotor angle difference deviation in the area.

According to these results, it is safe to assume that maximum level of wind power generation provide the worst case scenario in terms of rotor angle difference deviation. This is very important since the rotor angles in the area determine the flow of the power across the system.

Figures 6.63 through 6.65 show the transient frequency dynamics following investigated faults.

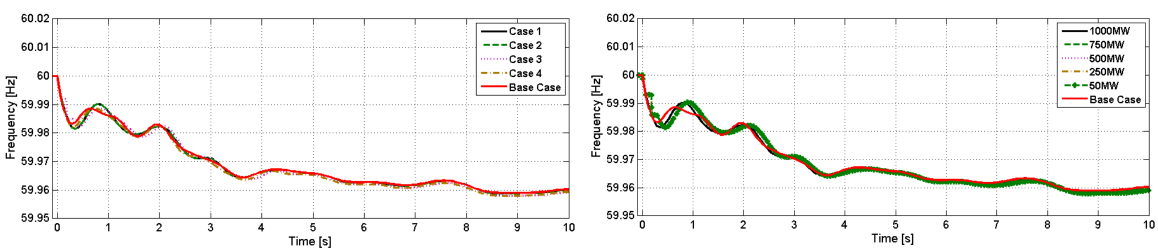

(a) Comparison of studied cases (b) Comparison of level of wind power

Figure 6.63: Area frequency following loss of Davis-Besse generator in studied cases

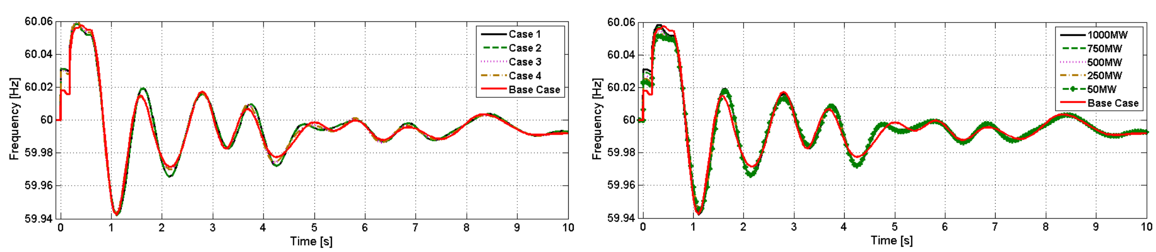

(a) Comparison of studied cases (b) Comparison of level of wind power

Figure 6.64: Area frequency following loss of Davis-Besse to Leymon line in studied cases

From the results presented in Figures 6.63 and 6.64, it can be seen that the frequency trajectory following the investigated faults on onshore assets, including the

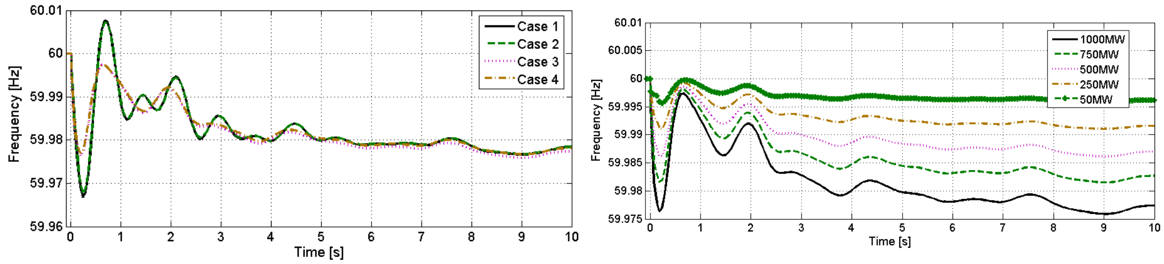

(a) Comparison of studied cases

(b) Comparison of level of wind power

Figure 6.65: Area frequency following loss of half of the offshore collector system in studied cases

generator and the transmission line, is identical in all of the studied cases and for all levels of offshore wind power and identical as was in the base case.

However, the area frequency following a fault on the offshore collector system, as shown in Figure 6.65, is a function of operation of Perry and independent from operation of SVC at the POI. The results from case 1 and case 2 and from case 3 and case 4 are identical. The transient frequency dynamics also is a function of level of power generation by offshore wind farm. As the higher the level of offshore wind power was, high level drop in frequency was. These results are consistent with the results from small signal stability analysis where the source of disturbance was the variability of the wind farm.

In all of the studied cases, nadir frequency remained above the UFLS threshold. The lowest settling frequency was at 59.96 Hz following loss of Davis-Besse generator and the lowest transient frequency was at 59.94 Hz following loss of the David-Besse to Leymon line.

However, the frequency response of a power system is defined by the area frequency behavior in respect to the level of blocked power. Values shown in Table 6.23 lists the proposed frequency response metric, SBFR, for studied cases. This metric is a function of blocked active electrical power and area frequency swing during a fault.

Table 6.23: *SBFR* index for studied cases in the FirstEnergy/PJM system

Fault	**Base Case**	**Case 1**	**Case 3**
Davis-Besse Generator	2,217	2,252	2,233
Davis-Besse to Leymon Line	411	390	391
Offshore Collector System	—	1,223	2,075

The results shown in Table 6.23 outline that the frequency response of the system following a long term fault on the Davis-Besse generator has been slightly improved upon offshore wind farm integration while for the fault on the Davis-Besse to Leymon line has been slightly degraded. It should be noted that the influence of the wind farm is, however, insignificant.

Since the frequency swing as well as blocked power remained unchanged following faults on the generator and the line for all levels of offshore wind power, the SBFR shown in this table is valid for the complete operational range of the wind farm. The metric shown for the collector system is calculated based on 1000MW offshore wind farm. The SBFRs for case 1 and case 2 and for case 3 and case 4 are identical. This metric is practical to assess impact of integration of an offshore wind farm on frequency stability of the grid.

It should be noted that although the frequency response of the system to fault on the Davis-Besse to Leymon line is the weakest among all, the area frequency was recovered to 60 Hz within first 10 seconds. The weak frequency response of the line was because of the fact that the fault on the line remained for 12.5 cycles before its trip. But, the faults on the generator and the collector system were immediate trip of the units. The persisted fault on the line was meant to increase severity of the fault since it transmitted a lower level of power relative to the studied generator. The results of frequency response from this section are consistent with the results from the small signal stability analysis.

Figures 6.66 through 6.68 demonstrate the relationship between rotor angle difference deviation and maximum voltage deviation dynamics in the area for studied cases.

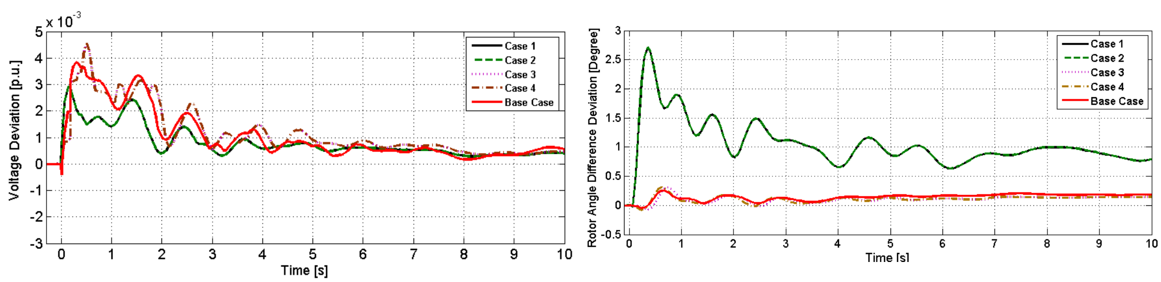

(a) Maximum voltage deviation

(b) Rotor angle difference

Figure 6.66: Maximum voltage deviation and rotor angle difference deviation dynamics in the area following loss of Davis-Besse generator in studied cases

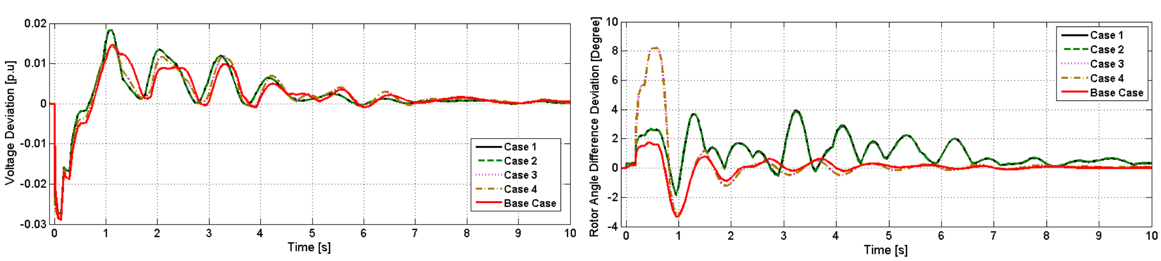

(a) Maximum voltage deviation

(b) Rotor angle difference

Figure 6.67: Maximum voltage deviation and rotor angle difference deviation dynamics in the area following loss of Davis-Besse to Leymon line in studied cases

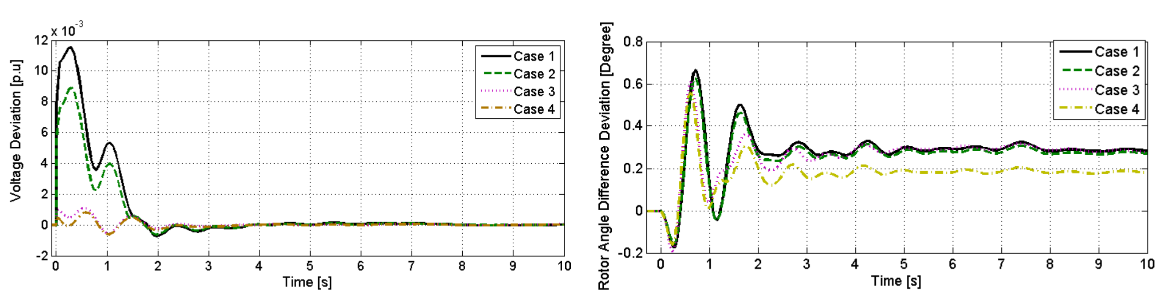

(a) Maximum voltage deviation

(b) Rotor angle difference

Figure 6.68: Maximum voltage deviation and rotor angle difference deviation dynamics in the area following loss of half of the offshore collector system in studied cases

From the results shown in Figures 6.66 through 6.68, it can be seen that the influence of integration and operation of the offshore wind farm on transient voltage stability following a fault on onshore components is very insignificant. Figures 6.67 and 6.66 indicate that following the faults on Davis-Besse generator and Davis-Besse to Leymon line, the voltage stability margin for all of the studies cases remains nearly as it was in their base case. From these results, it also could be seen that the transient voltage stability following a fault on onshore components was almost independent from the rotor angle difference dynamics for all levels of wind power.

However, in case of the fault of the offshore collector system, the transient voltage stability in Case 1 and Case 2 was weaker than in Case 3 and Case 4. This shows that the voltage stability was a function of operation of Perry while it had an adverse influence. The rotor angle differences in the area followed the same pattern in all of the studied cases. Thus, similar to the fault on onshore components, it could be stated that for all levels of wind power, the transient voltage stability was almost independent from the rotor angle difference dynamics in the area.

It should be noted that the amplitude of the voltage and rotor angle difference deviations following loss of the studied line was greater than loss of the generator and collector system. This was because of the fact that during investigation of the line fault, the fault was remained for 12.5 cycles on the line and then the line was tripped. The faults on the generator and the collector system were immediate trip of the units. The sustained fault on the line for 12.5 cycles prior to its trip was meant to increase severity of the fault.

The settling voltage deviation in all of the studied cases and for all level of wind power was zero. This indicated that following long term faults, voltage at the faulted components recovers to its pre-fault value within first 10 seconds following the fault. Thus, measures of transient voltage stability in the FirstEnergy/PJM system exist.

Chapter 7

Conclusions and Future Work

7.1 Summary

Electrical energy from offshore wind is relatively a new source of electrical energy in contrast to the conventional hydro and fossil fuel-based sources and yet certain aspects of it are to explore.

The overall goal of this project has been to develop a comprehensive guideline to identify transmission system upgrades needed to facilitate offshore wind projects. These tools were meant to determine operational effects of offshore generation on steady state operations and dynamic stability of the transmission systems.

This study used a computer simulation model of the US Eastern Interconnection as the test system and focused on the integration of a 1000MW offshore wind farm operating in Lake Erie into FirstEnergy/PJM service territory as a case study.

The contents of this research provided recommendations on development of offshore wind integration scenarios, identification of the locations of the POIs, wind profile modeling and simulation and computational methods to quantify performance, along with operating changes and equipment upgrades needed to mitigate system performance issues introduced by offshore wind projects.

7.2 Findings and Recommendations

- Measures of stability and security in FirstEnergy/PJM power system with 1000MW integrated offshore wind farm exist.
- Using statistical and stochastic tools allows quantification of variability of wind power in large power systems for planning and operation analysis.
- The wind integration projects are typically added to an existing power system. Therefore, it is safe to assume them as generation expansion study.
- Due to highly variable nature of the wind power, it is required to conduct reliability studies and compute the reliability for all levels of contribution of the wind farm in power generation, from 0% to 100% of its capacity with a credible

step size. If the safe reliability level is not reached, additional generation units may improve the reliability.

- The step size to model the wind variability could be chosen depending on the planner's preference and experience.
- In practice, the wind power change with a moderate ramp. However, to examine the most severe case such as wind gusts which in many occasions force to a sudden shut down of entire wind farm or a part of it for safety reasons, sudden changes of wind power should be applied to the system.
- The proposed tool in this study was fully capable to determine how integration of offshore wind generation may affect operation of large scale transmission systems. This tool provides an understanding of how associated factors with operation wind generation and integration scenarios might affect the system performance that is a key concern in choosing the best wind integration scenario.
- In this study, it was found out that the integration of offshore wind farms could improve the voltage regulation across the system. This is because of the fact the wind farm helps with managing the excessive reactive power available in the FirstEnergy/PJM power area.
- Using the wind machines with a greater capability to provide reactive power support result in a greater voltage regulation in the area.
- Operation of SVC at the wind POIs could compensate for lack of capability of wind machine to provide sufficient reactive power support.
- Point of voltage regulation by wind farm does not influence on steady state stability of the power area.
- The results of this study showed that in lightly loaded power systems such as FirstEnergy/PJM power area, the line congestion is not a concern for adding the wind generation capacity.
- Level of capability of the wind machine in providing reactive power support and operation of SVC at the wind POIs do not impacts on loading level of transmission system in the power area.
- The developed analytical tool for contingency operation of large scale power systems for offshore wind farm integration studies. This tool relied on a proposed risk based approach to quantify variability of the wind power as a single index. This allows in addition to comparing and ranking the severity of events, identifying the most secure integration scenario. This approach is also applicable to integration studies of all other forms of variable generation units such as onshore wind farms and solar farms.

- The results of contingency analysis showed that operation of Perry power plant significantly improves the system's security. However, its presence is not vital since lack of its operation does not lead to any stability or security violation.

- Operation of SVC at the wind POIs does not significantly impacts on security and resiliency of the power system.

- Prony analysis a superb tool for assessing large scale power system's voltage stability. The analysis completed in this research demonstrates that voltage oscillatory modes for small signal voltage stability analysis could be captured by applying Prony analysis directly to a time-domain voltage signal following a small disturbance. This finding is useful for large scale power system in which applying modal analysis is computationally burdening or impossible.

- The introduced frequency response metric in this study is practical for measuring frequency small signal stability of the power systems following variability of the wind farms. This metric measures the level of frequency swing in respect to the level of wind variability. This metric is useful for both events of increase and decrease in the level of power generation by offshore wind farm.

- Integration of the offshore wind farm through a POI where a power plant without an active governor such as a nuclear power plant, amplifies the oscillations caused by the wind farm and degrades the dynamics stability of the system.

- Upon integration of the offshore wind farm, the CCT in the FirstEnergy/PJM system was not degraded following a short term fault with a successful clearance. Conversely, it could be improved significantly in the majority of the cases in a fashion that the system could remain stable after 900 cycles of persisting fault.

- For faults on generators; Integration and operation of the offshore wind farm did not improve the CCT for faults on large generators. The significant improvement of the CCT was for faults on medium capacity generators.

- For faults on transmission lines; Integration and operation of the offshore wind farm improved the CCT for the lines depended on their distance from large capacity generators. The CCT for the fault on the lines close to large generators did not change significantly while for lines close to medium generators, the CCT was significantly improved.

- The CCT and dynamics of active power, rotor angle, reactive power and voltage following a short term fault are highly correlated. Upon integration and operation of the offshore wind farm, as the CCT is improved, all other aforementioned variables are improved. Thus, the CCT directly determines short term transient rotor angle and voltage stability margins of system.

- Additional reactive power support by SVC operating at the wind POI, does not improve the transient stability of the system following a short term fault.

- Integration and operation of the offshore wind farm improved the long term transient stability of the system by decreasing the number and amplitude of the oscillatory modes.

- Operation of SVC at the wind POIs does not influence the rotor angle stability of the system following an outage.

- The operation of the wind farm at it maximum capacity yielded the worst case scenario in terms of rotor angle oscillations following long term faults.

- Upon integration and operation of the offshore wind farm, the transient frequency stability following a short term fault depends on the size of the faulted component and its inertia contribution.

- As the larger the capacity of the generators are, the more robust and stable the frequency response following faults on them are. This is because of the higher inertia of the larger generators.

- Following short term faults on medium and small capacity generators and transmission lines, the frequency response relies on the inertial support by the large generators which provide major inertia contribution in the system. Therefore, in cases in which Perry was offline, the frequency response was degraded.

- Following short term faults on medium and small capacity generators and transmission lines, the second factor that determined the frequency response was the distance of the faulted component from the large generators. The more distant they were, the weaker the frequency response was.

- For faults on large capacity generators, frequency response was stronger and independent from the other inertia contributor units.

- The frequency response of the system was improved upon offshore wind farm integration and operation following long term faults.

- Integration and operation of the offshore wind farm improved the short term transient voltage stability of the system. In fact, maximum voltage deviation amplitude and oscillations were reduced following short term faults.

- The long term transient voltage stability of the system remained unchanged upon integration and operation of the offshore wind farm. It was not significantly improved or degraded.

- The transient voltage stability of the system following outage of the grid components was independent from behavior of rotor angle and rotor speeds in the area, for all levels of wind power.

7.3 Scope for Future Work

The following describes suggestions for further development in future research:

- Development of offshore wind farms in areas where thermal and voltage stability problems already exist may result in some generation not being properly dispatched for some period of time. Because of the fact that the generation dispatch is managed through market processes, it will be necessary to develop and implement methodologies that incorporate stability constraints and market processes. These models will reflect the actual operation of the wind farms that are ultimately deployed in practice. Such studies will give an indication as to whether the offshore wind generation will be economically and technically feasible and viable.

- Additional work is needed to completely understand how operation of neighboring generation units to the POI of the offshore wind farms and their controller systems affect the dynamics and control of both grid and the offshore wind farm.

- Additional work is needed to completely understand how energy storage systems such as battery and ultracapacitor can provide additional support to the power system by preventing or reducing the oscillatory modes in response to the external disturbances. This investigation should be extended to electrochemical effects on those systems including aging effect and ambient conditions such as drastic temperature change. For instance in Cleveland, OH, the summer temperature could reach beyond 100°F whereas the Polar Vortex in the winter could drop the temperature below -30°F. This analysis will allow understanding of their dynamic interaction with the grid and the consequences of these phenomena on the stability and operation of the grid in the presence of large scale offshore wind farms.

Bibliography

[1] D. Y. Goswami and F. Kreith, *Energy conversion*. CRC press, 2007.

[2] E. A. DeMeo, W. Grant, M. R. Milligan, and M. J. Schuerger, “Wind plant integration [wind power plants],” *Power and Energy Magazine, IEEE*, vol. 3, no. 6, pp. 38–46, 2005.

[3] E. Ela, V. Diakov, E. Ibanez, and M. Heaney, “Impacts of variability and uncertainty in solar photovoltaic generation at multiple timescales,” *Contract*, vol. 303, p. 2753000, 2013.

[4] J. Hill, “Us wind energy tops new electric capacity in 2015,” 2016.

[5] US Department of Energy, “Energy dept. reports: U.s. wind energy production and manufacturing reaches record highs,” 2013.

[6] US Department of Energy, “Wind vision,” 2016.

[7] C. Morris, “2015: Germanys record wind year,” 2016.

[8] S. Knight, “14% german wind market expansion below expectations,” 2013.

[9] WINDBIZ, “Germany installs 1,143 mw of wind power in 1st half of 2013,” 2013.

[10] A. Morales, “Spain installed no wind power for first time since 80s in 2015,” 2016.

[11] S. Kumar, “Growth of global solar and wind energy continues to outpace other technologies,” 2013.

[12] N. O. Pearson, “Growth of global solar and wind energy continues to outpace other technologies,” 2013.

[13] S. Han and S. Park, “S. korea to invest 9 billion in largest offshore wind farm,” 2011.

[14] Cape Wind Association, “Cape wind association,” 2015.

[15] R. Katakey, “India to build first offshore wind power project,” 2014.

[16] Wind Power Monthly, "Ewea offshore: India could have offshore wind by 2019," 2015.

[17] P.-L. Wen, J.-X. Lin, C.-C. Feng, F.-K. Ko, and S.-M. Lin, "Feasibility of taiwans offshore wind power development,"

[18] H. Guo, K. Rudion, and Z. Styczynski, "Integration of large offshore wind farms into the power system," in *Science and Technology, 2011 EPU-CRIS International Conference on*, pp. 1–6, IEEE, 2011.

[19] A. Sajadi, R. Kolacinski, and K. Loparo, "Impact of wind turbine generator type in large-scale offshore wind farms on voltage regulation in distribution feeders," in *Innovative Smart Grid Technologies Conference (ISGT), 2015 IEEE Power & Energy Society*, pp. 1–5, IEEE, 2015.

[20] J. Bebic, "Power system planning: emerging practices suitable for evaluating the impact of high-penetration photovoltaics," tech. rep., National Renewable Energy Laboratory (NREL), Golden, CO (United States), 2008.

[21] N. W. Miller, W. W. Price, and J. J. Sanchez-Gasca, "Dynamic modeling of ge 1.5 and 3.6 wind turbine-generators," *GE-Power systems energy consulting*, 2003.

[22] S. Barnes, "Progress Report - Great Lakes Offshore Wind: Utility and Regional Integration Study," tech. rep., General Electric (GE), Pittsburgh, Pennsylvania (United States), 2014.

[23] S. Barnes, R. D'Aquila, and B. Thomas, "GE PSLF User Manual," tech. rep., General Electric (GE), Schenectady, New York (United States), 2011.

[24] J. Machowski, J. Bialek, and J. Bumby, *Power system dynamics: stability and control*. John Wiley & Sons, 2008.

[25] R. Gutman, "Application of line loadability concepts to operating studies," *Power Systems, IEEE Transactions on*, vol. 3, no. 4, pp. 1426–1433, 1988.

[26] J. Machowski, J. Bialek, and J. R. Bumby, *Power system dynamics and stability*. John Wiley & Sons, 1997.

[27] S. C. Savulescu, *Real-time stability assessment in modern power system control centers*, vol. 42. John Wiley & Sons, 2009.

[28] M. Pai, D. S. Gupta, and K. Padiyar, *Small signal analysis of power systems*. Alpha Science Int'l Ltd., 2004.

[29] J. Paserba, J. Sanchez-Gasca, P. Kundur, E. Larsen, and C. Concordia, "Small signal stability and power system oscillations," *Power system Stability and Control, Ed. LL Grigsby, Boca Raton: CRC Press*, p. 9, 2007.

[30] Y. Zhang, J. Bank, Y.-H. Wan, E. Muljadi, and D. Corbus, "Synchrophasor measurement-based wind plant inertia estimation," in *Green Technologies Conference, 2013 IEEE*, pp. 494–499, IEEE, 2013.

[31] E. Muljadi, V. Gevorgian, M. Singh, and S. Santoso, *Understanding inertial and frequency response of wind power plants.* IEEE, 2012.

[32] P. W. Sauer and M. Pai, "Power system dynamics and stability," *Urbana*, 1998.

[33] P. M. Anderson and A. A. Fouad, *Power system control and stability.* John Wiley & Sons, 2008.

[34] P. Kundur, N. J. Balu, and M. G. Lauby, *Power system stability and control*, vol. 7. McGraw-hill New York, 1994.

[35] E. L. Petersen, I. Troen, S. Frandsen, and K. Hedegaard, *Danish Wind Atlas. A Rational Method of Wind Energy Siting.* Roskilde: Risø National Laboratory, 1981.

[36] D. L. Elliott, C. Holladay, W. Barchet, H. Foote, and W. Sandusky, "Wind energy resource atlas of the united states," *NASA STI/Recon Technical Report N*, vol. 87, p. 24819, 1987.

[37] US Department of Energy, "Utility-scale land-based 80-meter wind maps," 2016.

[38] S. Traup and B. Kruse, "Wind und windenergiepotentiale in deutschland. winddaten für windenergienutzer," *German. Selbstverlag des Deutschen Wetterdienstes, Offenbach am Main*, 1996.

[39] US Department of Energy, "Offshore 90-meter wind maps and wind resource potential," 2016.

[40] R. Swart, C. Coppens, H. Gordijn, M. Piek, P. Ruyssenaars, J. Schrander, P. de Smet, M. Hoogwijk, M. Papalexandrou, E. de Visser, *et al.*, "Europe's onshore and offshore wind energy potential: An assessment of environmental and economic constraints," tech. rep., European Environment AGency, 2009.

[41] J. Stonington, "Era of fast growth ends for wind energy in europe," 2013.

[42] R. Lopez, "Us wind power fastest-growing energy source in 2012, report says," 2013.

[43] Grantham Research Institute, "Onshore wind energy: what are the pros and cons?," 2012.

[44] M. Garcia-Sanz, "Lecture notes on wind energy." University Lecture, 2011.

[45] London Array, "Onshore wind energy: what are the pros and cons?," 2016.

[46] M. Garcia-Sanz and C. H. Houpis, *Wind energy systems: control engineering design*. CRC press, 2012.

[47] M. Eremia and M. Shahidehpour, *Handbook of electrical power system dynamics: modeling, stability, and control*, vol. 92. John Wiley & Sons, 2013.

[48] GE Energy, 2016.

[49] Enercon, 2016.

[50] Vestas, 2016.

[51] R. Maclean, "Electrical system design for the proposed one gigawatt beatrice offshore wind farm," *Faculty of Engineering*, 2004.

[52] J. Green, A. Bowen, L. J. Fingersh, Y.-H. Wan, *et al.*, "Electrical collection and transmission systems for offshore wind power," in *Offshore technology conference*, Offshore Technology Conference, 2007.

[53] P. Mackin, "Dynamic simulation studies of the frequency response of the three us interconnections with increased wind generation," *Lawrence Berkeley National Laboratory*, 2011.

[54] A. Sajadi, Ł. Rosłaniec, M. Kłos, P. Biczel, and K. A. Loparo, "An emulator for fixed pitch wind turbine studies," *Renewable Energy*, vol. 87, pp. 391–402, 2016.

[55] I. A. Hiskens, "Dynamics of type-3 wind turbine generator models," *Power Systems, IEEE Transactions on*, vol. 27, no. 1, pp. 465–474, 2012.

[56] P. Pourbeik, "Proposed changes to the wecc wt3 generic model for type 3 wind turbine generators," *Prepared under Subcontract No. NFT-1-11342-01 with NREL, Issued to WECC REMTF and IEC TC88 WG27*, vol. 12, no. 16, p. 43, 2014.

[57] O. Anaya-Lara, D. Campos-Gaona, E. Moreno-Goytia, and G. Adam, "Fully-rated converter wind turbine (frc-wt)," *Offshore Wind Energy Generation: Control, Protection, and Integration to Electrical Systems*, pp. 73–112, 2014.

[58] P. Pourbeik, "Proposed changes to the wecc wt4 generic model for type 4 wind turbine generators," *Prepared under Subcontract No. NFT-1-11342-01 with NREL, Issued to WECC REMTF and IEC TC88 WG27*, vol. 12, no. 16, p. 11, 2013.

[59] M. R. Islam, Y. Guo, and J. Zhu, "A review of offshore wind turbine nacelle: technical challenges, and research and developmental trends," *Renewable and Sustainable Energy Reviews*, vol. 33, pp. 161–176, 2014.

[60] S. Chuangpishit, A. Tabesh, Z. Moradi-Sharbabk, and M. Saeedifard, "Topology design for collector systems of offshore wind farms with pure dc power systems," *Industrial Electronics, IEEE Transactions on*, vol. 61, no. 1, pp. 320–328, 2014.

[61] G. Quinonez-Varela, G. Ault, O. Anaya-Lara, and J. McDonald, "Electrical collector system options for large offshore wind farms," *Renewable Power Generation, IET*, vol. 1, no. 2, pp. 107–114, 2007.

[62] G. Ault, S. Gair, and J. McDonald, "Electrical system designs for the proposed 1gw beatrice offshore windfarm," in *IEA Annex XXIII: Offshore wind energy technology and deployment: WORKSHOP ON WIND INTEGRATION OF OFFSHORE WIND POWER*, pp. 326–333, 2005.

[63] T. Ackermann, "Transmission systems for offshore wind farms," *Wind Power in Power Systems, T. Ackermann, ed*, pp. 479–504, 2005.

[64] Z. Chen, J. M. Guerrero, and F. Blaabjerg, "A review of the state of the art of power electronics for wind turbines," *Power Electronics, IEEE Transactions on*, vol. 24, no. 8, pp. 1859–1875, 2009.

[65] R. Grünbaum, "Facts for grid integration of wind power," in *Innovative Smart Grid Technologies Conference Europe (ISGT Europe), 2010 IEEE PES*, pp. 1–8, IEEE, 2010.

[66] F. Renaudin, "Integration and stability of a large offshore wind farm with hvdc transmission in the norwegian power system," 2009.

[67] O. Gomis-Bellmunt, J. Liang, J. Ekanayake, R. King, and N. Jenkins, "Topologies of multiterminal hvdc-vsc transmission for large offshore wind farms," *Electric Power Systems Research*, vol. 81, no. 2, pp. 271–281, 2011.

[68] R. B. Biggs and W. Jewell, "Summary of multiterminal high-voltage direct current transmission technology," tech. rep., Oak Ridge National Lab., TN (USA), 1984.

[69] J. Zhu and C. Booth, "Future multi-terminal hvdc transmission systems using voltage source converters," in *Universities Power Engineering Conference (UPEC), 2010 45th International*, pp. 1–6, IEEE, 2010.

[70] Siemens HVDC, 2011.

[71] J. P. Daniel, S. Liu, E. Ibanez, K. Pennock, G. Reed, and S. Hanes, "National offshore wind energy grid interconnection study," tech. rep., ABB Inc, 2014.

[72] D. Van Hertem and M. Ghandhari, "Multi-terminal vsc hvdc for the european supergrid: Obstacles," *Renewable and sustainable energy reviews*, vol. 14, no. 9, pp. 3156–3163, 2010.

[73] J. Schachner, *Power connections for offshore wind farms.* na, 2004.

[74] Siemens Mechanical Switched Capacitor (MSC/MSCDN), 2016.

[75] T. Wenzel and T. Leibfried, "Voltage stability with mechanically switched capacitors using vacuum circuit breakers in the high-voltage grid," in *Optimization of Electrical and Electronic Equipment (OPTIM), 2010 12th International Conference on*, pp. 41–47, IEEE, 2010.

[76] M. Iizarry-Silvestrini and T. Vélez-Sepúlveda, "Mitigation of back-to-back capacitor switching transients on distribution circuits," *Department of Electrical and Computer Engineering*, pp. 1–8, 2006.

[77] M. Marques, *Steady State Analysis of the Interconnection of Offshore Energy Parks.* PhD thesis, Master Thesis, Instituto Superior Técnico, Lisbon, 2010.

[78] T. D. Liacco, "The adaptive reliability control system," *IEEE Transactions on Power Apparatus and Systems*, vol. 5, no. PAS-86, pp. 517–531, 1967.

[79] NERC, "Accommodating high levels of variable generation," tech. rep., NERC (North American Electric Reliability Corporation), Princeton, NJ (United States), 2009.

[80] C. Herig, "Using photovoltaics to preserve californias electricity capacity reserves," *National Renewable Energy Laboratory, Golden, CO, Report No. NREL/BR-520-31179*, 2001.

[81] L. Garver, "Effective load carrying capability of generating units," *IEEE Transactions on Power Apparatus and Systems*, vol. 8, no. PAS-85, pp. 910–919, 1966.

[82] A. Keane, M. Milligan, C. J. Dent, B. Hasche, C. D'Annunzio, K. Dragoon, H. Holttinen, N. Samaan, L. Söder, and M. O'Malley, "Capacity value of wind power," *Power Systems, IEEE Transactions on*, vol. 26, no. 2, pp. 564–572, 2011.

[83] G. Strbac, A. Shakoor, M. Black, D. Pudjianto, and T. Bopp, "Impact of wind generation on the operation and development of the uk electricity systems," *Electric Power Systems Research*, vol. 77, no. 9, pp. 1214–1227, 2007.

[84] J. Saintcross, R. Piwko, X. Bai, and other authors, "The effects of integrating wind power on transmission system planning, reliability, and operations," tech. rep., General Electric (GE), Albany, New York (United States).

[85] R. Zavadil, J. King, N. Samaan, and other authors, "Final report - 2006 minnesota wind integration study," tech. rep., EnerNex Corporation, Knoxville, Tennessee (United States).

[86] B. Hasche, A. Keane, and M. O'Malley, "Capacity value of wind power, calculation, and data requirements: the irish power system case," *Power Systems, IEEE Transactions on*, vol. 26, no. 1, pp. 420–430, 2011.

[87] M. Milligan, "Methods to model and calculate capacity contributions of variable generation for resource adequacy planning (ivgtf1-2): Additional discussion (presentation)," tech. rep., National Renewable Energy Laboratory (NREL), Golden, CO., 2011.

[88] L. Xu, L. Yao, and C. Sasse, "Comparison of using svc and statcom for wind farm integration," in *Power System Technology, 2006. PowerCon 2006. International Conference on*, pp. 1–7, IEEE, 2006.

[89] L. Holdsworth, X. Wu, J. Ekanayake, and N. Jenkins, "Comparison of fixed speed and doubly-fed induction wind turbines during power system disturbances," in *Generation, Transmission and Distribution, IEE Proceedings-*, vol. 150, pp. 343–352, IET, 2003.

[90] L. Holdsworth, N. Jenkins, and G. Strbac, "Electrical stability of large, offshore wind farms," in *IEE conference publication*, pp. 156–161, Institution of Electrical Engineers, 2001.

[91] A. Sajadi, H. Farag, P. Biczel, and E. El-Saadany, "Voltage regulation based on fuzzy multi-agent control scheme in smart grids," in *2012 IEEE Energytech*.

[92] V. Donde, V. Lopez, B. Lesieutre, A. Pinar, C. Yang, and J. Meza, "Identification of severe multiple contingencies in electric power networks," in *Power Symposium, 2005. Proceedings of the 37th Annual North American*, pp. 59–66, IEEE, 2005.

[93] B. Pal and B. Chaudhuri, *Robust control in power systems*. Springer Science & Business Media, 2006.

[94] A. Miri, C. Sihler, and T. Zöller, "Active damping of torsional modes in turbine-generator shafts," 2009.

[95] J. L. Domínguez-García, O. Gomis-Bellmunt, F. D. Bianchi, and A. Sumper, "Power oscillation damping supported by wind power: a review," *Renewable and Sustainable Energy Reviews*, vol. 16, no. 7, pp. 4994–5006, 2012.

[96] J. NARAIN, "Turbines turned off... because it's too windy! they automatically shut down as gusts of 85mph swept country," 2015.

[97] Frequency Load Shedding, "C37. 117," 2007.

[98] A. Exhibit, "Prc-006-npcc-1automatic underfrequency load shedding regional reliability standard proposed and implementation plan for approval," 2012.

[99] J. H. Eto, "Use of frequency response metrics to assess the planning and operating requirements for reliable integration of variable renewable generation," *Lawrence Berkeley National Laboratory*, 2011.

[100] A. Ulbig, T. S. Borsche, and G. Andersson, "Impact of low rotational inertia on power system stability and operation," *arXiv preprint arXiv:1312.6435*, 2013.

[101] NERC, "Standard bal0031frs, frequency response standard background document," tech. rep., NERC (North American Electric Reliability Corporation), Princeton, NJ (United States), 2012.

[102] N. Miller, M. Shao, S. Pajic, and R. DAquila, "Eastern frequency response study," *Contract*, vol. 303, pp. 275–3000, 2013.

[103] Michelle DiFrangia, "New study suggests pjm could benefit from increasing its renewable resources," 2014.

[104] FirstEnergy, "Firstenergy territory map," 2013.

[105] J. Mackauer, J. Syner, P. Bowers, and J. Detweiler, "FirstEnergy/PJM Requirements for Transmission Connected Facilities," tech. rep., FirstEnergy, Akron, Ohio (United States), 2013.

[106] E. Vittal, M. O. Malley, and A. Keane, "Rotor angle stability with high penetrations of wind generation," *Power Systems, IEEE Transactions on*, vol. 27, no. 1, pp. 353–362, 2012.